Dissertation der Fakultät für Biologie

der Ludwig-Maximilians-Universität München

The trypanosomatid protein kinase A activation mechanism - a target for structure-based inhibitor development

Qingping Wu

Dissertation zur Erlangung des Doktorgrades der Naturwissenschaften

Doctor rerum naturalium (Dr. rer. nat.) an der Fakultät für Biologie der

Ludwig-Maximilians-Universität München

München, 2021

Diese Dissertation wurde angefertigt
unter der Leitung von Prof. Dr. Michael Boshart
im Bereich von Genetik
an der Ludwig-Maximilians-Universität München

Erster Gutachter: Prof. Dr. Michael Boshart
Zweiter Gutachter: Prof. Dr. Daniel Krappmann

Datum der Abgabe: 20.04.2021

Datum der mündlichen Prüfung: 14.07.2021

Eidesstattliche Versicherung

Ich versichere hiermit an Eides statt, dass die vorgelegte Dissertation von mir selbständig und ohne unerlaubte Hilfe angefertigt ist.

München, 16-07-2021	Qingping Wu
(Ort, Datum)	(Unterschrift)

Erklärung

Ich versichere hiermit an Eides statt, dass meine Dissertation selbständig und ohne unerlaubte Hilfsmittel angefertigt worden ist.

Die vorliegende Dissertation wurde weder ganz, noch teilweise bei einer anderen Prüfungskommission vorgelegt.

Ich habe noch zu keinem früheren Zeitpunkt versucht, eine Dissertation einzureichen oder an einer Doktorprüfung teilzunehmen.

München, 16-07-2021	Qingping Wu
(Ort, Datum)	(Unterschrift)

Content

Abbreviation

7-CN-7-C-inosine	7-cyano-7-deaza-inosine
AC	adenylate cyclase
AKAP	a kinase anchoring protein
BLE	bleomycin resistance protein
BSA	bovine serum albumin
BSD	blasticidin S deaminase
BSF	bloodstream form
cAMP	3'-5'-cyclic adenosine monophosphate
cGMP	3'-5'-cyclic guanosine monophosphate
CNB	cyclic nucleotide binding domain
Ctrl	control
D/D domain	dimerization and docking domain
DAPI	4,6-diamidino-2-phenylindole
DMSO	dimethyl sulfoxide
DTT	dithiothreitol
EDTA	ethylenediamine tetra acetate
FACS	fluorescence activated cell sorting
FCS	fetal calf serum
GPCR	G protein-coupled receptor
HAT	Human African Trypanosomiasis
HMI-9	Hirumi’s modified Iscove’s medium 9
HYG	hygromycin phosphotransferase
IPTG	Isopropyl-β-D-thiogalactoside
K/N	kinetoplast/nucleus configuration analysis
kDa	kilo Dalton
LB medium	lysogeny broth medium
LRR	leucine-rich repeat
LS	long slender
M/V	mass per volume
MCF	mesocyclic form
mRNA	messenger RNA
Mw	molecular weight
NBD	nucleoside binding domain
NEO	neomycin phosphotransferase
ORF	opening reading frame
PAC	puromycin N-acetyl transferase
PAGE	polyacrylamide gel electrophoresis

PBC	phosphate binding cassette
PBS	phosphate-buffered saline
PCF	procyclic form
PDE	phosphodiesterase
PDT	population doubling time
PFR	paraflagellar rod
PKA	Protein kinase A
PKAC	PKA catalytic subunit
PKAR	PKA regulatory subunit
PKG	protein kinase G
PKI	PKA inhibitor polypeptide
PVDF	polyvinylidene fluoride
RBC	ribose binding cassette
RNAi	RNA interference
SDS	sodium dodecyl sulphate
SIF	stumpy induction factor
SS	short stumpy
T7Pol	T7 polymerase
TAC	tripartite attachment complex
TAE buffer	Tris-acetate-EDTA buffer
TbPKA	*T. brucei* PKA
TbPKAR/TbR	*T. brucei* PKAR
TbPKAC/TbC	*T. brucei* PKAC
TcPKA	*T. cruzi* PKA
TcPKAR/TcR	*T. cruzi* PKAR
LdPKA	*L. donovani* PKA
LdPKAR/LdR	*L. donovani* PKAR
TEMED	N, N, N', N-Tetramethylethylen-diamin
Tet	tetracyclin
TetO	tetracycline operator
TetR	tetracycline repressor
UTR	untranslated region
V/V	volume per volume
VASP	vasodilator-stimulated phosphoprotein
VSG	variant surface glycoprotein
WHO	World health organization
WT	wild type

Abstract

The Protein kinase A (PKA) is a universal serine/threonine kinase that is highly conserved from low unicellular eukaryotes to humans. PKA plays a pivotal role in regulating a plethora of physiological processes, including metabolism, apoptosis, cell cycle progression and differentiation. Although PKA has been widely studied both structurally and functionally in model eukaryotes, PKA in *Trypanosoma brucei* and other kinetoplastid parasites has surprisingly distinct properties. Previous work from the group showed that TbPKA is not activated by cAMP and does not bind cAMP. Instead, it can be regulated by nucleoside analogs and is activated by cold shock *in vivo*. Compared to the mammalian orthologs, the TbPKA holoenzyme is a heterodimer consisting of the single R and one of three C subunit isoforms, that are differentially expressed in the life cycle of the parasite. TbPKAR contains an unusual large N-terminal domain and an extended C-terminal α-subdomain (α-D helix) with unknown functions. Previous studies revealed a critical role of PKA for the survival and proliferation of *T. brucei.*

In this thesis, we established a robust *in vivo* protein-protein interaction assay (NanoBiT) based on the complementary split NanoLuc to detect R-C association and dissociation. NanoBiT assay is proven to be highly sensitive, fast and convenient in operation and shows a wide dynamic range in measuring PKA activation. Unbiased compound screening by this assay has been achieved using membrane permeabilized trypanosomes, the resulting EC_{50} values are comparable with the radioactive *in vitro* kinase assay on purified kinase. Using this assay and mutagenesis, we found that without the unusual N-terminal domain, PKAR can hardly form holoenzyme with the C-subunit *in vivo*. However, the attempt to identify its interaction sites with the C-subunit based on a simulated holoenzyme model was not conclusive. Interestingly, we found the P-site (T205) phosphorylation is critical for PKA activation and plays an antagonistic role to the N-terminal domain in PKA activation. By gene manipulation, we found that PKAR devoid of the C-terminal α-D helix acts like a dominant-negative mutant that traps the C-subunits, and the host cells show severe growth and cytokinesis phenotype. A comprehensive investigation of the α-D helix using NanoBiT assay reveals a key residue Y485, its interaction with N438 and H440 of the B-site is critical for PKA activation. Mutation of the two interacting amino acids in the back of the B pocket confirmed the result. Combining this result and the analysis of the crystal structure of TbR bound to inosine, we concluded that the α-D helix is confining the

ligand in the B pocket in a lid-like fashion and is important for ligand binding. We speculate that the movement of the lid upon ligand binding is initiating the conformation change required for activation. An attempt to design bulky inhibitors allosterically targeting PKAR by blocking the interactions of the α-D helix and mimicking the dominant-negative effect, was performed. The designed compounds were examined by computational docking. Although a potent inhibitor has not been obtained so far, nucleoside-related compounds were found with high binding affinity but low activation potency, indicating that the separation of binding affinity from activation potency is possible. These compounds can serve as the basis for further inhibitor development. More importantly, they provide a chemical tool for further exploration the TbPKA activation mechanism.

Although the essentiality of PKAC1 catalytic activity and the possible redundancy of the PKAC subunits were reevaluated by reverse genetics in the thesis, the result is puzzling in comparison to previous studies. Interestingly, no difference was found in the activation of different PKA holoenzymes in the bloodstream and procyclic life cycle stages. To further investigate the functions and possible redundancy of the C subunit isoforms, a dominant-negative strategy using a SuperDN PKAR mutant was designed.

1 Introduction

1.1 cAMP-dependent protein kinase

Protein kinases are of vital importance in regulating a plethora of biological events in eukaryotic cells. Over 500 kinase genes were found in human genome accounting for ~2% of the genome (Manning *et al.*, 2002). According to the sequence similarity and evolutionary distance of their catalytic domain, they were clustered into 7 major groups containing a number of families and subfamilies (Manning *et al.*, 2002). cAMP-dependent protein kinase (PKA), a universal serine/threonine kinase that belongs to the AGC superfamily, was first described in 1968 (Walsh *et al.*, 1968) and serves in many ways as a prototype for the entire eukaryotic protein kinases (ePK) since it is one of the best understood kinases both in structure and mechanism. Higher eukaryotic PKA is a heterotetrametric complex (R_2C_2) comprising a regulatory subunit (PKAR or the R subunit) dimer and two catalytic subunits (PKAC or the C subunit). PKAR is the main receptor of cyclic adenosine monophosphate (cAMP), the binding of cAMP results in the dissociation of C subunits from the R-subunit dimer, which in turn phosphorylate a wide variety of substrates. The process is known as PKA activation. In mammalian, PKA family possesses two principal PKAR classes, RI and RII. Each type contains two isoforms (α and β). PKAC has two isoforms (Cα, Cβ). An extra Cγ subunit is only found in primates (Skalhegg & Tasken, 2000). Despite the four PKAR isoforms, different PKAs are functionally non-redundant due to the spatiotemporal distribution of these isoforms. As one of the main effectors of the second messenger cAMP, PKA together with G-protein coupled receptor (GPCR), adenylyl cyclase (AC) and phosphodiesterase (PDE) constitute the key components of cAMP/PKA signaling pathway. The signaling pathway has been found in most eukaryotes, ranging from protozoa to humans, regulating a wide range of biological events which includes metabolism, apoptosis, differentiation, proliferation, etc., in responding to extracellular stimuli. In animals, the spatiotemporal specificity of cAMP/PKA signaling can be achieved by the following mechanisms: 1) cell type and/or tissue-specific expression of PKA isoforms as well as distinct GPCRs and PDEs (Trotter *et al.*, 1999; Wong & Scott, 2004); 2) different PKA holoenzymes are transported by AKAPs and sequestered into various cellular compartments that contain distinctive substrates (Colledge *et al.*, 2000; Skalhegg & Tasken, 2000); 3) AKAPs bind other signaling proteins, e.g., GPCR (Shih *et al.*, 1999; Tao *et al.*, 2003) and PKC (Perkins *et al.*, 2001),

creating a signaling hub at certain sites enabling crosstalk between different signaling pathways. Dysregulation of cAMP/PKA signaling pathway is related to a number of human diseases, such as Carney complex (CNC), which is mostly caused by the mutation of PRKAR1A gene on chromosome 17 (Kirschner *et al.*, 2000; Stratakis *et al.*, 2001; Bertherat *et al.*, 2009). CNC causes tumors in heart, skin and endocrine glands which is manifested as Cushing's syndrome (Sandrini & Stratakis, 2003; Beuschlein *et al.*, 2014; Zhang *et al.*, 2020).

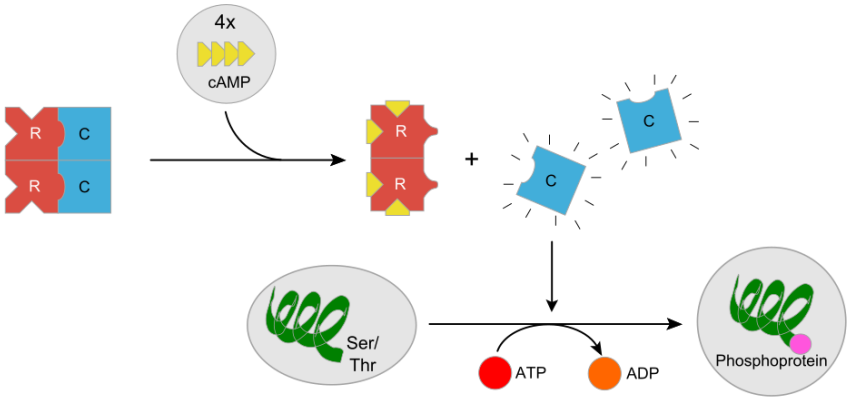

Fig 1.1 PKA activation by cAMP. (https://www.wikiwand.com/en/Protein_kinase_A).

1.1.1 PKAC

The kinase activity of PKA resides in the catalytic subunit (PKAC). Like all kinases in the AGC subfamily, PKAC contains a conserved catalytic core characterized by a prototypical bi-lobal kinase fold that consists of an N-terminal small lobe (N-lobe) and a C-terminal large lobe (C-lobe), as shown in Fig 1.2. One ATP molecule is sandwiched between the two lobes and poised for transferring the γ-phosphate to the phosphorylation site of the captured protein substrate or RII subunit captured by the C-lobe. Based on sequence alignment and structural analysis, many conserved motifs were identified and characterized in the last decades (Hanks *et al.*, 1988; Taylor *et al.*, 1993a; Taylor *et al.*, 1993b). The activation loop is the most flexible and diverse region on the activation segment, which regulates PKAC activity by the phosphorylation of Thr197 (human PKACα). This phosphorylation triggers the conformation change of the linked α-C helix, resulting in the formation of a crucial hydrogen bond network between the α-C helix, the phosphates of ATP and Lys72 (human PKACα) of β-3 strand of the N-lobe (Kornev *et al.*, 2006); this network is required for optimal catalytic activity (Yang *et al.*, 2002; Komander *et al.*, 2005). It is worth mentioning that Thr197 was shown to be autophosphorylated in *E. coli* and *in vitro* (Shoji *et al.*, 1979; Steinberg *et al.*, 1993;

Yonemoto *et al.*, 1993a), whereas other studies indicate it is phosphorylated by other kinases (Cauthron *et al.*, 1998; Cheng *et al.*, 1998; Nirula *et al.*, 2006). PKA substrates bind to the peptide-binding groove of PKAC via their PKA-specific phosphorylation motif (RxxS/T), which are common for all PKA substrates. A small endogenous heat-stable protein (HSP) containing the pseudosubstrate sequence was discovered to inhibit the free active PKAC (Walsh *et al.*, 1971). The core of the protein, PKI-(5-24), was identified to inhibit PKA specifically and efficiently (Cheng *et al.*, 1985; Scott *et al.*, 1985). It is therefore broadly used as a tool in biochemical assays. The N- and C-terminal tails of protein kinases are intrinsically disordered regions (IDRs) flanking the well-folded kinase core. In PKAC, the N-tail containing a myristoylation site and a long α-A helix that docks onto the surface of both the N- and C-lobes is found to be involved in the catalytic process and localization (Yonemoto *et al.*, 1993b; Herberg *et al.*, 1997; Sastri *et al.*, 2005; Bastidas *et al.*, 2012). Wrapping around both lobes, the C-tail acts not only as a *cis*-regulatory element that is required for PKAC enzyme activity but also as a *trans*-regulatory element that modulates the quaternary structure of PKA holoenzyme (Kannan *et al.*, 2007; Romano *et al.*, 2009; Ilouz *et al.*, 2012).

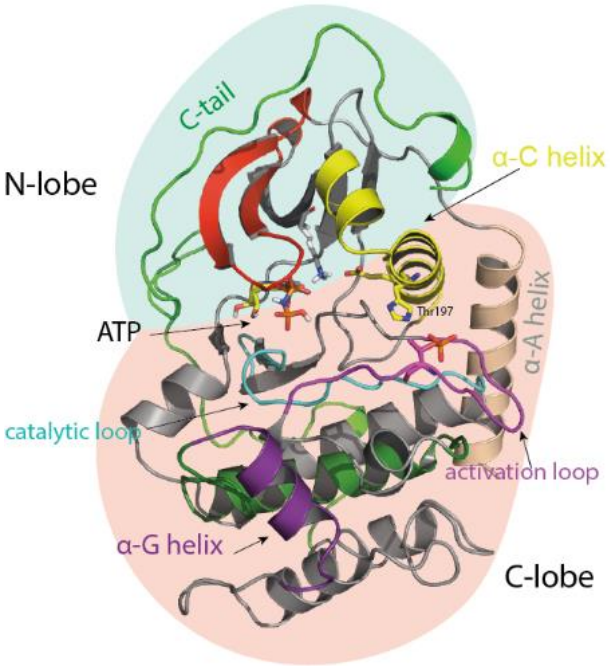

Fig 1.2, Cartoon representation of human PKACα structure. The kinase core is flanked by the N-tail and the C-tail. Important subdomains and motif were highlighted and labeled with different colors. The strucuture is from a heterodimer PKA holoenzyme (PDB: 2QCS), thus the PKACα is in inactive state. The figure is adapted from (Kim *et al.*, 2007).

1.1.2 PKAR

As the regulatory subunit of PKA, PKAR inhibits PKAC activity by binding and forming inactive holoenzyme in the absence of cAMP. As mentioned above, mammals possess four functionally non-redundant PKAR isoforms (RIα, RIβ, RIIα and RIIβ). RIα and RIIα

subunits are expressed in almost every cell, whereas RIβ and RIIβ subunits are tissue-specific. RIβ is found in brain and spinal cord and concentrated in dendrites, whereas RIIβ is mostly expressed in brain and enriched in axons (Cadd & McKnight, 1989; Ilouz *et al.*, 2017). Besides, RIIβ is also found in endocrine, fat, liver and reproductive tissues (Jahnsen *et al.*, 1986; Cadd & McKnight, 1989). The R subunits are highly homologous in amino acid sequence and conserved in domain organization: An N-terminal dimerization and docking (D/D) domain, followed by a variable linker region and two tandem cyclic-nucleotide binding domains (CNB-A and CNB-B) at the carboxyl-terminus, as shown in Fig 1.4 A. The D/D domain is responsible for forming PKAR homodimer and interacting with A-kinase anchoring proteins (AKAPs). AKAPs selectively bind different PKAs through an amphipathic helix composed of 14-18 residues (Carr *et al.*, 1991; Newlon *et al.*, 1997; Newlon *et al.*, 2001), tethering PKAs to distinct subcellular sites or compartments. The variable linker region contains an inhibitor sequence (IS), also termed substrate phosphorylation motif, which docks into the active cleft of the C subunit and can be phosphorylated at the P-site. The inhibitor sequence of RII subunits is RRXS or RRXT, where the X represents any amino acids and the serine or threonine residue can be phosphorylated by PKAC in the presence of Mg-ATP. This sequence stretch is the common character of PKA-specific substrates. RI subunits contain a pseudophosphorylation motif, RRXA or RRXG, where the alanine or glycine residue cannot be phosphorylated. The phosphorylation of RII by the bound PKAC was proven to destabilize PKA holoenzyme, enabling PKA activation in lower cAMP concentration (Rangel-Aldao & Rosen, 1976). In addition, the Ser101 at the P+2 site of bovine RI subunit was reported to be phosphorylated by cGMP-dependent protein kinase (PKG). The latter phosphorylation was shown to cause conformation change of the tetrameric complex and sensitize PKAC kinase activity while in holoenzyme state (Haushalter *et al.*, 2018). The C-terminal CNB domains are conserved in all cAMP-binding proteins throughout bacteria to human. The CNB domain consists of an 8-stranded β barrel flanked by three N-terminal helices (N3A motif) and a C-terminal B/C helix. A highly conserved helix, termed phosphate-binding cassette (PBC), is located between β-strand 6 and 7 and being the signature motif of the CNB domain. The PBC motif is a key for cAMP binding, it contains several conserved residues that interact with the exocyclic oxygens attached to the phosphate group and the 2'OH group from the ribose of cAMP. It also coordinates with a C-terminal tail aromatic capping residue, which forms π-stacking with the adenine ring of cAMP, stabilizing cAMP in the ligand pocket (Su *et al.*, 1995; Das *et al.*, 2007). CNB domain also exists in other cyclic nucleotide-related proteins, e.g., PKG, cAMP-

regulated guanine nucleotide exchange factor (Epac) and Cyclic nucleotide–gated ion (CNG) channels. In bacteria, cAMP receptor protein (CRP) contains a CNB domain at the N-terminus and a C-terminal DNA binding domain. It is also known as catabolite activator protein (CAP) owing to its function to regulate the transcription of genes involved in energy metabolism upon binding and activation by cAMP (Schultz *et al.*, 1991; Lawson *et al.*, 2004).

1.1.3 PKA holoenzyme structure

To understand the R-C interaction and the allosteric regulation of PKA, the holoenzyme structure is necessary. The RIα (91-379):C heterodimeric structure reveals 4 interfaces between the R-C complex (Kim *et al.*, 2007). They are the inhibitor sequence (site 1), CNB-A (site 2), the α-C helix (site 3) and CNB-B (site 4) in the R subunit. The inhibitor sequence docks into the acitve site cleft of the C-subunit while CNB-A, specifically the hydrophobic part of the PBC-A, docks onto the hydrophobic surface of the G helix of the C-lobe of the C subunit (Kim *et al.*, 2005). Fig 1.3 shows the overall R-C holoenzyme structure (left) and the amplified interaction surfaces at site 3 and site 4. At site 3, the completely extended B/C helix in RIα covers the activation loop of the C subunit. Here, the CNB-A capping residue W260 docks into the N-terminal moiety of the activation loop. This residue undergoes a movement over 30 Å towards PBC-A upon cAMP binding. The fourth interaction site is between the CNB-B and the αH-αI loop on the C-lobe of PKAC. A conserved Arg355 residue forms multiple interactions with the C-subunit. The binding of PKAR not only occupies the active site cleft but also blocks the substrate binding surfaces at the C-lobe of the C-subunit. Furthermore, the tetrameric PKA holoenzyme structures have been revealed, e.g., $RII\beta_2:C_2$ (Zhang *et al.*, 2012), $RI\beta_2:C_2$ (Ilouz *et al.*, 2012) and $RI\alpha_2:C_2$ (Lu *et al.*, 2019), providing more information about the allosteric activation and structure-function relationship of PKA isozymes (Taylor *et al.*, 2012).

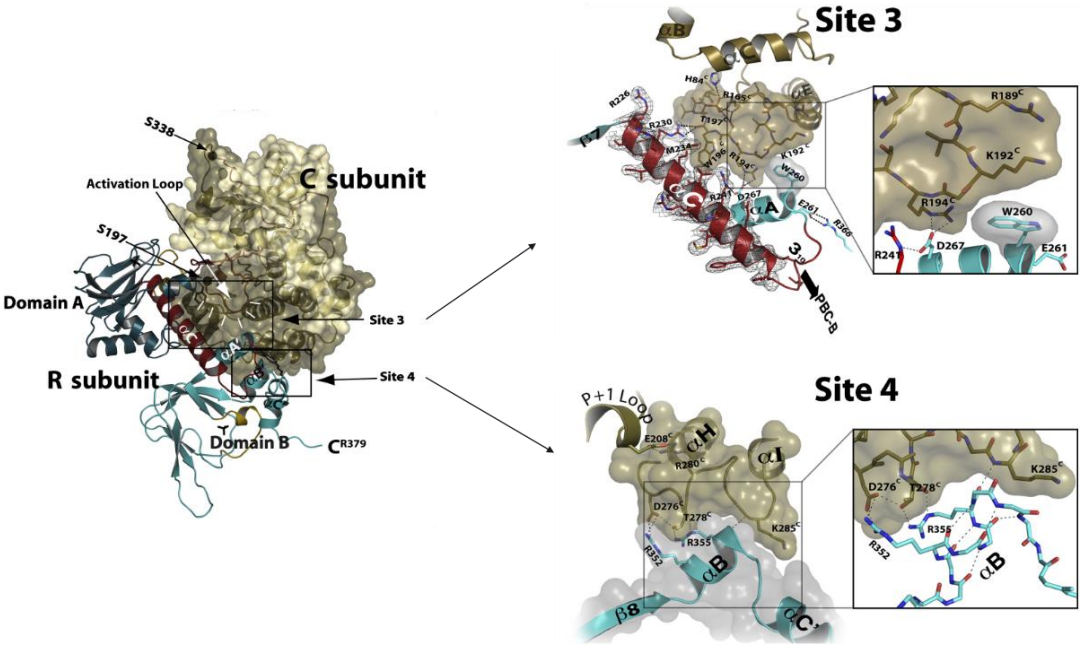

Fig 1.3 RIα$_1$:C$_1$ heterodimer structure is shown on the left. C subunit is shown as surface representation colored in amber, The R subunit is shown bound to it in cartoon representation. The R-C interface 3 is shown in upper right and interface 4 is shown in bottom right. The figure is adapted from (Kim *et al.*, 2007).

1.1.4 PKA activation mechanism

PKA activation is driven allosterically by the two contiguous CNB domains of PKAR in the presence of cAMP molecules (Kim *et al.*, 2007; Zhang *et al.*, 2015; Guo & Zhou, 2016). Fig 1.4 B shows the transition of a mammalian PKAR from holoenzyme form (H-form) to cAMP bound form (B form). In H-form, CNB-A is masked by the R/C interface so it is structurally less accessible and cAMP binds into CNB-B at first. To stabilize cAMP, the C-tail α-B and α-C helices of CNB-B are recruited and a critical π-stacking interaction is formed between the capping residue Y371 (α-C helix) and cAMP. The motion of α-B and α-C helices results in the breakage of the E261-R366 salt bridge, unleashing the coupled capping residue W260 and inducing a large conformation change of PKAR marked by the kinked α-B/C helix (red) and the accessible CNB-A. Binding of a second cAMP into CNB-A is stabilized by PBC-A and W260 that forms π-stacking interaction with cAMP. N3A motif of CNB-A then undergoes conformation change, stabilizing the final cAMP-bound form PKAR (Hao *et al.*, 2019). As a consequence, the C subunit dissociates from the R and phosphorylates a wide variety of downstream substrates. PKAR domain organization is conserved in all PKA orthologues found so far, which therefore suggests the cooperative ligand binding triggered allosteric activation mechanism is conserved in PKA family. PKG contains

the regulatory and catalytic domains within a single polypeptide, while the activation mechanism is similar to PKA. In addition to cAMP, PKA is found to be activated in a cyclic-nucleotide independent manner in yeast. *Saccharomyces cerevisiae* PKA, for example, can be activated by re-addition of missing nutrient such as nitrogen and phosphate (Hirimburegama *et al.*, 1992; Steyfkens *et al.*, 2018) as well as micro-nutrient iron and zinc (Schothorst *et al.*, 2017) in specifically starved fermenting cells.

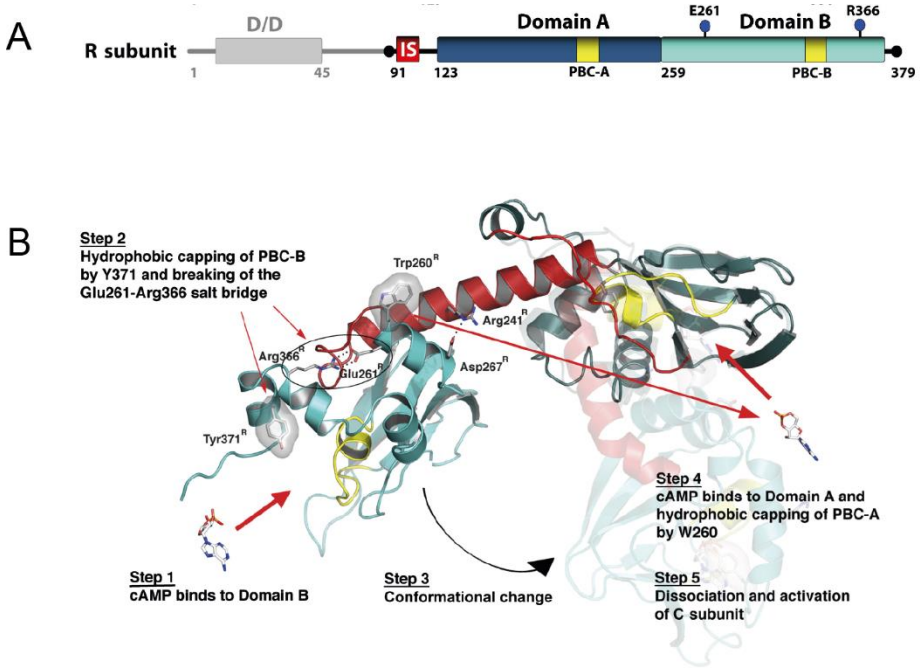

Fig 1.4 A, PKAR domain organization; B, PKAR conformation change upon activation. The figures are adapted from (Kim *et al.*, 2007).

1.1.5 Conservation of PKA in eukaryotes

PKA has been discovered in most eukaryotes, including protozoans, fungi and all animals, where the other key components of cAMP/PKA signaling coexist. However, the existence of PKA in plant cell is highly controversial, so is PKG. To date, genes with significant sequence homology to PKA or PKG have not been identified from plants (Wang *et al.*, 2003). Secondly, the typical R_2C_2 composition of a PKA holoenzyme is not conserved in some lower, unicellular eukaryotes. For example, heterodimeric PKAs comprising one regulatory subunit and one catalytic subunit were discovered in *Dictyostelium discoideum* (Mutzel *et al.*, 1987; Simon *et al.*, 1992) and *Amphidinium operculatum* (Leighfield *et al.*, 2002). Some PKAR orthologues lack the prototypical sequence of the D/D domain, these PKA holoenzymes have been confirmed to be heterodimeric, e.g., PKA in *Plasmodium falciparum* (Haste *et al.*, 2012; Bandje *et al.*, 2016) and kinetoplastids species, *Trypanosoma brucei* (Bachmaier *et al.*,

2019) and *Trypanosoma equiperdum* (Bubis *et al.*, 2018).

Among the C subunit variants from the same or different organisms, the catalytic core is highly conserved and the general 3D structure is shared by all protein kinases (Ten Eyck *et al.*, 2008; Kornev & Taylor, 2010). The N- terminal part, which is deemed as an intrinsically disordered region (Taylor *et al.*, 2013), are very variable even among different isoforms of the same organism. As for PKAR, the general domain organization, the substrate sequence and the tertiary structure of the CNB domain are highly conserved features. While the capping residues and the salt bridge residues that are important for PKA activation are conserved, several key amino acids on the PBC motif are different (PhD thesis Githure, 2014). These variances were then identified to be critical for ligand switch (Bachmaier *et al.*, 2019). The N-terminal part of PKAR can be very different. For example, kinetoplastid PKARs are characterized with a large N-terminal domain with unknown function while mammalian PKARs usually contain a much smaller N-terminal domain.

1.2 PKA in kinetoplastids

Kinetoplastids are flagellated protozoa, many members of which are parasitic. Three notorious pathogens in the group are *Trypanosoma brucei*, *Trypanosoma cruzi*, and *Leishmania* species causing African trypanosomiasis (HAT), Chagas disease and Leishmaniasis, respectively. They have caused serious endemics or epidemics in the last century and are threatening millions of people especially for people in poor, less developed regions. In kinetoplastid genomes, there are usually one PKAR gene and 2 to 3 copies of PKAC genes (Bachmaier & Boshart, 2013). When the first kinetoplastid PKAR was identified and characterized from *T. brucei*, it was initially thought that PKA was activated by cGMP rather than cAMP according to protein kinase assay (Shalaby *et al.*, 2001). However, the K_d of cGMP to TbPKA is extremely high (> 10 μM) and not physiologically achievable in living cells, compared to the low nanomolar K_d of cAMP of mammalian PKA. Similarly, *Trypanosome equiperdum* PKAR was found not binding cAMP (Bubis *et al.*, 2018). It is not until recently that an inosine derivative, 7-cyano-7-deaza-inosine, and some tubercidin analogs were found to activate TbPKA with high potency and high binding affinity to TbPKAR, suggesting nucleoside-related metabolites as endogenous ligands for TbPKA and other kinetoplastid PKAs (PhD thesis Githure, 2014; Bachmaier *et al.*, 2019)

1.2.1 Kinetoplastid PKAR and PKAC

PKAR isoforms have been cloned and characterized from the three pathogenic parasites, *T. brucei* (Shalaby *et al.*, 2001; Bachmaier *et al.*, 2019), *T. cruzi* (Huang *et al.*, 2006) and *L. donovani* (Bhattacharya *et al.*, 2012) in in last decades. Amino acid sequence alignment of kinetoplastid and mammalian PKARs reveals some common but also kinetoplastid-specific features. The common features include the consensus substrate sequence (RRXT) and two tandem cAMP binding domains, albeit several highly conserved residues in the PBC motif of mammalian PKARs are substituted. On the other hand, all identified kinetoplastid PKARs contain an atypical large N-terminal domain containing some leucine-rich repeats (LRR) while showing no homology to other proteins. Moreover, the D/D domain is missed from kinetoplastid PKARs. The absence of D/D domain is in agreement with the heterodimeric (R_1C_1) composition of trypanosomal PKAs (Bubis *et al.*, 2018; Bachmaier *et al.*, 2019). Most importantly, nucleoside analogs instead of cAMP were discovered to activate *T. brucei* PKA (Bachmaier *et al.*, 2019). This explains the long-standing mystery in previous studies (Shalaby *et al.*, 2001; Bubis *et al.*, 2018). The co-crystal structure of TcPKAR bound to 7-cyano-7-deaza-inosine unraveled the mechanism of nucleoside analog binding (Bachmaier *et al.*, 2019). The CNB domain and PBC motif are therefore renamed to nucleoside binding domain (NBD) and ribose binding cassette (RBC) respectively for kinetoplastid PKAR. As shown in Fig 1.5, the ligand interaction network in *B. taurus* CNB-B and *T. brucei* NBD-B are compared. NBD-B interacts with the ribose group through the RBC motif and the conserved capping residue (Y482). The conserved arginine residue (R333) responsible for neutralizing the negative phosphate of cAMP in mammalian PKAR is substituted by a neutral amino acid. Kinetoplastid PKARs are predominantly localized in the flagellum of cells. In *T. brucei*, PKAR was found to be differentially expressed in the life cycle stages. It is much more abundant in bloodstream form (BSF) than procyclic forms (PCF) (Shalaby *et al.*, 2001).

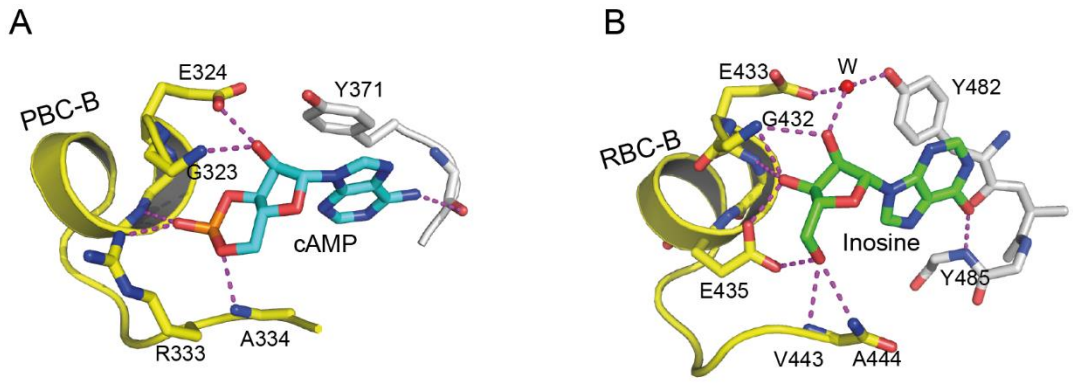

Fig 1.5 Comparison of the B-site of *B. taurus* PKAR (PDB:1rgs) (A) and *T. brucei* PKAR (PDB:6flo) (B). PBC-B and RBC-B are represented as cartoon in yellow. The ligands and the

interacting residues are represented as sticks. Hydorgen bonds are represented as purple dashed line. The water molecule is represented as sphere in red.

In *T. brucei*, three PKAC isoforms that are differentially expressed in the lifecycle stages were identified, termed PKAC1, PKAC2 and PKAC3 (PhD thesis Kramer, 2004). PKAC1 is exclusively expressed in bloodstream form (BSF) cells, while PKAC2 predominantly expressed in procyclic form (PCF) cells and barely expressed in BSF. In contrast, PKAC3 is expressed throughout the life stages of *T. brucei*. PKAC1 and PKAC2 are highly homologous, sharing 95% identity in general and a completely identical kinase core. The different amino acids reside predominantly in the N- and C-terminal tails. PKAC3, however, only shares 55% homology with PKAC1 and PKAC2. Similarly, three orthologous PKAC isoforms were identified in *T. cruzi* (Huang *et al.*, 2002) and *Leishmania major* (Siman-Tov *et al.*, 1996; Siman-Tov *et al.*, 2002).

1.2.2 Unconventional PKA signaling in kinetoplastids

cAMP/PKA signaling in kinetoplastids is distinct from the well-studied canonical one (chapter 1.1.5), since kinetoplastid PKA is cAMP-independent and no GPCR genes were found in kinetoplastid genomes (Tagoe *et al.*, 2015). Kinetoplastid adenylyl cyclases represent a different structure containing a single trans-membrane domain, an unusually large variable extracellular N-terminal domain and a conserved intracellular C-terminal domain (Pays *et al.*, 1989). In contrast, mammalian ACs are characterized by a variable intracellular N-terminal domain, two trans-membrane bundles consisting of six transmembrane helices each and two large intracellular catalytic domains (Cooper, 2005; Dessauer, 2009). The large N-terminal domain of trypanosomal ACs was deemed to function as receptors taking over GPCRs, similar to mammalian receptor-type guanylyl cyclases (Garbers *et al.*, 2006). The loss of PKA as the main cAMP effector is compensated by a group of cAMP Response Proteins (CARPs) (Gould *et al.*, 2013). In addition to nucleosides, some environmental factors have been discovered to activate PKA in *T. brucei*. Cold shock, for instance, can increase cellular PKA activity (PhD thesis Kramer, 2004; PhD thesis Bachmaier, 2015). Dipyridamole, a PDE inhibitor, was surprisingly found to activate PKA indirectly (Bachmaier *et al.*, 2019). These observations suggest unknown upstream regulatory mechanisms of kinetoplastid PKA.

1.2.3 The role of PKA in *T. brucei*

In the last years, a number of reverse genetics studies were carried out to elucidate the role of PKA in *T. brucei* in the lab. In BSF, PKAR and the three catalytic subunits

were depleted by knockout or RNAi, respectively (PhD thesis Kramer, 2004). The RNAi designed to target PKAC1 was found to target PKAC2 as well due to their high homology, which was therefore denoted as PKAC1/2 RNAi. The cells suffered severe growth and cytokinesis phenotype and died 2 days post induction of PKAC1/2 RNAi. PKAC1/2 protein was decreased by 80-90% after 4-8 hours as revealed by immunoblotting. Knocking out both PKAC2 alleles was achieved and a mild growth and cytokinesis phenotype was observed, indicating PKAC2 is not essential for BSFs. Cell lines with one PKAC1 allele knocked out were easily obtained, but further attempts to delete the second allele or replace it with PKAC2 were not achieved. Interestingly, a PKAC1/2 RNAi utilizing a hairpin siRNA based on pHD615 vector resulted in cells with very slight phenotype while the PKAC1/2 proteins decreased also by 80-90% (PhD thesis Bachmaier, 2015). RNAi of PKAC3 resulted in a more significant growth and cytokinesis phenotype than PKAC2 knockout. In summary, PKAC1 is important for the viability of BSFs while whether it is an essential gene and whether it can be replaced by PKAC2 is not clear. As mentioned, PKA can be activated by cold shock. This might be relevant to cell differentiation since trypanosomes experience a cold shock when they enter tsetse fly midgut and it was proven to promote the differentiation of *in vitro* cultured pleomorphic BSFs (Engstler & Boshart, 2004). This phenomenon persisted in the PKAC2 or PKAC3 knockout cell lines but was absent in all PKAC1/2 RNAi cell lines. Depletion of PKAR by knockout or RNAi resulted in severe cell growth and cytokinesis phenotype. The absence of R subunit actually decreased intracellular PKAC concentration, this might be because the active C subunit is unstable or susceptible to degradation. In addition, reduced PKAR resulted in impaired cell motility, which is most prominent in cells with outgrowing daughter flagellum (PhD thesis Krumbholz, 2006), and abnormal basal body movement which is marked by the extended distance between the 2 kinetoplasts of 2K2N cells (PhD thesis Kramer, 2004). Besides of cell growth and proliferation, a gene ontology (GO) enrichment analysis of PKA induced phosphoproteome predicts that PKA might be related to gene posttranscriptional regulation, dynamics of cytoskeletal and organellar structures and signaling (Bachmaier *et al.*, 2019).

1.3 *Trypanosoma brucei* as a model

1.3.1 *Trypanosoma brucei* epidemiology

The unicellular flagellated eukaryotic parasite *Trypanosoma brucei* (*T. brucei*) belongs to the order *Kinetoplastida*. Subspecies of *Trypanosoma brucei* are the causative

agents of Human African Trypanosomiasis (HAT), also known as sleeping sickness, in human (*T. brucei gambiense* and *T. brucei rhodesiense*) and Nagana in cattle (*T. brucei brucei*) (Brun *et al.*, 2010). They distribute in the sub-Saharan Africa, where their insect host, tsetse fly (*Glossina spp.*), inhabits. The WHO intended to eliminate HAT before 2020, which has not been achieved yet but the situation has been improved significantly according to a recent investigation (Franco *et al.*, 2020). *T. brucei brucei* is not pathogenic to human due to a trypanosome lytic factor possessed by humans and primates (Vanhollebeke *et al.*, 2008), it is therefore a perfect model for safe research. *T. brucei gambiense and T. brucei rhodesiense* are however resistant to the lytic factor. *T. cruzi* (Chagas disease) and *Leishmania. spp* (leishmaniasis) are the other two kinetoplastid pathogens which are more challenging for eradication. As the population motility, urbanization and emigration, increased cases of the two diseases have been detected in many countries including developed countries (WHO report, https://www.who.int/health-topics/chagas-disease). Studies based on *T. brucei brucei* can increase our understanding of kinetoplastids and help develop targeted therapies for the pathogens.

1.3.2 *Trypanosoma brucei* phylogeny and morphology

T. brucei and other members in family *Trypanosomastidae* of order *Kinetoplastida* are characterized by a single flagellum and the name-giving kinetoplast that contains condensed mitochondrial DNA within the single extended mitochondrion. As shown in Fig 1.6, the kinetoplast is located close to the basal body of the flagellum. The single flagellum attached to the membrane of cell body is originated from

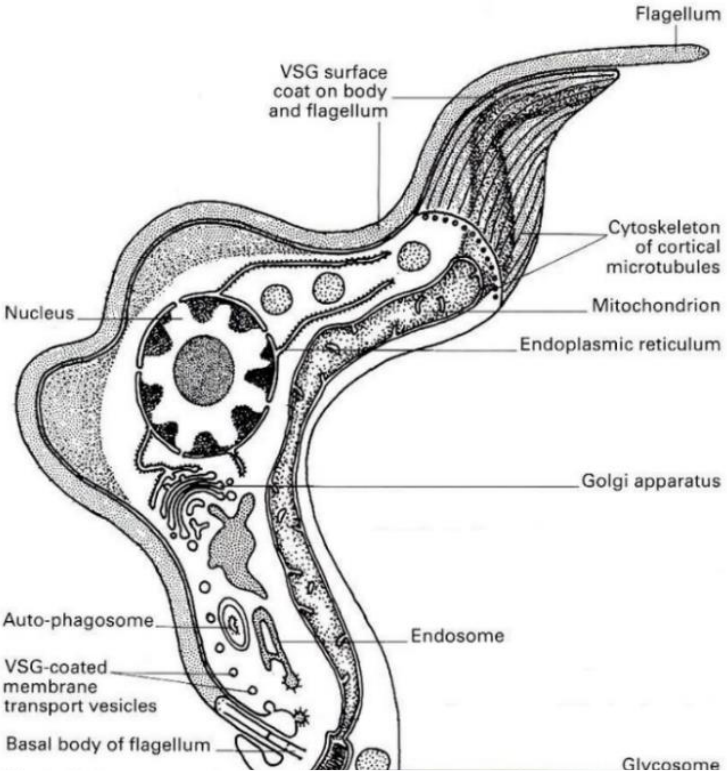

Fig 1.6 Schmatic representation of a bloodstream form *T. brucei* subcellualr structure. The figure is adapted from (Vickerman K, 1993).

the flagellar pocket, which is the only site of endo- and exocytosis (Field & Carrington, 2009). It extends towards the anterior end and only the tip is free (Matthews, 2005).

1.3.3 Life cycle and cell division

To transmit between mammalian and insect hosts and survive in the different host environments, *T. brucei* has developed a complex life cycle (Fig 1.7). Cells undergo major changes in morphology and metabolism during differentiations. Metacyclic trypanosomes can be transferred to mammals from the infected tsetse fly via injection of its saliva into the dermal tissue during a bloodmeal. Thereby, the parasite transforms into long slender form (LS) and proliferates rapidly in the nutrious blood by binary fission. Patients usually suffer from chronic and intermittent fever, headache and pruritus at this stage. At late stage of trypanosomiasis, LS trypanosomes penetrate the blood-brain barrier and invade the central nervous, resulting in more severe symptoms, such as chronic sleep disorders, neuro-psychiatric disorders and paralysis (Grab & Kennedy, 2008). A portion of LS trypanosomes transit to the cell-cycle arrrested short stump form (SS) when parasite density reaches to a certain level. The mechanism is known as quorum sensing. Stumpy Induction Factor (SIF), which is secreted by the parasite itself, has been found to trigger the differentiation as it accumulates (Vassella *et al.*, 1997; Seed & Wenck, 2003; Dean *et al.*, 2009). SS trypanosomes are charaterised by compact shape and shorter flagellum, they are pre-adapted for living in the tsetse fly metabolically by turning on part of respiratory chain (Flynn & Bowman, 1973; Priest & Hajduk, 1994). Transforming to non-dividing SS form decreases the parasitemia of the host, restricting the parasite virulence and preventing an early death of the host (Rico *et al.*, 2013). Moreover, LS trypanosomes can evade immune clearance by alteration of the cell surface coat (VSG). It is therefore a paradigm for antigenic variation (Pays *et al.*, 1989; Chaves *et al.*, 1999; Barry & McCulloch, 2001; Pinger *et al.*, 2018). Trypanosomes are transferred to tsetse fly during the bloodmeal from infected animals. They firstly accommodate in midgut lumens, where the quiescent SS form cells diffentiate to the proliferating procyclic form (PCF) which uses proline as the main energy source via the fully activated mitochondrion (Haston, 1972; Priest & Hajduk, 1994; van Weelden *et al.*, 2003; Riviere *et al.*, 2004). The changes of cell morphology include cell body elongation and mitochondrion enlargement. Besides, the VSG coat is degraded fastly and replaced with a new coat composed of procyclin proteins (Gruszynski *et al.*, 2006). After about 6 days, some of the procyclic form cells penetrate the peritrophic matrix to the proventriculus (Gibson & Bailey, 2003; Rose *et al.*, 2020). Thereby, the trypanosomes transform to the cell cylcle arrested mesocyclic

form (MCF) and then migrate into the salivary gland, where they further differentiate to the dividing epimastogotes, whose flagellum is attached to the microvilli of the epithelial cells. Epimastigotes can differentiate to the non-proliferating metacyclics which expresses VSGs again and is prepared to live in mammals. Metacyclics are transferred to mammalian host by injection of saliva during a bloodmeal and the life cycle starts again (Vickerman, 1985).

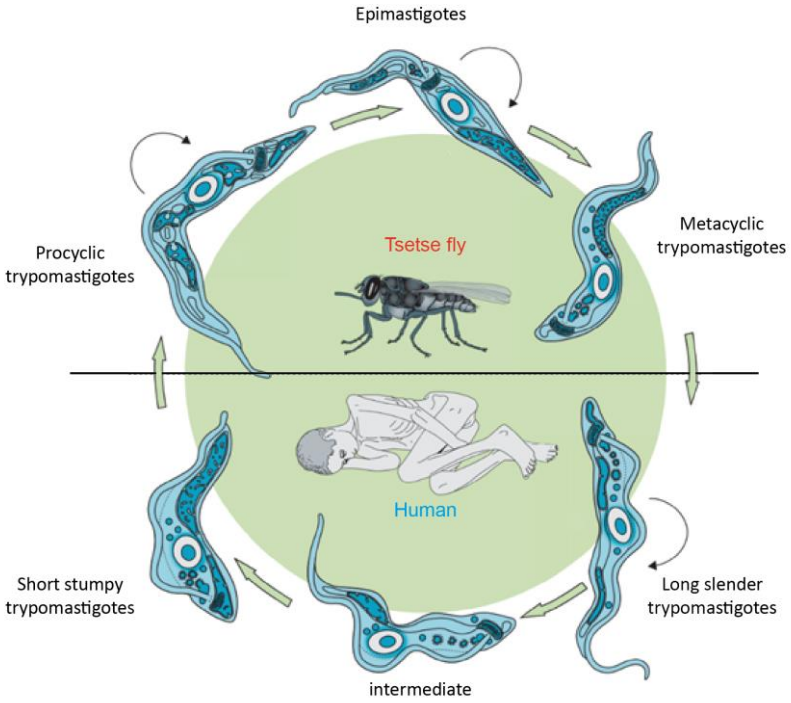

Fig 1.7 Schematic representation of *T. brucei* life cycle. The picture was adapted from (Brun *et al.*, 2010).

The cell cycle of *T. brucei* shows features of typical mitosis that consists of G0/G1, S, G2 and M phases but also some unique features. As a number of single-copy organelles and structures e.g., nucleus, kinetoplast, mitochondrion, flagellum, Golgi and basal body have to be correctly replicated and segregated to daughter cells, the cell cycle is fine-tuned temporally and spatially (McKean, 2003; Hammarton, 2007; Li, 2012; Zhou *et al.*, 2014). The earliest detectable event of trypanosome cell division is the formation of a pro-basal body (Vaughan & Gull, 2015), following by the outgrowth of the daughter flagellum and duplication of the Golgi apparatus. In the meantime, the kinetoplast is replicated prior to the nucleus duplication. Early in G2 phase, the motion of basal bodies towards cell posterior drives the separation of the duplicated kinetoplast as they are physically connected by the tripartite attachment complex (TAC) (Robinson & Gull, 1991; Ogbadoyi *et al.*, 2003). *T. brucei* undergoes a closed mitosis

that the nuclear envelope remains intact during division, like many other lower eukaryotes. Cytokinesis, as the last step of the cell division, is marked by the cleavage furrow formation along the longitudinal axis of the dividing cell. Many factors have been identified to impact trypanosome cytokinesis, such as aurora kinase (Tu *et al.*, 2006) and PKA (PhD thesis Kramer, 2004)

A convenient method to analyze the cell cycle of a trypanosome is through its K/N configuration, as kinetoplast (K) is duplicated before nucleus. During a cell cycle, a trypanosome cell progresses from 1K1N to 2K1N as kinetoplast duplicates in early S phase. As the replication of nucleus, the K/N configuration becomes 2K2N, which persists until the completion of cytokinesis. Disruption of the cell cycle, for example, by depletion of basal body duplication regulators (Kobayashi & Dynlacht, 2011) or decrease PKA activity (PhD thesis Kramer, 2004), could result in abnormal K/N configurated or cytokinesis deficient cells. Remarkably, the position of kinetoplast and the distance between it and nucleus are variable in different stages of the insect forms, this feature has been used for distinguishing early procyclics, epimastigotes and metacyclics (Rotureau & Van Den Abbeele, 2013).

1.3.4 *Trypanosome brucei* as a model for laboratory research

As a human non-infective *T. brucei* subspecies and the close evolutionary relationship with the pathogenic subspecies*, T. brucei brucei* has been a perfect and safe model for lab research. The genome sequence of the *T. brucei* strain TREU927/4 GUTat10.1, along with the genome sequences of *T. cruzi* and *L. major*, were released in 2005 (Berriman *et al.*, 2005; El-Sayed *et al.*, 2005; Ivens *et al.*, 2005). The genome information including sequences, gene annotations can be conveniently obtained from TriTryp database (https://tritrypdb.org/tritrypdb/app). The establishment of the genome database has greatly promoted the research of trypanosomes. Besides, the development of genetics tools, in particular the availability of RNAi and CRISPR technique in *T. brucei*, enables functional characterization and decoding of complex pathways.

1.3.4.1 *in vitro* axenic cultivation and differentiation of trypanosomes

Trypanosomes freshly isolated from the blood of animals contain both the proliferating LS form and the quiescent SS form cells, the isolates are hence called pleomorphic strains. Axenic culturing of pleomorphic cells *in vitro* had been a major challenge in the past until the development of extracellular matrix-dependent culturing method that uses agarose or other additives such as methylcellulose to increase the viscosity of

the culture medium mimicking the blood environment preferred by bloodstream form trypanosomes (Vassella & Boshart, 1996) (Bachmaier *et al.*, 2020). Cultivation of the non-adapted pleomorphic strains is critical for the studies of stage differentiation, fly transmission and metabolic regulation (Schuster *et al.*, 2017; Alfituri *et al.*, 2020). After high numbers of passages, some subclones of the pleomorphic strain were adapted to liquid medium while showing comparable growth rate as in the matrix medium while maintain the pleomorphic features, namely differentiation ability. These strains were termed matrix-independent pleomorphic strains (Bachmaier *et al.*, 2020). Serial passages of bloodstream form cells between laboratory rodents resulted in the so-called monomorphic strains that can be cultured to relatively high density without differentiation to the SS form (Ashcroft, 1960).

1.3.4.2 Homologous recombination for gene manipulation in trypanosomes

Homologous recombination is the key mechanism in introducing transgenes to the trypanosome genome. Stable transformants result from the integration of the DNA of interest along with a selection marker, usually a drug resistance gene, into the target locus. Two types of targeting plasmid vectors that use different integration mechanisms are applied in *T. brucei*. The first one is the ends-out recombination vectors. As shown in Fig 1.8 A, a cloned sequence that contains the DNA of interest, selection marker and the homologous regions on both ends can be produced by digestion of the targeting vector or PCR. After transfecting into the cells, the sequence can be inserted into the chromosomal target. The second type is called ends-in plasmid, see Fig 1.8 B, which uses a linearized plasmid resulting from a restriction digestion for transfection. The integration of the transfected DNA into the homologous chromosomal sequence is via a gene conversion mechanism and a followed crossing over event.

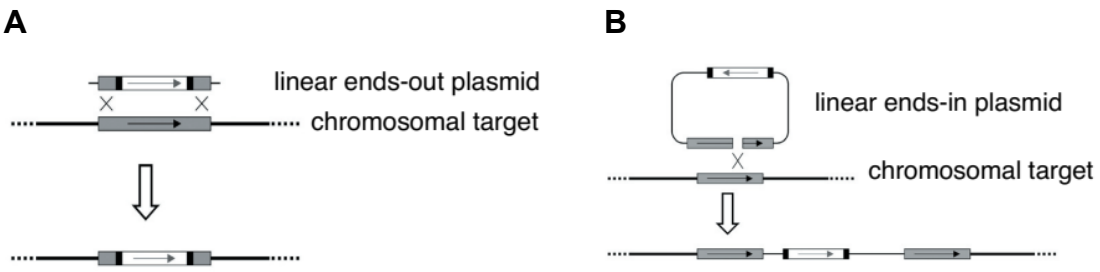

Fig 1.8 Two mechanism of homologous recombination. A, ends-out recombination. B, ends-in recombination. (Modified from **McCulloch et al., 2004**)

1.3.4.3 Reverse and forward genetics approaches

Reverse genetics is commonly used to understand the function of a gene by analyzing

the phenotypic effects caused by knockout or RNA interference (RNAi). In *T. brucei*, ablation of a target gene by knockout is usually accomplished through homologous recombination conveniently as introduced above, but it might be complicated in some cases due to the diploid genome of *T. brucei*. Currently, there are only 6 recommended drug resistance markers for *T. brucei* selection. They can be in some cases in shortage, especially for strains that harbor multiple transgenes, such as Tet repressor or T7 polymerase. Moreover, gene knockout is difficult for multicopy genes and those gene families consisting of highly homologous gene isoforms arranged in tandem (Seebeck *et al.*, 1983; Bringaud & Baltz, 1993; Sanchez *et al.*, 2002), if no valid multigene manipulation tool like CRISPR are available. RNA interference (RNAi) is an alternative approach devoid of the restrictions of knockout. In *T. brucei*, RNAi can be conducted by transfecting with *in vitro* synthesized dsRNA or a plasmid vector expressing stem-loop RNA (Ngo *et al.*, 1998). However, RNAi is unavailable for *T. cruzi* and *Leishmania spp*., due to the lack of key components in the RNAi pathway such as TbAGO1 (Ullu *et al.*, 2002). Another powerful tool is Cas9-based gene editing, which has been progressed rapidly to trypanosomatids in the last few years, providing alternative gene manipulation tool for *T. cruzi* (Peng *et al.*, 2014) and *Leishmania spp* (Zhang & Matlashewski, 2015). Various CRISPR/Cas9 methods have also developed in *T. brucei* recently (Rico *et al.*, 2018; Shaw *et al.*, 2020). Forward genetics approach determines genes responsible for an identified phenotype. As the development of the RNAi libraries in *T. brucei* (Morris *et al.*, 2002) and later a more powerful version (Alsford *et al.*, 2011), remarkable progresses have been made in gene function studies (Alsford & Horn, 2008; Wurst *et al.*, 2009; Verner *et al.*, 2010; Baker *et al.*, 2011; Genovesio *et al.*, 2011; Luis García-Fuentes, 2011; Alsford *et al.*, 2012; Gould *et al.*, 2013; Moreau & Schaeffer, 2013; Glover *et al.*, 2015; Moss *et al.*, 2015; Fernandez-Cortes *et al.*, 2017; Stortz *et al.*, 2017). Other forward genetics approaches can also be used, such as transposable element-based methods (Shi *et al.*, 2002; Leal *et al.*, 2004).

1.4 PKA as a drug target

The essential role of PKA in *T. brucei* proliferation makes it a promising drug target, which could be a kinetoplastids-specific drug target considering the conservation between kinetoplastid PKARs and their diversities from the mammalian counterparts. Rp-cAMPS is an inhibitor for mammalian PKAs, which binds both the CNB-A and CNB-B while not inducing R subunit conformation change and thereby blocking activation (Dostmann & Taylor, 1991; Wu *et al.*, 2004b). Finding inhibitors specifically targeting

the R subunit of *T. brucei* and inhibiting the holoenzyme dissociation, constraining not only PKAC1 but also PKAC2 and PKAC3 in inactive state appears possible. The effect is supposed to be stronger than the PKAC1/2 RNAi which kills most of BSF trypanosomes within 2 days *in vitro* (PhD thesis Bachmaier, 2015). This strategy was investigated in chapter 3.4. In fact, many diseases in human are implicated with aberrant PKA signaling, while the widespread tissue distribution and multiple physiological functions of PKA makes it a challenging pharmacological target. Poor selectivity means low drug efficacy and increased undesirable side effect. Alternatively, other components of cAMP/PKA signaling, such as GPCR and PDE, have been targeted to selectively modulate cAMP/PKA signaling. Selective β2-adrenergic receptor agonist salmeterol and PDE3 inhibitor milrinone, for example, have been used to treat asthma or chronic obstructive pulmonary disease (COPD) (Ellison & Gandhi, 2005; McKeage & Keam, 2009) and improve vasodilation and cardiac contraction after heart failure (Jaski *et al.*, 1985), respectively. In addition, there are some strategies focusing on inhibiting the catalytic subunit and disrupting PKA targeting by targeting AKAP proteins, while no drugs to our knowledge are available commercially (Taylor *et al.*, 2008; Kleppe *et al.*, 2011).

The current drugs for treating sleeping sickness include suramin, pentamidine, melarsoprol, nifurtimox, eflornithine and the recently approved fexinidazole (Deeks, 2019; Lindner *et al.*, 2020). Nifurtimox-Eflornithine combination therapy (NECT) shows high efficacy in curing patients suffering second stage *gambiense* HAT with considerable adverse effect, and has been a common therapeutic recommendation for second stage *gambiense* HAT (Yun *et al.*, 2010). Oral monotherapy fexinidazole shows a comparable efficacy in treating second stage *gambiense* HAT and the treatment is much easier than NECT. Nevertheless, drug resistance and the second stage rhodesiense HAT are still problematic (Koning, 2020). For Chagas disease, nifurtimox and benznidazole are the only commercially available options since the 1970s (Sales Junior *et al.*, 2017; Ribeiro *et al.*, 2020). However, their effect for the chronic phase patients is questionable (Francisco *et al.*, 2020). Initial efficacy tests of fexinidazole in treating chronic Chagas disease seems encouraging (Francisco *et al.*, 2016), while a comprehensive assessment is ongoing (DNDi, https://dndi.org/research-development/portfolio/fexinidazole-chagas/). Whereas many drugs and vaccines are available for treating leishmaniasis, studies showed they cannot eradicate the parasite completely and are limited due to high cost, toxicity and drug resistance, especially in long-term treatment (Sundar, 2001; Croft & Coombs, 2003; Freitas-Junior *et al.*, 2012; Duthie *et al.*, 2016). In the past years, as the accumulation of fundamental and

mechanism studies, many new drug targets have been proposed (Gadelha *et al.*, 1989; Andriani *et al.*, 2013; Villalta & Rachakonda, 2019; Saye *et al.*, 2020), while developing new drug is always a marathon. Therefore, there is large unmet need for new efficient trypanocidal and anti-leishmaniasis drugs. The kinetoplastids-specific structural and activation features of PKA are conserved in *T. cruzi* and *Leishmania spp*, thus inhibitor development based on *T. brucei* PKA could be used to obtain candidates for a multi-parasite drug, the only commercially attractive solution for neglected tropical diseases of the poor.

1.5 Aims of the thesis

Although PKA as a prototype kinase has drawn abundant attention and has been well studied in most eukaryotes, *T. brucei* and other kinetoplastid PKAs are poorly understood. The large N-terminal domain and the extended C-terminal α-D helix of TbPKAR are the most prominent differences from its mammalian counterparts, while their functions are unclear. Rapid temperature downshift (cold shock) and dipyridamole are identified as indirect TbPKA activation triggers, but the activation mechanisms are still unresolved.

The major goal of the thesis is therefore to understand the activation mechanism of TbPKA. To achieve it, in the first step I aim to establish a sensitive and convenient *in vivo* assay that detects PKA activation and can be used for compound screening (see chapter 3.1). Previous pull down data suggests the N-terminal domain is important for R-C holoenzyme formation (PhD thesis Krumbholz, 2006). In chapter 3.2.1, I aim to study it *in vivo* and try to find the interaction sites with the C subunit. The TcPKAR crystal structure revealed that the α-D helix strongly traps ligands within the B-site. The following aspects are planned to be investigated: 1) Is the α-D helix involved in PKA activation? 2) If yes, how does it impact PKA activation? 3) Is its role conserved in other kinetoplastid PKARs? 4) Is it possible to develop a specific TbPKA inhibitor targeting the unusual B-site? (Chapter 3.2.2 and chapter 3.4).

TbPKAC1 and TbPKAC2 are highly homologous but differentially expressed in the life cycle of *T. brucei*. Although several results from RNAi and knockout experiments suggest PKAC1 is essential, no direct evidence has been obtained so far. Therefore, another goal of the thesis is to clarify whether PKAC1 is essential and whether it can be replaced by PKAC2 for BSFs. I aim to delete both PKAC1 alleles in the presence of an expression-controllable rescue C subunit (see chapter 3.3.1). Moreover, the

activation of different PKA holoenzymes will be compared in BSF and PCF (chapter 3.3.2). The last goal of the thesis is to establish a screening assay for identification of the regulators involved in cold shock and dipyridamole induced PKA as well as candidate compounds for specific activation or inhibition of kinetoplastid PKA activation (see chapter 3.5).

2 Materials and methods

2.1 Materials

2.1.1 *Trypanosoma brucei* cell lines

Here, only the cell lines used for experiments in the thesis were listed. Some intermediate cell lines can be found in the detailed inventory. The cell line ID (Tb-QWxxx) refers to the inventory.

2.1.1.1 *Trypanosoma brucei* parental cell lines

	Lister 427 MiTat1.2 (NY subclone)
Made by	(Cross & Manning, 1973; Cross, 1975)
Description	This cell line is a wild type monomorphic BSF cell line.

	AnTat1.1 E 1313
Genotype	*TET^R TET^R BLE*
Made by	S. Bachmaier (PhD thesis Bachmaier, 2015)
Constructs	pHD1313 (BLE)
Selection m	Phleomycin (0.2 µg/ml)
Description	This pleomorphic cell line was made to express Tet repressor proteins (TetR) for inducibly expressing the gene of interest.

	MiTat1.2 1313 VASP
Genotype	*TET^R TET^R BLE RDNA::VASP HYG*
Clone number	Clone 1(PhD thesis Bachmaier, 2015)
Made by	S. Bachmaier (PhD thesis Bachmaier, 2015)
Constructs	pHD1313 (BLE), pTSArib (HYG)VASP
Selection	Phleomycin (0.2 µg/ml), Hygromycin (4 µg/ml)
Description	The cell line was made for performing VASP assay.

	AnTat1.1 90-13
Genotype	*T7POL NEO TETR HYG*
Made by	(Engstler & Boshart, 2004)
Constructs	plew13, plew90
Selection	Neomycin (2 µg/ml), Hygromycin (4 µg/ml)
Description	This cell line expresses T7 polymerase and Tet repressor proteins

2.1.1.2 NanoBiT cell lines

Tb-QW007	**MiTat1.2 SmBiT-PKAC1**
Genotype	*SmBiT::PKAC1 NEO*
Clone number	Clone 1, 2 and 3
Made by	Q. Wu
Constructs	pPOTv4(NEO)SmBiT_linker
Selection	Neomycin (2 µg/mL)
Description	*SmBiT-linker* coding sequence 5' flanking with a *NEO* expression cassette was in situ tagged to the 5' of one of the endogenous *PKAC1* alleles in the parental cell line MiTat1.2 by homologous recombination. This cell line constitutively expresses SmBiT-PKAC1 and was used for generation of TB-QW012 and TB-QW013.

Tb-QW008	MiTat1.2 LgBiT-PKAR
Genotype	*LgBiT::PKAR BSD*
Clone number	Clone 1, 2, 3 and 4
Made by	Q. Wu
Constructs	pPOTv4(BSD)LgBiT_linker
Selection	Blasticidin (2 µg/ml)
Description	*LgBiT-linker* coding sequence 5' flanking with a *BSD* expression cassette was in situ tagged to the 5' of one of the endogenous *PKAR* alleles in the parental cell line MiTat1.2 by homologous recombination. LgBiT-PKAR is constitutively expressed in this cell line.

Tb-QW010	MiTat1.2 PKAR-LgBiT
Genotype	*PKAR::LgBiT BSD*
Clone number	Clone 1, 2, 3 and 4
Made by	Q. Wu
Constructs	pPOTv4(BSD)-linker_LgBiT
Selection markers	Blasticidin (2 µg/ml)
Description	*Linker-LgBiT* coding sequence 3' flanking with *a BSD* expression cassette was in situ tagged to the 3' of one of the endogenous *PKAR* alleles in the parental cell line MiTat1.2 by homologous recombination. PKAR-LgBiT is constitutively expressed in this cell line.

Tb-QW012	MiTat1.2 SmBiT-PKAC1/LgBiT-PKAR
Genotype	*SmBiT::PKAC1 NEO LgBiT::PKAR BSD*
Clone number	Clone 1, 2 and 3
Made by	Q. Wu
Constructs	pPOTv4-SmBiT_linker Neo), pPOTv4(BSD)LgBiT_linker
Selection	Neomycin (2 µg/ml), Blasticidin (2 µg/ml)
Description	One of the NanoBiT cell lines. pPOTv4(BSD)LgBiT_linker was transfected in Tb-QW007. The cell line expresses SmBiT-PKAC1 and LgBiT-PKAR constitutively.

Tb-QW013	MiTat1.2 SmBiT-PKAC1/PKAR-LgBiT
Genotype	*SmBiT::PKAC1 NEO PKAR::LgBiT BSD*
Clone number	Clone 1, 2 and 3
Made by	Q. Wu
Constructs	pPOTv4-SmBiT_linker Neo, pPOTv4-linker_LgBiT BSD
Selection	Neomycin (2 µg/mL), Blasticidin (2 µg/ml)
Description	One of the NanoBiT cell lines. pPOTv4(BSD)linker-LgBiT was transfected in Tb-QW007. The cell line expresses SmBiT-PKAC1 and PKAR-LgBiT constitutively.

Tb-QW016	MiTat1.2 SmBiT-PKAR LgBiT-PKAR
Genotype	*SmBiT::PKAR NEO PKAR::LgBiT BSD*
Clone number	Clone 1, 2 and 3
Made by	Q. Wu
Constructs	pPOTv4(NEO)SmBiT_linker, pPOTv4-linker_LgBiT BSD
Selection	Neomycin (2 µg/mL), Blasticidin (2 µg/ml)
Description	The cell line was used as control examining the background luminescence produced by spontaneous interaction of PKAR proteins in the compacted flagellum

2.1.1.3 BRET cell lines

Tb-QW022	MiTat1.2 HA-Nluc-PKAC1
Genotype	*HA-Nluc::PKAC1 PAC*
Clone number	Clone 1
Made by	Q. Wu
Constructs	pPOTv4(PAC)HA_Nluc_linker
Selection markers	Puromycin (0.1 µg/ml)
Description	A fragment including a *PAC* expression cassette and HA-Nluc coding sequence was inserted into the 5' of one of the endogenous *PKAC1* alleles by homologous recombination. This cell line constitutively expresses HA-Nluc-PKAC1 and was

	used for generation of TB-QW025 and TB-QW028.

Tb-QW025	MiTat1.2 HA-Nluc-PKAC1 Ty-mCherry-PKAR
Genotype	*HA-Nluc::PKAC1 PAC Ty-mCherry::PKAR NEO*
Clone number	Clone 1, 2 and 3
Made by	Q. Wu
Constructs	pPOTv4(PAC)HA_Nluc_linker, pPOTv4(NEO)Ty_mCherry_linker
Selection markers	Puromycin (0.1 µg/ml), Neomycin (2 µg/ml)
Description	A fragment including a *NEO* expression cassette and Ty-mCherry coding sequence was inserted into the 5' end of one endogenous *PKAR* allele in cell line Tb-QW022.

Tb-QW028	MiTat1.2 HA-Nluc-PKAC1 Ty-YFP-PKAR
Genotype	*HA-Nluc::PKAC1 PAC Ty-YFP::PKAR NEO*
Clone number	Clone 1 and 2
Made by	Q. Wu
Constructs	pPOTv4(PAC)HA_Nluc_linker, pPOTv4(NEO)Ty_YFP_linker
Selection	Puromycin (0.1 µg/ml), Neomycin (2 µg/ml)
Description	A fragment including a *NEO* expression cassette and Ty-YFP coding sequence was inserted into the 5' of one endogenous *PKAR* allele in cell line Tb-QW022.

2.1.1.4 Cell lines used and produced for knocking out PKAC1

Tb-QW047	AnTat1.1 E 1313 Ty-PKAC2^{Ti}
Genotype	*TET^{R} TET^{R} BLE RDNA::Ty-PKAC2^{Ti} PAC*
Clone number	Clone 1, 2 and 4
Made by	Q.Wu
Constructs	pHD1313 (BLE), pHD615 (PAC)Ty-PKAC2
Selection	Phleomycin (0.2 µg/ml), Puromycin (0.1 µg/ml)
Description	This cell line inducibly expresses Ty-PKAC2 in the presence of Tet.

Tb-QW051	AnTat1.1 E 1313 Ty-PKAC2^{Ti} Δ*pkac1/PKAC1*
Genotype	*TET^{R} TET^{R} BLE RDNA::Ty-PKAC2^{Ti} PAC ΔPKAC1::BSD/PKAC1*
Clone number	Clone 2, 3 and 4
Made by	Q.Wu
Constructs	pHD1313 (BLE), pHD615 (PAC)Ty-PKAC1, pΔPKAC1 (BSD),
Selection	Phleomycin (0.2 µg/ml), Puromycin (0.1 µg/ml), Blasticidin (2 µg/ml)
Description	The is a hemizygous PKAC1 knockout cell line that one of its *PKAC1* alleles was replaced by a *BSD* expression cassette by transfection in the presence of the rescue Ty-PKAC2 protein.

Tb-QW055	AnTat1.1 E 1313 Ty-PKAC2^{Ti} Δ*pkac1/*Δ*pkac1*
Genotype	*TET^{R} TET^{R} BLE RDNA::Ty-PKAC2^{Ti} PAC ΔPKAC1::BSD/ ΔPKAC1::NEO*
Clone number	Clone 2, 3 and 4
Made by	Q.Wu
Constructs	pHD1313 (BLE), pHD615 (PAC)Ty-PKAC1, pΔPKAC1 (BSD), pΔPKAC1 (NEO),
Selection	Phleomycin (0.2 µg/ml), Puromycin (0.1 µg/ml), Blasticidin (2 µg/ml), Neomycin (2 µg/ml)
Description	A homozygous PKAC1 knockout cell line generated from Tb-QW051. The second *PKAC1* allele was replaced by a *NEO* expression cassette by transfection in the presence of the rescue Ty-PKAC2.

Three other cell lines that inducibly expresses Ty-PKAC1, the chimeric Ty-C1C2 and Ty-C2C1 were made in the same manner as Tb-QW047, resulting in cell line Tb-QW046, Tb-QW049 and Tb-QW048. The *PKAC1* alleles of these cell lines were

sequentially deleted by homologous recombination using pΔPKAC1(BSD) and pΔPKAC1(NEO). The following table briefly summarizes these cell lines.

Cell line ID	Cell line	Constructs	Selection marker
Tb-QW046	AnTat1.1 E 1313 Ty-PKAC1^{Ti}	pHD1313 (BLE), pHD615 (PAC)Ty-PKAC1	Phl, Puro
Tb-QW049	AnTat1.1 E 1313 Ty-C1C2^{Ti}	pHD1313 (BLE), pHD615 (PAC)Ty-C1C2	Phl, Puro
Tb-QW048	AnTat1.1 E 1313 Ty-C2C1^{Ti}	pHD1313 (BLE), pHD615 (PAC)Ty-C2C1	Phl, Puro
Tb-QW052	AnTat1.1 E 1313 Ty-C1C2^{Ti} *Δpkac1/PKAC1*	pHD1313 (BLE), pHD615 (PAC)Ty-C1C2, pΔPKAC1 (BSD)	Phl, Puro, Blas
Tb-QW053	AnTat1.1 E 1313 Ty-C2C1^{Ti} *Δpkac1/PKAC1*	pHD1313 (BLE), pHD615 (PAC)Ty-C2C1, pΔPKAC1 (BSD)	Phl, Puro, Blas
Tb-QW056	AnTat1.1 E 1313 Ty-C1C2^{Ti} *Δpkac1/Δpkac1*	pHD1313 (BLE), pHD615 (PAC)Ty-PKAC1, pΔPKAC1 (BSD), pΔPKAC1 (NEO)	Phl, Puro, Blas, Neo
Tb-QW057	AnTat1.1 E 1313 Ty-C2C1^{Ti} *Δpkac1/Δpkac1*	pHD1313 (BLE), pHD615 (PAC)Ty-PKAC1, pΔPKAC1 (BSD), pΔPKAC1 (NEO)	Phl, Puro, Blas, Neo

2.1.1.6 Cell lines produced for studying the role of the α-D helix

	MiTat1.2 1313 VASP PKAR^{Ti}
Genotype	*TET^R TET^R BLE RDNA::VASP HYG RDNA::PKAR^{Ti} PAC*
Made by	Y. Volpato
Constructs	pHD1313 (BLE), pTSArib (HYG)VASP, pHD615(PAC)PKAR
Selection	Phleomycin (0.2 µg/ml), Hygromycin (4 µg/ml), puromycin (0.1µg/ml)
Description	A transgenic PKAR was inserted into ribosomal DNA spacer for inducible expression

	MiTat1.2 1313 VASP PKAR(Δ480-499)^{Ti}
Genotype	*TET^R TET^R BLE RDNA::VASP HYG RDNA::PKAR(Δ480-499)^{Ti} PAC*
Made by	Y. Volpato
Constructs	pHD1313 (BLE), pTSArib (HYG)VASP, pHD615(PAC)-PKAR(Δ480-499)
Selection	Phleomycin (0.2 µg/ml), Hygromycin (4 µg/ml), puromycin (0.1µg/ml)
Description	A transgenic α-D helix truncated PKAR was inserted into ribosomal DNA spacer for inducible expression

	MiTat1.2 1313 VASP PKAR-Ty^{Ti}
Genotype	*TET^R TET^R BLE RDNA::VASP HYG RDNA::PKAR-Ty^{Ti} PAC*
Made by	Y. Volpato
Constructs	pHD1313 (BLE), pTSArib (HYG)VASP, pHD615(PAC)-PKAR-Ty
Selection	Phleomycin (0.2 µg/ml), Hygromycin (4 µg/ml), puromycin (0.1µg/ml)
Description	A transgenic PKAR-Ty was inserted into ribosomal DNA spacer for inducible expression

	MiTat1.2 1313 VASP PKAR(Δ480-499)-Ty^{Ti}
Genotype	*TET^R TET^R BLE RDNA::VASP HYG RDNA::PKAR(Δ480-499)-Ty^{Ti} PAC*
Made by	Y. Volpato
Constructs	pHD1313 (BLE), pTSArib (HYG)VASP, pHD615(PAC)-PKAR(Δ480-499)-Ty
Selection	Phleomycin (0.2 µg/ml), Hygromycin (4 µg/ml), puromycin (0.1 µg/ml)
Description	A transgenic PKAR(Δ480-499)-Ty was inserted into ribosomal DNA spacer for inducible expression

2.1.1.7 Cell lines produced for studying the α-D helix by NanoBiT assay

Tb-QW039	**MiTat1.2 1313 VASP SmBiT-PKAC1**
Genotype	*TET^R TET^R BLE RDNA::VASP HYG SmBiT::PKAC1 NEO*

Clone number	Clone 1, 2, 3 and 4
Made by	J. Hammerl (Bachelor thesis Hammerl, 2018)
Constructs	pHD1313 (BLE), pTSArib (HYG)VASP pPOTv4 (NEO)SmBiT_linker
Selection	Phleomycin (0.2 µg/ml), Hygromycin (4 µg/ml), Neomycin (2 µg/ml)
Description	SmBiT_linker coding sequence was in situ tagged to the 5' of one endogenous *PKAC1* allele. This cell line constitutively expresses SmBiT-PKAC1 and was used as the parent cell line for transfection of different Ty-LgBiT-PKARs

Tb-QW040	**MiTat1.2 1313 VASP SmBiT-PKAC1 Ty-LgBiT-PKAR^{Ti}**
Genotype	*TET^{R} TET^{R} BLE RDNA::VASP HYG* *SmBiT::PKAC1 NEO RDNA::Ty-LgBiT-PKAR^{Ti} PAC*
Clone number	Clone 1 and 2
Made by	J. Hammerl (Bachelor thesis Hammerl, 2018)
Constructs	pHD1313 (BLE), pTSArib (HYG)VASP pPOTv4 (NEO)SmBiT_linker, pHD615(PAC)Ty-LgBiT-PKAR
Selection	Phleomycin (0.2 µg/ml), Hygromycin (4 µg/ml), Neomycin (2 µg/ml), puromycin (0.1 µg/ml)
Description	Ty-LgBiT-PKAR inducible expression cassette was inserted into the ribosomal DNA spacer of Tb-QW039 by transfection. The other cell lines in this section were generated in the same manner.

Tb-QW042	**MiTat1.2 1313 VASP SmBiT-PKAC1 Ty-LgBiT-PKAR(∆480-499)^{Ti}**
Genotype	*TET^{R} TET^{R} BLE RDNA::VASP HYG* *SmBiT::PKAC1 NEO NEO RDNA:: Ty-LgBiT-PKAR(∆480-499)^{Ti} PAC*
Clone number	Clone 1, 2 ,4 and 5
Made by	J. Hammerl (Bachelor thesis Hammerl, 2018)
Constructs	pHD1313 (BLE), pTSArib (HYG)VASP, pPOTv4(NEO)SmBiT_linker, pHD615(PAC)Ty-LgBiT-PKAR(∆480-499)
Selection	Phleomycin (0.2 µg/ml), Hygromycin (4 µg/ml), Neomycin (2 µg/ml), puromycin (0.1 µg/ml)

Tb-QW058	**MiTat1.2 1313 VASP SmBiT-PKAC1 Ty-LgBiT-PKAR(Y484A)^{Ti}**
Genotype	*TET^{R} TET^{R} BLE RDNA::VASP HYG* *SmBiT::PKAC1 NEO RDNA::Ty-LgBiT-PKAR(Y484A)^{Ti} PAC*
Clone number	Clone 2, 3 and 4
Made by	Q. Wu
Constructs	pHD1313 (BLE), pTSArib (HYG)VASP pPOTv4(NEO)SmBiT_linker, pHD615(PAC) Ty-LgBiT-PKAR(Y484A)
Selection	Phleomycin (0.2 µg/ml), Hygromycin (4 µg/ml), Neomycin (2 µg/ml), puromycin (0.1 µg/ml)

Tb-QW059	**MiTat1.2 1313 VASP SmBiT-PKAC1 Ty-LgBiT-PKAR(Y485A)^{Ti}**
Genotype	*TET^{R} TET^{R} BLE RDNA::VASP HYG* *SmBiT::PKAC1 NEO RDNA::Ty-LgBiT-PKAR(Y485A)^{Ti} PAC*
Clone number	Clone 1, 3 and 4
Made by	Q. Wu
Constructs	pHD1313 (BLE), pTSArib (HYG)VASP pPOTv4(NEO)SmBiT_linker, pHD615(PAC) Ty-LgBiT-PKAR(Y485A)
Selection	Phleomycin (0.2 µg/ml), Hygromycin (4 µg/ml), Neomycin (2 µg/ml), puromycin (0.1 µg/ml)

Tb-QW060	**MiTat1.2 1313 VASP SmBiT-PKAC1 Ty-LgBiT-PKAR(Y484A, Y485A)^{Ti}**
Genotype	*TET^{R} TET^{R} BLE RDNA::VASP HYG* *SmBiT::PKAC1 NEO RDNA::Ty-LgBiT-PKAR(Y484A, Y485A)^{Ti} PAC*
Clone number	Clone 2, 3 and 4
Made by	Q. Wu
Constructs	pHD1313 (BLE), pTSArib (HYG)VASP pPOTv4(NEO)SmBiT_linker, pHD615(PAC) Ty-LgBiT-PKAR(Y484A, Y485A)
Selection	Phleomycin (0.2 µg/ml), Hygromycin (4 µg/ml), Neomycin (2 µg/ml), puromycin (0.1 µg/ml)

Tb-QW069	MiTat1.2 1313 VASP SmBiT-PKAC1 Ty-LgBiT-PKAR(N438A, H440A)^{Ti}
Genotype	*TET^R TET^R BLE RDNA::VASP HYG SmBiT::PKAC1 NEO RDNA:: Ty-LgBiT-PKAR(N438A, H440A)^{Ti} PAC*
Clone number	Clone 3 and 5
Made by	Q. Wu
Constructs	pHD1313 (BLE), pTSArib (HYG)VASP, pPOTv4(NEO)SmBiT_linker, pHD615(PAC) Ty-LgBiT-PKAR(N438A, H440A)
Selection	Phleomycin (0.2 µg/ml), Hygromycin (4 µg/ml), Neomycin (2 µg/ml), puromycin (0.1 µg/ml)

Tb-QW070	MiTat1.2 1313 VASP SmBiT-PKAC1 Ty-LgBiT-PKAR(N438A)^{Ti}
Genotype	*TET^R TET^R BLE RDNA::VASP HYG SmBiT::PKAC1 NEO RDNA:: Ty-LgBiT-PKAR(N438A)^{Ti} PAC*
Clone number	Clone 1, 2 and 4
Made by	Q. Wu
Constructs	pHD1313 (BLE), pTSArib (HYG)VASP, pPOTv4(NEO)SmBiT_linker, pHD615(PAC) Ty-LgBiT-PKAR(N438A)
Selection	Phleomycin (0.2 µg/ml), Hygromycin (4 µg/ml), Neomycin (2 µg/ml), puromycin (0.1 µg/ml)

Tb-QW071	MiTat1.2 1313 VASP SmBiT-PKAC1 Ty-LgBiT-PKAR(H440A)^{Ti}
Genotype	*TET^R TET^R BLE RDNA::VASP HYG SmBiT::PKAC1 NEO RDNA:: Ty-LgBiT-PKAR(H440A)^{Ti} PAC*
Clone number	Clone 2, 3 and 4
Made by	Q. Wu
Constructs	pHD1313 (BLE), pTSArib (HYG)VASP, pPOTv4(NEO)SmBiT_linker, pHD615(PAC) Ty-LgBiT-PKAR(H440A)
Selection	Phleomycin (0.2 µg/ml), Hygromycin (4 µg/ml), Neomycin (2 µg/ml), puromycin (0.1 µg/ml)

Tb-QW073	MiTat1.2 1313 VASP SmBiT-PKAC1 Ty-LgBiT-PKAR(∆480-499,_T205A)^{Ti}
Genotype	*TET^R TET^R BLE RDNA::VASP HYG SmBiT::PKAC1 NEO RDNA:: Ty-LgBiT-PKAR(∆480, T205A)^{Ti} PAC*
Clone number	Clone 2, 3 and 4
Made by	Q. Wu
Constructs	pHD1313(BLE), pTSArib (HYG)VASP, pPOTv4(NEO)SmBiT_linker, pHD615(PAC)Ty-LgBiT-PKAR(∆480, T205A)
Selection	Phleomycin (0.2 µg/ml), Hygromycin (4 µg/ml), Neomycin (2 µg/ml), puromycin (0.1 µg/ml)

2.1.1.8 Cell lines produced for studying the N-terminal domain by NanoBiT assay

Tb-QW061	MiTat1.2 1313 VASP SmBiT-PKAC1 PKAR-LgBiT-Ty^{Ti}
Genotype	*TET^R TET^R BLE RDNA::VASP HYG SmBiT::PKAC1 NEO RDNA::PKAR-LgBiT-Ty^{Ti} PAC*
Clone number	Clone 1, 2 and 3
Made by	Q. Wu
Constructs	pHD1313 (BLE), pTSArib (HYG)VASP pPOTv4(NEO)SmBiT_linker, pHD615(PAC) PKAR_LgBiT-Ty
Selection	Phleomycin (0.2 µg/ml), Hygromycin (4 µg/ml), Neomycin (2 µg/ml), puromycin (0.1 µg/ml)
Description	PKAR-LgBiT-Ty inducible expression cassette was inserted into the ribosomal DNA spacer of Tb-QW039 by transfection. The other cell lines in this section were generated in the same manner.

Tb-QW062	MiTat1.2 1313 VASP SmBiT-PKAC1 PKAR(T205A)-LgBiT-Ty^{Ti}

Genotype	*TET^R TET^R BLE RDNA::VASP HYG SmBiT::PKAC1 NEO RDNA::PKAR(T205A)-LgBiT-Ty^{Ti} PAC*
Clone number	Clone 1, 3 and 4
Made by	Q. Wu
Constructs	pHD1313 (BLE), pTSArib (HYG)VASP, pPOTv4(NEO)SmBiT_linker, pHD615(PAC) PKAR(T205A)-LgBiT-Ty
Selection	Phleomycin (0.2 µg/ml), Hygromycin (4 µg/ml), Neomycin (2 µg/ml), puromycin (0.1 µg/ml)

Tb-QW063	**MiTat1.2 1313 VASP SmBiT-PKAC1 PKAR(R207S)-LgBiT-Ty^{Ti}**
Genotype	*TET^R TET^R BLE RDNA::VASP HYG SmBiT::PKAC1 NEO RDNA::PKAR(R207S)-LgBiT-Ty^{Ti} PAC*
Clone number	Clone 5
Made by	Q. Wu
Constructs	pHD1313 (BLE), pTSArib (HYG)VASP, pPOTv4(NEO)SmBiT_linker, pHD615(PAC) PKAR(R207S)-LgBiT-Ty
Selection	Phleomycin (0.2 µg/ml), Hygromycin (4 µg/ml), Neomycin (2 µg/ml), puromycin (0.1 µg/ml)

Tb-QW064	**MiTat1.2 1313 VASP SmBiT-PKAC1 PKAR(T205A, R207S)-LgBiT-Ty^{Ti}**
Genotype	*TET^R TET^R BLE RDNA::VASP HYG SmBiT::PKAC1 NEO RDNA::PKAR(T205A, R207S)-LgBiT-Ty^{Ti} PAC*
Clone number	Clone 1, 2 and 4
Made by	Q. Wu
Constructs	pHD1313 (BLE), pTSArib (HYG)VASP, pPOTv4(NEO)SmBiT_linker, pHD615(PAC) PKAR(T205A, R207S)-LgBiT-Ty
Selection	Phleomycin (0.2 µg/ml), Hygromycin (4 µg/ml), Neomycin (2 µg/ml), puromycin (0.1 µg/ml)

Tb-QW065	**MiTat1.2 1313 VASP SmBiT-PKAC1 PKAR(R89A, R137A)-LgBiT-Ty^{Ti}**
Genotype	*TET^R TET^R BLE RDNA::VASP HYG SmBiT::PKAC1 NEO RDNA::PKAR(R89A, R137A)-LgBiT-Ty^{Ti} PAC*
Clone number	Clone 2, 3 and 4
Made by	Q. Wu
Constructs	pHD1313 (BLE), pTSArib (HYG)VASP, pPOTv4(NEO)SmBiT_linker, pHD615(PAC) PKAR(R89A, R137A)-LgBiT-Ty
Selection	Phleomycin (0.2 µg/ml), Hygromycin (4 µg/ml), Neomycin (2 µg/ml), puromycin (0.1 µg/ml)

Tb-QW066	**MiTat1.2 1313 VASP SmBiT-PKAC1 PKAR(R89K, R137K)-LgBiT-Ty^{Ti}**
Genotype	*TET^R TET^R BLE RDNA::VASP HYG SmBiT::PKAC1 NEO RDNA::PKAR(R89K, R137K)-LgBiT-Ty^{Ti} PAC*
Clone number	Clone 2
Made by	Q. Wu
Constructs	pHD1313 (BLE), pTSArib (HYG)VASP, pPOTv4(NEO)SmBiT_linker, pHD615(PAC) PKAR(R89K, R137K)-LgBiT-Ty
Selection	Phleomycin (0.2 µg/ml), Hygromycin (4 µg/ml), Neomycin (2 µg/ml), puromycin (0.1 µg/ml)

Tb-QW067	**MiTat1.2 1313 VASP SmBiT-PKAC1 PKAR(∆1-191)-LgBiT-Ty^{Ti}**
Genotype	*TET^R TET^R BLE RDNA::VASP HYG SmBiT::PKAC1 NEO RDNA::PKAR(∆1-191)-LgBiT-Ty^{Ti} PAC*
Clone number	Clone 1, 3 and 4
Made by	Q. Wu
Constructs	pHD1313 (BLE), pTSArib (HYG)VASP, pPOTv4(NEO)SmBiT_linker, pHD615(PAC) PKAR(∆1-191)-LgBiT-Ty
Selection	Phleomycin (0.2 µg/ml), Hygromycin (4 µg/ml), Neomycin (2 µg/ml), puromycin (0.1 µg/ml)

Tb-QW068	MiTat1.2 1313 VASP SmBiT-PKAC1 PKAR(∆1-191, T205A, R207S)-LgBiT-Ty^{Ti}
Genotype	*TET^{R} TET^{R} BLE RDNA::VASP HYG SmBiT::PKAC1 NEO RDNA::PKAR(∆1-191, T205A, R207S)-LgBiT-Ty^{Ti} PAC*
Clone number	Clone 2 and 3
Made by	Q. Wu
Constructs	pHD1313 (BLE), pTSArib (HYG)VASP, pPOTv4(NEO)SmBiT_linker, pHD615(PAC) PKAR(∆1-191, T205A, R207S)-LgBiT-Ty
Selection	Phleomycin (0.2 µg/ml), Hygromycin (4 µg/ml), Neomycin (2 µg/ml), puromycin (0.1 µg/ml)

2.1.1.9 Cell lines used and produced for studying PKAC1 and PKAC2

TB-QW075	AnTat1.1 90-13 LgBiT-PKAR
Genotype	*T7POL NEO TETR HYG LgBiT::PKAR BSD*
Clone number	Clone 4
Made by	Q. Wu
Constructs	plew13, plew90, pPOTv4 (BSD)LgBiT_linker
Selection	Neomycin (2 µg/ml), Hygromycin (4 µg/ml), Blasticidin (2 µg/ml)
Description	LgBiT_linker coding sequence was in situ tagged to the 5' of one endogenous *PKAR* allele. This cell line constitutively expresses LgBiT-PKAR and was used as the parent cell line for transfection of different SmBiT-PKACs.

TB-QW077	AnTat1.1 90-13 LgBiT-PKAR SmBiT-PKAC1^{Ti}
Genotype	*T7POL NEO TETR HYG LgBiT::PKAR BSD RDNA::SmBiT-PKAC1^{Ti} PAC*
Clone number	Polol and clone 3
Made by	Q. Wu
Constructs	plew13, plew90, pPOTv4 (BSD)LgBiT_linker, pHD615(PAC) SmBiT-PKAC1
Selection	Neomycin (2 µg/ml), Hygromycin (4 µg/ml), Blasticidin (2 µg/ml), puromycin (0.1 µg/ml)
Description	SmBiT-PKAC1 inducible expression cassette was inserted into the ribosomal DNA spacer of Tb-QW075 by transfection. The other cell lines in this section were generated in the same manner.

TB-QW078	AnTat1.1 90-13 LgBiT-PKAR SmBiT-PKAC2^{Ti}
Genotype	*T7POL NEO TETR HYG LgBiT::PKAR BSD RDNA:: SmBiT-PKAC2^{Ti} PAC*
Clone number	Pool and clone 2
Made by	Q. Wu
Constructs	plew13, plew90, pPOTv4 (BSD)LgBiT_linker, pHD615(PAC) SmBiT-PKAC2
Selection markers	Neomycin (2 µg/ml), Hygromycin (4 µg/ml), Blasticidin (2 µg/ml), puromycin (0.1 µg/ml)

TB-QW079	AnTat1.1 90-13 LgBiT-PKAR SmBiT-C1C2^{Ti}
Genotype	*T7POL NEO TETR HYG LgBiT::PKAR BSD RDNA:: SmBiT-C1C2^{Ti} PAC*
Clone number	Pool and clone 3
Made by	Q. Wu
Constructs	plew13, plew90, pPOTv4 (BSD)LgBiT_linker, pHD615(PAC) SmBiT-C1C2
Selection	Neomycin (2 µg/ml), Hygromycin (4 µg/ml), Blasticidin (2 µg/ml), puromycin (0.1 µg/ml)

TB-QW080	AnTat1.1 90-13 LgBiT-PKAR SmBiT-C2C1^{Ti}
Genotype	*T7POL NEO TETR HYG LgBiT::PKAR BSD RDNA:: SmBiT-C2C1^{Ti} PAC*
Clone number	Pool and clone 3
Made by	Q. Wu
Constructs	plew13, plew90, pPOTv4 (BSD)LgBiT_linker, pHD615(PAC) SmBiT-C2C1
Selection	Neomycin (2 µg/ml), Hygromycin (4 µg/ml), Blasticidin (2 µg/ml), puromycin (0.1 µg/ml)

TB-QW081	AnTat1.1 90-13 LgBiT-PKAR SmBiT-PKAC1(S315A, S320A, T324A)^{Ti}
Genotype	*T7POL NEO TETR HYG* *LgBiT::PKAR BSD RDNA:: SmBiT-PKAC1(S315A, S320A, T324A) PAC*
Clone number	Pool and clone 3
Made by	Q. Wu
Constructs	plew13, plew90, pPOTv4 (BSD)LgBiT_linker, pHD615(PAC) SmBiT-PKAC1(S315A, S320A, T324A)
Selection	Neomycin (2 µg/ml), Hygromycin (4 µg/ml), Blasticidin (2 µg/ml), puromycin (0.1 µg/ml)

2.1.2 Bacteria strain

Strain	Genotype	Purpose
***E. coli* SURE (Stratagene)**	*e14^{-}(McrA^{-}) Δ(mcrCB-hsdSMR-mrr) 171 endA1 supE44 thi-1 gyrA96 relA1 lac recB recJ sbcC umuC::Tn5 (Kan^{r}) uvrC [F´ proAB lacI^{q} ZΔM15 Tn10 (Tet^{r})]]]*	Plasmid amplification
***E. coli* XL 10-Gold (Stratagene)**	*endA1 glnV44 recA1 thi-1 gyrA96 relA1 lac Hte Δ(mcrA)183 Δ(mcrCBhsdSMR-mrr)173 tetR F'[proAB lacI^{q}ZΔM15 Tn10(Tet^{r} Amy CmR)]*	Plasmid amplification
***E. coli* Rosetta (DE3) (Novagen)**	*F – ompT hsdSB(rB– mB–) gal dcm (DE3) pRARE27 (CamR)*	Recombinant protein expression

2.1.3 Primers

Name	Sequence	Target Gene	Purpose
LgLr-fwd	GGGGTACCATGGTCTTCACACTCGAAGAT	*LgBiT*	Cloning of LgBiT-linker into pPOTv4 vector
LgLr-rev	CGGGATCCGCTGTTGATGGTTACTCG	*LgBiT*	
SmLr-fwd	GGGGTACCATGGTGACCGGCTACCGGCTGTTCGAGG AGATTCTGGGATCCGGATCGAGCGGT	*SmBiT*	Cloning of SmBiT-linker into pPOTv4 vector
SmLr-rev	CGAGCTCACCTGACGACCCTCCACCTCCGCTCCCGC CACCACCGCTCGATCCGGATCCCAGA	*SmBiT*	
LrLg-fwd	CGGGATCCGTCTTCACACTCGAAGATTTC	*LgBiT*	Cloning of linker-LgBiT into pPOTv4 vector
LrLg-rev	CGAGCTCTTAGCTGTTGATGGTTACTCG	*LgBiT*	
5'-PKAC1-fwd	TCTTTTTCGTTTCTCTTTGCCTTTTTTTTTGTATAATTAA GGTAATAACAAGGTGGGTAAAAGCAACTAGCCGCGCA AATGTATAATGCAGACCTGCTGC	*TbPKAC1*	In situ tagging to the 5' end of PKAC1 gene
5'-PKAC1-rev	ATTTCAAAGTCACTCAGCTTCCATCCCGATGTGTCAG GCTTGGTAAACAGTTGGCCATCACCAGTGGGAGTTGT CGTCATACCTGACGACCCTCCACC	*TbPKAC1*	
5'-PKAR-fwd	TAAGACAAAACAACGAAATAAAACCAGAAGGGTAGTTT TTCCTTTGTTTTCTTTTCTTTTTGTTTTTTTTTCTGGTTT CCGTATAATGCAGACCTGCTGC	*TbPKAR*	In situ tagging to the 5' end of PKAR gene
5'-PKAR-rev	AGAAATGTGTTGGGTTGCTTCACACCCTCCTTTTGGC AGGCGGCGAGGAATAGGTTTAACGATGTTCCCTTTTC AGACATACCTGACGACCCTCCACC	*TbPKAR*	
3'-PKAR-fwd	TGAAACGAACCTCGCAGCAGCCAAACTATGAGTACTA CCAGTCGAAACTGAAAACTACTTTAAGGGCAGAGGG GAGGAAGGGATCGAGCGGTGGTGGCGG	*TbPKAR*	In situ tagging to the 3' end of PKAR gene
3'-PKAR-rev	TACTCCCCAAAAGAAAACAAAAACAAGAAAACAAACA AAAAAAACACGAAAAGCAATCCAATGCATATTTTACGA GCCACCCAATTTGAGAGACCTGTGC	*TbPKAR*	
HA-Nluc-Lr-fwd	GGGGTACCATGTACCCATACGATGTTCCAGATTACGCT ACTAGTGTCTTCACACTCGAAGAT	*Nluc*	Cloning of HA-Nluc-linker into pPOTv4 vector

HA-Nluc-Lr-rev	CGGGATCCCGCCAGAATGCGTTCGCA	*Nluc*	
Ty-YFP-Lr-fwd	GGGGTACCTATGGAGGTCCATACTAACCAAGATCCAC TTGACAAGCTTGTGAGCAAGGGCGAGGAG	*Ty-YFP*	Cloning of Ty-YFP-linker into pPOTv4 vector
Ty-YFP-Lr-rev	CGGGATCCCTTGTACAGCTCGTCCAT	*Ty-YFP*	
PKAR_N438A_ H440A fwd	GAGCTGGAATTCCTTGCCAATGCCGCCAATGTAGCAG ATGTTGTG	*TbPKAR*	Mutagenesis of PKAR_N438A_H440A
PKAR_N438A_ H440A rev	ATCTGCTACATTGGCGGCATTGGCAAGGAATTCCAGC TCACCCAC	*TbPKAR*	
PKAR_N438A fwd	GAGCTGGAATTCCTTGCCAATCACGCCAATGTAGCAG AT	*TbPKAR*	Mutagenesis of PKAR_N438A
PKAR_N438A rev	TACATTGGCGTGATTGGCAAGGAATTCCAGCTCACCC AC	*TbPKAR*	
PKAR_H440A fwd	GAATTCCTTAACAATGCCGCCAATGTAGCAGATGTTGT G	*TbPKAR*	Mutagenesis of PKAR_H440A
PKAR_H440A rev	ATCTGCTACATTGGCGGCATTGTTAAGGAATTCCAGCT C	*TbPKAR*	
AvrII_TcPKAR fwd	ACACCTAGGATGGCGGAGGAAGAA	*TcPKAR*	Cloning of TcPKAR into pHD615 vector
BamH I-TcPKAR rev	CGCGGATCCTTATACATCATCCAC	*TcPKAR*	
AvrII_LdPKAR fwd	AAACCTAGGATGTCCGCGGAAGAC	*LdPKAR*	Cloning of LdPKAR into pHD615 vector
BamH I-LdPKAR rev	AAAGGATCCTTACTGGACCGCCGC	*LdPKAR*	

2.1.4 Plasmids

	pPOTv4-(BSD)-GS-BirA-GS-(HYG)
Description	pPOT plasmid was developed for inserting a sequence of DNA into the genome of trypanosome, usually the 5' or 3' of a target gene ORF in combination with long-primer PCR and transfection
Made by	Matt. Gould
Selection markers	Blasticidin (2 µg/ml) for 5' tagging; Hygromycin (2 µg/ml) for 3' tagging; Ampicillin (100 µg/ml) for *E. coli*

pQW-009	**pPOTv4-(BSD)-LgBiT-Linker**
Description	It was used to insert the LgBiT-linker to the 5' of a target gene
Construction	The LgBiT-linker was amplified from the pBiT1.1-C [TK/LgBiT] Vector provided by the NanoBiT® PPI MCS Starter System kit. It was inserted into the pPOTv4 vector using KpnI and SacI. The original HYG gene of pPOTv4-(BSD)-GS-BirA-GS-(HYG) was replaced by BSD gene through *Nhe*I and *Xho*I
Made by	Q. Wu
Selection markers	Blasticidin (2 µg/ml) for BSF; Ampicillin (100 µg/ml) for *E. coli*

pQW-010	**pPOTv4-Linker-LgBiT-(BSD)**
Description	It was used to insert the linker-LgBiT to the 3' of a target gene
Construction	It was developed in similar manner as pQW-009.
Made by	Q. Wu
Selection markers	Blasticidin (2 µg/ml) for BSF; Ampicillin (100 µg/ml) for *E. coli*

pQW-011	**pPOTv4-(NEO)_SmBiT-Linker**
Description	It was used to insert the SmBiT-Linker to the 5' of a target gene
Construction	The SmBiT-linker fragment was generated by denaturing and annealing of a pair of partially complementary long primers. It was thereafter inserted into the pPOTv4 vector using *Kpn*I and *Sac*I.
Made by	Q. Wu

Selection markers	Neomycin (2 µg/ml) for BSF; Ampicillin (100 µg/ml) for *E. coli*

pQW-012	**pPOTv4_Linker-SmBiT-(NEO)**
Description	It was used to insert the linker-SmBiT to the 3' of a target gene
Construction	It was developed in similar manner as pQW-011
Made by	Q. Wu
Selection markers	Neomycin (2 µg/ml) for BSF; Ampicillin (100 µg/ml) for *E. coli*

pQW-013	**pPOTv4-(NEO)_TY-mCherry-Linker**
Description	It was used to insert the Ty-mCherry-linker to the 5' of a target gene
Construction	It was developed from pQW-11 by replacing the SmBiT-linker with Ty-mCherry-linker
Made by	Q. Wu
Selection markers	Neomycin (2 µg/ml) for BSF; Ampicillin (100 µg/ml) for *E. coli*

pQW-017	**pPOTv4-(PAC)_HA-Nluc-Linker**
Description	It was used to insert the HA-Nluc-linker to the 5' of a target gene
Construction	It was developed from pQW-009 by replacing the LgBiT-linker with the HA-Nluc-linker. The BSD marker was replaced by PAC marker through *Eco*RI and *Nco*I
Made by	Q. Wu
Selection markers	Puromycin (0.1 µg/ml) for BSF; Ampicillin (100 µg/ml) for *E. coli*

pQW-020	**pPOTv4_TY-YFP-Linker**
Description	Developed from pQW011 to insert Ty-YFP-linker to the 5' of a target gene
Construction	It was developed from pQW-013 by replacing Ty-mCherry-linker with Ty-YFP-linker
Made by	Q. Wu
Selection markers	Neomycin (2 µg/ml) for BSF; Ampicillin (100 µg/ml) for *E. coli*

	pΔPKAC1 (BSD)
Description	Deletion of one *PKAC1* allele
Made by	Paul Hassan
Linearization	*Eco*RI / *Bgl*II
Selection markers	Blasticidin (2 µg/ml) for BSF; Ampicillin (100 µg/ml) for *E. coli*

pQW-001	**pΔPKAC1 (NEO)**
Description	Deletion of one *PKAC1* allele
Construction	It was developed from pΔPKAC1 (BSD) where the BSD marker was replaced by NEO using *Xba*I and *Blp*I
Made by	Q. Wu
Linearization	*Eco*RI / *Bgl*II
Selection markers	Neomycin (2 µg/ml) for BSF; Ampicillin (100 µg/ml) for *E. coli*

	pHD615 (PAC)_PKAR
Description	For inducible expression of PKAR
Construction	The PKAR ORF was inserted to the vector by *Hind*III and *BamH*I. Three similar constructs were also made in the same way, they are pHD615 (PAC)PKAR(Δ480-499), pHD615 (PAC)PKAR-Ty and pHD615 (PAC)PKAR(Δ480-499)-Ty. They were used for study the function of the α-D helix
Made by	Yuri Valpoto
Linearization	*Not*I

Selection markers	Puromycin (0.1 µg/ml) for BSF; Ampicillin (100 µg/ml) for *E. coli*

	pHD615 (PAC)_Ty-LgBiT-PKAR
Description	Inducible expression of Ty-LgBiT-PKAR that can form holoenzyme with SmBiT-PKAC1. The activation of the specific holoenzyme can be monitored by NanoBiT assay
Construction	The construct was developed from pHD615 (PAC)PKAR. A short sequence containing some extra restriction enzyme sites (*Apa*I, *Hpa*I and *Xba*I) was inserted to the 5' of PKAR ORF at first. The Ty-LgBiT amplified from pQW-009 was then inserted by *Apa*I and *Xba*I. Note: there is a *Hind*III site in PKAR ORF, that's why the *Hind*III site was not used in this and the following pHD615 constructs
Made by	Q. Wu
Linearization	*Not*I
Selection markers	Puromycin (0.1 µg/ml) for BSF; Ampicillin (100 µg/ml) for *E. coli*

pQW-036	**pHD615 (PAC)_Ty-LgBiT-PKAR(Y484A)**
Description	Inducible expression of Ty-LgBiT-PKAR_Y484A
Construction	The construct was developed from pHD615 (PAC)_Ty-LgBiT-PKAR. The PKAR(Y484A) sequence was generate by PCR and introduced to the backbone by *Xba*I and *BamH*I. There were more PKAR mutants made in the same way. Please check the table in the end of this section
Made by	Q. Wu
Linearization	*Not*I
Selection markers	Puromycin (0.1 µg/ml) for BSF; Ampicillin (100 µg/ml) for *E. coli*

pQW-048	**pHD615 (PAC)_PKAR-LgBiT-Ty**
Description	Inducible expression of PKAR-LgBiT-Ty.
Construction	The construct was developed from pHD615 (PAC)PKAR. *Apa*I and *Avr*II sites were introduced in between the original *Hind*III and *BamH*I. PKAR ORF was inserted between *Apa*I and *Avr*II, LgBiT-Ty was inserted by *Avr*II and *BamH*I. Many other PKAR mutants that contain mutations on N-terminal were made using this construct as backbone. They are listed in the table of the end of this section
Made by	Q. Wu
Linearization	*Not*I
Selection markers	Puromycin (0.1 µg/ml) for BSF; Ampicillin (100 µg/ml) for *E. coli*

	pHD615 (PAC)_Ty-PKAC1
Description	Inducible expression of Ty-PKAC1
Construction	The construct is developed from pHD615(PAC)Ty-LgBiT-PKAR, where the Ty-PKAC1 was introduced through *Apa*I and *BamH*I. A *Nhe*I site is in between of the Ty epitope and PKAC1 sequences. Based on this construct, the other 3 constructs respectively expressing Ty-PKAC2, Ty-C1C2 and Ty-C2C1 were made.
Made by	Q. Wu
Linearization	*Not*I
Selection markers	Puromycin (0.1 µg/ml) for BSF; Ampicillin (100 µg/ml) for *E. coli*

	pHD615 (PAC)_SmBiT-PKAC1
Description	Inducible expression of SmBiT-PKAC1
Construction	The construct is developed from pHD615(PAC)Ty-PKAC1, where the Ty epitope was replaced by the SmBiT-linker generated by PCR via *Apa*I and *Nhe*I. Based on this construct, the other 3 constructs 3 constructs respectively expressing SmBiT-PKAC2, SmBiT-C1C2 and SmBiT-C2C1 were made. The four constructs were used for studying the activation of different PKA holoenzymes.
Made by	Q. Wu

Linearization	*Not*I
Selection markers	Puromycin (0.1 µg/ml) for BSF; Ampicillin (100 µg/ml) for *E. coli*

pQW-065	**pLew82 (BLE)_Ty-PKAR(∆480-499, T205A)**
Description	Inducible overexpression of Ty-LgBiT-PKAR(∆480-499, T205A)
Construction	Ty-PKAR(∆480-499, T205A) was cloned from PKAR_T205A using a forward primer containing the Ty epitope tag coding sequence and the reverse primer cloning the PKAR(∆480-499). A *Spe*I restriction site was introduced to the N-end of Ty, *BamH*I is at the C-end of the mutated PKAR.
Made by	Q. Wu
Linearization	*Not*I
Selection markers	Phleomycin (0.2 µg/ml) for BSF; Ampicillin (100 µg/ml) for *E. coli*

2.1.4.1 The constructs used for expressing different PKA subunits

Plasmid	Expression	Linearization for transfection	Selection marker
PKAR α-D helix truncation & mutations			
pHD615 (PAC)_Ty-LgBiT-PKAR(Δ480-499)	Ty-LgBiT-PKAR(Δ480-499)	*Not*I	Puromycin 0.1 µg/ml
pHD615 (PAC)_Ty-LgBiT-PKAR(Y484A)	Ty-LgBiT-PKAR(Y484A)	*Not*I	Puromycin 0.1 µg/ml
pHD615 (PAC)_Ty-LgBiT-PKAR(Y485A)	Ty-LgBiT-PKAR(Y485A)	*Not*I	Puromycin 0.1 µg/ml
pHD615 (PAC)_Ty-LgBiT-PKAR(Y484A, Y485A)	Ty-LgBiT-PKAR(Y484A, Y485A)	*Not*I	Puromycin 0.1 µg/ml
pHD615 (PAC)_Ty-LgBiT-PKAR(N438A)	Ty-LgBiT-PKAR(N438A)	*Not*I	Puromycin 0.1 µg/ml
pHD615 (PAC)_Ty-LgBiT-PKAR(H440A)	Ty-LgBiT-PKAR(H440A)	*Not*I	Puromycin 0.1 µg/ml
pHD615 (PAC)_Ty-LgBiT-PKAR(N438A, H440A)	Ty-LgBiT-PKAR(N438A, H440A)	*Not*I	Puromycin 0.1 µg/ml
PKAR N-terminal truncation & mutations			
pHD615 (PAC)_PKAR(T205A)-LgBiT-Ty	PKAR(T205A)-LgBiT-Ty	*Not*I	Puromycin 0.1 µg/ml
pHD615 (PAC)_PKAR(R207S)-LgBiT-Ty	PKAR(R207S)-LgBiT-Ty	*Not*I	Puromycin 0.1 µg/ml
pHD615 (PAC)_PKAR(T205A, R207S)-LgBiT-Ty	PKAR(T205A, R207S)-LgBiT-Ty	*Not*I	Puromycin 0.1 µg/ml
pHD615 (PAC)_PKAR(Δ1-191)-LgBiT-Ty	PKAR(Δ1-191)-LgBiT-Ty	*Not*I	Puromycin 0.1 µg/ml
pHD615 (PAC)_PKAR(Δ1-191, T205A, R207S)-LgBiT-Ty	PKAR(Δ1-191, T205A, R207S)-LgBiT-Ty	*Not*I	Puromycin 0.1 µg/ml
pHD615 (PAC)_PKAR(R89A, R137A)-LgBiT-Ty	PKAR(R89A, R137A)-LgBiT-Ty	*Not*I	Puromycin 0.1 µg/ml
pHD615 (PAC)_PKAR(R89K, R137K)-LgBiT-Ty	PKAR(R89K, R137K)-LgBiT-Ty	*Not*I	Puromycin 0.1 µg/ml
PKAC1 chimeras & mutations			
pHD615 (PAC)_SmBiT-PKAC1	SmBiT-PKAC1	*Not*I	Puromycin 0.1 µg/ml
pHD615 (PAC)_SmBiT-PKAC2	SmBiT-PKAC2	*Not*I	Puromycin 0.1 µg/ml
pHD615 (PAC)_SmBiT-C1C2	SmBiT-C1C2	*Not*I	Puromycin 0.1 µg/ml

pHD615 (PAC)_SmBiT-C2C1	SmBiT-C2C1	*Not*I	Puromycin 0.1 µg/ml
pHD615 (PAC)_SmBiT-PKAC1(S315A, S320A, T324A)	SmBiT-PKAC1(S315A, S320A, T324A)	*Not*I	Puromycin 0.1 µg/ml

2.1.5 Antibiotic stock solutions

Name	Stock solution	Supplier
Ampicillin	100 mg/ml in H_2O	Boehringer, Mannheim
Tetracycline	10 mg/ml in Ethanol	Sigma, Steinheim
Hygromycin	10 mg/ml in H_2O	Calbiochem, Darmstadt
Phleomycin	10 mg/ml in H_2O	Cayla, Toulouse, France
Blasticidin	10 mg/ml in H_2O	Merck, Darmstadt
Neomycin	10 mg/ml in H_2O	Sigma, Steinheim
Puromycin	10 mg/ml in H_2O	Sigma, Steinheim

2.1.6 Antibodies

2.1.6.1 Primary antibodies

Name	Source	Type	Dilution	Origin
α-PKAC1/2	Rabbit	Polyclonal	1/1000	Recombinant expression of GST-tagged PKAC1 truncation (AA277-334), (PhD thesis Klöckner, 1996), Hybridoma pGex2
α-PKAR	Rabbit	Polyclonal	1/1000	(PhD thesis Schulte zu Sodingen, 1996), Hybridoma 9430
α-PFR A/C	Mouse	Monoclonal	1/2000	(Kohl *et al.*, 1999) (Manchester), Hybridoma L13D6
α-PKAC1 ps36	Rabbit	Polyclonal	1/250	Hybridoma SA1024
α-RxxS/T	Rabbit	Polyclonal	1/1000	Cell signaling technology, Cat.No 9621
α-Ty	Mouse	Monoclonal	1/2000	(Kohl *et al.*, 1999) (Manchester), lgG1-Hybridoma BB2
α-HA	Mouse	Monoclonal	1/1000	By Elisabeth Kremmer, Hybridoma 12CA5

2.1.6.2 Secondary antibodies

Name	Type	Dilution	Usage	Catalog N	Origin
IRDye 800CW	goat anti-mouse	1/15000	Western Blot	926-32210	LI-COR, Bad Homburg
IRDye 680LT	goat anti-rabbit	1/50000	Western Blot	926-68021	LI-COR, Bad Homburg
Alexa Fluor 633	goat anti-rabbit	1/2000	Immuno-fluorescence	A21094	ThermoFisher Scientific, Darmstadt
Alexa Fluor 594	goat anti-mouse	1/2000	Immuno-fluorescence	A11005	ThermoFisher Scientific, Darmstadt

2.1.7 Enzymes

Name	Catalog	Origin
Q5® DNA polymerase	M0491L	NEB, Frankfurt
Taq DNA polymerase	M0267S	NEB, Frankfurt
T4 DNA ligase	M0202S	NEB, Frankfurt
Restriction endonucleases	Various	NEB, Frankfurt
Calf intestine alkaline phosphatase	M0290	NEB, Frankfurt

2.1.8 Chemicals and compounds

2.1.8.1 Compounds

Compound	Stock solution	Catalog Number	Supplier
1-Benzyl-Inosine	20 mM, DMSO	An aliquot from Yuri Volpato	Santa Cruz
2'-deoxyadenosine	50 mM, DMSO	099K1642V	Sigma Aldrich
5-Iodo-Tubercidin	50 mM, DMSO	An aliquot from Sabine Bachmaier	BioLog, Bremen
7-cyano-7-deaza-Inosine	20 mM, DMSO	C214-05	BioLog, Bremen
Adenosine	50 mM, H_2O	SLBL0630V	Sigma Aldrich
cAMP	50 mM, H_2O	BCBX5560	Sigma Aldrich
Dipyridamole	50 mM, DMSO	Lot No: 12809MA	Sigma Aldrich
Guanosine	50 mM, H_2O	BCBQ4147V	Sigma Aldrich
Inosine	50 mM, H_2O	SLBP5740V	Sigma Aldrich
Sangivamycin	50 mM, DMSO	An aliquot from Sabine Bachmaier	Berry & associates
Tubercidin	50 mM, DMSO	T0642	Sigma Aldrich
Toyocamycin	50 mM, DMSO	T3580	Sigma Aldrich

2.1.8.2 Chemicals

Agarose	**Roth, Karlsruhe**
BSA	Roth, Karlsruhe
dNTPs	Roche, Mannheim
DAPI (4, 6 Diamidino-2-phenylindole)	Sigma Aldrich, Taufkirchen
Ethidium bromide 1% solution (Cat No: SH3A8023.01)	Roth, Karlsruhe
Fetal Calf Serum	Capricorn scientific, Germany
IMDM powder	Life technologies, California
Ni-NTA	Thermo Scientific Pierce, Schwerte
Protease inhibitor tablet (EDTA-free)	Roche, Mannheim
Streptomycin-Penicillin 100x	Sigma Aldrich, Darmstadt
SDM-79 CGGGPPTA powder (Custom made deficient carbon source)	GE Healthcare Life Sciences, München
Standard chemicals	AppliChem, Darmstadt; Merck Millipore, Darmstadt; Roth, Karlsruhe
Common organic solvents	AppliChem, Darmstadt; Merck Millipore, Darmstadt; Roth, Karlsruhe

2.1.9 Medium and buffers

Medium and buffers used in the thesis are listed with individual methods.

2.1.10 Kits

PureYield™ Plasmid Miniprep System	Promega, Mannheim
PureYield™ Plasmid Midiprep System	Promega, Mannheim
ReliaPrep™ gDNA Tissue Miniprep System	Promega, Mannheim
Hi Yield® Gel/PCR DNA fragment Extraction Kit	SLG, München
NanoBiT® PPI Starter System	Promega, Mannheim
Nano-Glo® Luciferase Assay System	Promega, Mannheim

2.1.11 Consumables

1 kb DNA ladder	NEB, Frankfurt
96-well plate (white, opaque)	Greiner Bio-one, Frickenhausen
Amicon® Ultra 15 mL Centrifugal Filters (3000 NMWL)	Merck Millipore, Darmstadt
Blue Pre-stained Protein Standard (11-250 kDa)	NEB, Frankfurt
BTX cuvette, 2mm gap	VWR International, Darmstadt
Cell culture flask	Greiner Bio-one, Frickenhausen
CELLSTAR® Polypropylene Tube (15 ml & 50 ml)	Greiner Bio-one, Frickenhausen
PD-10 desalting column	GE Healthcare Life Sciences, München
Dialysis membrane (Cut-off, 14 kDa)	Sigma Aldrich, Taufkirchen
Sterile filter 0.22 µm	Merck Millipore, Darmstadt
Odyssey® blocking buffer (TBS)	LI-COR, USA

2.1.12 Equipment

Amaxa Nucleofector II	Lonza, Köln
CASY I Cell Analyzer (Modell TTC)	Schärfe System, Reutlingen
Geldoc 2000	Bio-Rad Munich
Nano Drop-1000 Spectrophotometer	Peqlab, Erlangen
French® pressure cell press	Glen Mills Inc, USA
BD FACSAria™ III cell sorter	Becton Dickinson, Heidelberg
ÄKTA pure protein purification system	GE Healthcare Life Sciences, München
Incubator Thermo Heracell 240	Thermo Scientific, Darmstadt
DeltaVision Elite microscope	GE Healthcare Life Sciences, München
Axiovert 25 microscope	Carl Zeiss, Jena
PowerPac™ HC Power Supply	Bio-Rad, München
Odyssey® CLx Imaging system	LI-COR Biosciences, Bad Homburg
Prometheus NT.48 nanoDSF analyzer	Nano Temper, München
MicroCal PEAQ-ITC	Malvern Panalytical, United Kingdom
GloMax® Discover plate reader	Promega, Mannheim
TECAN Infinite M200 Pro, plate reader	TECAN group, Männedorf, Schweiz

2.1.13 Software

CLC Main workbench 7.9	CLC bio, a QIAGEN® company
EndNote X9	Thomson Reuters, USA
Fiji is ImageJ	https://imagej.net/Fiji
GraphPad Prism 8	GraphPad, San Diego, USA

Image Studio™ Lite	LI-COR, USA
PR. Stability Analysis	Nano Temper, München
PyMol 2.3	Schrödinger, USA
Schrödinger Maestro	Schrödinger, USA
UCSF Chimera 1.14	University of California, USA
Affinity Photo	Serif, UK

2.2 Methods

2.2.1 *Trypanosoma brucei*

2.2.1.1 Cultivation of BSF cells

HMI-9 (1 L)	Iscoves modified medium (IMDM) powder (+ L-Glutamine, - $NaHCO_3$), pH 7.4
HMI-9 supplements (1 L)	3.024 g $NaHCO_3$; 136 mg hypoxanthine; 28.2 mg bathocuproine sulfonate; 20 mM 2-mercaptoethanol; 39 mg thymidine; 100,000 U penicillin; 100 mg streptomycin; 182 mg cysteine; 10% FCS

The BSF cells of Lister 427, variant monomorphic strain MiTat1.2 (Cross and Manning, 1973) and Matrix independent clones of pleomorphic strain AnTat1.1(Delauw *et al.*, 1985; Bachmaier *et al.*, 2020) were cultured in complete HMI-9 medium in ventilated flasks in a 37°C incubator. The HMI-9 medium supplements are listed above. The incubator is humidified and contains 5% CO_2 atmosphere. Cells were grown at exponential phase and the density was regularly monitored by manually counting with Neubauer cell chamber. The cell density was kept under 1×10^6 cell/ml. Antibiotics were added according to the selectable marker expressed by the cells. All the operations concerning *T. brucei* cell culturing were done in sterile ventilation hood to avoid contamination.

2.2.1.2 Cultivation of PCF cells

SDM-79 stock (850 mL)	100 g SMD-79 CGGGPPTA powder, 0.091 M Sodium pyruvate, 50 mM L-threonine, 0.265 mM L-proline, 200 mM L-glutamine
SDM-79 complementation (1 L)	SDM-79 stock (850 ml), 10 mg hemin, 0.01 M D-Glucose, 0.01 M Glycerol, 100 mg penicillin/streptomycin, 10% FCS

The PCF cells of pleomorphic strain AnTat1.1 were cultured in complete SDM-79 medium at 27°C in flasks with sealed cap in a non-humidified incubator. The SDM-79 medium was supplemented as shown above. Cells were grown at exponential phase and regularly monitored by microscope and counting with a CASY cell counter. Cell density was kept between 2×10^6 to 2×10^7 cell/mL. Antibiotics were added according

to the selectable marker expressed by the cells.

2.2.1.3 Freezing and thawing cells

BSF freezing medium	Complemented HMI-9 medium, 10% (v/v) FCS, 10% (v/v) glycerol, filtered by 0.22 µm Millipore membrane filter
PCF freezing medium	Complemented SDM-79 medium, 10% (v/v) FCS, 10% (v/v) glycerol, filtered by 0.22 µm Millipore membrane filter

To prepare a stabilate, 5 x 10^6 BSF cells or 5 x 10^7 PCF cells were harvested at 1400 g (BSF) or 900 g (PCF) at 4°C for 10 min. Cell pellet was resuspended in 1 ml pre-cooled BSF or PCF freezing medium. The cell suspension was transferred to a cryo-tube placed in a strata cooler box. The box was immediately stored at -80°C. For long-term storage, stabilates were stored at -150°C.

To thaw frozen cells, a stabilate was quickly thawn in a 37°C (BSF)/27°C (PCF) water bath and washed by 9 ml pre-warmed HMI-9 (BSF)/SDM-79 (PCF) medium by centrifugation. After that, the cells were resuspended in the corresponding culture medium and cultured with appropriate conditions.

2.2.1.4 Stable transfection of BSF cells

Electroporation stock buffer (3x stock)	200 mM Na_2HPO_4, 70 mM NaH_2PO_4, 15 mM KCl, 150 mM HEPES pH 7.3
Electroporation buffer (1x fresh)	600 µl ddH_2O, 350 µl Electroporation stock buffer, 100 µl 1.5 mM $CaCl_2$

2 x 10^7 BSF cells in mid-log phase (5 to 8 x 10^5 cells/ml) were harvested by centrifugation at 1400g for 10 min, RT. After resuspension with 100 µL cold electroporation buffer, the cell suspension was transferred to a 2 mm gap transparent cuvette containing 10 µL linearized DNA (1 µg/µL in H_2O) on the bottom and mixed. The electroporation was performed with the AMAXA Nucleofector® II using program X-001 for mouse T-cell (CD8+). Subsequently, the cell-DNA mixture was transferred to 30 mL prewarmed complemented HMI-9 medium. For clonal selection, 10-fold serial dilutions were performed in 2 tubes contain 27 mL HMI-9 medium. Transfected cells of different density were plated in three 24-well tissue culture plates (1mL/well) individually. 1 mL complemented HMI-9 medium containing 2x concentration of antibiotics were added to each well 6-18 h post transfection.

2.2.1.5 Differentiation of pleomorphic long-slender BSF cells

DTM medium	DTM basic medium (Overath *et al.*, 1986)

DTM supplements (1L)	10 mM glycerol, 28.2 mg bathocuproine sulfonate, 182 mg cysteine, 7.5 mg hemin

For each differentiation, 10 mL long-slender BSF cells at a density of 5 x 10^5 cells/mL were cultured for 36-48 h until reaching maximal density and the majority of cells transformed to short-stumpy BSF. The cells were harvested and resuspended with 5 mL modified DTM medium supplemented with 6 mM cis-aconitate in order to induce the differentiation. After culturing at 27°C for 24 h, 5 mL SDM-79 medium supplemented with 1x concentration of antibiotics was added to the DTM culture. The cell density was kept under 2x10^7 cells/ml. Newly differentiated PCFs usually grow a bit slower but recover in few days.

2.2.1.6 PCF cells counting

CASYton	135.7 mM NaCl, 1.3 mM EDTA, 5.35 mM KCl, 1.37 mM Na_2HPO_4, 5.44 mM NaH_2PO_4, 7.14 mM NaF

PCF cell counting was performed by CASY cell counter. 25 µL cell culture was diluted 200-fold by transferring to 5 mL CASYton. The diluted cells were subjected to CASY counter using program 02 (settings for PCF).

2.2.2 Bacteria

2.2.2.1 *E. coli* culture

LB liquid medium (1 L)	10 g tryptone, 5 g yeast extract, 10 g NaCl, pH 7
LB agar plate	1 L LB liquid medium, 16 g agar

Fresh *E. coli* colonies on the agar plate were inoculated to a glass tube containing 5 mL liquid LB medium with a toothpick or a sterile pipette tip. After inoculation, the bacteria were cultured overnight at 37°C, 200 rpm in a shaking incubator. For protein expression, the 5 mL cell culture is further inoculated to 500 mL LB liquid medium. For plasmid extraction, 5 mL overnight cell culture is usually enough.

2.2.2.2 Chemical competent *E. coli* cell preparation

An *E. coli* XL-10 gold or SURE colony was inoculated to 5 mL LB medium and cultured overnight. The second day, 200 mL LB medium was inoculated with 1/100 volume of the overnight culture and incubated at 37°C, 250 rpm to an optical density (OD_{600}) between 0.3 to 0.5. The cell culture was then cooled down on ice for 20 min and harvested at 4000 g for 10 min by a pre-cooled centrifuge. The cell pellet was

resuspended gently with 20 mL ice-cold sterile CaCl2 (100 mM) buffer and incubated on ice for 1 h. After that, the cells were harvest (4000 g, 10 min, 4°C) again and resuspended gently with 2 mL 100 mM CaCl2 containing 15% glycerol. 100 µL aliquots were made in Eppendorf tubes, frozen in liquid nitrogen and stored at -80°C. All washes and resuspensions were done on sterile bench.

2.2.2.3 Chemical transformation of *E. coli*

50 µL frozen competent *E. coli* cells were thawn on ice for 5-10 min, mixed with 1-3 µL plasmid DNA (> 10 pg) or alternatively 5 µL of ligation mixture and incubated on ice for 30 min. After incubation, cells were heat-shocked for 45 sec at 42°C by a heat-block and chilled for 2-3 min on ice. Cells were added to 450 µL LB medium and incubated at 37°C for 45 min, 150 rpm, on a shaker. Afterwards, appropriate volume of cells (50 µL for plasmid transfection, 500 µL for ligation mixture) was plated on LB agar plate containing required antibiotics and incubated overnight at 37°C.

2.2.2.4 Expression of recombinant *T. brucei* PKAR in *E. coli* Rosetta DE3

E. coli cells transformed with a *T. brucei* PKAR expression plasmid were plated on LB agar plate and grown at 37°C overnight. A fresh colony was inoculated to 5 mL LB medium and cultured overnight. Afterwards, the 5 mL overnight cell culture was inoculated to 500 mL LB medium in a glass flask and incubated at 37°C, 250 rpm in a shaking incubator until the OD_{600} density reaches 0.8. The flask was chilled at 4°C for 30 min while the incubator temperature was set and dropped to 16°C. From now on, the cells were ready for induction. IPTG was added to the flask with a final concentration of 0.2 mM, bacteria were further cultured at 16°C, 160 rpm overnight to obtain a maximum protein expression. After induction,1 L *E. coli* culture were harvested (5000g, 4°C, 15 min) and washed by 30 mL washing buffer (50 mM Hepes, pH 7.5, 50 mM NaCl) and centrifuging at 5000g, 4°C for 15 min. The pellet can be stored at -20°C for short-term or -80°C for long-term.

2.2.3 Nucleic acid methods

2.2.3.1 Polymerase chain reaction (PCR)

Q5® High-fidelity polymerase (NEB) was used for error free DNA amplification. The annealing temperature can be calculated on the website (https://tmcalculator.neb.com/), the extension time depends on and the length of target fragment (2 kb/min). Q5 High GC Enhancer was optional but necessary in the case

that the target DNA fragment has high GC-content and for long-primer PCR. *Taq* DNA polymerase was used for integration PCR using genomic DNA as template. The long-primer PCR reaction and program setups are following.

Template DNA (pPOT plasmids)	1	µL (25 ng)
Forward primer (10 µM)	2.5	µL
Reverse primer (10 µM)	2.5	µL
dNTP (10 mM)	1	µL
5x Q5 reaction buffer	10	µL
5x Q5 High GC enhancer	10	µL
Q5 polymerase	0.5	µL
ddH_2O	22.5	µL
Total	50	µL

Initial denaturation	94°C	5 min
30 cycles	94°C	15 sec
	65°C	30 sec
	72°C	2 min
Final extension	72°C	7 min
Hold	12°C	∞

2.2.3.2 DNA digestion and gel extraction

Plasmids and DNA fragments were digested with restriction endonucleases from NEB using the recommended conditions. Agarose gel electrophoresis was performed to ensure the efficient digestion especially for plasmid digestion. DNA gel extraction was performed using Hi Yield® Gel/PCR DNA Fragment Extraction Kits of SLG®.

2.2.3.3 DNA ligation

Plasmid and insert ligation used T4 DNA ligase (NEB) and was performed according to the instruction. A total volume of 10 µL of ligation mixture was incubated at RT for 20 min or at 16°C for 2-3 h. Plasmid: insert molar ratio is always kept between 1:3 and 1:5.

2.2.3.4 Extraction plasmid DNA from *E. coli*

Plasmid extraction was performed using Promega PureYield™ Plasmid Miniprep System or Midiprep system, depending on the demand.

2.2.3.5 Phenol-Chloroform DNA extraction

PCI solution	Phenol/Chloroform/isoamyl alcohol solution (25:24:1), Sigma-Aldrich
Elution solution	10 mM Tris-HCl, pH 8.5

PCR products used for transfection were subjected to phenol-chloroform extraction to ensure a high purity and therefore promote transfection efficiency. PCR product was topped up to 200 µL with Elution buffer and mixed with the same volume of the PCI solution in tube A. After vortex vigorously for 1 min and centrifugation at 15000g or higher speed for 5 min, the mixture separated to two phases including the aqueous phase on the top and organic phase on the bottom. DNA was dissolved in the aqueous

phase. ~180 µL of the top aqueous solution was removed and transferred to tube B. Never pick up any organic solution while removing. The left solution of tube A was mixed with 200 µL Elution buffer and subjected to vortex and centrifugation again, the top aqueous solution was removed carefully and transferred to tube B. Equal volumes of the freshly made chloroform/isoamyl alcohol solution (24:1) was added to tube B, mixed by vortex and centrifugation. The top aqueous solution was removed and transferred to tube C and ready to be precipitated.

2.2.3.6 DNA ethanol precipitation

Linearized plasmid DNA or DNA extracted by Phenol/chloroform/isoamyl alcohol was supplemented with 1/10 volume of 3M sodium-acetate, pH 7.0 and 3x volume of 100% ethanol. The mixture was mixed well and incubated at -20°C for 3 h or -80°C for half hour. Afterwards, the solution was centrifuged at 15000g, 4°C for 20 min. The DNA pellet was washed twice with 70% ethanol by centrifugation at 15000g, 4°C for 15 min. After the second wash, the ethanol was the removed and the pellet was air dried under a sterile bench and dissolved in sterile H_2O to a final concentration of 10 µg/µL.

2.2.4 Protein methods

2.2.4.1 Protein extraction from *E. coli*

The frozen *E. coli* pellet (section 2.2.2.4) can be stored at -20°C for months or -80°C for long-term. To extract protein, the pellet was resuspended with 30 mL Wash buffer supplemented with PMSF (500 µM stock in ethanol absolute), 0.5 mL DNase (10 mg/mL) and 1 mL lysozyme (10 mg/mL) at RT for 10 – 15 min on a roller shaker. During the resuspending, the French press compressor was cleaned, greased and assembled, thereby ready to use. The *E. coli* resuspension was incubated on ice for 15 min and then compressed at 20,000 psi twice by French Press. The crude lysate was centrifuged at 20,000g, 4°C for 20 min and the supernatant was kept for purification or stored at -80°C.

2.2.4.2 Ni-NTA affinity purification of His-tagged TbPKAR

Equilibration buffer	50 mM Hepes, pH 7.5, 50 mM NaCl, sterilized by autoclave
Wash buffer	50 mM Hepes, pH 7.5, 50 mM NaCl, 30 mM Imidazole, sterilized by autoclave
Elution buffer	50 mM Hepes, pH 7.5, 50 mM NaCl, 250 mM Imidazole, sterilized by autoclave

The purification was performed on Ni-NTA (HisTrap™ HP, 5 mL, GE Healthcare) by

ÄKTA Pure. HisTrap column was assembled and washed with 10 column volumes (CV) water, followed by 10 CVs equilibration buffer until the conductivity curve reaches the plateau. The *E. coli* lysate supernatant (section 2.2.4.1) was thawn and filtered through a 0.22 µm Millipore membrane to exclude debris and aggregation and then topped up to 50 mL by Wash buffer. The sample was injected to a clean Superloop column by a syringe and the Superloop was then connected properly on ÄKTA Pure. The program was set to 'manual load' and the flow rate was 2 mL/min. HisTrap column was washed with Wash buffer after the sample was loaded completely. Elution was conducted with Elution buffer, the resulting eluate was collected manually and stored at -20°C for short term.

2.2.4.3 Dialysis

ITC buffer	50 mM Hepes, pH 7.5, 50 mM NaCl

To get rid of the imidazole, the elution fraction (section 2.2.4.3) was transferred to a prepared cellulose membrane (Mw cut-off: 12,000 Da) and dialyzed against 100x volume of ITC buffer overnight at 4°C.

2.2.4.4 His-tag removal

TEV reaction buffer	50 mM Hepes, pH 7.5, 50 mM NaCl, 5 mM KCl, 5 mM $CaCl_2$

To remove the His-tag, TEV enzyme was added to the protein at a 1:500 mass ratio and dialyzed overnight against ITC buffer supplemented with 5 mM KCl and 5 mM $CaCl_2$ to enable efficient cleavage. The separation of His-tag and non-tagged TbPKAR was performed with a manual assembled Ni-NTA column containing 2 mL Ni-agarose resin. The column was washed and equilibrated with 10 column volumes (CVs) of water and ITC buffer, respectively. The TEV cleaved recombinant protein was mixed with the resin and incubated at 4°C for 30 min. The elution started with washing by ITC buffer and then by different imidazole buffers (20 mM, 40 mM, 60 mM). All fractions were collected and later analyzed by SDS-PAGE.

2.2.4.5 Removal of the ligand bound to the recombinant TbPKAR

Denaturation buffer	50 mM Hepes, 50 mM NaCl, 8 M urea, pH 7.5

In order to obtain Apo TbPKAR, 2.4 g urea and appropriate water was added to 2 mL purified protein to reach a concentration of 8 M urea. 2.5 mL denatured protein was loaded to a PD-10 desalting column (Sephadex G-25, GE Healthcare) pre-washed and pre-equilibrated with respective 5 CVs water and 5 CVs PD-10 Buffer. 3 mL

denaturation buffer was added into the column when the protein sample had entered completely. The flow-through from this step contained the protein and was collected. The PD-10 column was washed by 10 CVs with water and stored in 20% ethanol for reuse.

2.2.4.6 Refolding and purification of Apo TbPKAR

10x Refolding buffer stock	0.5 M Tris-Cl, 2.40 M NaCl, 100 mM KCl, 20 mM $MgCl_2$, 2 mM $CaCl_2$
1x refolding buffer (1 L)	100 mL 1x refolding buffer stock, 0.4 M sucrose, 1 mM DTT, top up the volume to 1 L by adding water

The stock buffer was supplemented with sucrose and DTT to make fresh Refolding buffer for dialysis. 1 mg/mL denatured Apo TbPKAR (section 2.2.4.5) was added into cellulose membrane (no more than 5 mL) and dialyzed in pre-cooled 1x Refolding buffer overnight. Denatured Apo TbPKAR refolded gradually as urea be dialyzed. For TbPKAR_RBCA mutant where the A-site was modified to bind to cAMP, 1 mM cAMP was added to the protein to aid the refolding.

The purification of refolded Apo TbPKAR was performed by size exclusion chromatography on ÄKTA Pure. After dialysis, the protein sample was concentrated to 1 mL using Amicon® Ultra-15 centrifugal filter (5.000xg, 4°C, 30 min) with a MW cut-off of 2 KDa, followed by injection to a 1 mL sample loop on ÄKTA. Refolded monomer TbPKAR passed through the size exclusion column (Superdex 200 Increase 10/30 GL) was collected manually according to the UV-280 curve.

2.2.4.7 SDS-PAGE

6x loading buffer	350 mM Tris-HCl, pH 6.8, 10% SDS, 30% v/v glycerol, 0.06% w/v Bromophenol blue, 0.6 M DTT
SDS-PAGE running buffer	25 mM Tris-Base, 200 mM glycine, 0.1% w/v SDS
Separating buffer	1.5 M Tris-HCl, pH 8.8, 0.4 % w/v SDS
Stacking buffer	0.5 M Tris-HCl, pH 6.8, 0.4 % w/v SDS

SDS polyacrylamide gelelectrophoresis (PAGE) were performed as described by (Laemmli, 1970). An SDS-PAGE gel contains stacking gel and separating gel. The recipes of stacking gel and separating gel are listed below. 10 gels were cast by Multi-Casting Chambers (Bio-Rad). Cell pellet dissolved in 6x loading buffer or protein samples were denatured at 95°C for 5 min in a heat block (Eppendorf) and sonicated 2x 30 sec in the Diagenode Bioruptor. Proteins were separated according to their molecular weight at 20 mA/gel in a vertical electrophoresis apparatus (Bio-Rad). A pre-

stained protein marker was used as the reference of protein molecular weight and for monitoring the running.

Stock solution	Separating Gel		Stacking Gel
	10%	12%	
Acrylamide/Bisacrylamide 37, 5:1	4 ml	4.8 ml	0.78 ml
Separation gel buffer/ Stacking gel buffer	3 ml	3 ml	1.5 ml
Distilled H_2O	5 ml	4.2 ml	3.7 ml
10% w/v APS (Ammonium Persulfate)	40 µl	40 µl	30 µl
TEMED	8 µl	8 µl	6 µl

2.2.4.8 Coomassie staining of SDS-PAGE gels

Staining solution	0.02% w/v Coomassie Brilliant Blue G-250, 10% w/v ammonium sulfate, 10% v/v ethanol (96%), 2% v/v phosphoric acid (85%)
Destaining solution	10% v/v ethanol (96%), 2% v/v phosphoric acid (85%)

The SDS-PAGE gel was incubated in deionized water for 10 min with 3 changes after running. The gel was placed in a staining dish covered with staining solution on a shaking incubated for 2-12 h. After that, the gel was washed by deionized water for 10 min, 2 times and followed by incubation with destaining solution for 1-2 h. To accelerate the process, the staining/destaining solution can be heated up shortly in a microwave oven. The staining solution can be reused several times.

2.2.4.9 Western Blot

Anode buffer	300 mM Tris-HCl, pH 10.4, 20 % v/v Methanol
Cathode buffer	25 mM Tris-HCl, pH 7.6, 40 mM ε-aminop cypronic acid, 20 % v/v Methanol
PBS	12 mM Na_2HPO_4, 1.8 mM KH_2PO_4, 137 mM NaCl, 2.7 mM KCl, pH 7.4
0.1% PBS-T	PBS buffer supplemented with 0.1% v/v Tween 20
0.2% PBS-T	PBS buffer supplemented with 0.2% v/v Tween 20

The protein sample resolved in SDS-PAGE gel was transferred to PVDF by semi-dry Western Blot (Kyhse-Andersen, 1984). One PVDF membrane and five Whatman papers (0.5 mm thick) were cut to the dimensions of the SDS-PAGE gel with the stacking gel removed, 6 x 9 cm. The PVDF membrane was soaked in pure methanol for 30 sec for moistening (activation) prior to washing in deionized water. In a western blot “sandwich”, three pieces of Whatman paper soaked with anode buffer should be

on the bottom and covered sequentially by a PVDF membrane, the polyacrylamide gel and two other pieces of Whatman paper soaked with cathode buffer soaked. Air bubbles between the layers were removed by pressing with a roller tool. The assembly was placed and locked in a semi-dry Western Blot chamber (Bio-Rad) and the transfer was carried out at 0.8 mA/cm^2 for 70 min.

After the protein transfer, the PVDF membrane was placed carefully in a 50 mL falcon tube and blocked with 5% non-fat milk in PBS for 1 h at RT. Primary antibodies were diluted in 0.1% PBS-T buffer supplemented with 1% w/v milk powder. Incubation was 1 hour at RT or overnight at 4°C prior to washing with 0.2% PBS-T buffer for 5 min for 3 times. Species specific fluorophore conjugated secondary antibodies were diluted in 0.1% PBS-T buffer containing 1% (w/v) milk powder and 0.02% (w/v) SDS. The incubation was performed in dark for 1 h. After washing by 0.2% PBS-T buffer for 5 min, 4 times, the membrane was quickly rinsed with running water and dried between two Whatman papers. The membrane was scanned by Odyssey® CLx imaging system. Signal analysis and quantification were performed with the software Image Studio™ Lite. For the purpose of PKA substrate phosphorylation analysis, the membrane was blocked by Odyssey blocking buffer (Li-COR) and incubated with anti-RxxS/T diluted in the buffer overnight at 4°C.

2.2.5 Immunofluorescent assay (IFA)

- **Silanization of microscope cover slip**

Cover slips were incubated with 2 N HCl for 5 min prior to rinsing with deionized water and following acetone. Subsequently, they were incubated with 2% 3-aminopropyltriethoxysilane in acetone for 2 min, followed by rinsing with deionized water. After drying between Whatman papers, the cover slips can be stored for up to one year at RT.

- **Cell fixation**

For each microscope slide 3 x 10^6 cells were harvested by centrifugation at 4℃ , 1400 g (BSF)/900 g (PCF) for 10 min. The pellet was resuspended gently with 500 µl pre-cooled medium followed by treatment with 500 µl 4% (w/v) paraformaldehyde (PFA) for 5 min at 4°C. The fixed cells were washed 3 times with 1 mL PBS and resuspended with 50 µl PBS per slide. These cells now can be used for immunostaining or stored at 4°C for several days.

- **Immunostaining**

To treat multiple groups of cells simultaneously, the silanized cover slips were placed in 6-well plates. Fixed cells from the last step were dropped (approx. 50 µl) onto the center of cover slip and incubated for 10 – 30 min. The cover slips were subsequently gently washed twice with 1 mL PBS to remove unattached cells. Cell permeabilization was performed by incubation with 0.2% Nonidet-P40 in PBS for 5 min, following with 2 times washing with PBS.

For immunostaining, the cells were blocked with 2 mL 1% BSA in PBS for 1 h. Primary antibodies were added directly to the blocking solution with appropriate dilution (α-Ty1 = 1:500, α-PKAR = 1: 25) and incubated for 1 h. After washing 3 times with PBS for 5 min, the cells were incubated with Alex-Fluor conjugated secondary antibodies diluted in 1% BSA in PBS for 1 h in the dark, followed by 3 times washing with PBS for 5 min. Nuclei and kinetoplasts were stained with 0.1 µg/mL DAPI in PBS for 5 min. After 3 times wash with PBS and one time with deionized water, the cover slips were dried carefully using the edge of Whatman paper and mounted with one drop of Vectashield Mounting Medium (vector Laboratories Burlingame) on microscopic slides for anti-fading. The four edges of the cover slip were sealed with nail polish carefully while not moving the cover slip. Cells were imaged with the GE DeltaVision Elite microscope using 100-fold oil objective lens. The images were analyzed with software Fiji.

2.2.6 Live cell imaging on agar pads

Live trypanosomes were temporarily fixed on agar pads for microscopic imaging. The agar pads were prepared as following. 2% agarose were dissolved in PBS by heating. 2-3 layers of adhesive tape was pasted up along the two short edges of a microscope glass slide, creating a mold (2 mm in depth) in between. The agarose PBS solution was pipetted in the middle of the mold and then covered by a second slide, resulting in a ‘sandwich’ architecture. The big agar pad formed in between the slides was cut to small squares and transferred to individual microscope slides.

1 x 10^7 BSF or PCF cells were harvested by centrifugation at 1400 g or 900 g and washed twice with PBS, followed by resuspending with 100 µl PBS supplemented with 1% (w/v) glucose. 10 µl cell suspension was pipetted on an agar pad and covered with a cover slip, the cells were imaged with GE DeltaVision Elite microscope.

2.2.7 NanoBiT assay

PBSG buffer	PBS buffer, 1% w/v D-glucose
NanoLuc substrate	Furimazine, from Nano-Glo® Luciferase Assay system, Promega
Cell lysis buffer	Nano-Glo® Luciferase Assay Buffer, Promega

NanoBiT reporter assay was performed in trypanosomes expressing Nano-luciferase fragments, LgBiT and SmBiT, according to (Dixon *et al.*, 2016). 5 x 10^6 cells were harvested by centrifugation (37°C, 10 min, BSF: 1400 g; PCF: 900 g) and washed by pre-warmed PBSG. After washing, cell pellet was resuspended with 1 mL 37°C pre-warmed PBSG. The cell suspension was incubated at 37°C for 10 min for equilibrating and subsequently transferred to 96-well plates (100 µL/well) by multi-channel pipette. NanoLuc substrate was diluted 100-fold by PBSG and added to the wells (25 µL/well). Luminescence signal detection was carried out in Tecan Infinite® 200 Pro Plate reader (TECAN). The plate chamber of Tecan should be pre-warmed to 37°C before measurement. The reading program settings are: Orbital shaking, duration 6 s, amplitude 2 mm; integration time, 500 ms.

To measure the dose response curve of PKA activation by a compound, the stock solution of the compound was firstly diluted to 10 mM and then serially diluted 1:10 in its solvent (mostly DMSO), resulting in a serial of concentrations, 100 nM, 1 µM, 10 µM, 100 µM, 1 mM, 10 mM. Different concentrations of the compound were added into different rows of a 96-well plate. 3 wells of a row were added with the same concentration of compound (1 µL/well) for technical triplicates. Now, one can add either live trypanosomes or permeabilized trypanosomes to the plate for assessing PKA activation.

To perform NanoBiT assay with live cells, the cells were washed and resuspended as described above. After transferring the cell suspension to the prepared 96-well plate by a multi-channel pipette (100 µL/well), a 15 min incubation was performed. 25 µL 100-fold diluted substrate was added to each well post incubation. Luminescence measurement was carried out with the same settings as described above.

To perform NanoBiT assay with permeabilize cells, 5 % (v/v) Nano-Glo® Luciferase Assay Buffer (Promega) was added to the prepared cell suspension after equilibrating at 37°C. Then the permeabilized cells were added to the 96-well plate by a multi-channel pipette (100 µL/well). The plate should be incubated at 37°C for 5 min prior to addition of Nluc substrate (25 µL/well, same as above). The Tecan plate reader settings were the same as described above.

To perform a competition assay, the antagonist, for example, 10 µM compound MB052, was added to the permeabilized cells and stood for 2 min. After that, the treated cells were transferred immediately to a 96-well plate added with different concentrations of agonist (like adenosine). The plate was incubated at 37°C for 5 min prior to addition of Nluc substrate (25 µL/well, same as above). The Tecan plate reader settings were the same as described above.

2.2.8 NanoLuc-BRET assay

The BRET assay based on the ultrabright Nano-luciferase was designed and developed to monitor *T. brucei* PKA dissociation and achieve cell sorting by FACS as described by (Kim & Grailhe, 2016). 1 x 10^6 BSF cells expressing Nanoluc-PKAC1 and mCherry-PKAR were harvested by centrifugation (37°C, 10 min, 1400 g) and washed by pre-warmed PBSG, followed by resuspending with 1 mL pre-warmed PBSG. Compound of various concentrations (3 replicates/concentration) and 100 µL cells were added into 96-well plate sequentially using multichannel pipette. NanoLuc substrate was diluted 100-fold by PBSG and added to the wells, 25 µL/well. WT cells were treated in the same way and served as control. The measurement was performed with GloMax® plate reader (Promega). The settings are listed following: Filter 450 BP (8 nm), 600 LP; Integration time, 300 ms; temperature, 37°C; orbital shaking for 10 sec, 300 rpm, amplitude 1 mm. The BRET ratio was calculated automatically after measurement. Normalization was done by subtracting the background signal measured from wild type cells.

2.2.9 BRET signal detection by flow cytometry

NanoBRET cells were harvested and resuspended with PBSG at a density of 1x 10^6 cells/mL and incubated at a 37ºC incubator. NanoLuc substrate was added to the cells at the ratio of 1: 100 prior to FACS sorting. Samples were analyzed with the FACSAria™ II cell sorter (Becton Dickinson). Since at least one excitation had to be included while measuring, the near UV laser (375 nm) for DAPI was used, which has the minimal crossbleeding into YFP and mCherry channels. The resulting data were evaluated by the software FlowJo 8.8.6.

2.2.10 Isothermal Titration Calorimetry

The interactions between a variety of biomolecules, either protein-ligand interaction, intra-protein interaction or protein-nucleic acid (DNA/RNA) interaction, involve the molecular recognition process, which is accomplished by multiple non-covalent bonds

between the complementary binding partners. Characterization of thermodynamic parameters during a binding event as well as the correlation with protein/chemical structures is pivotal for understanding the molecular recognition process. Isothermal titration calorimetry (ITC) is the only label-free quantitative technique that determines a number of thermodynamics parameters, including binding affinity (K_d), enthalpy (ΔH) and binding stoichiometry (n) with calorimetric titration. From the measured parameters, Gibbs free energy changes (ΔG) and entropy (ΔS) can be determined using the following formula, $\Delta G = -RT \ln K_d = \Delta H - T\Delta S$, where *R* is the gas constant and *T* is the absolute temperature (Jelesarov & Bosshard, 1999; Luis García-Fuentes, 2011). Thus, ITC can provide a full thermodynamic description of an interaction system. With the development of techniques, ITC has become increasingly sensitive and been widely used in pharmaceuticals in a bid to obtain the thermodynamic features of potential compounds for further optimization (Holdgate, 2007).

ITC bufffer	50 mM Hepes, pH 7.5, 50 mM NaCl

Proteins used for ITC were freshly produced (see section 2.2.4.6). The natural nucleosides like inosine, guanosine and adenosine were dissolved in ITC buffer to 20 mM, the synthesized nucleoside derivatives were dissolved in 100% DMSO to make a 20 mM stock. A 100 µM compound of working concentration was made by adding 5 µL stock solution to 995 µL the same ITC buffer that used for protein purification by size exclusive chromatography to minimize the buffer mismatches which could cause extra heat release when ligand be injected to the protein chamber. Protein sample was diluted to either 5 µM or 10 µM according to the expected stoichiometry value. For example, WT TbPKAR199-499 APO is expected to have a stoichiometry of 2 and thus was diluted to 5 µM. On the other hand, TbPKAR199-499_RBCA APO mutant has only one nucleoside binding site and was diluted to 10 µM. To minimize the buffer mismatch, protein sample was supplemented with the same percentage of DMSO when titrated with 100 µM the synthesized compounds.

The ITC measurement was performed with MicroCal PEAQ-ITC machine (Malvern). Approximately 280 µL protein sample was loaded slowly but continuously to the sample cell using a syringe to avoid air bubbles which causes significant noise. The measurement was carried out at 25ºC with a standard difference power (DP) of 10 µcal/s between the reference and sample cells. The compound was loaded into the syringe (approx. 40 µL) and then placed into the sample cell. A series of 13 to 19 injections (1.5 to 2 µL per injection) was set to titrate the protein. The difference power in between the two cells was calculated and the peak was recorded per injection. After

titration, the data was analyzed by software MicroCal ITC Analysis v1.1. The sample cell and syringe were cleaned with detergent and rinsed after every measurement.

2.2.11 nanoDSF

nanoDSF determines protein stability during thermal denaturation by measuring the intrinsic fluorescence intensity change, while the conventional DSF methods determine the fluorescence intensity change of the fused GFP **(Moreau & Schaeffer, 2013)** or labeled protein dye **(Semisotnov *et al.*, 1991)**. Protein's intrinsic fluorescence is mainly originated from tryptophan and partially tyrosine. Tryptophan emission peak and fluorescence intensity are dependent on the close surroundings and therefore they vary during the process of protein unfolding. The ratio of 350 nm and 330 nm fluorescence (F350/F330) has been used to indicate the conformation change of protein during unfolding. In the nanoDSF instrument, Prometheus (NanoTemper), protein sample in glass capillary is subjected to progressive heating from 20°C to 95°C, the fluorescence at 350 nm and 330 nm are measured constantly. The correlation of F350/F330 and temperature gradient can be used to calculate the melting temperature (Tm), which indicates the temperature point that 50% protein are unfolded.

In order to assess a large number of compounds, the nano Differential Scanning Fluorimetry (nanoDSF) was used to evaluate the protein stability change upon compound binding. Proteins produced from (section 2.2.4.6) was diluted to 10 µM using ITC buffer and transferred to PCR 8-strip tubes, followed by addition of 1 µL 10 mM compound stock (dissolved in pure DMSO) resulting in a 100 µM final concentration. Control group was set by adding 1 µL DMSO to the protein. The mixture was incubated at RT for 10 min to get complete binding reactions. High sensitivity glass capillaries (Nano Temper) were subsequently applied to take the protein sample (approx. 10 µL/capillary) and arrayed on the sample tray sequentially. A maximum of 48 capillaries can be measured at a time. For each compound or each concentration of a certain compound, a least two replicates were applied. In most of our experiments, temperature increased from 20°C to 90°C and the heating rate was set to 1°C per min. The data was analyzed by software PR. Stability Analysis (nanoTEMPER).

3 Results

3.1 Establishment of NanoBiT assays for assessing dynamic PKA dissociation *in vivo*

PKA activation is a dynamic and reversible process presenting as holoenzyme dissociation in the presence of ligand. In order to identify the domains involved in R-C holoenzyme activation and explore the mechanisms behind, a sensitive reporter assay directly measuring PKA activation is of great importance. The approach currently applied for measuring PKA activation *in vivo* is a reporter assay based on VSAP phosphorylation (PhD thesis Kramer, 2004). This assay indirectly indicates PKA activation by the phosphorylation of a PKA-specific substrate, VSAP, upon different stimuli such as cold shock and activators *in vivo*. Another approach applied *in vitro* is a radioactive kinase activity assay (PhD thesis Githure, 2014), which uses γ-^{32}P labelled ATP and measures the radioactivity change of the PKA specific substrate kemptide to indicate the activity of purified kinase. Both approaches work well but do not directly measure the dynamic dissociation/association of PKA. Furthermore, they are technically complicated or labor intensive. VASP assay requires to perform a series of western blots for quantifying VASP phosphorylation. In comparison, *in vitro* kinase assay is more accurate and easier to operate, while the preparation of active *T. brucei* PKA holoenzymes is relatively difficult and the protein sample is unstable in storing. To solve the problems, we aimed to establish a convenient *in vivo* reporter assay that can be used for measuring real-time PKA dissociation/association with simplified steps.

3.1.1 Establishment of NanoBiT assay in *T. brucei*

NanoLuc Binary Technology (NanoBiT) is a structural complementation reporter assay that was developed based on an engineered luciferase, NLuc (Dixon *et al.*, 2016). It has been widely used for protein-protein interaction (PPIs) studies in many fields (Shetty *et al.*, 2020; Wells *et al.*, 2020; Azad *et al.*, 2021). According to the tertiary structure, the full length NLuc was cleaved into two fragments, LgBiT (17.6 kDa) and SmBiT (11 amino acids), which undergo further engineering to diminish their individual enzymatic activity as well as the intrinsic binding affinity to an extend (K_D = 190 μM) so the behavior of their fusion proteins is not affected. The two fragments are able to form a functional complex when brought in proximity less than 10 nm by the interacting proteins like PKAR and PKAC1 (Fig 3.1).

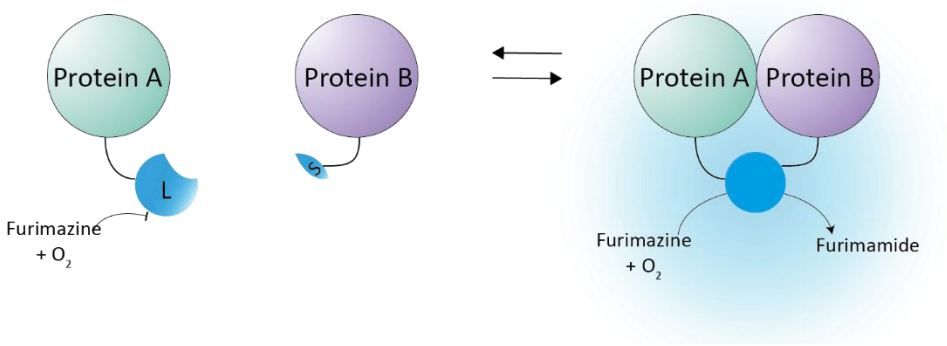

Fig 3.1 schematic representation of NanoBiT assay

3.1.1.1 Screening for the optimal fusion pattern

Appropriate fusion of the NanoBiT fragments to the target proteins is critical for the functional complementation assay. For the mammalian PKA holoenzyme, N-terminal fusion to PKAR and PKAC has proven to be feasible (Dixon *et al.*, 2016). However, in consideration of the unconventional large N-terminal domain of TbPKAR, the feasible fusion pattern maybe different. A total of 8 different combinations can be generated as depicted on Fig 3.2. The constructs of the 8 combinations were made.

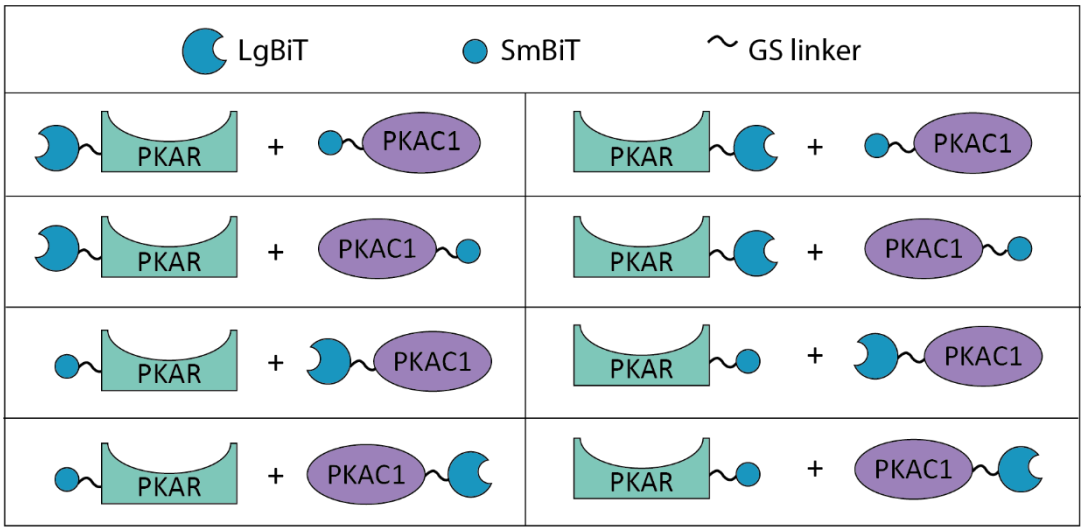

Fig.3.2 8 possible combinations of NanoBiT fragments and PKA subunits.

3.1.1.2 Generation of NanoBiT cell lines

In order to minimize the side effects caused by changes of cellular PKA level, LgBiT and SmBiT were designed to insert to the endogenous PKA gene loci. The pPOTv4 plasmid vector was therefore used to insert NanoBiT fragments to either sides of the target gene through homologous recombination (Dean *et al.*, 2015). In the plasmid, SmBiT (Fig 3.3, A) or LgBiT (Fig 3.3, B) flanked by a linker sequence encoding

GSSGGGGSGGGGSSG at one site was placed between two resistance marker genes. The GS linker was expected to improve the flexibility of the NanoBiT fragments and thereby promote the complementation. 5' and 3' untranslated regions (UTRs) from various trypanosomal genes such as *actin*, *aldolase* and *PFR2* were used, enabling efficient processing and expression of the resistance markers and transgenes. As depicted in Fig 3.3 A, in order to insert a tag to the 3' end of the target gene, a long forward primer containing the last 80 bp, but excluding the stop codon, of the target gene and 20 bp of the GS linker was synthesized. The first 80 bp serves as homology arm for homologous recombination with the endogenous target gene, while the last 20 bp is used for amplifying the insert sequence from the pPOTv4 plasmid. Accordingly, the reverse primer contains the first 80 bp of the 3' UTR of the target gene and 20 bp of plasmid backbone. For N-terminal tagging, a forward long primer consisting of the last 80 bp of the 5' UTR of the target gene and 20 bp of the plasmid backbone and a reverse primer consisting of the first 80 bp of the target gene and then 20 bp of the GS linker were used (Fig 3.3 B).

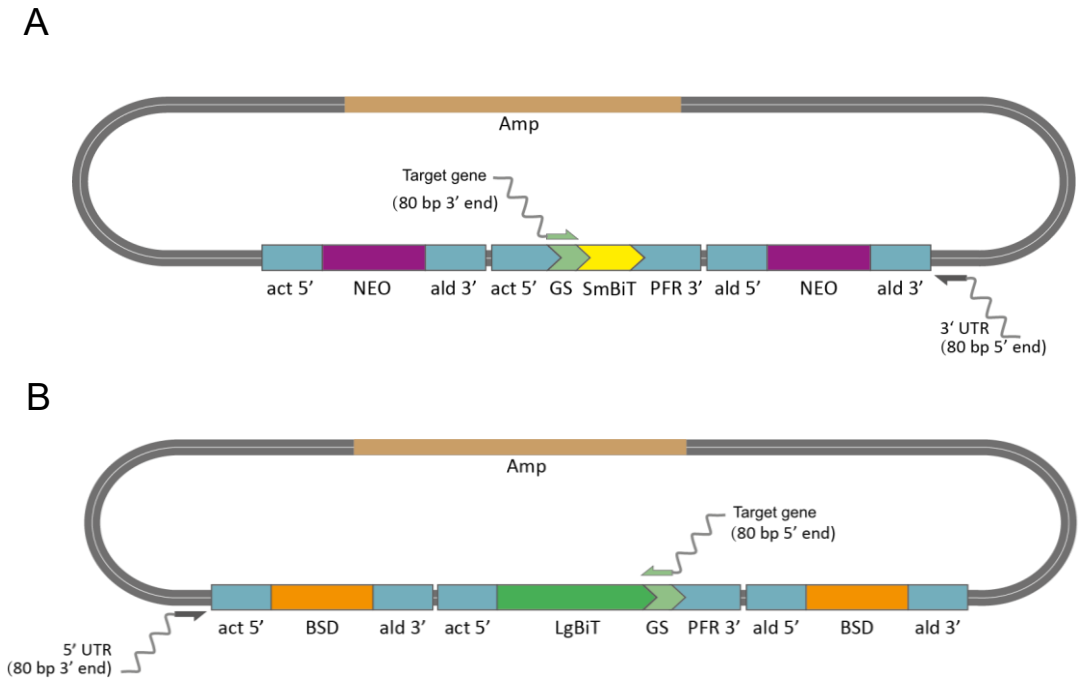

Fig 3.3 pPOTv4 plasmids for *in situ* tagging of PKA genes. A, pPOTv4_GS_SmBiT_NEO; B, pPOTv4_BSD_LgBiT_GS.

The inserts were amplified using the designed long primers as described in 2.2.3.1. Transfections were carried out as described in 2.2.1.4 using MITat1.2 wild type as parent cell line. A series of cell lines were obtained and 2 - 3 clones of each cell line

were analyzed by western blot. The tagging of *PKAC1* gene was problematic, only SmBiT_PKAC1 was detected by Western blot, as shown in Fig. 3.4 A. A similar phenomenon was observed previously in the lab when tagging *PKAC1* with fluorescent proteins, only N-terminal tagging was achieved. Thus, the possible combinations are limited to two. PKAR is detected as two bands on western blot, due to a genetic polymorphism (Schmitz, 2011). *LgBiT* sequence can be integrated to either alleles of *PKAR* in transfection. As a result, the detected bands of LgBiT-PKAR were slightly different in size among the clones. The cell line expressing SmBiT-PKAC1, which is denoted as SmC1, was used for further gene manipulation. *LgBiT* sequence was integrated to either terminal of *PKAR* by homologous recombination. The generated cell lines were referred to as SmC1/LgR and SmC1/RLg in the thesis. As shown in Fig 3.4 B and C, LgBiT_PKAR and PKAR_LgBiT were detected by Western blot, albeit their expression levels are much less than the endogenous PKAR.

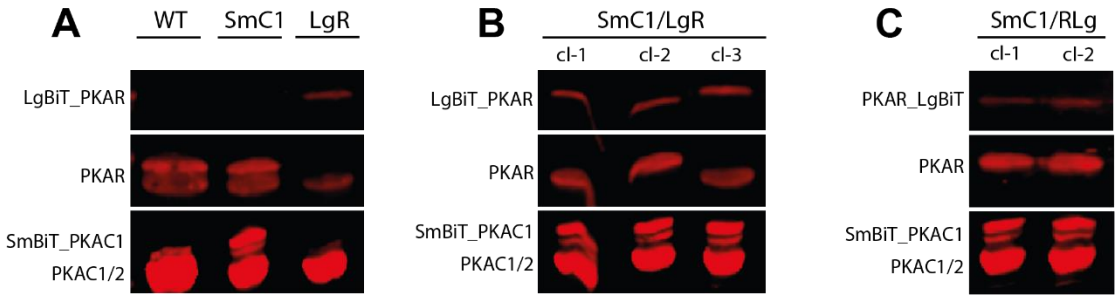

Fig 3.4 Western blot analysis of NanoBiT fused PKA subunits expression. Anti-PKAR and anti-PKAC1/2 were used in the experiment. The experiment was done as described in 2.2.4.9. Membranes were scanned by Image Studio™ Lite.

3.1.1.3 Luminescence was detected in SmC1/LgR and SmC1/RLg cell lines

Luminescence was measured in the generated cell lines. As shown in Fig 3.5 A, cell line SmC1 and LgR showed only background signal, while cells of SmC1/LgR emited strong luminescence signal. Luminescence intensity was compared between the clones of SmC1/LgR and SmC1/RLg cell lines. Cells were harvested and resuspended to the same density in PBSG. The luminescent intensity was measured as described in 2.2.6. For both cell line, clone1 showed the highest luminescence signal (Fig 3.5B and C). Clone 3 of SmC1/RLg showed a comparable signal intensity to clone 1. This result demonstrates that the fusion of LgBiT on either side of PKAR is able to complement with the SmBiT fused on the N-terminal of PKAC, suggesting N- and C-terminus of PKAR are in similar proximity to the PKAC N-terminus.

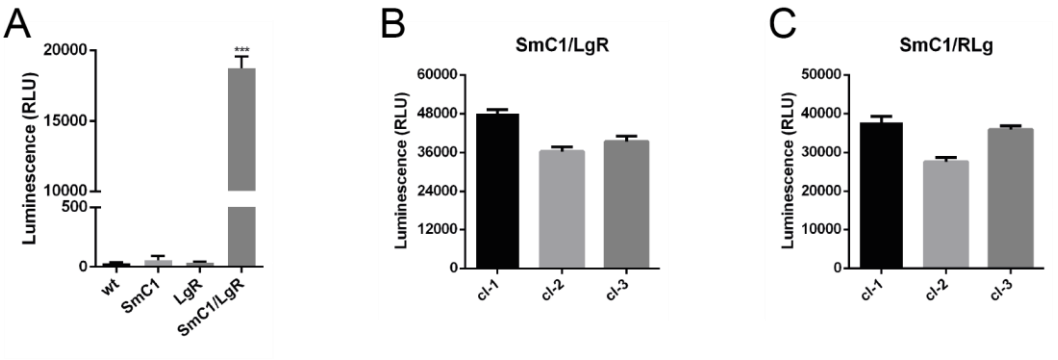

Fig 3.5, Measuring luminescence signal from the generated NanoBiT assay cells. A, luminescent signal in cells expressing one or both of the fusion proteins, the same cell number was used for each cell line, standard deviations were from 3 replicate wells. B, luminescent intensity comparison of SmC1/LgR clones. C, luminescent intensity comparison of SmC1/RLg clones. Same cell number was used for each clone in plot B and C. The standard deviations were calculated from 3 replicate wells.

3.1.1.4 Optimization of NanoBiT assay

Clone 1 of SmC1/LgR cell line was then used for further optimization of the assay. The NanoLuc substrate is commercially available from Promega but it is costly especially for large-scale compound screening. The recommended substrate dilution ratio in the official manual is 1/20, which is excessive. The details of the commercial substrate are not disclosed by Promega. Therefore, a range of substrate concentrations were tested as shown in Fig 3.6 A. The 100-fold diluted substrate is shown to sufficiently produce comparable luminescence signal without significant decrease of signal half-life (Fig 3.6 B). Therefore, a 1/100 dilution of substrate was used in the following experiments. The luminescence signal slightly rose or kept stable in the first 2 min of 1/20, 1/50 and 1/100 dilutions, but it dropped from the beginning in other higher dilutions. The luminescence decay is mainly due to the degradation of substrate in aqueous solution and the cytotoxicity of the solvent of substrate. Subsequently, the relationship between cell number and luminescence intensity was evaluated. Cells were harvested and resuspended to $1x10^7$ cells/ml, a 2-fold series dilution was performed afterwards. The same volume of cell suspension was transferred to wells of a 96-well plate and luminescence was measured. As shown in Fig 3.6 C, the luminescence intensity increased in proportion to cell number.

The half activation constant (EC_{50}) is the most important parameter for evaluating activation of PKA by ligands. Many factors can influence the EC_{50} value during *in vivo* measurement, such as temperature, pH, solution and incubation time. BSF

trypanosomes are in mammalian blood, so the temperature is strictly kept at 37°C during measurement. PBS buffer supplemented with 1% glucose (PBSG) was used to resuspend the cells and dilute the substrate. Compounds enter cells mainly through passive transport, which takes time to reach an equilibrium inside and outside the membrane. Thus, an investigation of appropriate incubation time was carried out. Cells were incubated with Toyocamycin (Bachmaier *et al.*, 2019) for different durations, luminescence was measured and the EC_{50} of Toyocamycin was calculated afterwards. As shown in Fig 3.6 D, fast incubation for 5 to 10 min results in higher EC_{50} values and lower dynamic range. One possible explanation is that the toyocamycin concentration is less in the cells than in the extracellular environment due to insufficient uptake and transport. 15-20 min incubation was found the most suitable. It provides a good dynamic range of about 10-fold or more upon treatment. Most importantly, the calculated EC_{50} is consistent with that of *in vitro* kinase assay and VASP assay ranging from 100 to 200 nM (Bachmaier *et al.*, 2019).

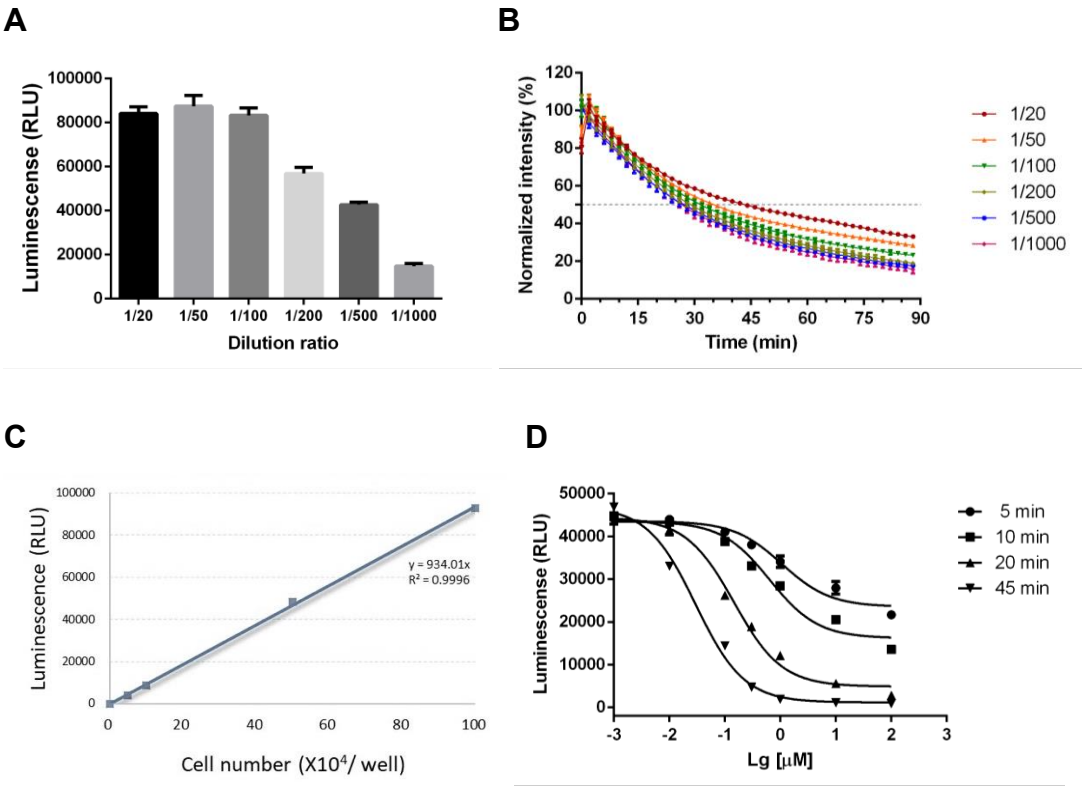

Fig 3.6, Optimization of NanoBiT assay. A, substrate concentration vs luminescence intensity. The same number of cells were used in each well. SD values were determined from three replicates. B, time-course curves of different substrate concentrations; C, standard curve of luminescent intensity to cell number; D, The span of incubation time impacts toyocamycin EC_{50}. ±SD values were determined from three technical replicates.

3.1.2 Assessing PKA activator and cold shock *in vivo*

3.1.2.1 NanoBiT assay measures comparable EC_{50} values of activators as other assays

A series of PKA activators identified previously by VASP reporter assay and *in vitro* kinase assay were evaluated by NanoBiT assay. As shown in Fig 3.7, Toyocamycin is among the best PKA activators with an EC_{50} of 354 nM; 5-Iodo-Tubercidin is slightly better in activating PKA than 5-Bromo-Tubercidin. Their EC_{50} values are 822 nM and 2.13 µM, respectively. Sangivamycin is the weakest activator and the dynamic range of the assay is much lower than other activators. This is probably due to its low membrane permeability. As a result, the calculated EC_{50} only demonstrates its potency in activating PKA in live trypanosomes. The PKA activation potency order is Toyocamycin > 5-I-Tubercidin > 5-Br-Tubercidin > Sangivamycin, the same as that of *in vitro* kinase assay and *in vivo* VASP assay. The EC_{50} values measured by NanoBiT assay are generally 2 to 3-fold higher than that measured by the other assays expect for Sangivamycin. Given that both the VASP assay and *in vitro* kinase assay measure the phosphorylation change of the PKA substrate, which is actually the secondary effect of PKA activation, a slight difference on EC_{50} is plausible. *In vivo* and *in vitro* assay can develop vast variance for some compounds due to their poor membrane permeability. Additionally, longer incubation time is required for *in vivo* assays.

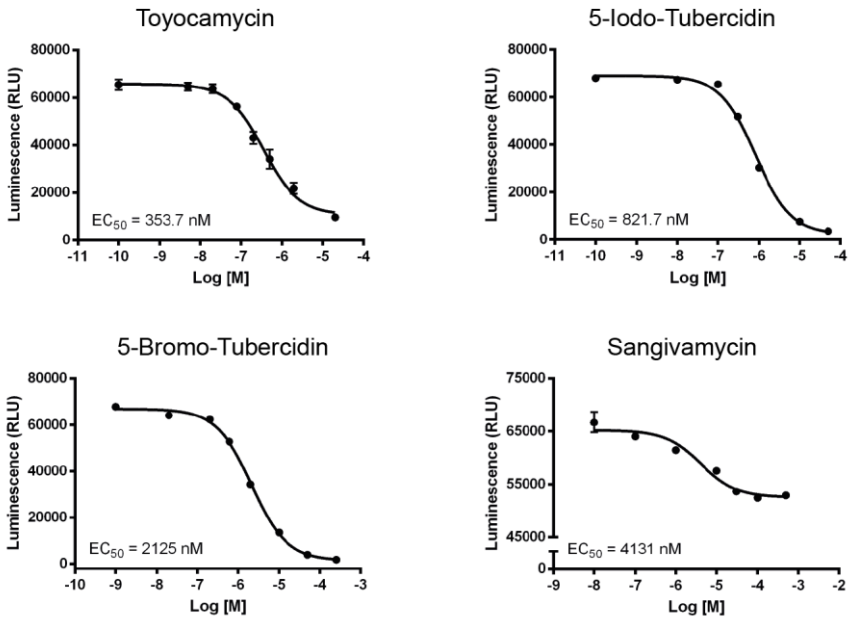

Fig 3.7, NanoBiT assay measuring PKA activation by differnt activators. Living trypanosomes were treated with different compound at 37 °C for 15 min. The luminescence signal was

measured by Tecan Infinite 200M plate reader. NanoBiT assays were performed as described in section 2.2.7. ± SD values were determined from three technical replicates The dose response curves were plotted by Graph-pad Prism 6.0.

Compound	*In vitro kinase assay EC_{50}[1,2]*	*In vivo VASP assay EC_{50}[2]*	*In vivo NanoBiT assay EC_{50}*
Toyocamycin	185 nM	88 ± 10 nM	354 ± 37 nM
5-I-Tubercidin	230 nM	390 ± 20 nM	822 ± 52 nM
5-Br-Tubercidin	≥ 700 nM	625 ± 66 nM	2.13 ± 0.12 µM
Sangivamycin	≥ 10 µM	> 10 µM	4.13 ± 1.10 µM

Table 1, A comparison of EC_{50} values measured by NanoBiT assay and other methods.

[1] data from (PhD thesis Githure, 2014)

[2] data from (Bachmaier *et al.*, 2019)

3.1.2.2 Measuring PKA activation using membrane permeabilized cells

As aforementioned, the membrane permeability of compounds has a large impact on the EC_{50} when measured with live cells. For example, the EC_{50} of inosine is measured as 37 nM by *in vitro* kinase assay, but this value is more than 1 µM by VASP assay and NanoBiT assay using live cells. The difference is mainly due to the poor membrane permeability of inosine and the limited uptake by transmembrane transporters. To quickly and accurately evaluate a number of compounds in PKA activation regardless of their membrane permeability, a modified method is needed.

To do it, the NanoGlo buffer that contains mild detergent provided in the Nano-Glo® Luciferase Assay kit (Promega) was used in the NanoBiT assay. The included detergent is able to permeabilize cell membrane without denaturing proteins in low concentrations and short incubation time. As shown in Fig 3.8 A, as more NanoGlo buffer was added, lower luminescence signal was detected. This is probably due to PKA degradation by proteases released from cell organelles. The structure complementation of LgBiT and SmBiT may also be disrupted by the detergent. Apparently, the longer the incubation takes, the lower the luminescence signal will be. Microscopic analysis found that cells were dead and floating around immediately after the addition of 5% NanoGlu buffer, indicating successful permeabilization. Therefore, 5% NanoGlu buffer and 5 min incubation were applied to the assay. After the above optimization, different activators were tested with permeabilized cells and the resulting

EC_{50} values were compared to those measured with live cells. As shown in Fig 3.8C and D, The EC_{50} values of toyocamycin and 5-Br-tubercidin are barely changed with the modified NanoBiT assay, indicating better membrane permeability of the two activators. The EC_{50} of 5-I-tubercidin, however, dropped to 161 nM. 7-cyano-7-deaza-inosine (7-CN-7-C-Inosine) is the strongest PKA activator identified so far, showing a EC_{50} of 6.5 nM by *in vitro* kinase assay (Bachmaier *et al.*, 2019). However, the measurements by *in vivo* VASP assay and NanoBiT assay with live cell revealed a EC_{50} of 838 nM and 265 nM, respectively. Using the modified NanoBiT assay, the EC_{50} of 7-CN-7-C-Inosine was measured as 12.7 nM, closing to that of the *in vitro kinase* assay. The assay dynamic range of sangivamycin improved significantly with the permeabilized cells, its EC_{50} was measured as 60 µM. In general, the measured EC_{50} values using the permeabilized cells are much closer to those measured by *in vitro* kinase assay. The modified NanoBiT assay can be used for high-throughput and unbiased PKA activator/inhibitor screening.

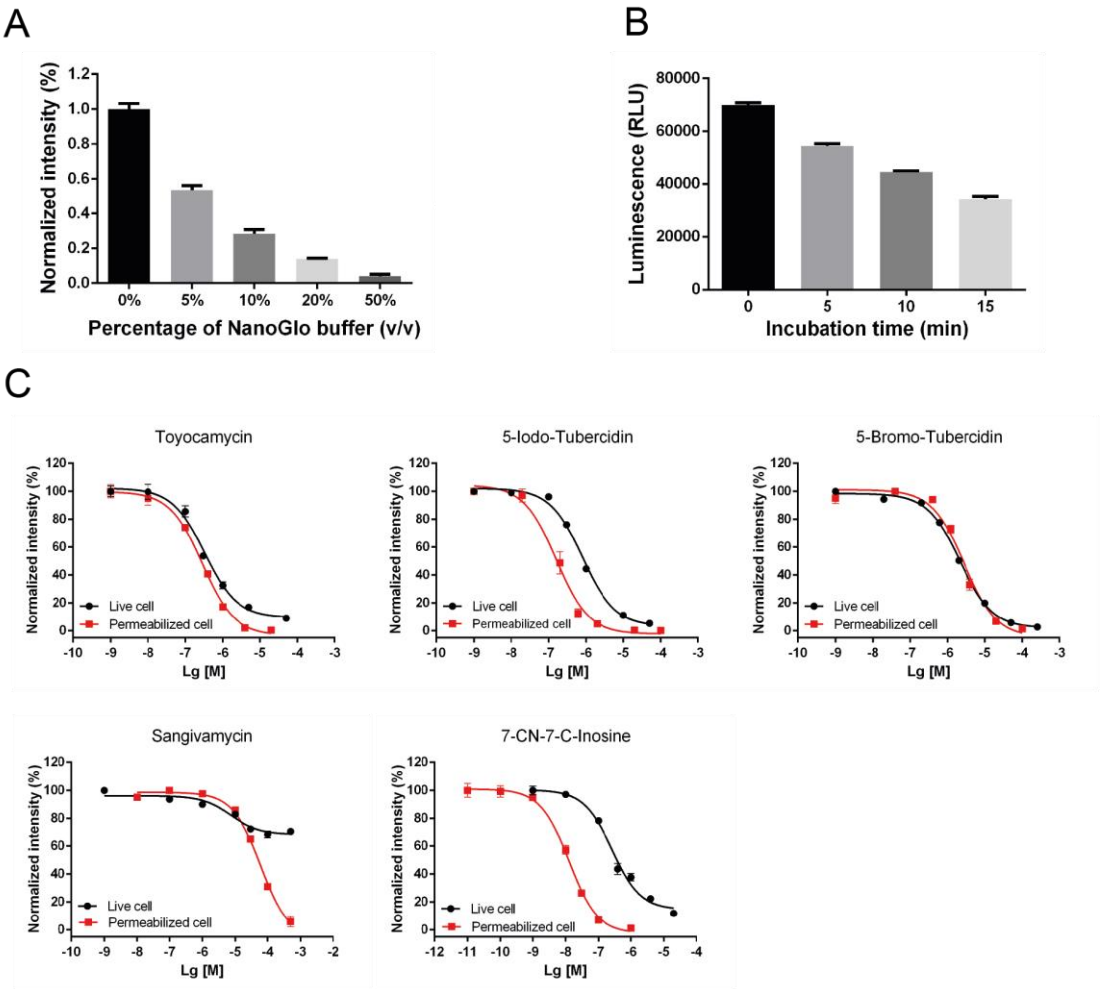

D

Compound / EC_{50}	Toyocamycin	5-I-Tubercidin	5-Br-Tubercidin	Sangivamycin	7-CN-7-C-Inosine
Live cell	329 ± 32 nM	803 ± 54 nM	2.13 ± 0.1 μM	7.47 ± 1.93 μM	265 ± 34 nM
Permeabilized cell	285 ± 20 nM	161 ± 19 nM	2.77 ± 0.32 μM	61.1 ± 4.84 μM	12.7 ± 0.9 nM

Fig 3.8, PKA activation in permeabilized cells. A, Investigation of NanoGlo buffer usage. Different percentages of NanoGlo buffer were supplemented into PBSG resuspended cells. Luminescent signal was measured immediately. B, Investigation of incubation time. Cells treated with 5% NanoGlo buffer were incubated for different time spans ranging from 5 min to 15 min. C, Comparison of the EC_{50} of compounds measured in live cells and permeabilized cells by NanoBiT assay. The black dots and curve represent live cell group and the red represents permeabilized cell group. D, A table of EC_{50} values measured by the two methods. ± SD values were calculated from 3 replicates. NanoBiT assays were performed as described in section 2.2.7. The EC_{50} and ±SD values were determined by GraphPad Prism 6.0.

3.1.2.3 PKA activation by cold shock is undetectable by NanoBiT assay

Cold-shock was shown to activate PKA (PhD thesis Kramer, 2004). Interestingly, trypanosomes undergo cold-shock upon transferring from mammalian blood to tsetse fly midgut and it has proven to co-induce differentiation in vitro (Engstler & Boshart, 2004). Therefore, PKA might mediate BSF differentiation to PCF, although the mechanism remains unknown. NanoBiT assay was tested as a possible tool to investigate the cold-shock induced PKA activation. To separate the impact of low temperature on kinase activation and catalytic activity as such of the complemented Nluc, a control cell line expressing LgBiT-GS linker-SmBiT was generated. This fusion protein served as a control of enzymatic activity change in low temperatures. The cell line emits strong luminescence in the presence of substrate (Fig 3.9), indicating the assembly of the linked SmBiT and LgBiT. Cell suspensions were incubated at 37°C for 20 min at first and then divided into 3 different 1.5 ml tubes, which were incubated at 4, 20 and 37°C for 15 min. PKA activation was measured immediately after incubation. As shown in Fig. 3.9, the luminescence of both NanoBiT cell line and control line decreases in lower temperatures as expected as the enzymatic activity of the structure complemented Nluc was reduced in lower temperatures. However, over-proportional reduction of the luminescence signal in cold shocked cells indicating kinase dissociation was not observed. This unexpected result was not followed up.

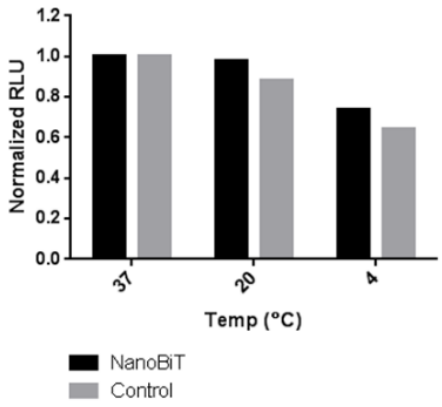

Fig 3.9, cold-shock activation of PKA measured by NanoBiT assay. Black bar indicates SmC1/LgR cell line, gray bar represents the control cell line. The experiments were done only once.

3.1.2.4 Dipyridamole induced PKA activation is assessed by NanoBiT assay

Dipyridamole was found to activate PKA by *in vivo* VASP assay while *in vitro* kinase assay suggested it does not activate PKA by binding (Bachmaier *et al.*, 2019). It is speculated that an undiscovered signal pathway upstream of trypanosome PKA

stimulated by dipyridamole. The PKA activation triggered by dipyridamole was assessed by NanoBiT assay using live cell in Fig. 3.10. The measured EC_{50} is 9.5 μM, closing to the value (22.4 μM) measured by VASP assay. Noteworthy, dipyridamole is an auto-fluorescent molecule, which can be problematic in BRET (see chapter 3.5) and FRET assays.

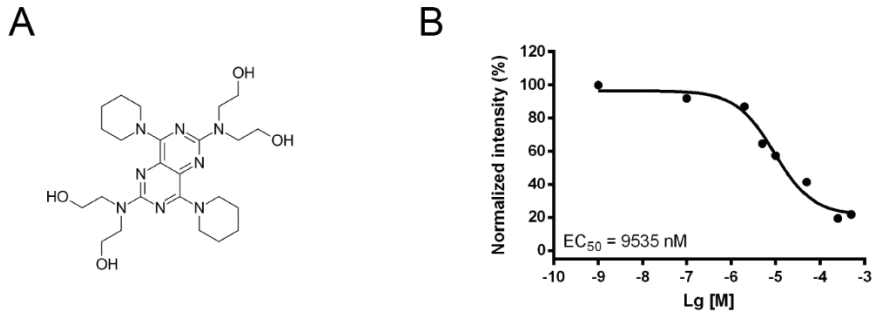

Fig 3.10, PKA activation by dipyridamole. A, molecular structure of dipyridamole. B, PKA activation by dipyridamole. This curve was measured using live cells. ± SD was calculated from 3 technical replicates. The assay was performed as described in section 2.2.7. The dose response curves were plotted by Graph-pad Prism 6.0.

3.1.3 Application of NanoBiT assay

The developed NanoBiT assay is a major improvement for easy and high throughput evaluation of kinase activity. The wide dynamic range of the assay presented in the above validations enables it precise estimation of the potency of new compounds to activate PKA. Moreover, its easy operation makes it possible for fast screening of compounds. Most importantly, the use of permeabilized cells in the assay enables the examination of compounds regardless of their membrane permeability. Taking advantage of the NanoBiT assay, a systematic study of *T. brucei* PKA activation mechanism was carried out. Chapter 3.2 focuses on the regulatory subunit, a series of PKAR mutants were generated and analyzed by NanoBiT assay. Based on the mechanism study of the α-D helix, potential PKA inhibitors were designed and screened by NanoBiT assay in chapter 3.4. Chapters 3.3 focuses on the catalytic subunits, NanoBiT assay was used to compare the activation of different PKA holoenzymes in both BSF and PCF.

3.2 Structural and functional characterization of PKAR N-terminal domain and the α-D helix

PKA has been well studied in higher eukaryotes over the last decades, the activation mechanisms are well understood. PKA-like proteins were also identified in kinetoplastids. However, structural comparison and sequence alignment revealed some specific features for kinetoplastid PKAR, 1) in the Phosphate Binding Cassette (PBC), some key residues responsible for ligand binding are different to mammalian PKAs but conserved in the kinetoplastid PKAs. These residues have been proven to be critical for the binding of purine nucleosides (Bachmaier *et al.*, 2019). 2) The kinetoplastid PKAR has an extended N-terminal domain comprising nearly 200 amino acids. In the previous study, the N-terminal domain truncation mutant was shown not to bind the C-subunits via pull down (PhD thesis Krumbholz, 2006). This suggests that the N-terminal domain might be involved in PKA holoenzyme formation and activation. 3) An extra α-helix is found at the PKAR C-terminus following the α-C helix. It is referred to as α-D helix. The crystal structure of TbPKAR bound to inosine reveals that inosine is buried in the B-site (NBD-B) and covered by the α-D helix relative to the solvent exposed cAMP in the B-site of mammalian PKA (Wu *et al.*, 2004a); In this study, we intended to answer the questions, 1) Whether and how the N-terminal domain is involved in PKA holoenzyme formation; 2) how and why the α-D helix covers the NBD-B like a lid.

Site-directed mutagenesis is a common strategy for protein structural and functional study. To assess the activation features of different PKA holoenzyme *in vivo*, we used the NanoBiT assay. The PKAR mutants were fused with Ty tag and the LgBiT on either the N- or C-terminal end depending on the mutation/truncation position. In order to evaluate PKA activation by NanoBiT assay, the MiTat1.2 1313 VASP SmC1 cell line (Hammerl, 2018) constitutively expressing SmBiT-PKAC1 was used as the parent cell line. LgBiT fused wild type or mutated PKAR was introduced and inducibly expressed in this cell line. The cell line expresses also VASP peptide, thus VASP assay can be performed to study the effect of mutated PKARs on substrate phosphorylation.

3.2.1 Role of the PKAR N-terminal domain and the linker region on R-C interaction

In comparison to mammalian PKAR, kinetoplastid PKAR has an extraordinary extended N-terminal domain. The previous study has shown that removing the N-

terminal domain or even only the first 10 amino acids from it resulted in the failure of PKAC pull-down, suggesting the N-terminal domain is involved in PKA holoenzyme formation (PhD thesis Krumbholz, 2006). The N-terminal domain of PKAR is followed by the linker hinge region, which contains the inhibitory sequence (RRTT*). The threonine marked by an asterisk can be phosphorylated by the catalytic subunit in the holoenzyme form. Curiously, mutation of this autophosphorylation site (T205) to Ala turned out to cause a dominant negative-like phenotype (Schmitz, 2011), though the mechanism was not clear. Combining the PKAR structure analysis and NanoBiT assay, this study aims to unravel the mechanism behind. The following cell lines were produced in this study (Table 2). Since the truncation or mutation sites were on the N-terminus of PKAR, *LgBiT* sequence was genetically tethered to the C-terminus to reduce the influence on PKA holoenzyme formation. Ty tag was added to facilitate the detection by western blot. A shortened name was applied to each cell line for convenience.

	Cell line	Shortened name	Inducible expression
1	MiTAT1.2 1313 VASP SmC1 PKAR-LgBiT-Ty^{Ti}	R-LgTy^{Ti}	R-LgTy
2	MiTAT1.2 1313 VASP SmC1 PKARΔ(1-191)-LgBiT-Ty^{Ti}	RΔ (1-191)-LgTy^{Ti}	RΔ(1-191)-LgTy
3	MiTAT1.2 1313 VASP SmC1 PKAR_T205A-LgBiT-Ty^{Ti}	R_T205A-LgTy^{Ti}	R_T205A-LgTy
4	MiTAT1.2 1313 VASP SmC1 PKAR_R207S-LgBiT-Ty^{Ti}	R_R207S-LgTy^{Ti}	R_R207S-LgTy
5	MiTAT1.2 1313 VASP SmC1 PKAR_T205A_R207S-LgBiT-Ty^{Ti}	R_T205A_R207S-LgTy^{Ti}	R_T205A_R207S-LgTy
6	MiTAT1.2 1313 VASP SmC1 PKARΔ191_T205A_R207S-LgBiT-Ty^{Ti}	RΔ(1-191)_T205A_R207S-LgTy^{Ti}	RΔ(1-191)_T205A_R207S-LgTy
7	MiTAT1.2 1313 VASP SmC1 PKAR_R89K_R137K-LgBiT-Ty^{Ti}	R_R89K_R137K- LgTy^{Ti}	R_R89K_R137K-LgTy
8	MiTAT1.2 1313 VASP SmC1 PKAR_R89A_R137A-LgBiT-Ty^{Ti}	R_R89A_R137A- LgTy^{Ti}	R_R89A_R137A-LgTy

Table 2, cell lines produced in the study. ^{Ti} means protein expression is inducible by Tet. The expression of the fused PKARs were probed by western blot (Fig S1)

3.2.1.1 The N-terminal domain of the R subunit is involved in PKA holoenzyme formation *in vivo*

Considering that a pull-down assay is intrinsically less sensitive for transient and weak

protein-protein interactions, a verification of the involvement of the N-terminal domain in PKA holoenzyme formation was carried out using NanoBiT assay. For this purpose, R-LgTy^{Ti} (control cell line) and RΔ(1-191)-LgTy^{Ti} were produced. The expression of R-LgTy and RΔ(1-191)-LgTy were probed by western blot (Fig S1). PKA activation was accessed by treating cells with different concentrations of the ligand toyocamycin. As shown in Fig 3.11, the luminescence intensity of the untreated RΔ(1-191)-LgTy^{Ti} cells was around 6-times lower than the control. Given the higher expression of RΔ(1-191)-LgTy, it was clear that the deletion of the N-terminal domain is detrimental to PKA holoenzyme formation. In contrast to the control, the truncated protein hardly responded to toyocamycin treatment of cells, indicating that the low luminescence more likely resulted from unspecific interaction of R and C subunits. It should be noted that the truncation of the N-terminal domain also causes mis-localization of the protein as expected (PhD thesis Krumbholz, 2006). The relatively high background luminescence was presumably due to the enrichment of RΔ(1-191)-LgTy and SmC1 in a vesicular compartment.

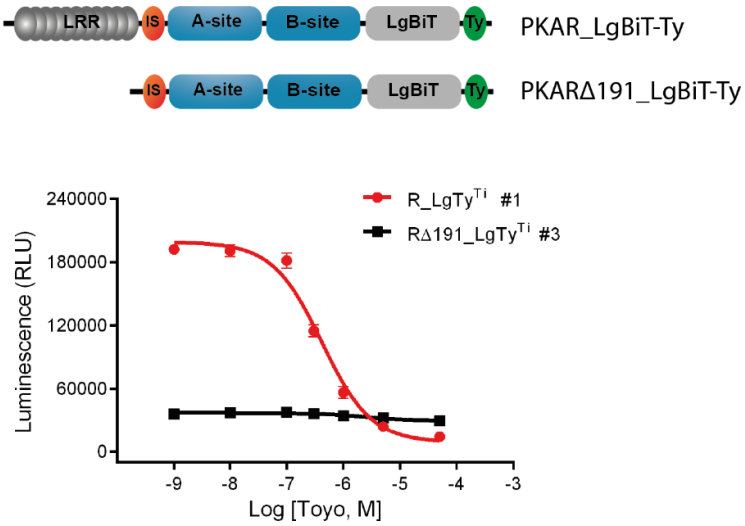

Fig 3.11, NanoBiT assay assessing the formation and activation of PKA. Upper panel shows the structure of R-LgTy and RΔ(1-191)-LgTy. The lower panel shows the activation of the PKA wild type and mutant holoenzymes in the two cell lines. Standard deviations were determined from three technical replicates and indicated as error bars. NanoBiT assays were performed as described in section 2.2.7. The dose response curves were plotted by Graph-pad Prism 6.0.

3.2.1.2 Test of a computational model of the PKAR N-terminal domain

A model of the N-terminal domain structure was made by ab-initio modeling as shown in Fig 3.12 (PhD thesis Githure, 2014). The barrel-like N-terminal domain comprises of

8 parallel β-strands typical for the LR repeats and several short α-helices. Three positively charged residues, R89, R137 and K21, are exposed at the surface likely to be the interaction interface with the C-subunit. The positively charged K21, R89 and R137 of the PKAR N-terminal domain were speculated to interact with S315 and S320 at the C-terminus of PKAC by ionic interaction. The two serine residues were predicted to be phosphorylated (PhD thesis Kramer, 2004). These interactions may contribute to the stabilization of the holoenzyme complex. Therefore, substitution of the two arginine residues for alanine residues was supposed to destabilize PKA holoenzyme or reduce the formation of holoenzyme, which can be reflected by low luminescence or left-shifted dose response curve in NanoBiT assay.

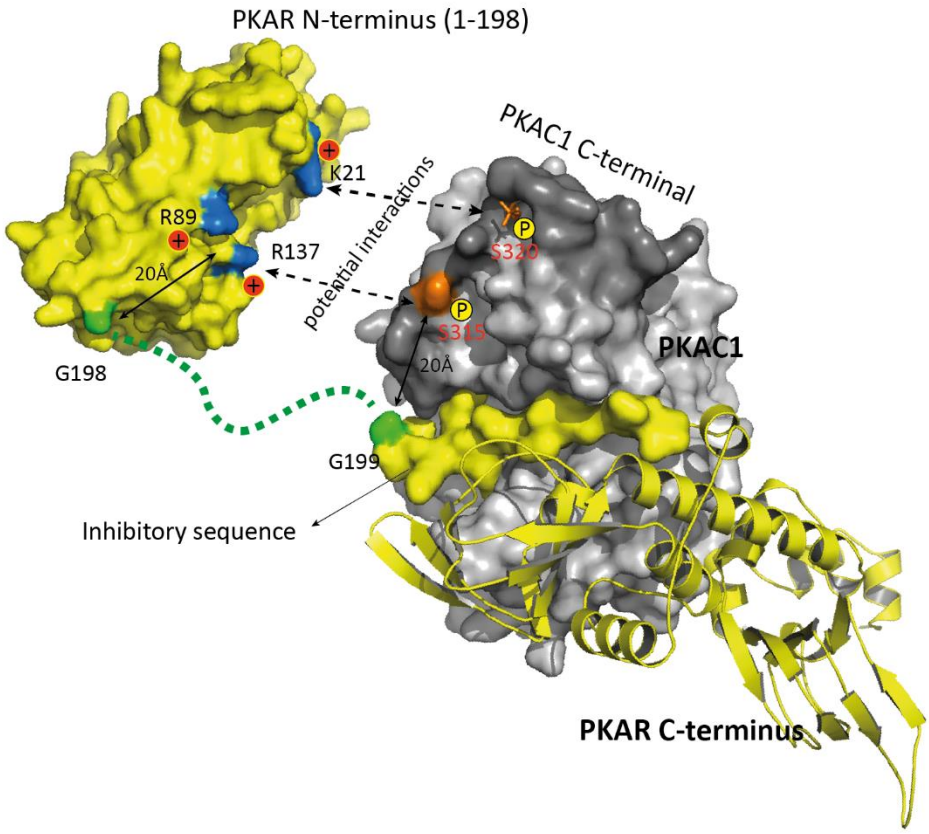

Fig 3.12 Potential interaction interface of PKAR N-terminal domain and PKAC C-terminus. PKAR N-terminal domain is represented as yellow surface. Positively charged residues R89, R137 and K21 are highlighted in blue. They were predicted to form a salt bridge with the negatively charged, phosphorylated residues S315 and S320 in the C-terminus of the C-subunit. The inhibitory sequence docked in the active site cleft of PKAC1 is represented as surface in yellow. PKAR C-terminus as carton representation in yellow. PKAR N-terminus and C-terminus parts are separated for visualization. A green dashed line connects the two parts. PKAC1 is represented as light gray surface, its C-terminal part is highlighted in dark gray. S315

and S320 are colored in orange.

To validate the speculation, a cell line expressing PKAR_R89A_R137A and a second cell line expressing PKAR_R89K-R137K were generated. Since Arg and Lys share comparable structure and both are positively charged, R→A mutation was expected to cause stronger effect than the R→K mutation. The control was R-LgTy^{Ti}. As shown in Fig 3.13, the R89K_R137K mutant showed a similar dose response curve as the control, indicating the R89K and R137K mutations have no effect on PKA activation. Curiously, the R→A mutant is harder to be activated. The EC_{50} of toyocamycin measured in this cell line was 4 times that of the control (750 nM vs 190 nM). This result suggests the two arginine residues do not interact with the serine residues at PKAC1 C-terminus, rejecting the hypothesis and the validity of the structural model. In addition, only 60% R→A mutated PKA holoenzymes were dissociated in the presence of 100 μM compared to more than 95% for the wild-type and R→K mutated PKA holoenzymes.

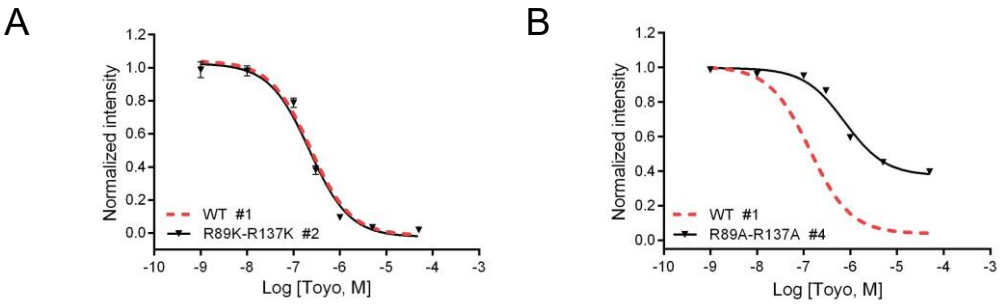

Cell line	Toyo EC_{50}
WT #1	190 nM
R89K-R137K #2	220 nM
R89A-R137A #4	750 nM

Fig 3.13 NanoBiT assay testing the activation of PKAR_R89K-R137K (A) and PKAR_R89A_R137A (B) formed PKA holoenzymes. Cells were incubated with a series of concentrations of toyocamycin before measurement. The table on the bottom lists the toyocamycin EC_{50} values. Standard deviations were determined from three technical replicates and indicated by error bars. NanoBiT assays were performed as described in section 2.2.7. The dose response curves were plotted by Graph-pad Prism 6.0.

3.2.1.3 Mutation of the autophosphorylation site T205 strengthens the holoenzyme complex

The inhibitory sequence (IS) of PKAR is in the hinge region that interacts with the active-site cleft of C subunit. There are two general classes of mammalian PKAR,

designated as type-I and type-II, due to the differences in the inhibitory sequence. As shown in Fig 3.14 A, the IS of R-I is RRxA/G, where the 'x' can be any amino acid and the Ala or Gly is the pseudo-phosphorylation site. On the other hand, the typical IS of R-II is RRxS*/T*, where the asterisk marked Ser or Thr is the auto-phosphorylation. Increased phosphorylation of human R-IIβ autophosphorylation site was shown to reduce PKA activation threshold, especially in some cellular compartments (Terrin *et al.*, 2012). *T. brucei* PKAR contains an auto-phosphorylation site (T205). In the previous study, the T205A mutation was found to cause non-responsiveness of PKA holoenzyme to the activation by toyocamycin and cold-shock (Schmitz, 2011). In order to validate the effect of T205 on PKA dissociation, a cell line expressing R_T205A-LgTy was made (Table 2). The control cell line was R-LgTy^{Ti}. As shown in Fig 3.14 B, both clones of R_T205A-LgTy^{Ti} showed significantly resistance to toyocamycin compared to the control. The EC_{50} measured in R_T205A-LgTy^{Ti} is more than 10 times that of the control. Hence, the result confirms the importance of T205 phosphorylation in PKA activation and explains the cause of the dominant-negative like phenotype in T205A mutant cell line.

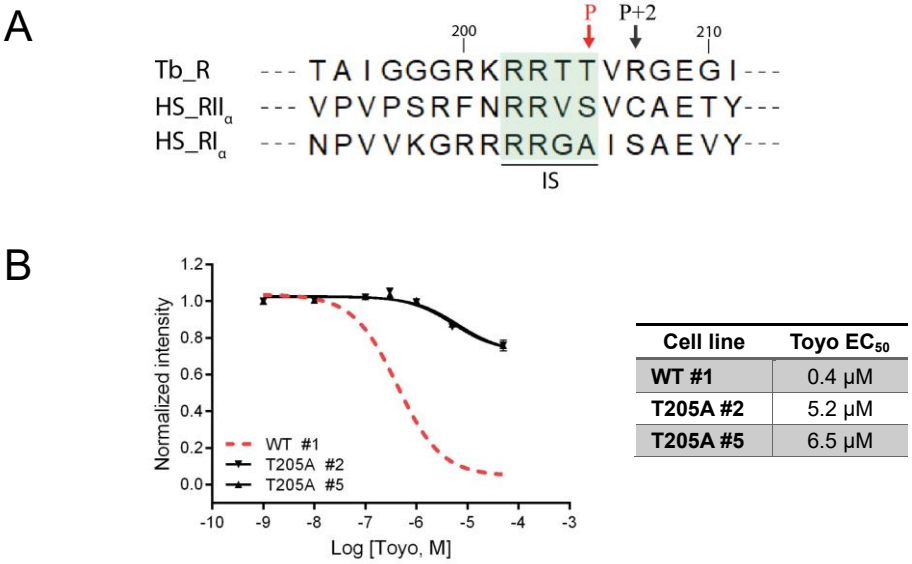

Cell line	Toyo EC_{50}
WT #1	0.4 µM
T205A #2	5.2 µM
T205A #5	6.5 µM

Fig 3.14, A, sequence alignment of the linker-hinge region of Tb, mammalian type-I and type-II PKARs. The inhibitory sequence (IS) is green shaded. The numbering refers to *T. brucei* PKAR (TbR). The phosphorylation or pseudo-phosphorylation site is marked by a red arrow. The second residue on the C-terminal of P-site referred to as P+2 site. B, Toyocamycin activation of PKAR_T205A. Standard deviations were determined from three technical replicates and indicated as error bars. Two clones of the PKAR_T205A cell line were tested. The table lists the measured EC_{50}. NanoBiT assays were performed as described in section 2.2.7. The dose response curves were plotted by Graph-pad Prism 6.0.

3.2.1.4 The P+2 site R207 is not relevant to PKA activation

In mammalian R-Iα, the P+2 site is a conserved serine (Fig 3.14 A). According to (Haushalter *et al.*, 2018), the phosphorylation of the Serine residue by cGMP-dependent protein kinase (PKG) transforms the R-Iα to the sensitized state, the resulting PKA holoenzyme is primed to be activated. Inspired by this study, a preliminary investigation on the P+2 site of TbPKAR was carried out, although it has an Arginine residue at that site. R207 was mutated to a serine and the activation of the mutant PKA was probed by NanoBiT assay. As shown in Fig 3.15, R207S mutation hardly influences PKA activation. The dose-response curve of toyocamycin in this cell line is highly similar to that of the control. However, the double mutation (T205A and R207S) of PKAR showed strong resistance to toyocamycin activation, confirming again the importance of T205 phosphorylation of T205 for PKA activation. This result suggests that R207 is not involved in PKA activation.

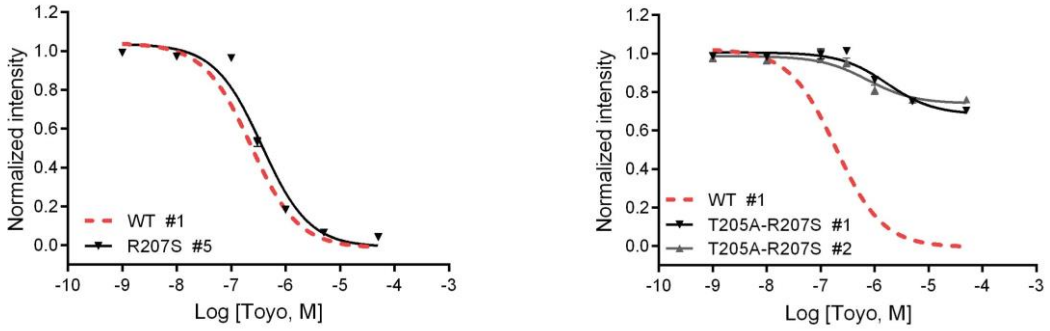

Cell line	Toyo EC_{50}
WT #1	230 nM
T207A #5	364 nM
T205A_R207S #1 & #2	> 1.3 µM

Fig 3.15 Toyocamycin activation of R207S and T205A_R207S PKAR mutants. Standard deviations were determined from three technical replicates and indicated as error bars. Two clones of the PKAR_T205A_R207S cell line were tested. The table lists the EC_{50} values measured. The presented EC_{50} value of the T205A_R207S cell line is the mean of two clones (2.55 µM and 1.1 µM, respectively). NanoBiT assays were performed as described in section 2.2.7. The dose response curves were plotted by Graph-pad Prism 6.0.

3.2.1.5 Antagonistic effects of T205 phosphorylation and the N-terminal domain on holoenzyme stability

Combining the above observations, T205 phosphorylation clearly promotes holoenzyme dissociation, while the N-terminal domain contributes to the formation or

stabilization of the holoenzyme complex. A mutant containing both T205A mutation and the N-terminal domain truncation was introduced and expressed in trypanosomes. R207S mutation was also introduced mimicking the typical mammalian R-Iα, although this residue was not relevant for PKA activation as revealed in 3.2.1.4 chapter. Hence, the mutant was PKARΔ(1-191)_T205A_R207S-LgTy. As shown in Fig 3.16, the combination of T205A restores the binding ability of the N-terminal domain truncated PKAR to C-subunits significantly. In another words, the T205A mutation cancels the effect of the N-terminus truncation which dissociates completely the holoenzyme (compare figures 3.11 and 3.16). Moreover, the resulting holoenzyme is harder to be activated by toyocamycin in comparison to the WT control, verifying the dominant role of T205 in PKA activation.

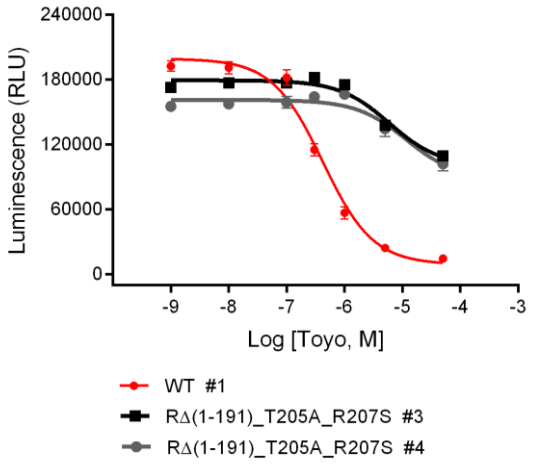

Cell line	Toyo EC_{50}
WT #1	420 nM
RΔ(1-191)_T205A_R207S #3	> 6 μM
RΔ(1-191)_T205A_R207S #4	> 10 μM

Fig 3.16 The activation of PKARΔ191_T205A_R207S:SmC1. Two clones (#3 and #4) were tested. The ± SD was determined from three technical replicates and indicated by error bar. NanoBiT assays were performed as described in section 2.2.7. The dose response curves were plotted by Graph-pad Prism 6.0.

3.2.2 Functional and structural characterization of the α-D helix

Unlike cAMP-dependent protein kinase A in most eukaryotes, the regulatory subunit of the nucleoside activated *T. brucei* PKA has an extended α-D helix on the C-terminus (Fig 3.17) with unknow function. Through analyzing the structure of PKAR bound to Inosine (PDB: 6FLO, Yuri Volpato - PhD Thesis), the helix was found wrapped around the B-site, resulting in the ligand being completely buried in the interior of the protein and therefore shielded from any contact with the solvent. Moreover, it was found interacting with the β-barrel of the NBD-B, the RBC-B motif and the ligand, mainly through the three Tyr residues, Y482, Y484 and Y485. Y482 is in the coil region between the α-C and α-D helix. We studied the function of the unique α-D helix by

making α-D helix deleted mutants and analyzing the cell growth and morphological phenotype upon expression of the mutated R subunit. Subsequently, the key residues involved in the interaction of the α-D helix were identified by site-directed mutagenesis.

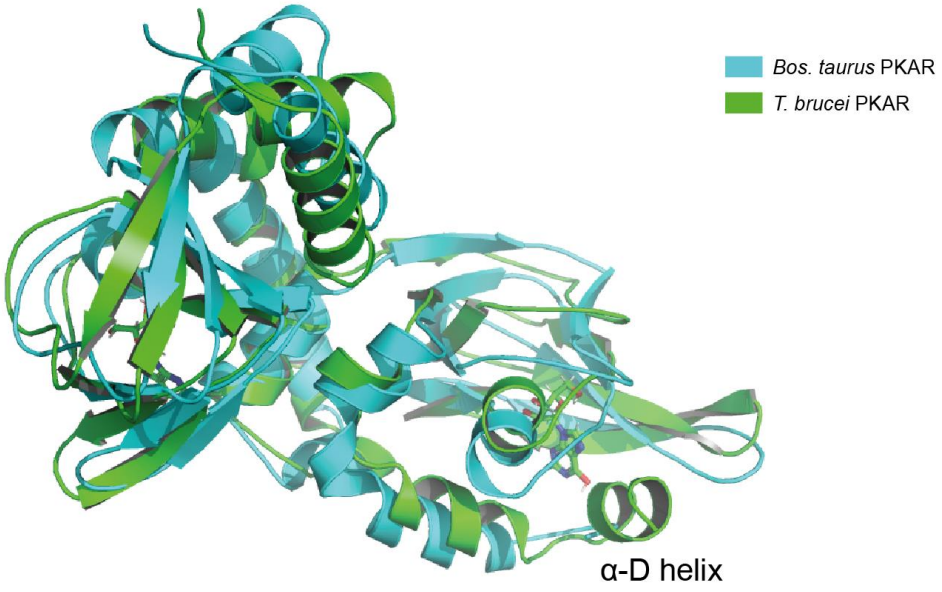

Fig 3.17, PKAR structures alignment. *T. brucei* PKAR (PDB: 6FLO) is represented in green as cartoon, *Bos.taurus* PKAR (PDB: 1RGS) is represented in cyan as cartoon. Only *T. brucei* PKAR has the α-D helix.

3.2.2.1 Expression of the a-D helix truncated PKAR causes a dominant negative-like phenotype

To investigate the function of the α-D helix, the wild type and the α-D helix truncated PKAR were expressed in trypanosomes so that the impact of the α-D helix truncation can be compared. The monomorphic BSF cell line MITat1.2 1313 VASP was used as the parent cell line in order to compare VASP phosphorylation of the resulting cell lines. However, it was found later that the VASP protein was not sufficiently expressed in this cell line, probably due to longer passage. The following four cell lines were made by Yuri Volpato as shown in Table 3. They express PKAR, PKAR(1-480), PKAR-Ty or PKAR(1-480)-Ty upon induction. Ty epitope tag was added on the C-terminal of the wild type and the α-D helix truncated PKAR not only for facilitating the detection by western blot but also to check whether an unrelated sequence can compensate the loss of the α-D helix.

	Cell line	Referred to as	Protein expression
1	MiTAT1.2 1313 VASP PKAR^{Ti}	PKAR^{Ti}	PKAR

2	MiTAT1.2 1313 VASP PKAR(1-480)^{Ti}	PKAR(1-480)^{Ti}	PKAR(1-480)
3	MiTAT1.2 1313 VASP PKAR-Ty^{Ti}	PKAR-Ty^{Ti}	PKAR-Ty
4	MiTAT1.2 1313 VASP PKAR(1-480)-Ty^{Ti}	PKAR(1-480)-Ty^{Ti}	PKAR(1-480)-Ty

Table 3, cell lines used for cell growth and morphological phenotype study. They were made by Yuri Volpato. ^{Ti} represents tetracyclin inducible.

The inducible expression of the recombinant PKARs was titrated by 5 different concentrations of Tet (0, 5, 25, 100 and 500 ng/ml) for 24 hours and probed by immunostaining. As shown in Fig 3.18 A, two PKAR bands are detected in each lane, because the expressed wild type PKAR overlapped with the upper band of the endogenous PKAR doublet. The total amount of PKAR was quantified in each lane. It revealed that the total amount of PKAR increased up to 200% when the Tet concentration was over 25 ng/ml (Fig 3.18 A, right panel). Interestingly, the total amount of PKAR including PKAR(1-480) just fluctuated a bit in PKAR(1-480)^{Ti} line as shown in Fig 3.18 B. A more accurate quantification was possible since PKAR(1-480) has a different molar mass compared to the endogenous PKAR. As shown on the right panel of Fig 3.18 B, the endogenous PKAR was decreasing as the increasing of PKAR(1-480). It reached the bottom as PKAR(1-480) reached the plateau. The PKAR-Ty^{Ti} line showed similar pattern in term of total PKAR amount change as the PKAR^{Ti} cell line in the titration, but the total PKA amount slightly decreased in high Tet concentrations (> 25 ng/ml), as shown in Fig 3.18 C. Alike, PKAR(1-480)-Ty^{Ti} line showed a similar pattern of total PKAR amount as PKAR(1-480)^{Ti} line (Fig 3.18 D). These results clearly indicate the down-regulation of the endogenous PKAR in response to the expression of α-D helix truncated PKAR mutant.

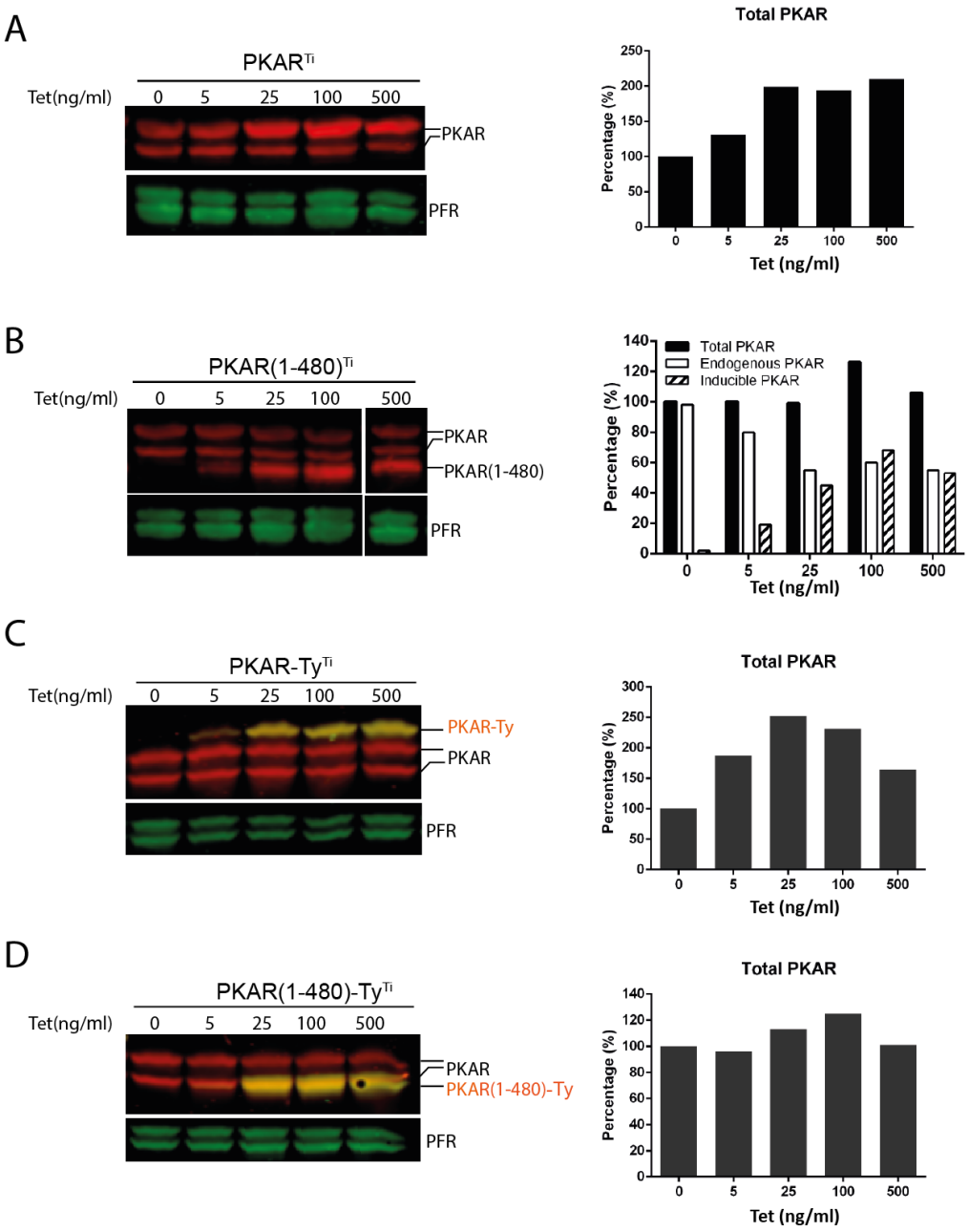

Fig 3.18, Western blot examining the expression of the inducible transgenes. A, titration of the inducible PKAR expression. B, titration of the inducible PKAR(1-480) expression. C, titration of the inducible PKAR-Ty expression. D, titration of the inducible PKAR(1-480)-Ty expression. Anti-Ty, anti-PKAR and anti-PFR were used in the experiment. Signal scanning and quantification were done by Image Studio™ Lite. The abundance of the proteins in each lane were normalized with the corresponding PFR signal. The PKAR abundance of the untreated cells was set to 100% in each titration. The total PKAR levels were compared and indicated in the right plot in blot A, C and D. The expression levels of endogenous PKAR, PKAR(1-480) and total PKAR were compared in blot B.

During the culturing with the addition of Tet, PKAR(1-480)^{Ti} and PKAR(1-480)-Ty^{Ti} cell lines showed a cell growth phenotype and more cell aggregations were found. The growth of each cell line in minus and plus Tet conditions was monitored in 7 consecutive days. As shown in Fig 3.19 A, all cell lines grew equally in minus Tet condition. Their PDTs were close, ranging from 5.6 to 5.8 h. However, in plus Tet condition, the cell lines expressing α-D helix truncated PKAR showed higher PDT as compared in the table (Fig 3.19B).

The drastically increased cell aggregation is a sign of aberrant cell division. During cell division, the duplication of kinetoplast happens prior to the nucleus division. K/N configuration analysis was therefore used to identify cells of different division stages. Cells incubated with Tet for 0h, 24h and 96h were fixed on silanized cover-slips and stained with DAPI before microscopy. As shown in Fig 3.19C, there are four types of cells, 1K1N, 2K1N, 2K2N and multinucleated (aberrant). The percentage of each cell type in each condition were then analyzed. As shown in Fig 3.19D, all four cell lines showed similar ratios for each cell type in -Tet condition. After induction, cell lines inducibly expressing the α-D helix truncated PKAR had increased proportion of 2K2N and aberrant cells. The phenomenon was maximal after 96 hours induction, whereas the ratios in PKAR^{Ti} and PKAR-Ty^{Ti} lines remained unchanged. It is worth to be mentioned that similar phenomenon was observed in the PKAC1 hemizygous knockout cell line (PhD thesis Kramer, 2004). It seems like the α-D helix deleted PKARs act like a dominant-negative mutant trapping the C subunits and the dominant-negative-like phenotype is due to the reduction of free catalytic subunits in cells.

A

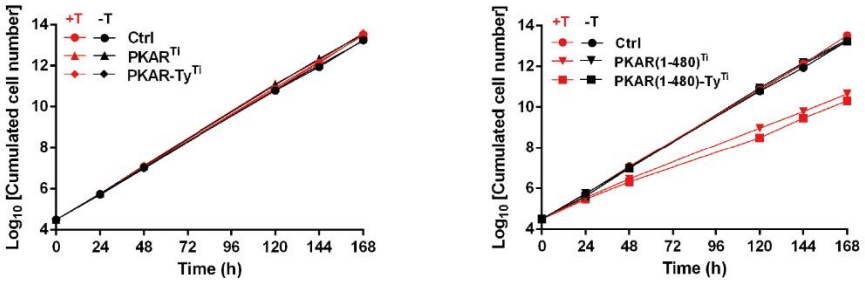

B

Cell lines	PDT (h) -Tet	PDT (h) +Tet
Ctrl	5.78	5.60
PKAR^{Ti}	5.59	5.55
PKAR(1-480)^{Ti}	5.73	8.20
PKAR-Ty^{Ti}	5.79	5.63
PKAR(1-480)-Ty^{Ti}	5.79	8.68

C

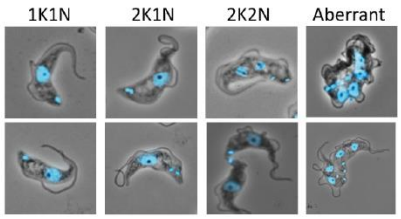

D

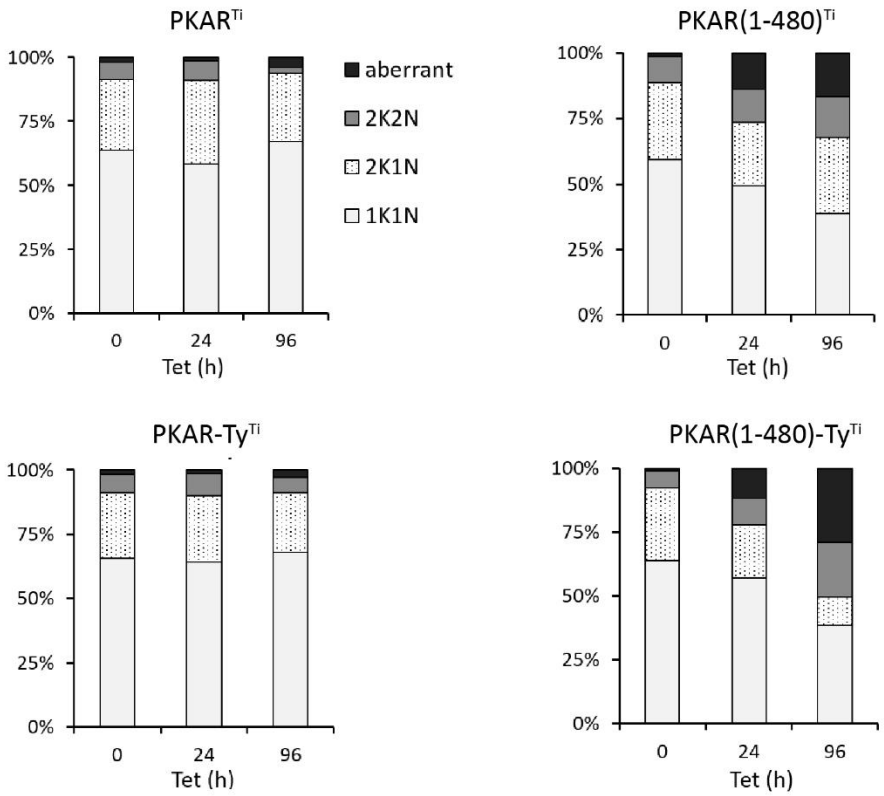

Fig 3.19, Growth and cell division analysis. A, the growth curve of the cell lines. B, the PDT of each cell line. C, representation of cells with different K/N configuration. The cell nucleus and kinetoplast were stained by DAPI. D, K/N configuration of each cell line after Tet induction for 0h, 24h and 96h. At least 200 cells of each time point were analyzed except for the PKAR(1-480)^{Ti} and PKAR(1-480)-Ty^{Ti} cells treated for 96 hours, since there were less than 200 individual cells left on the glass slide. For those data points, at least 100 cells were analyzed.

3.2.2.2 The α-D helix truncated PKAR traps C-subunits in the inactive state

According to the dominant negative-like effect presented above, we concluded that PKAR(1-480) should form a undissociated holoenzyme with catalytic subunits. To validate the hypothesis, NanoBiT assay was applied. As the cartoon representation in Fig 3.20 A, Ty epitope and LgBiT were fused on the N-terminus of PKAR and the α-D helix truncated PKAR. The parent cell line MITat1.2 1313 VASP SmC1 was transfected with the constructs pHD615-Ty-LgBiT-PKAR and pHD615-Ty-LgBiT-PKAR(1-480). The resulting cell lines were listed in Table 4. They are referred to as TyLg-R^{Ti} and TyLgR-(1-480)^{Ti} for convenience.

	Cell line	Inducible expression	Referred to as
1	MiTAT1.2 1313 VASP SmC1 Ty-LgBiT-PKAR^{Ti}	Ty-LgBiT-PKAR	TyLgR^{Ti}
2	MiTAT1.2 1313 VASP SmC1 Ty-LgBiT-PKAR(1-480)^{Ti}	Ty-LgBiT-PKAR(1-480)	TyLgR(1-480)^{Ti}

Table 4, NanoBiT cell lines produced for studying the role of the α-D helix.

The inducible expression of the engineered PKARs was checked by immunoblotting (Fig 3.20B). The cell growth in minus and plus Tet conditions was analyzed. As shown in Fig 3.20C, TyLg-R^{Ti} grew equally in minus and plus Tet conditions, whereas the two clones (#1 and #2) of TyLg-R(1-480)^{Ti} showed reduced growth under plus Tet induction. The PDT of the two clones were 5.4 h and 5.5 h in minus Tet condition and 8.4 h and 8.6 h in plus Tet condition, respectively. The PDTs are consistent with that measured in PKAR(1-480)^{Ti} and PKAR(1-480)-Ty^{Ti} lines. The activation of the TyLg-R/SmC1 and the TyLg-R(1-480)/SmC1 holoenzyme complexes is shown in Fig 3.20 D. Treatment of TyLg-R^{Ti} cells with different concentrations of toyocamycin revealed an expected dose response curve, from which the measured EC_{50} was 120 nM. However, the same treatment of TyLg-R(1-480)^{Ti} cells resulted in barely decreased luminescence even with high concentration of toyocamycin (> 100 μM). Both clones showed nearly flat dose response curves. It means that the TyLg-R(1-480)/SmC1 holoenzyme cannot be activated by toyocamycin. This validates the hypothesis that PKAR(1-480) traps the C-subunits in inactive state by forming undissociated PKA holoenzyme. PKAR(1-480) is therefore a dominant-negative mutant.

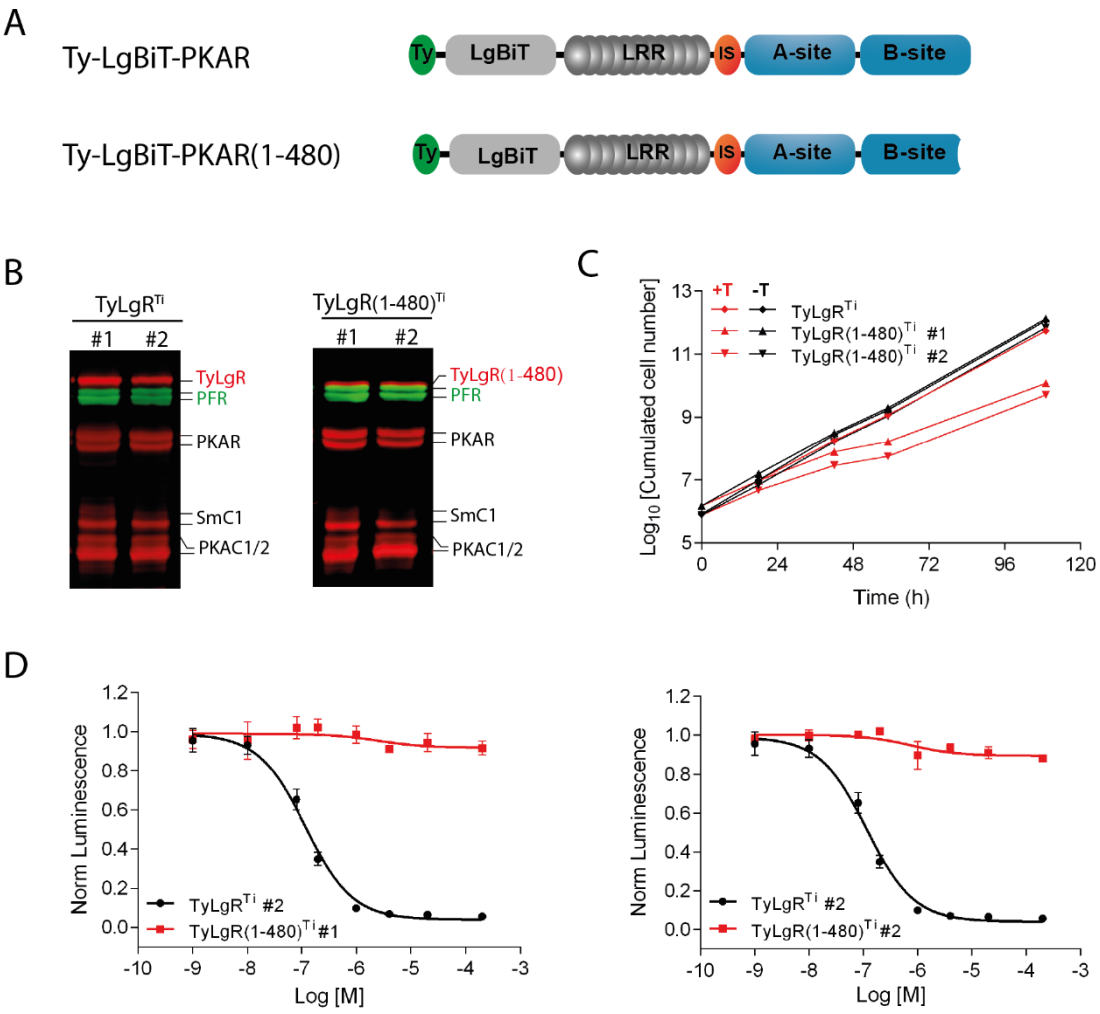

Fig 3.20 α-D helix deletion diminishes PKA activation. A, domian organization of TyLgR and TyLgR(1-480). B, Western blot probing TyLgR and TyLgR(1-480) expression. C, growth of the cell lines. D, NanoBiT assay of PKA holoenzyme dissociation. The luminescence intensity was normalized by the highest value measured in the assay. ±SD were determined from three technical replicates and indicated by error bars. NanoBiT assays were performed as described in section 2.2.7. The dose response curves were plotted by Graph-pad Prism 6.0.

3.2.2.3 The α-D helix is involved in ligand binding and PKA activation

The next step, structural analysis of TbR bound to inosine was performed to reveal the mechanism of the dominant-negative effect in collaboration with Yuri Volpato. Many interactions were found between the α-D helix and other motifs of the NBD-B. As shown in Fig 3.21A (left), Y485 interacts with N438 and H440 of the Ribose Binding Cassette B (RBC-B) by hydrogen bonding. Meanwhile, Y484 interacts with the main chain of V443 and R413. R413 forms a salt bridge with D445. It is noteworthy to mention that the backbone nitrogen of Y485 forms a hydrogen bond with the position 6 keto-group of inosine. On the other side, the ribose moiety of inosine forms multiple

hydrogen bonds with the RBC-B (Fig 3.21A, right). The surface representation of the α-D helix shows it is placed at the entrance of the ligand binding pocket after ligand binding, closing the pocket in a lid-fashion manner (Fig 3.21B). Y484 and Y485 are hypothesized to act as two latches that locking the lid by hydrogen bonding with the NBD-B in the pocket. The locked lid stabilizes the ligand inside the pocket. In the cAMP-bound conformation of mammalian PKAR, the α-C helix was thought to be repositioned by the capping residue, Y371 (Kim *et al.*, 2007). In *T. brucei* PKAR, it could be a cooperative process involving both the capping residue and the α-D helix. Therefore, the α-D helix truncation might be not only important for ligand binding but also for the PKAR conformation change from holoenzyme state to ligand-bound state.

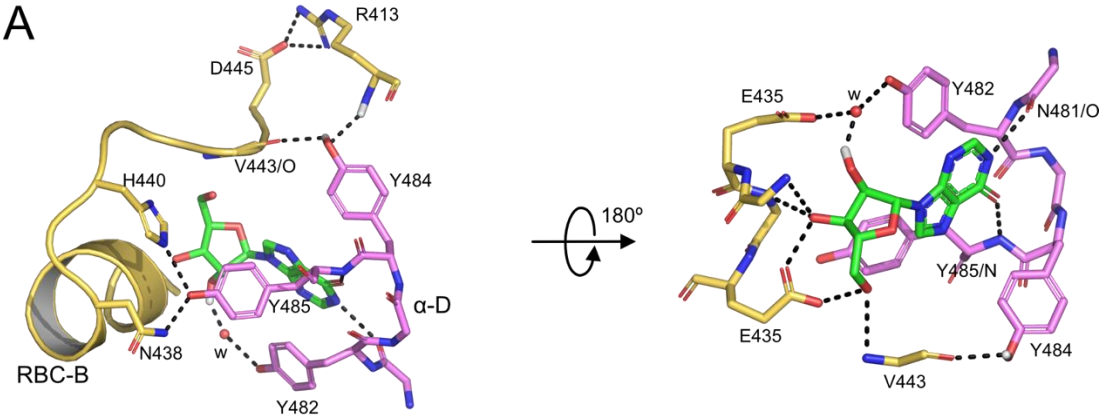

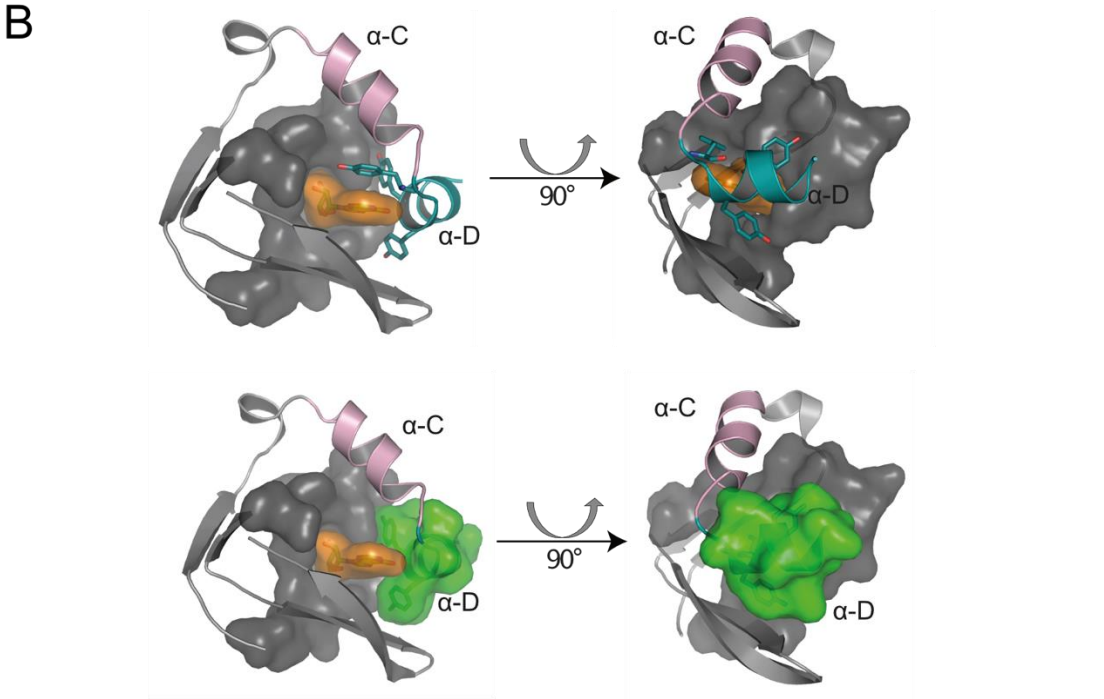

Fig 3.21 A, Inosine is stabilized tightly by the RBC-B morif and the α-D helix. The amino acids of RBC-B and the α-D helix involved in inosine binding are represented as sticks in yellow and pink, respectively. Inosine is represented as sticks in green. The hydrogen bonds are shown as black dashed line. B, Front and side views of inosine binding in pocket B. The RBC-B and inosine are shown as surface representation in grey and orange, respectively. The α-B, α-C and α-D helices are shown as cartoon representation in grey, pink and green, respectively. In the bottom, the α-D helix is shown as surface representation in green. The structures are adapted from TbPKAR bound to inosine (PDB: 6FLO; ligand chemical ID: NOS).

3.2.2.4 Y484 and Y485 are the key residues of the α-D helix

An alignment of kinetoplastid PKAR sequences was performed, as shown in Fig 3.22 A. Y484, Y485, N438, H440, R413, V443 and D445 of *T. brucei* PKAR were found highly conserved in the other PKARs. Thus, we supposed that Y484 and Y485 are the key residues to transform the α-D helix into a lid-like structure. To validate the hypothesis, the following cell lines were produced (Table 5). The inducible expression of the PKAR mutants were probed by western blot (Fig S2).

	Cell line	Shortened cell line name	Inducible expression
1	MiTAT1.2 1313 VASP SmC1 Ty-LgBiT-PKAR_Y484A^{Ti}	TyLg-R_Y484A^{Ti}	TyLg-R_Y484A
2	MiTAT1.2 1313 VASP SmC1 Ty-LgBiT-PKAR_Y485A^{Ti}	TyLg-R_Y485A^{Ti}	TyLg-R_Y485A
3	MiTAT1.2 1313 VASP SmC1 Ty-LgBiT-PKAR_Y484A-Y485A^{Ti}	TyLg-R_Y484A-Y485A^{Ti}	TyLg-R_Y484A-Y485A
4	MiTAT1.2 1313 VASP SmC1 Ty-LgBiT-PKAR_N438A^{Ti}	TyLg-R_N438A^{Ti}	TyLg-R_N438A
5	MiTAT1.2 1313 VASP SmC1 Ty-LgBiT-PKAR_H440A^{Ti}	TyLg-R_H440A^{Ti}	TyLg-R_H440A
6	MiTAT1.2 1313 VASP SmC1 Ty-LgBiT-PKAR_N438A-H440A^{Ti}	TyLg-R_N438A-H440A^{Ti}	TyLg-R_N438A-H440A

Table 5, cell lines expressing the α-D helix related PKAR mutants. Ty-LgBiT was fused on the N-terminus of the PKAR. The expression of the PKAR mutants were probed by western blot (Fig S2).

Activation of the PKA holoenzymes formed by the mutants with SmC1 was probed by NanoBiT assay. TyLg-R^{Ti} cell line produced in section 3.2.1.2 was used as control. As shown in Fig 3.22 B, in comparison to the control, Y484A mutation caused a slightly right-shifted dose response curve. Remarkably, Y485A mutation caused a prominently right-shifted curve, similar to the double mutation. Toyocamycin EC_{50} measured in these cell lines increased 2-fold, 20-fold and 67-fold for Y484A, Y485A and Y484A_Y485A, respectively (Table 6). The results indicate the importance of the two

tyrosine residues for activation, particularly Y485. Unlike the undissociated PKA holoenzyme caused by a-D helix truncation, the Y484 and Y485 mutated PKA can still be activated by toyocamycin, albeit at high concentration of toyocamycin (> 10 µM). This is likely due to the capping residue Y482, which was removed in the α-D helix truncated mutant but kept in the above mutants. This residue is critical for ligand binding in the mammalian PKAR and conserved in trypanosomal PKAR (Bachmaier *et al.*, 2019). However, mutagenesis analysis of Y482 is yet to be done.

The binding of Inosine to PKAR was measured via ITC (Isothermal Titration Calorimeter) by Yuri Volpato. He used a recombinant PKAR(199-499)_PBCA, in which the bulky N-terminal domain was removed and the RBC-A was modified to bind cAMP through the three mutations, E311A, T318R and V319A. Therefore, inosine should only bind the NBD-B. The K_D of inosine binding to the Y484 and Y485 mutated PKAR(199-499)_PBCA increased more than 100 times compared with the binding to PKAR(199-499)_PBCA. The K_D are 14 nM and 1.5 µM, respectively (unpublished data, Yuri Volpato). This proves that Y484 and Y485 are involved in ligand binding.

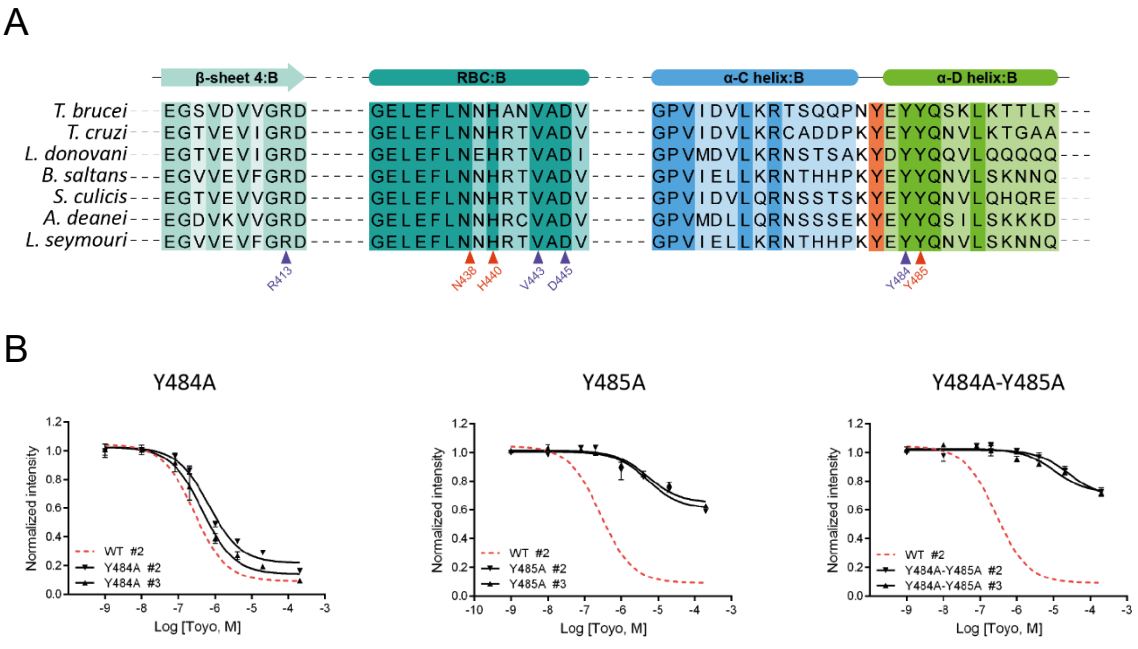

Fig 3.22 A, sequence alignment of the C-terminal part of kinetoplastid PKARs. The numbering of amino acids refers to *T. brucei* PKAR (TbR). B, NanoBiT assay testing the activation of the mutated PKA holoenzymes. Red dashed line represents the dose-response curve of TyLg-R:SmC1 measured from the control cell line. 2 clones of the other cell lines were tested. Standard deviations were determined from three technical replicates and indicated by error bars. NanoBiT assays were performed as described in section 2.2.7. The dose response curves were

plotted by Graph-pad Prism 6.0.

3.2.2.5 Y485 creates a three-way communication among α-D helix, the RBC-B and the bound ligand

Since Y485 was shown to be more critical at least in term of PKA activation, its interaction partners, N438 and H440, were studied by site-directed mutagenesis. As shown in Fig 3.23 A and Table 6, the EC_{50} increased from 267 nM for the WT to nearly 600 nM for PKAR-N438A and to more than 3.5 μM for PKAR-H440A. The double mutation results in a comparable increased EC_{50} as H440A single mutation. The structural analysis reveals that Y485 interacts not only with the RBC-B but also the bound ligand. Hydrogen bonds can be formed including Y485, H440, E435 and inosine in a network (Fig 3.23 B). This might stabilize ligand binding and be important for PKA activation.

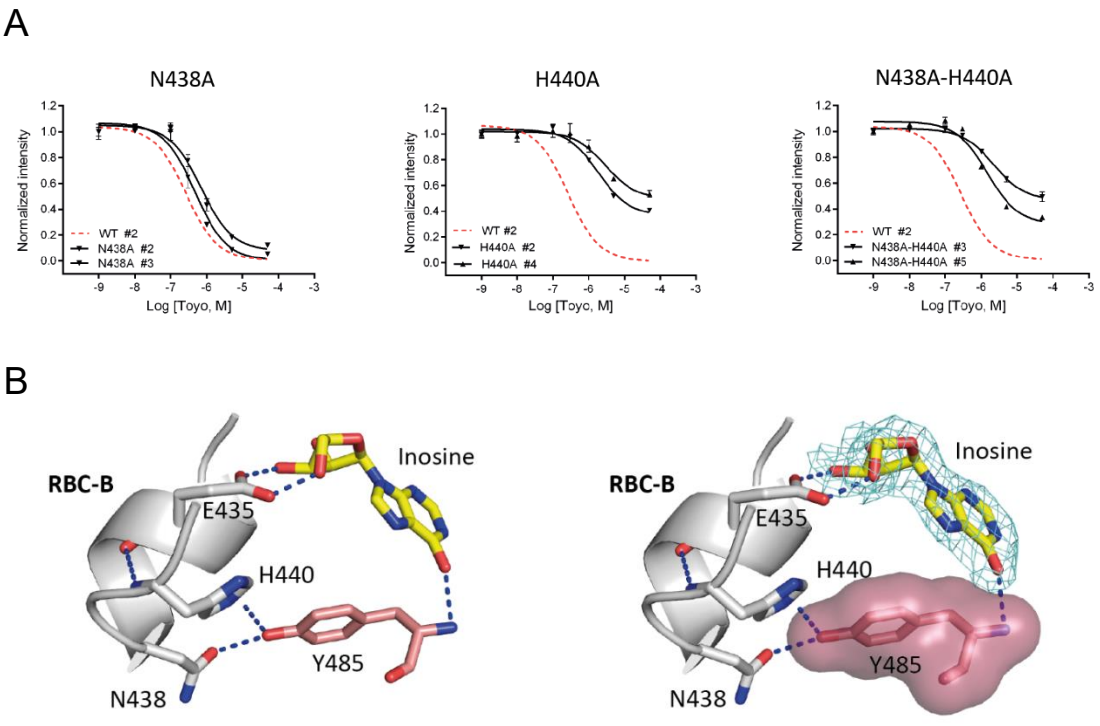

Fig 3.23 A, NanoBiT assay testing the N438A and H440A mutants. B, Hydrogen bonding network of Y485. Hydrogen bond is shown as blue dashed line. RBC-B is shown as grey cartoon. The right panel shows the surface representation of Y485 and the electron density map of inosine.

Mutant	EC_{50} (nM)	Fold change
WT	267	-
Y484A_Y485A	18080	67.0
Y484A	564	2.1
Y485A	5220	19.3
N438A_H440A	1850	7.0
N438A	593	2.2
H440A	3251	12.0

Table 6, Toyocamyin activation of α-D helix mutants. EC_{50} values are the mean of two clones of each cell line.

3.2.2.6 PKA substrate phosphorylation is attenuated by an enhanced dominant-negative mutant (SuperDN)

Both the α-D helix truncation and T205 mutation of PKAR lead to dominant negative (DN) phenotype in cells, see Fig 3.19 and (Schmitz, 2011). An attempt to overexpress a PKAR mutant that contains both the T205A mutation and the α-D helix truncation was carried out. This PKAR mutant is referred to as the SuperDN PKAR. It was cloned into the pLew82 plasmid vector and then transfected into Antat1.1 13-90 cell line. The expression of the superDN PKAR is directed by a T7 promotor that is recognized only by T7 RNA polymerase. However, the expected overexpression of the superDN PKAR was not realized in all clones analyzed, as can be seen in Fig 3.24 A. The molar mass of the endogenous PKAR and Ty-PKAR(1-480, T205A) are very close, so their bands overlap on western blot. Nevertheless, the change of PKA substrate phosphorylation level in the presence and absence of toyocamycin or cold shock were probed by western blot utilizing the anti-Phospho-(Ser/Thr) PKA substrate antibody. As shown in Fig 3.24 B, in minus Tet condition toyocamycin treatment (1 μM) and cold shock (16 °C) increased the substrate phosphorylation level by 5.6-fold and 4.2-fold, respectively. In the plus Tet condition, the overall phosphorylation level of all groups dropped over 2-fold in comparison with the counterparts of the minus Tet condition. In conclusion, PKA activation by two different ways was inhibited by the superDN PKAR.

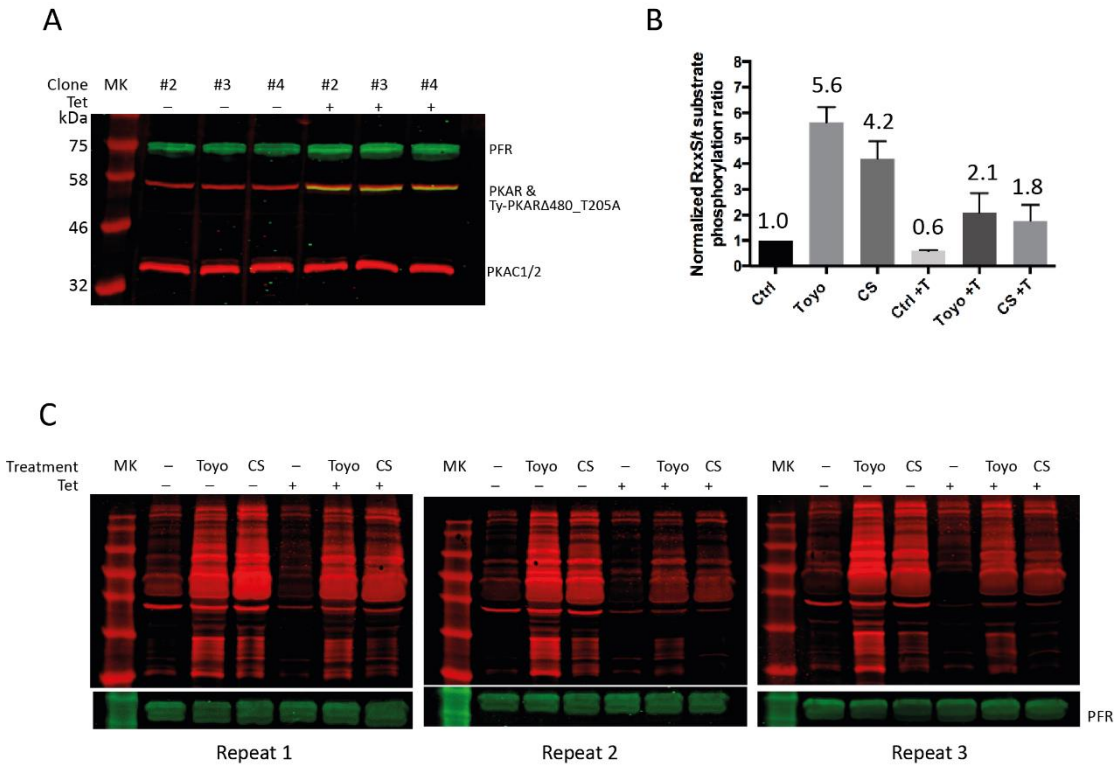

Fig 3.24 PKA substrate phosphorylation analysis of the SuperDN cell line. A, the expression of Ty-PKAR(1-480)_T205A. The following primary antibodies, anti-PKAR, anti-PKAC1/2, anti-PFR and anti-Ty were used. The molar mass of the endogenous PKAR (red band) and Ty-PKAR(1-480, T205A) (yellow band) are 56.7 and 55.7 kDa, respectively. B, quantification of the substrate phosphorylation. Cells were treated with 1 µM toyocamycin for 5 min at 37°C or incubated at 16°C for 5 min (cold shock). PKA substrate phosphorylation was detected by the anti-Phospho-(Ser/Thr) PKA substrate antibody (1:1000 diluted in Odyssey buffer). PFR is the loading control and its signal in each lane was used for normalization. The substrate phosphorylation intensity of the control was set as 1. The normalized intensity of PKA substrate was labelled above the coloumns. The experiment was performed in independent triplicates. Standard deviations are indicated by error bars. C, Western blot detection of the PKA substrate phosphorylation change.

3.2.2.8 The α-D helix is critical for PKA activation in *T. cruzi* and *L. donovani*

The amino acid sequence of *T. cruzi* and *L. donovani* PKAR reveals that they all contain the extended α-D helix, while whether the α-D helix is essential for TcPKA and LdPKA activation is yet to be validated. A fast but effective strategy is to inducibly express the TyLgBiT fused TcR and LdR in the *T. brucei* cell line MiTat1.2 1313 VASP SmC1, which constitutively expresses SmBiT-TbPKAC1. We expected the TyLg-TcR and TyLg-LdR to form holoenzymes with SmBiT-TbPKAC1 so that the holoenzyme activation can be assessed by NanoBiT assay. As the PKAC1 orthologs are highly homologous among the three species (Fig S8), the heterologous PKA holoenzymes are expected to function like the homologous holoenzymes. The MiTat1.2 1313 VASP SmC1 cell line was used as the parent cell line for transfection. The generated cell lines are listed in Table 7. The inducible expression of the PKAR fusion proteins was probed by immunostaining (Fig S3).

	Cell line	Referred to as	Inducible expression
1	MiTAT1.2 1313 VASP SmC1 Ty-LgBiT-TcPKAR^{Ti}	TyLg-TcR^{Ti}	TyLg-TcR
2	MiTAT1.2 1313 VASP SmC1 Ty-LgBiT-LdPKAR^{Ti}	TyLg-LdR^{Ti}	TyLg-LdR
3	MiTAT1.2 1313 VASP SmC1 Ty-LgBiT-TbPKAR(1-482)^{Ti}	TyLg-TbR(1-482)^{Ti}	TyLg-TbR(1-482)
4	MiTAT1.2 1313 VASP SmC1 Ty-LgBiT-TcPKAR(1-483)^{Ti}	TyLg-TcR(1-483)^{Ti}	TyLg-TcR(1-483)

Table 7, NanoBiT cell lines produced for studying *T. cruzi* and *L. donovani* PKARs.

Activation of the resulting PKA holoenzymes was assessed by NanoBiT assay using permeabilized cells as described in chapter 3.1.2.2. As shown in Fig 3.25, the heterologous PKA holoenzymes were activated by various ligand. The EC_{50} values measured by NanoBiT assay are in general close to those measured by *in vitro* kinase assay (data taken for comparison from (PhD thesis Githure, 2014)), albeit the catalytic subunits involved in the two assays are different. The potency order of the three endogenous nucleosides is inosine > guanosine > adenosine for both TcR:TbC1 and LdR:TbC1, which is the same as for TbR:TbC1. The result is in agreement with that of *in vitro* kinase assays. Interestingly, guanosine is a better activator for TbR:TbC1 relative to TcR:TbC1 and LdR:TbC1 holoenzymes as revealed by both assays. These results indicate that the heterologous TcR:TbC1 and LdR:TbC1 holoenzymes do not differ from the corresponding TcR:TcC2 and LdR:LdC1 holoenzymes with respectiv to kinase in activation. Therefore, mutagenesis studies on TcPKAR and LdPKAR can be done and analyzed by NanoBiT assay in *T. brucei*.

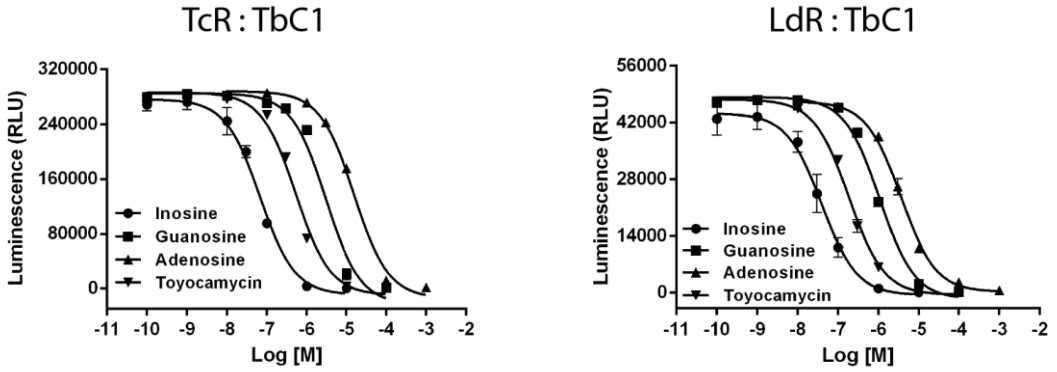

	NanoBiT assay[1]			*In vitro* Kinase assay[2] (for comparison)		
	TbR:TbC1	TcR:TbC1	LdR:TbC1	TbR:TbC1	TcR:TcC2	LdR:LdC1
Inosine	38 nM	60.4 nM	34 nM	14 nM	150 nM	47 nM
Guanosine	140 nM	2.27 µM	1.0 µM	150 nM	3.5 µM	1.7 µM
Adenosine	5.2 µM	12.8 µM	3.5 µM	5.6 µM	8.3 µM	6.5 µM
Toyocamycin	354 nM	464 nM	280 nM	185 nM	n.d.	n.d.

Fig 3.25, NanoBiT assay assessing TcR:TbC1 and LdR:TbC1 activation by nucleosides and toyocamycin. The cells used in the assay were membrane permeabilized by 2% NanoGlo buffer. The experiment was performed by three technical replicates and independently in two clones. NanoBiT assays were performed as described in section 2.2.7. The curves shown above are from one of the two clones tested.

[1] the values are the mean of two independent experiments using different clones

[2] data from George Githure, manuscript in preparation

As studying TcR and LdR in trypanosomes has been verified to be feasible, we aimed to study the role of the α-D helix in TbR, TcR and LdR. In order to dissect the role of the α-D helix alone, only the α-D helix part was deleted in the PKARs in this study, the capping residue of the B-site was kept as in mammalian PKAR. Two cell lines inducibly expressing the α-D helix truncated TbR(1-482) and TcR(1-483) were generated as listed in Table 7. A cell line expressing LdR(1-483) has not yet been obtained. NanoBiT assay was performed to assess the activation of these PKAs using membrane permeabilized cells. As shown in Fig 3.26, TbR(1-482):TbC1 and TcR(1-483):TbC1 are resistant to inosine activation compared to the untruncated holoenzymes. The EC_{50} of inosine increased more than 100-fold in both cell lines expressing the α-D helix deleted PKAR. These results indicate that the critical role of α-D helix in PKA activation is conserved in TbPKA, TcPKA and most likely also LdPKAR, in accordance with the

sequence alignment presented in Figure 3.22A. Interestingly, unlike the complete resistance of TbR(1-480) to toyocamycin activation, TbR(1-482) can still be activated by inosine in high concentrations. Presumably, the capping residue stabilizes the bound inosine weakly in the absence of the α-D helix.

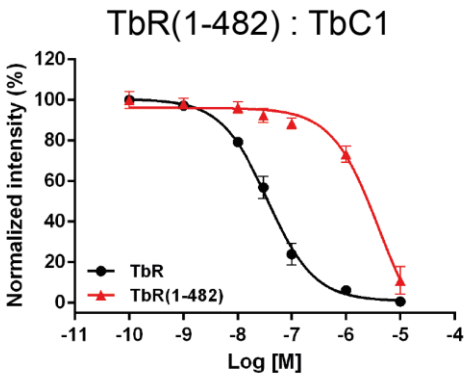

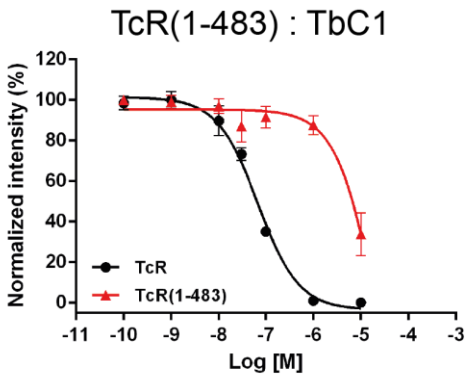

Holoenzyme	Inosine EC_{50}
TbR:TbC1	35.8 nM
TbR(1-482):TbC1	4.05 µM

Holoenzyme	Inosine EC_{50}
TcR:TbC1	68.1 nM
TcR(1-483):TbC1	> 10 µM

Fig 3.26, inosine activation of the α-D helix truncated PKAs. NanoBiT assay was conducted with membrane permeabilized cells as described in chapter 2.2.7.

3.3 Functional characterization of PKAC1 and PKAC2

In T. brucei, PKAC1 and PKAC2 are highly homologous, their amino acid sequences are 94% identical. The differences between the two isoforms reside exclusively on the N- and C-termini. The two genes locate adjacently at the same gene locus, probably resulting from an evolutionarily recent duplication event. Interestingly, the two isoforms are differentially expressed in the life cycles of the parasite: PKAC1 is expressed only in BSF while PKAC2 is expressed prominently in the PCF. Their expression is controlled by posttranscriptional regulation. PKAC1 and PKAC2 together is referred to as PKAC1/2 in the thesis since the antibody (anti-PKAC1/2) available recognizes both of them. As introduced in chapter 1.3.5, reverse genetics approaches have suggested the essential role of PKAC1 in BSF. To provide direct and doubtless evidence for the essentiality, *PKAC1* was knocked out in the presence of a rescue PKAC isoform (inducible knockout). To address the question whether PKAC1 can be replaced by PKAC2 or parts thereof, PKAC2 and the chimeras, C1C2 and C2C1, were expressed as the rescue isoform in the pleomorphic cell line Antat1.1 E 1313. *PKAC1* knockout was conducted in the presence of these rescue isoforms. We also asked whether the two isoforms formed PKA holoenzymes different in activation. To avoid confusing, all the cell lines generated in this study were listed in the following table (Table 8).

Cell line	Gene manipulation	Referred to as
Antat1.1 E 1313 *Ty-PKAC1*^{Ti}	*Ty-PKAC1* Tet inducible expression cassette inserted	[*Ty-PKAC1*^{Ti}]
Antat1.1 E 1313 *Ty-PKAC2*^{Ti}	*Ty-PKAC2* Tet inducible expression cassette inserted	[*Ty-PKAC2*^{Ti}]
Antat1.1 E 1313 *Ty-C1C2*^{Ti}	*Ty-C1C2* Tet inducible expression cassette inserted	[*Ty-C2C1*^{Ti}]
Antat1.1 E 1313 *Ty-C2C1*^{Ti}	*Ty-C2C1* Tet inducible expression cassette inserted	[*Ty-C1C2*^{Ti}]
Antat1.1 E 1313 Δ*pkac1/PKAC1 Ty-PKAC2*^{Ti}	*Ty-PKAC2* Tet inducible expression cassette inserted One endogenous *PKAC1* allele deleted	[Δ*pkac1/PKAC1 Ty-PKAC2*^{Ti}]
Antat1.1 E 1313 Δ*pkac1/PKAC1 Ty-C1C2*^{Ti}	*Ty-C1C2* Tet inducible expression cassette inserted One endogenous *PKAC1* allele deleted	[Δ*pkac1/PKAC1 Ty-C2C1*^{Ti}]
Antat1.1 E 1313 Δ*pkac1/PKAC1 Ty-C2C1*^{Ti}	*Ty-C2C1* Tet inducible expression cassette inserted One endogenous *PKAC1* allele deleted	[Δ*pkac1/PKAC1 Ty-C1C2*^{Ti}]
Antat1.1 E 1313 Δ*pkac1/PKAC1 Ty-PKAC2*^{Ti}	*Ty-PKAC2* Tet inducible expression cassette inserted both endogenous *PKAC1* alleles were deleted	[Δ*pkac1/*Δ*pkac1 Ty-PKAC2*^{Ti}]
Antat1.1 E 1313 Δ*pkac1/PKAC1 Ty-C1C2*^{Ti}	*Ty-C1C2* Tet inducible expression cassette inserted both endogenous *PKAC1* alleles deleted	[Δ*pkac1/*Δ*pkac1 Ty-C1C2*^{Ti}]
Antat1.1 E 1313 Δ*pkac1/PKAC1 Ty-C2C1*^{Ti}	*Ty-C2C1* Tet inducible expression cassette inserted both endogenous *PKAC1* alleles deleted	[Δ*pkac1/*Δ*pkac1 Ty-C2C1*^{Ti}]

Table 8, cell lines inducibly express rescue PKAC isoforms.

3.3.1 Deletion of *PKAC1* in the presence of a rescue PKAC

The previous RNAi and knockout studies have suggested the essentiality of PKAC1, albeit in part from negative data. To solve the problem, a new approach was used. The strategy was to knock out both endogenous PKAC1 alleles while expressing a Ty epitope tagged rescue gene. The rescue gene integrated into ribosomal RNA spacer in the genome and the transcription should be controlled by a Tet inducible promoter. The deletion of both *PKAC1* alleles needs two successive transfections. The rescue gene was expressed constantly until both the endogenous PKAC1 alleles were confirmed as deleted. Cell viability, growth and differentiation in the context of *PKAC1* knockout were to be studied. Furthermore, to investigate whether PKAC2 or a chimera of PKAC1 and PKAC2 are able to replace PKAC1 in BSF, three cell lines that individually express Ty epitope tagged PKAC2, C1C2 and C2C1 upon Tet induction were made. The composition of the rescue genes was depicted in Fig 3.27 A. The parent cell line used in the study is AnTat1.1 E 1313 (Bachmaier *et al.*, 2020). It expresses the Tet repressor (construct pHD1313) and can be differentiated to PCF, so the Tet-controlled expression system is available and the resulting cell lines can be used for further differentiation studies. The two plasmids pΔPKAC1-BSD and pΔPKAC1-NEO were used to replace the endogenous *PKAC1* alleles with a *BSD* or *NEO* expression cassette.

3.3.1.1 Expression of rescue genes causes no growth phenotype

The cell lines inducibly express the rescue PKAC isoforms were obtained after transfection. 3 to 4 transfected clones were subjected to immunoblotting analysis. As shown in Fig 3.27B, the expression of Ty-PKAC1, Ty-PKAC2 and Ty-C1C2 was all tightly controlled by Tet in the clones. In [*Ty-C2C1*^{Ti}], only clone #1 was useful. The #2 did not express the target protein while the #3 was leaky. Interestingly, all the clones grew at similar rate as the parent cell line, although the robust expression of the rescue PKAC increased the total level of intracellular PKAC1/2.

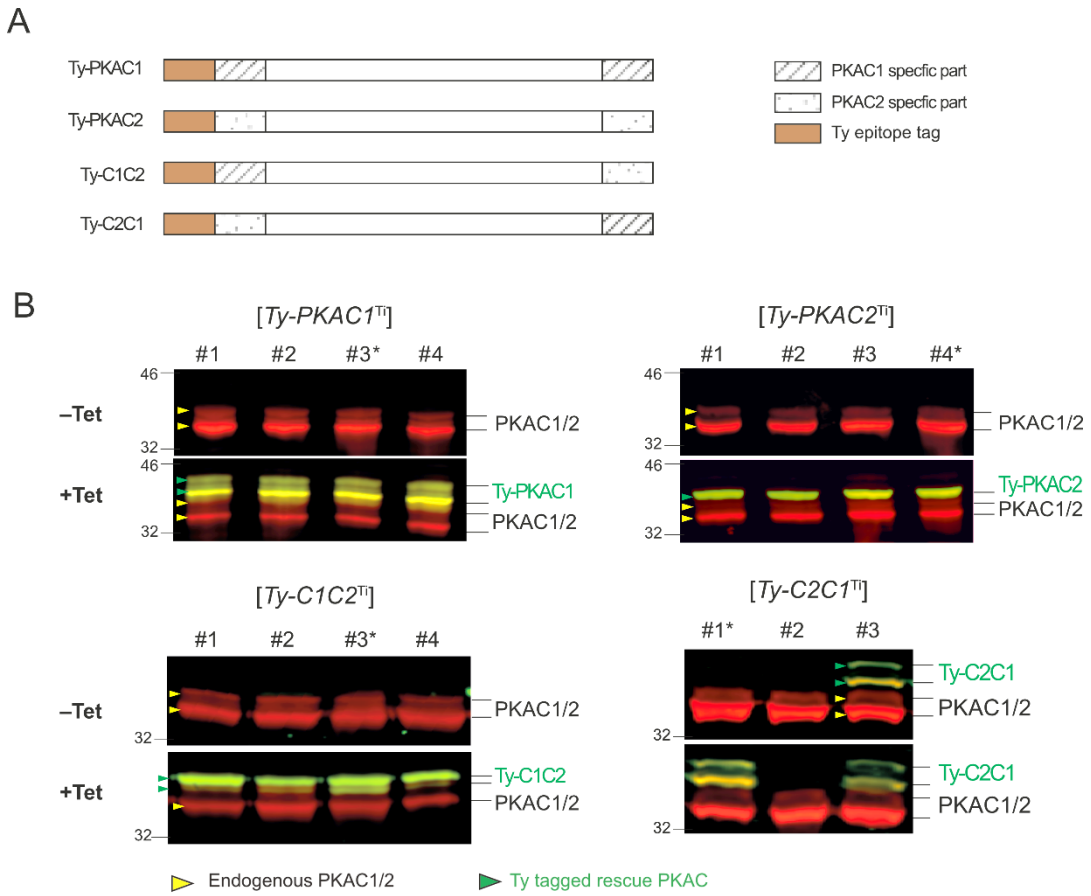

Fig 3.27, Expression of Ty epitope tagged rescue *PKAC* genes upon Tet induction. A, the structure of rescue genes. The plasmid vector used is pHD615, the target gene is expected to be integrated in RDNA spacer sequence. B, Expression of rescue genes. At least 3 clones of each cell line were analyzed by Western blot. Cells treated with or without Tet were harvested after 24 h. Clones marked with an asterisk were used for further studies.

3.3.1.2 Deletion of the first *PKAC1* allele

The clone #3 of cell line [*Ty-PKAC1*^{Ti}], clone #4 of [*Ty-PKAC2*^{Ti}], clone #3 of [*Ty-C1C2*^{Ti}] and clone #1 of [*Ty-C2C1*^{Ti}] were selected for *PKAC1* knockout. The construct pΔPKAC1-BSD designed to replace *PKAC1* gene with the blasticidin resistance gene *BSD* was transfected in these clones. Tet was added in the process for expressing the corresponding rescue PKACs. The resulting cell lines were referred to as [Δ*pkac1/PKAC1 Ty-PKAC*^{Ti}]. The integration of *BSD* in the resulting cell lines was probed by PCR using different primers as depicted in Fig 3.28A. Primer pair 1 and pair 2 were used to examine the endogenous *PKAC1* allele, primer pair 3 and 4 were used to examine the integration of *BSD* into *PKAC1* allele. In addition, the house keeping gene *PDEB1* was amplified in a bid to examine the quality of the extracted genomic DNA of each cell line. 3 to 4 transfected clones of each cell line were analyzed. As

shown in Fig 3.28B, clone #1, #4 and #5 of cell line [Δ*pkac1/PKAC1 Ty-PKAC2*^{Ti}], clone #3 and #4 of [Δ*pkac1/PKAC1 Ty-C1C2*^{Ti}] and clone #1 and #2 of [Δ*pkac1/PKAC1 Ty-C2C1*^{Ti}] showed the expected bands in the gels with the primer pair 3 and 4, indicating correct integration of *BSD*. However, no bands were amplified from the three clones of what we expected to be [Δ*pkac1/PKAC1 Ty-PKAC1*^{Ti}], albeit the amplified *PDEB* bands suggesting the extracted genomic DNA was applicable. A further PCR with primer pair 1 and 2 were done and expected PCR products were obtained (Fig 3.28B). These results indicate no integration of *BSD* into either endogenous *PKAC1* allele. Western blot analysis revealed that the rescuing Ty-PKAC1 protein was gone (Fig 3.28C), suggesting the ribosomal DNA spacer integrated *Ty-PKAC1* gene was replaced by the *BSD* expression cassette. Mistargeting to *Ty-PKAC1* is possible, because the homology arms on the pΔPKAC1-BSD construct contain sequences of *PKAC1* gene. A repeat transfection was done, but unfortunately still clones correctly integrated by *BSD* were not obtained.

A

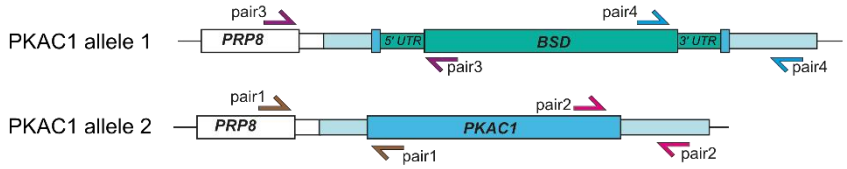

B

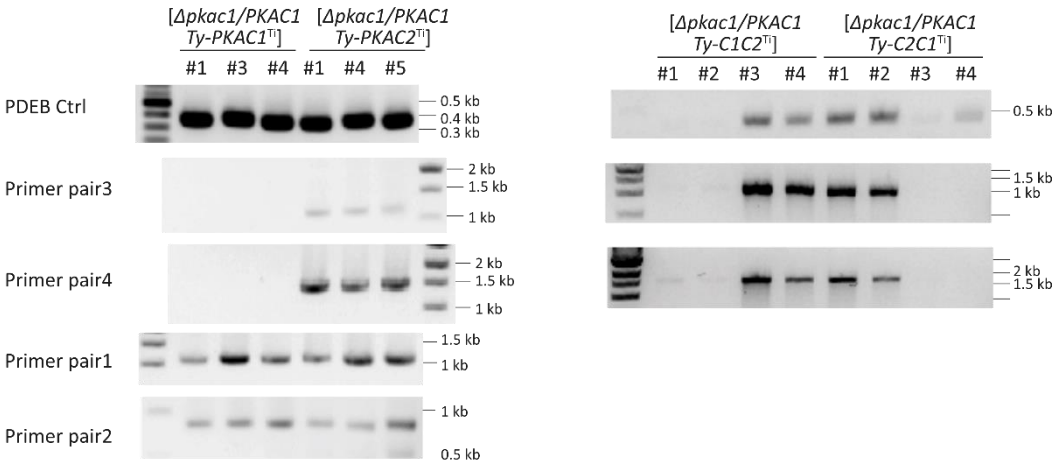

C

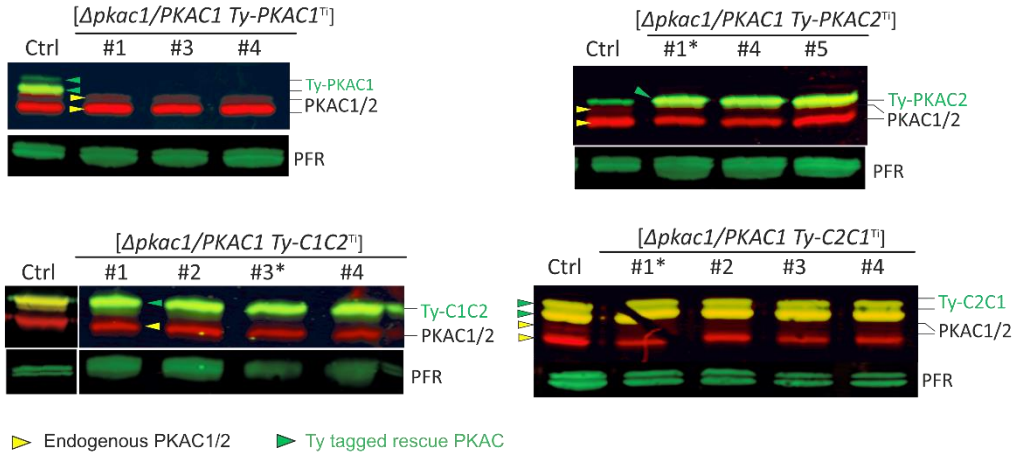

Fig 3.28 Knockout of the first PKAC1 allele. A, primer pairs used for PCR verification. B, PCR probing the integration of *BSD* expression cassette into the endogenous PKAC1 locus. C, Western blot probing the expression of rescue PKAC in each cell line; The corresponding parent cell line of each was used as control (Ctrl). Anti-PKAC1/2, anti-PFR and anti-Ty were used.

3.3.1.3 Deletion of the second endogenous PKAC1 allele

Although knocking out of *PKAC1* in the Ty-PKAC1 expressing cell line was not possible, *PKAC1* knocking out was continued in the other three cell lines. The construct pΔPKAC1-NEO was transfected in each *PKAC1* hemizygous knockout cell line. Tet was added during cell culturing and transfection. The resulting cell lines were referred to as [Δ*pkac1/*Δ*pkac1 Ty-PKAC*^{Ti}]. The integration of neomycin resistant gene *NEO* in the resulting cell lines was probed by PCR using primer pair 5 and pair 6 as depicted in Fig 3.29A. As shown in Fig 3.29B, clone #2 and #3 of [Δ*pkac1/*Δ*pkac1 Ty-PKAC2*^{Ti}], clone #2, #3 and #4 of [Δ*pkac1/*Δ*pkac1 Ty-C1C2*^{Ti}] and clone #2, #3 and #5 of [Δ*pkac1/*Δ*pkac1 Ty-C2C1*^{Ti}] showed the expected bands on the gel, indicating successful integration of *NEO*. These clones were further analyzed by immunoblotting as shown in Fig 3.29C. In comparison to the respective parent cell line, the bands of endogenous PKAC1 (commonly two bands due to phosphorylation) disappeared in the three resulting *PKAC1* homozygous knockout cell lines. Interestingly, there was a faint band in between of the unphosphorylated and phosphorylated endogenous PKAC1 bands. It is very likely the endogenous PKAC2, since the size of PKAC2 is slightly bigger than PKAC1 (38.5 versus 38 kDa) and it used to be overlapped by PKAC1 bands. These results indicate the successful deletion of both *PKAC1* alleles.

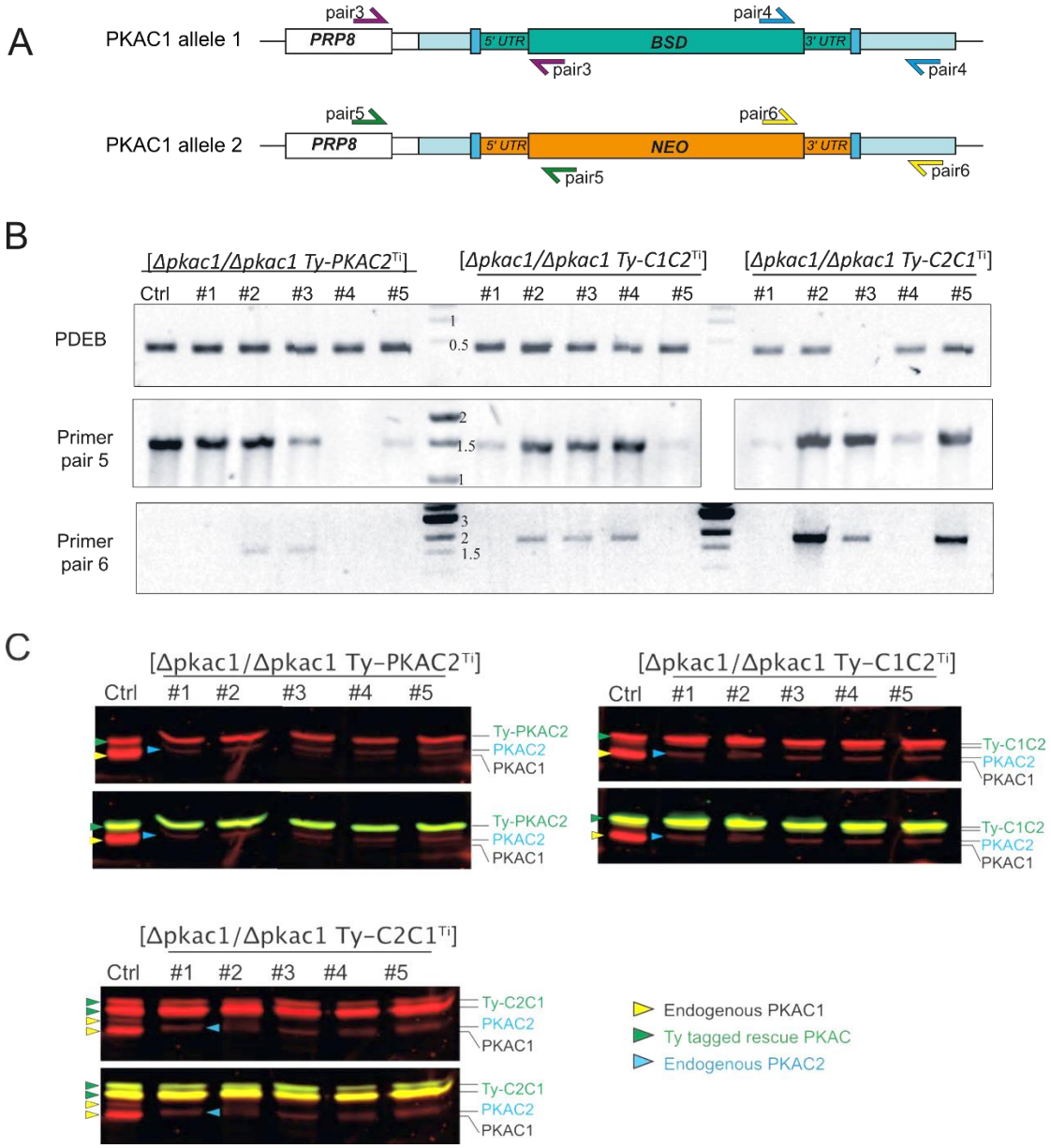

Fig.3.29 Knockout of the second *PKAC1* allele. A, Primers used for examining the integration of *NEO* expression cassette into the second *PKAC1* allele. B, PCR probing the integration of *NEO*. C, Western blot probing C subunits expression. anti-PKAC1/2, anti-Ty and anti-PFR were used; the Ty signal of the rescue Ty-PKAC was shown in green in a duplicate image. All cells were treated with Tet. The corresponding parental *PKAC1* hemizygous knockout cell line was used as control (Ctrl).

3.3.1.4 No significant phenotype observed in the cell lines lacking PKAC1

Clone #2 and #3 of each PKAC1 homozygous knockout cell line were used for further growth phenotype characterization. The cells cultured in the absence or presence of Tet for 48 hours were harvested for immunoblotting analysis. As shown in Fig 3.30B

and C, neither PKAC1 nor the rescue Ty-PKAC were shown in the clones of [Δ*pkac1/*Δ*pkac1 Ty-C1C2*^{Ti}] and [Δ*pkac1/*Δ*pkac1 Ty-C2C1*^{Ti}] in the absence of Tet. The two clones of [Δ*pkac1/*Δ*pkac1 Ty-C2*^{Ti}], however, were still expressing Ty-C2, indicating leaky expression not observed prior to knockout of the first allele. As shown in Fig 3.30D, the overall PKAC1/2 signal intensity of the three cell lines in the absence of Tet was quantified and normalized by the house-keeping gene PFR. [Δ*pkac1/*Δ*pkac1 Ty-C2*^{Ti}] showed the highest intensity as expected due to the leakiness of Ty-C2. [Δ*pkac1/*Δ*pkac1 Ty-C2C1*^{Ti}] showed the lowest signal. The growth curve of the three cell lines revealed that [Δ*pkac1/*Δ*pkac1 Ty-PKAC2*^{Ti}] and [Δ*pkac1/*Δ*pkac1 Ty-C1C2*^{Ti}] had identical growth rate in the absence and presence of Tet as indicated by their PDTs (Fig 3.30E, table), even though both *PKAC1* alleles were removed. [Δ*pkac1/*Δ*pkac1 Ty-C2C1*^{Ti}] showed slightly reduced growth in the absence of Tet, likely due to the low PKAC activity with the loss of both PKAC1 and rescue Ty-C2C1 expression.

These results suggest PKAC1 is not essential for BSF, at least in this Antat1.1 E 1313 cell line. A previous study knocking down PKAC1 or PKAC1/2 by a hairpin-based RNAi in Antat1.1 1313 cell line resulted in transfectants that showed no growth or cytokinesis phenotypes, albeit over 90% PKAC1 or PKAC1/2 was depleted (PhD thesis Bachmaier, 2015). However, we cannot exclude that whether the loss of PKAC1 was compensated by endogenous PKAC2 or PKAC3.

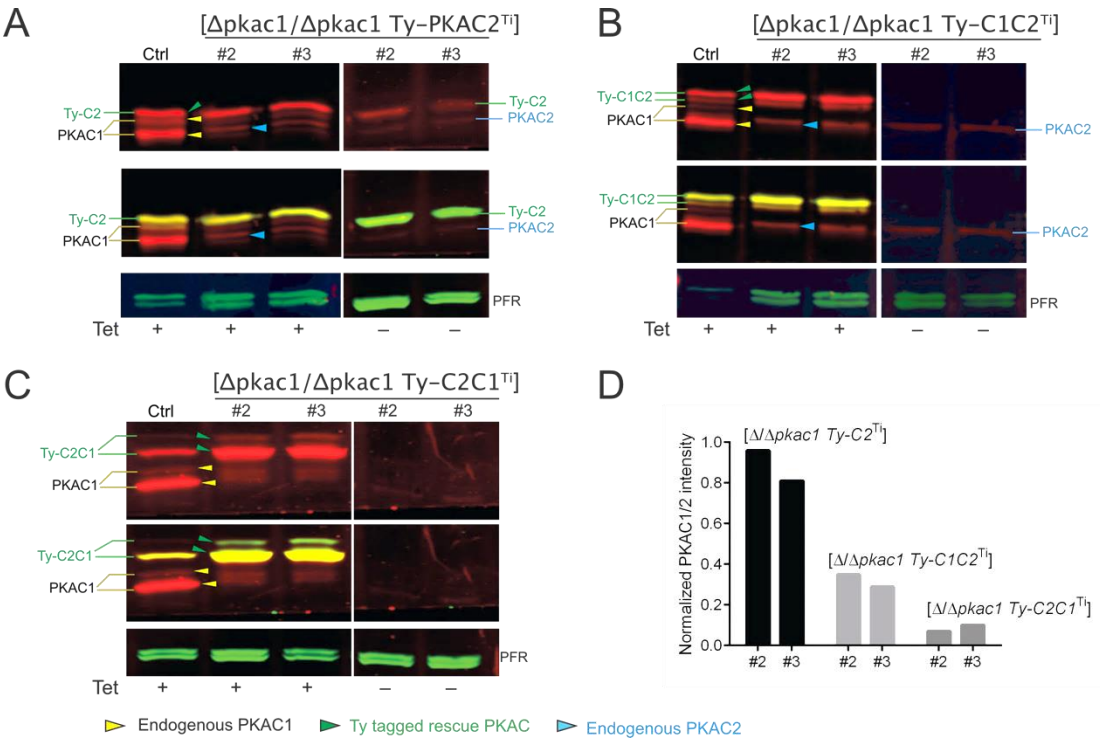

E

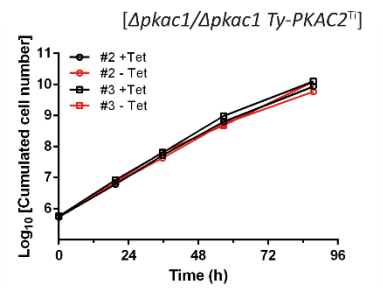

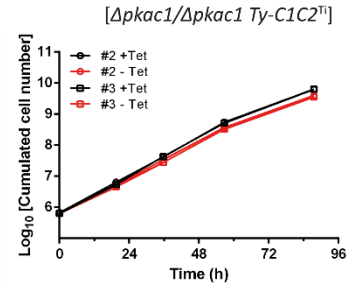

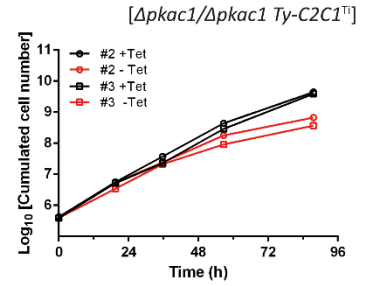

Cell line	clone	-Tet	+Tet
[Δpkac1/Δpkac1 Ty-PKAC2Ti]	#2	6.3	6.5
	#3	6.1	6.1
[Δpkac1/Δpkac1 Ty-C1C2Ti]	#2	6.6	7.0
	#3	6.6	7.0
[Δpkac1/Δpkac1 Ty-C2C1Ti]	#2	6.6	8.2
	#3	6.6	8.9

Fig 3.30, Characterization of the *PKAC1* knockout cell lines in the absence of rescue PKAC. Western blot probing the expression of the C-subunits in [Δ*pkac1*/Δ*pkac1 Ty-PKAC2*^{Ti}] (A), [Δ*pkac1*/Δ*pkac1 Ty-C1C2*^{Ti}] (B) and [Δ*pkac1*/Δ*pkac1 Ty-C2C1*^{Ti}] (C) in the absence of Tet; Anti-PKAC1/2, anti-Ty and anti-PFR were used; the Ty signal of the rescue Ty-PKAC was shown in green in a duplicate image. The corresponding parental *PKAC1* hemizygous knockout cell lines was used as control (Ctrl). D, quantification of PKAC1/2 signal intensity of the cell lines in the absence of Tet. Data was normalized by the corresponding PFR signal. E, growth curve of the cell lines in the presence and absence of Tet. The table at the bottom right lists their PDTs (h).

3.3.2 Comparing the activation of different PKA holoenzymes in BSF and PCF

The functional diversity of PKAC isoforms is unclear so far. The N- or C- end of PKAC1 and PKAC2 are divergent in amino acid sequence, which are speculated to be related to different properties or function of the two isoforms. Given the fact that the N-terminal domain deleted PKAR has shown not binding to PKAC1/2 (PhD thesis Krumbholz, 2006), it was speculated that this N-terminal domain and its interaction with N- or C-terminal of PKAC are critical for PKA holoenzyme formation. To compare the activation of different PKA holoenzymes. SmBiT N-terminally fused PKAC isoforms, including Sm-PKAC1, Sm-PKAC2, Sm-C1C2 and Sm-C2C1, were transfected in a cell line

constitutively expressing LgBiT-PKAR. These SmBiT-PKAC subunits were expected to form different PKA holoenzymes with LgBiT-PKAR so that their activations can be evaluated by NanoBiT assay. Furthermore, the BSF transfectants were differentiated to PCF, PKA activation were studied in both BSF and PCF cells.

3.3.2.1 Establishment of NanoBiT assay in a pleomorphic cell line

To study the PKA activation in both BSF and PCF forms, the pleomorphic AnTat1.1 13:90 strain was used in this study. Initially, *LgBiT* sequence was inserted into the 5' end of one of the endogenous *PKAR* genes in this cell line by *in situ* tagging, obtaining the AnTat1.1 13:90 LgR cell line. Subsequently, pHD615(PAC)-SmBiT_PKAC1, pHD615(PAC)-SmBiT_PKAC2, pHD615(PAC)-SmBiT_C1C2 and pHD615(PAC)-SmBiT_C2C1 were transfected in this cell line, respectively. The resulting four cell lines were referred to as *Sm-PKAC1*^{Ti}, *Sm-PKAC2*^{Ti}, *Sm-C1C2*^{Ti} and *Sm-C2C1*^{Ti} in the thesis. Protein expression of the resulting cell lines in the absence and presence of Tet was analyzed by immunoblotting. All SmBiT fused PKAC isoforms were expressed and detected by immunoblotting as shown in Fig 3.31A. The growth curve of each cell line in the absence and presence of Tet was studied. The parent cell line was included as a control. As shown in Fig 3.31B and C, the four cell lines cultured in the absence of Tet showed similar PDT ranging from 6.5 to 6.9 h, closing to that of the parent cell line. However, a mild growth phenotype (PDTs increased by 4 to 6 hours) was seen in the presence of Tet, suggesting the elevated PKAC activity is also detrimental to cell proliferation or viability in this experiment.

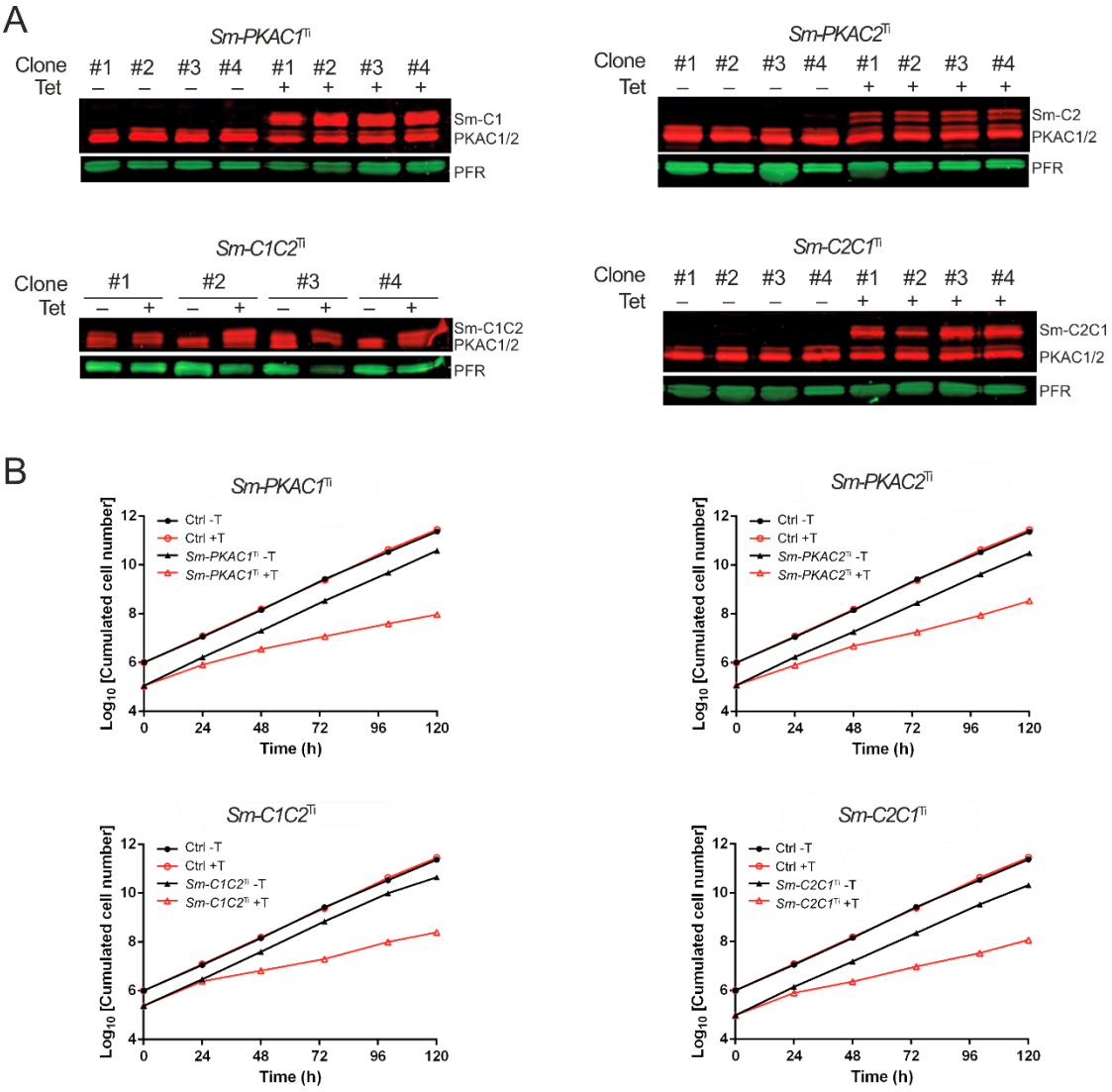

C

	Ctrl	*Sm-PKAC1*^{Ti}	*Sm-PKAC2*^{Ti}	*Sm-C1C2*^{Ti}	*Sm-C2C1*^{Ti}
-Tet	6.7	6.5	6.7	6.9	6.8
+Tet	6.6	12.4	10.5	12.0	11.7

Fig 3.31 Generation of SmBiT-PKAC^{Ti} cell lines. A, Western blot probing the inducible expression of SmBiT-PKACs. The following antibodies were used: anti-PKAC1/2, anti-PFR and anti-PKAR (band not shown). B, Growth curve of the cell lines. Cell density was measured daily using cell counting chamber. C, cell population doubling time (PDT), the unit is hour.

3.3.2.2 Comparison of different PKA holoenzymes activation in BSF

The activation of the different PKA holoenzymes was evaluated by NanoBiT assay. The cells were harvested after 24 h Tet induction. Cell suspension was supplemented with 2% (v/v) NanoGlo buffer for permeabilizing the membrane and incubated with different concentrations of ligands. 2% was found efficiently permeabilizing cells while

not reducing luminescence, thus 2% rather than 5% was used in the experiments. PKA activation by toyocamycin and inosine were firstly assessed. Interestingly, the activation of different holoenzymes is very similar as shown in Fig 3.32A. To see if the PKA holoenzymes are differentially activated by natural nucleosides. Sm-PKAC1^{Ti} and Sm-PKAC2^{Ti} were treated with guanosine and adenosine. As listed in Fig 3.32B, the EC_{50} of either ligand is very similar in different cell lines, indicating these holoenzymes (R:C1, R:C2, R:C1C2 and R:C2C1) are similarly sensitive to ligand activation and rejecting the working hypothesis.

A

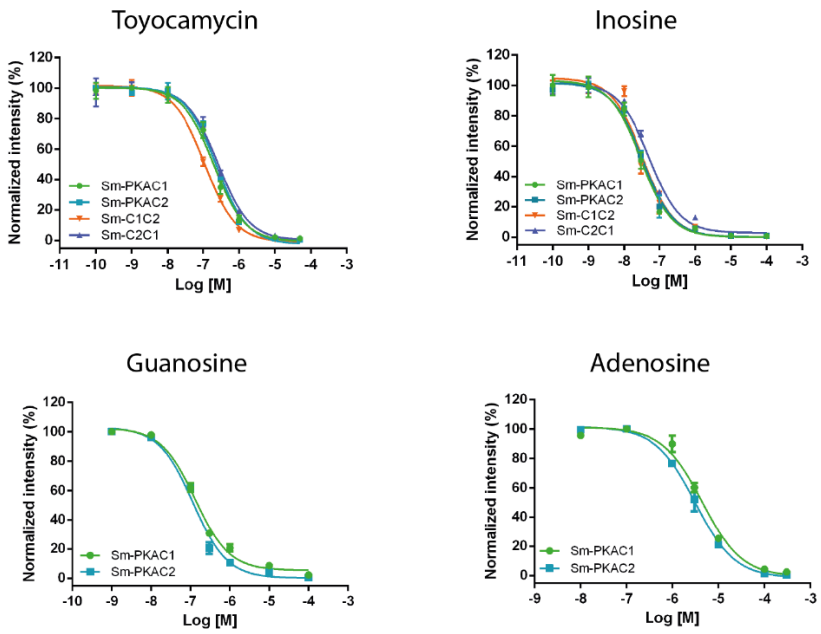

B

Cell line	Toyocamycin (nM)	Inosine (nM)	Guanosine (nM)	Adenosine (μM)
Sm-PKAC1^{Ti}	197.8	29.7	131.9	4.49
Sm-PKAC2^{Ti}	236.6	34.3	116.7	3.15
Sm-C1C2^{Ti}	262.9	51.8	–	–
Sm-C2C1^{Ti}	111.0	33.9	–	–

Fig 3.32 Activation of different PKA holoenzymes in BSF. A, NanoBiT assay measuring PKA holoenzyme activation by different compounds. The data is normalized to the highest value of each measurement. The Standard deviation of each data point was calculated from three replicates. B, the EC_{50} of compounds in activating different PKA holoenzymes.

3.3.2.3 Comparison of different PKA holoenzyme isoforms in PCF

The phosphorylation of PKAC isoforms in PCF have shown to be different to BSF. To further investigate PKA activation in PCF, the four cell lines obtained above were differentiated to PCF as described in section 2.2.1.5. The expression of SmBiT fused

PKAC isoforms was probed by immunoblotting. As shown in Fig 3.33A, Sm-PKAC1 and Sm-C2C1 were well expressed upon Tet induction. However, the expression of Sm-PKAC2 and Sm-C1C2 was very low. Nevertheless, the luminescence was detected from the two cell lines. Permeabilized cells were treated with different concentrations of inosine and the PKA activation was assessed by NanoBiT assay. As shown in Fig 3.33B, the EC_{50} of inosine is very similar in the four cell lines, ranging from 11 nM to 15 nM. This indicates these PKA holoenzymes perform similarly in response to inosine activation. Interestingly, in comparison to the values measured in BSF, the EC_{50} measured in PCF is in general 2 to 3-fold lower, suggesting PKA might be more sensitive to inosine activation in PCF.

In summary, PKAC1 and PKAC2 have same properties in BSF and PCF with respect to kinase activation. The two isoforms and probably PKAC3 are functionally redundant. Therefore, the best way to study the role of the C subunits is to diminish the activity of all three kinases simultaneously. A dominant-negative PKAR mutant has been verified to block PKAC kinase activity in chapter 3.2.2. In the next chapter, we attempted to design an inhibitor targeting PKAR, expecting it to inhibit PKA holoenzyme activation.

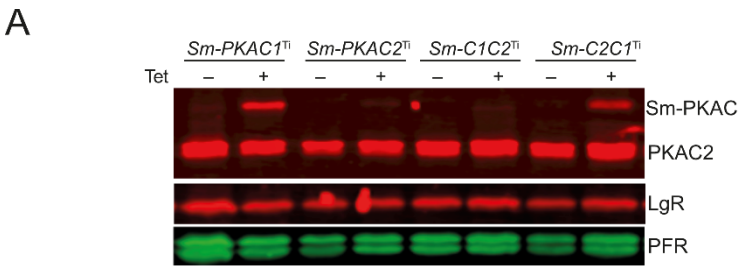

B

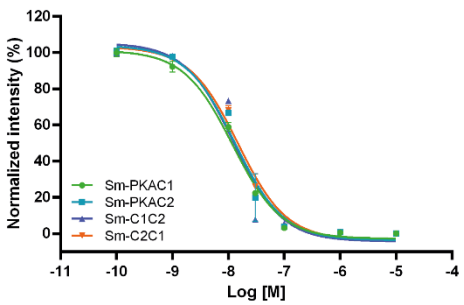

EC_{50} of Inosine (nM)

	PCF	BSF
Sm-PKAC1^{Ti}	11.8	29.7
Sm-PKAC2^{Ti}	13.7	34.3
Sm-C1C2^{Ti}	12.4	51.8
Sm-C2C1^{Ti}	14.8	33.9

Fig 3.33 Activation of different PKA holoenzymes in PCF by inosine. A, Western blot probing PKAC expression in PCF cells. The following antibodies were used: anti-PKAC1/2, anti-PFR and anti-PKAR. B, inosine activation of different PKA holoenzymes. The measured luminescence was normalized by the highest value of each measurement. The Standard deviation of each data dot was calculated from three technical replicates.

3.4 A strategy for inhibition of PKAC activity and validation

In contrast to the PKAC1 Knockout (chapter 3.3.1) and RNAi data (PhD thesis Bachmaier, 2015), inhibition of all C subunits by a dominant-negative PKAR mutant resulted in serious growth phenotype and suggested the importance of active PKA for the surviving and proliferation of trypanosomes (see chapter 3.2.2). The particular α-D helix of *T. brucei* PKAR is involved in the ligand binding and was hypothesized to initiates PKAR conformation change by moving toward the B-site (NBD-B) upon ligand binding. PKAR conformation change is essential for PKA activation. In chapter 3.3.2, the truncation of the α-D helix in both *T. brucei* and *T. cruzi* PKAR resulted in barely dissociated PKA holoenzymes, suggesting the essentiality of the α-D helix for *T. brucei* and *T. cruzi* PKA activation *in vivo*. These findings uncover the possibility of inhibiting PKA activation by interfering or blocking the movement of the α-D helix. This is expected to be achieved by a properly designed bulky inosine analog, which interacts the B-site via the ribose moiety but interferes with the interactions between Y484 and Y485 and the NBD-B via spatial hindrance. Our strategy of developing a PKA inhibitor is therefore starting from modifying inosine, expecting to convert it to an PKA inhibitor by adding well-designed side groups. Converting an activator to an inhibitor is a popular strategy in drug development and has seen many successes (Tolbert *et al.*, 2007; Courter *et al.*, 2014). The obtained inosine bound PKAR crystal structure (PDB: 6FLO) has helped us understand better the ligand binding mechanism. First computational docking and design of few compounds was initiated by Yuri Volpato in our group. Compounds were synthesized by Dr. Andreas Rentsch of Dr. Frank Schwede team, BIOLOG Life Science Institute GmbH & Co.KG, and Dr. Matjaz Brvar of Prof. Dr. Oliver Plettenburg group, Helmholtz Zentrum München, with whom we now conduct a large-scale program of design, docking, synthesis and testing in collaboration. These activities have also been funded by the BMBF (Target validation).

3.4.1 Converting inosine to PKA inhibitor by adding side chain

As shown in Fig 3.34, inosine forms one hydrogen bond with N481, a π-stacking with the capping residue (Y482) and one hydrogen bond with Y485 of the α-D helix. These interactions stabilize inosine binding and in turn pull the α-D helix towards the B-site. In order to disrupt the interactions, we planned to modify the 3 highlighted positions (N1, C6 and N7) of inosine by adding side groups (Fig 3.35). These side groups are expected to reside at the spatial localization of the α-D helix (inosine bound state), forcing the α-D helix staying away from the NBD-B. In this case, Y484 and Y485 are

supposed to not form interactions with the NBD-B and thus not result in a conformation change of PKAR. One concern is that the inhibitor may have lower binding affinity relative to inosine as a consequence of the lost or weakened interactions with the α-D helix.

A B

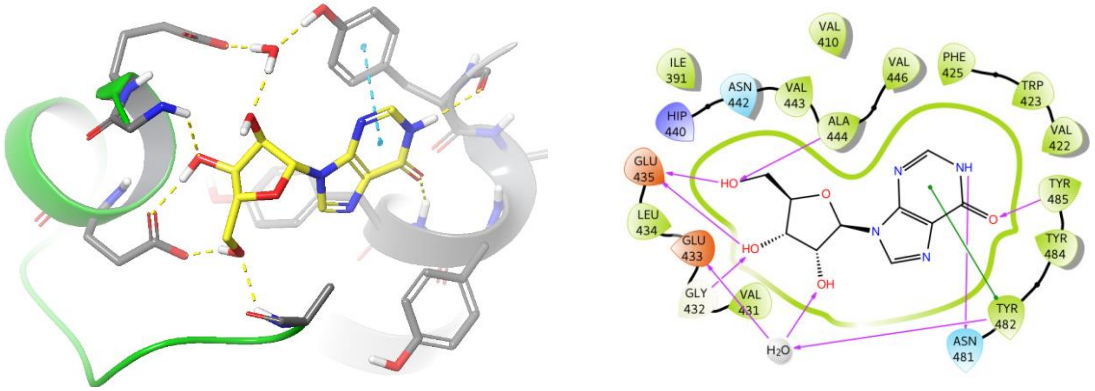

Fig 3.34, A, the interaction network of inosine in the NBD-B of PKAR. Inosine is represented as stick in yellow. The RBC-B domain and the α-D helix are represented as ribbon in green and gray, respectively. Hydrogen bond and π-stacking are shown as dashed line in yellow and cyan, respectively. B, 2D representation of the hydrogen bond network of inosine in NBD-B. The arrow of the magenta lines indicates hydrogen donating effect.

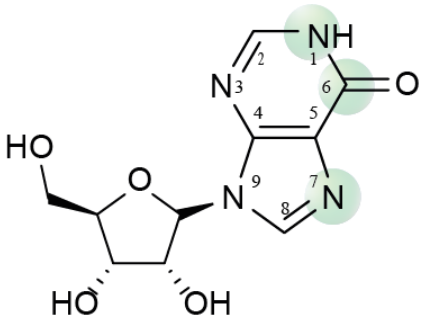

Figure 3.35, the structure of inosine. The numbering of the purine ring is indicated. The three green shaded atoms, N1, C6 and N7 are sites of substitution.

3.4.1.1 Inosine analogs with a single side group reveals a more complex activation mechanism of TbPKA

The 3 sites on the purine ring of inosine were separately modified by different side groups. A benzyl group was added to N1, resulting in 1-benzyl-inosine (Fig 3.36A, the bottom left corner). Docking of 1-benzyl-inosine to the B-site of PKAR was performed.

Before running a docking, the α-D helix was computationally deleted from PKAR structure as if it would adopt a flexible structure, so it would not interfere with the binding of bulky inosine analog. As shown in Fig 3.3.6A, docking suggested a π-stacking interaction between the benzyl group of this compound and W423 on the β-barrel of the B-site. Superposition of a second PKAR structure including the α-D helix showed clashes between the benzyl group and residues (N481 and Y482) of the α-D helix. This suggests the α-D helix cannot approach the B-site upon binding of 1-benzyl-inosine as it used to be. Unexpectedly, NanoBiT assay revealed that 1-benzyl-inosine is still a PKA activator. It means 1-benzyl-inosine binding still induces a conformation change of PKAR. Its EC_{50} is 1.2 μM, approximately 34-fold higher than that of inosine. All NanoBiT assays conducted in this chapter used membrane permeabilized cells by 2% NanoGlo buffer. The binding of 1-benzyl-inosine to NBD-B was measured by isothermal titration calorimetry (ITC). A PKAR mutant, PKAR(199-499)_PBCA, was used in the measurement. Three key residues in the RBC-A of this protein are replaced by their counterparts in the PBC-A of mammalian PKAR, resulting in a cAMP binding A-site (E311A, T318R and V319A (George Githure & Yuri Volpato, manuscript, 2021)). After purification, this protein was denatured to remove all bound ligands and then refolded properly in the presence of cAMP, so that the B-site is empty and compound binding to B-site can be assessed separately. ITC revealed a K_D of 63.6 nM of 1-benzyl-inosine to the B-site. The value is nearly 10 times higher than that of inosine, likely due to the loss of the interaction the α-D helix. These results suggest adding a benzyl group at N1 is not sufficient to inhibit PKA activation. Thus, we have to reject our first working hypothesis in its simplest form.

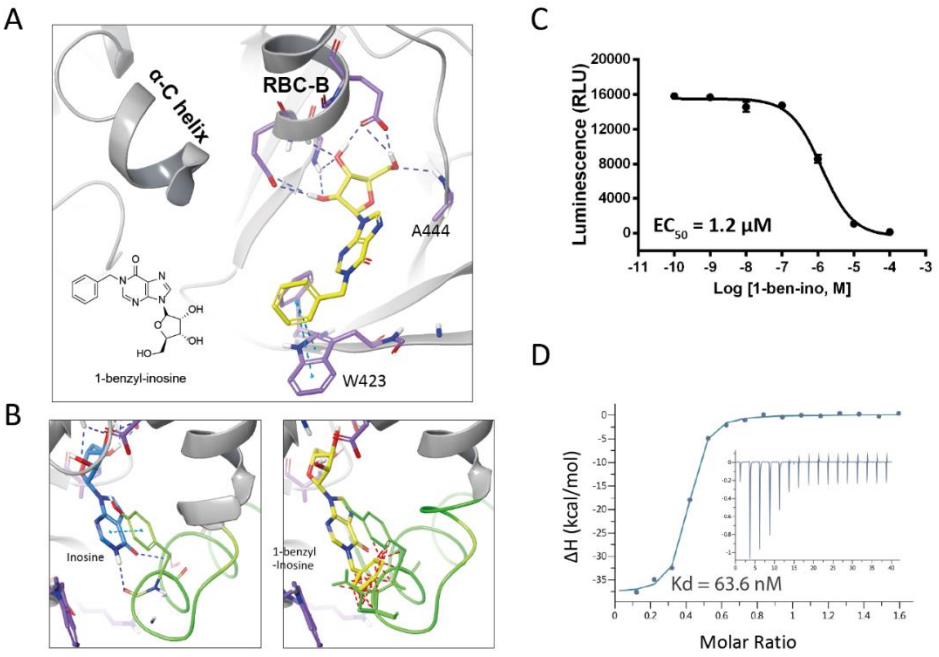

Fig 3.36, A, cartoon representation of 1-benzyl-inosine docking in NBD-B. 1-benzyl-inosine and the residues involved in ligand-receptor interaction are shown in stick representation in yellow and purple, respectively. PKAR was shown in cartoon representation in gray. Hydrogen bond and π-stacking are shown in dashed line in deep blue and sky blue, respectively. The structure of 1-benzyl-inosine is on the bottom left of the panel. B, Comparison of the binding of inosine (left) and 1-benzyl-inosine (right). The α-D helix from a duplicated PKAR structure was overlapped and presented in thin tube representation in lime. The red dashed lines represent the clashes. C, NanoBiT assay testing the EC_{50} of 1-benzyl-inosine. Membrane permeabilized cells were used. The presented EC_{50} is the mean of two independent experiments, both of which were performed by technical triplicates. D, ITC measurement of the binding affinity. The presented K_D is the mean of two independent experiments.

More inosine analogs were synthesized and tested. To add a side group to the N7 of inosine, 7-deaza-7-bromo-inosine was used as building block. The building block itself is a strong activator as inosine, while its C7 bromo atom can be conveniently replaced by designed groups in synthesis. A 2-hydroxy-4-methoxy-styryl group and a 2-ethyl-5-methoxyphenol group were added to the C7, resulting in two candidates, D238 or D239 (Fig 3.37A and C). As shown in Fig 3.37, docking suggests 2 possible poses of each compound in the B-site. Except for the pose 2 of D239, the other poses of D238 and D239 are very similar. They allow interaction of K420 or R413 with the stretched C7 side group. In pose 2, the C7 side group of D239 is kinked and forms a π-stacking with F425 and a hydrogen bond with H430 (Fig 3.37B and D). Superposition of an unmodified PKAR structure demonstrates that the C7 side group of D238 (pose 1 and

2) and D239 (pose 1) occupies the spatial position of Y484, while the side group of the pose 2 D239 occupies the position of Y485 (Fig 3.37E). Although the C7 side group of D238 and D239 thus creates spatial hindrance preventing the α-D helix to approach the B-site (Fig 3.37E), NanoBiT assay reveals that both compounds are still strong activators. The EC_{50} of D238 and D239 is 306 nM and 142 nM, respectively. The slightly higher activation potency for D239 is probably due to the higher flexibility of the side group. Interestingly, the K_D of D238 and D239 binding is about 10 nM as revealed by ITC, the value is close to that of inosine (4~6 nM). Compared to 1-benzyl-inosine, the higher binding affinity of the two compounds might result from 1) a stronger interaction of the C7 side group with the residues of the B-site relative to the benzyl group with W423; 2) possible interactions with the α-D helix.

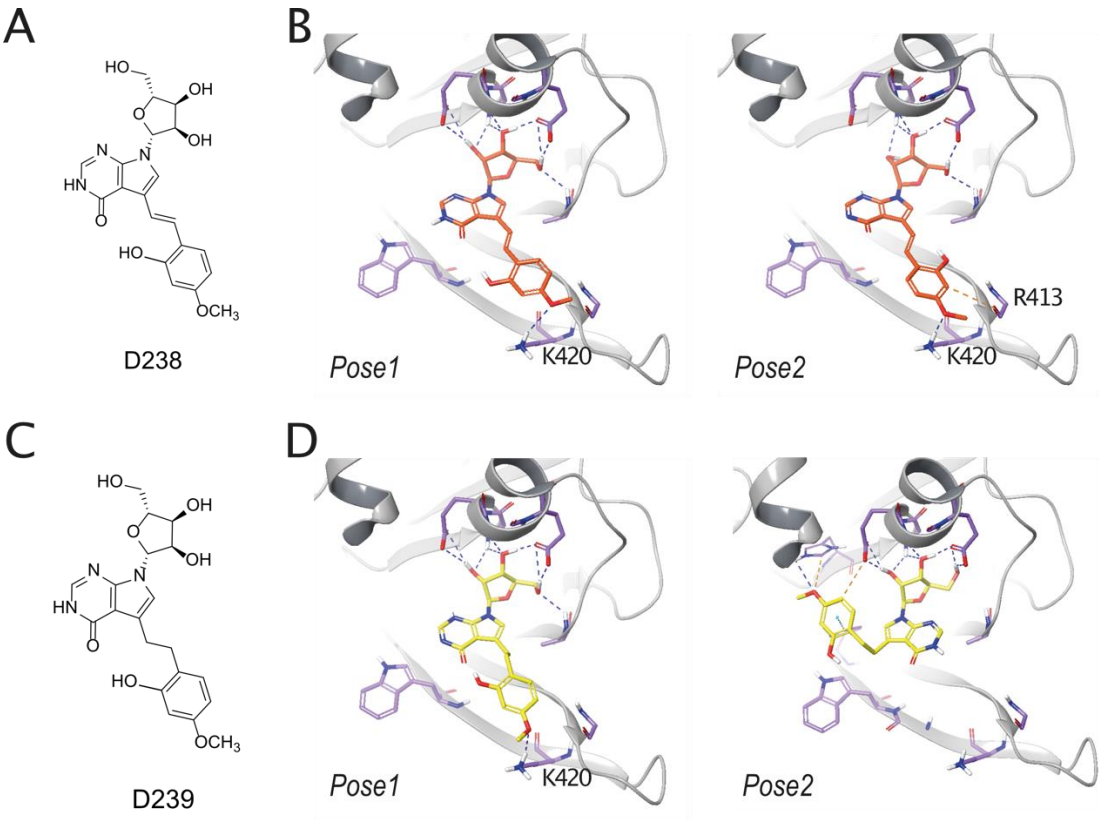

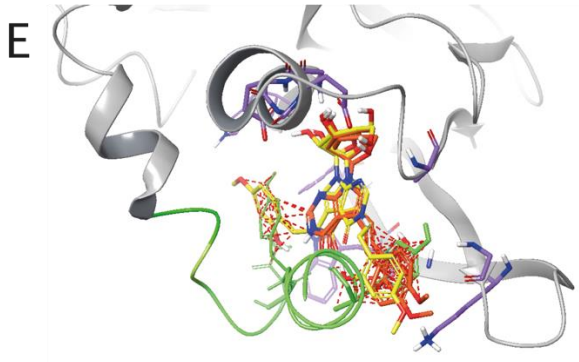

F

Compound	EC_{50} (nM)	K_D (nM)	EC_{50}/K_D
Inosine	37	4	9.3
1-benzyl-ino	1210	63.6	19
D238	306	9.9	31
D239	141	10.5	13.4

Fig. 3.37, A, chemical structure of D238; B two poses of D238 docking in the NBD-B. C, chemical structure of D239; D, two poses of D239 docking in the NBD-B D239. E, D238 or D239 occupies the spatial position of the α-D helix. The red dashed lines represent clashes. F, Comparison of EC_{50} and K_D values of inosine, 1-benzyl-inosine, D238 and D239. In the docking images, D238 and D239 were shown in sticks representation in orange and yellow, respectively. Hydrogen bond was represented by dashed line in deep blue. The α-D helix from a overlaid full-length PKAR structure was represented as thin tube in lime.

The following 3 C6 modified inosine analogs (MB037, MB055 and MB058) were then generated and tested. These compounds have poorer docking scores in comparison to 1-benzyl-inosine, D238 and D239, since the C6 side groups do not form interactions with the residues of the B-site backbone. Instead, they seem to traverse the spatial localization of the α-D helix as shown in Fig 3.38. To our surprise, these compounds were activators, the EC_{50} of MB058 is only 140 nM. The binding of the three compounds to the B-site were not measured, but it is most likely in low nanomolar range as suggested by the EC_{50} value.

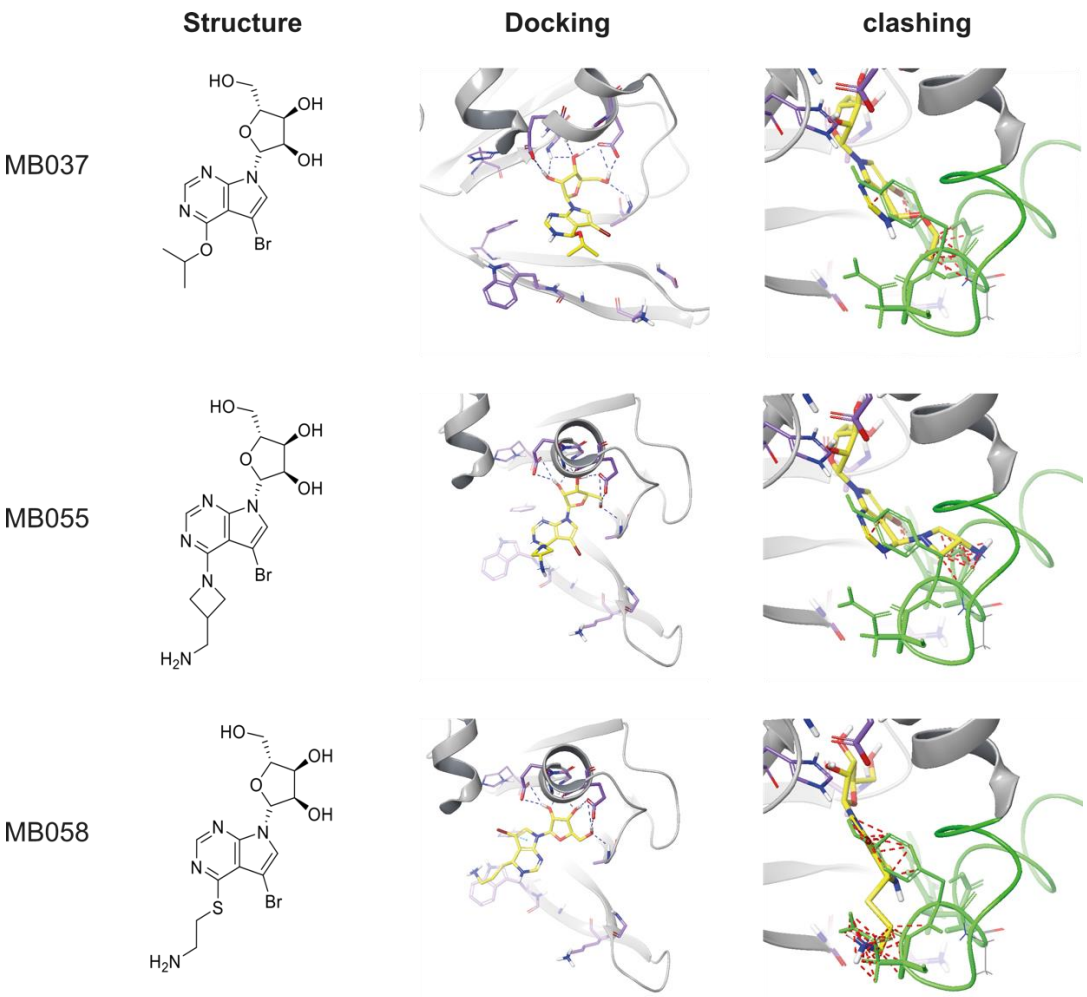

Fig. 3.38, The structures, docking poses and clashings with the α-D helix of the C6 modified inosine analogs. The representation of the structural components is similar as Fig 3.36.

Combining the results from these single site modified inosine analogs, we speculate that the α-D helix moves more flexibly. Presumably, the α-D helix bypasses the spatial hindrances caused by the side groups and still interacts with the B-site. The proline residue in the linkage region between the α-B and α-C helices as well as another proline between the α-C and α-D helix may enable the flexible movement of both α-C and α-D helices.

3.4.1.2 Inosine analogs containing N1 and C7 side groups show dissociation of binding affinity from activation potency

A benzyl group and a 2-ethyl-5-methoxyphenol group were installed to the N1 and C7 positions of the backbone compound, generating a bulkier compound, B294 (Fig 3.39) ITC showed that it retains high binding affinity to the B-site with a K_D of 26.5 ± 4.0 nM. The value is close to that of D238 and D239, although B294 scored better for binding the B-site in docking. The EC_{50} of B294 is 2.4 μM as revealed by NanoBiT assay. The EC_{50}/K_D ratio is near 100, being the highest among the compounds tested above.

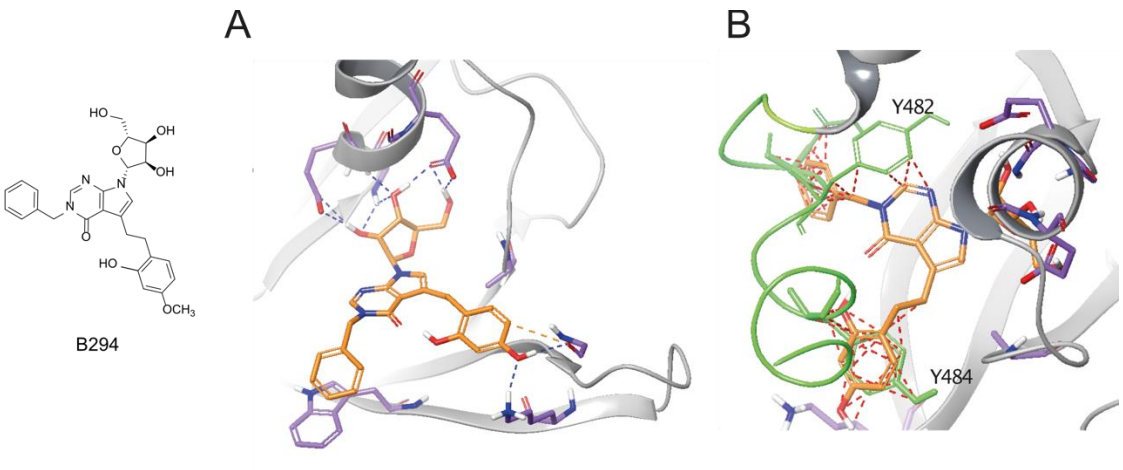

Fig 3.39, Chemical structure and the docking of B294. A, docking of B294 in NBD-B. B, clashes between B294 and the α-D helix. B294 is shown in stick representation in orange. The representations of other structural components are similar as Fig 3.36.

More analogs with combined modifications at N1 and C7 were generated and tested. The test results can be found in Table S1 in the supplement. Almost all of them have a EC_{50} in micromolar range. Among them, a series of 5 compounds showed strikingly increased separation of binding affinity and activation potency as shown in Fig 3.40.

The only difference between the first 3 compounds (MB017, MB018 and MB026) is the number of chlorines on the C7 phenyl group. A major difference in EC_{50} was seen between MB018 and MB026. Addition of a second chlorine to the phenyl group increases the EC_{50} by 8 times (8.8 μM vs 1.1 μM) and resulted in the highest EC_{50}/K_D ratio, 371, so far. Interestingly, the binding affinity of the three compounds are similar, ranging from 18 to 24 nM. MB035 contains a 4-chlorobenzyl group instead of a benzyl group at N1, which increases both EC_{50} and K_D by around 2 times. MB052 has an extended phenethyl group at N1. Its EC_{50} is over 64 μM, the highest so far. Curiously, the binding affinity was undetectable by ITC, probably due to its low solubility in aqueous solution. Nevertheless, it binding to NBD-B increased the stability of PKAR as revealed by nanoDSF (Fig S5).

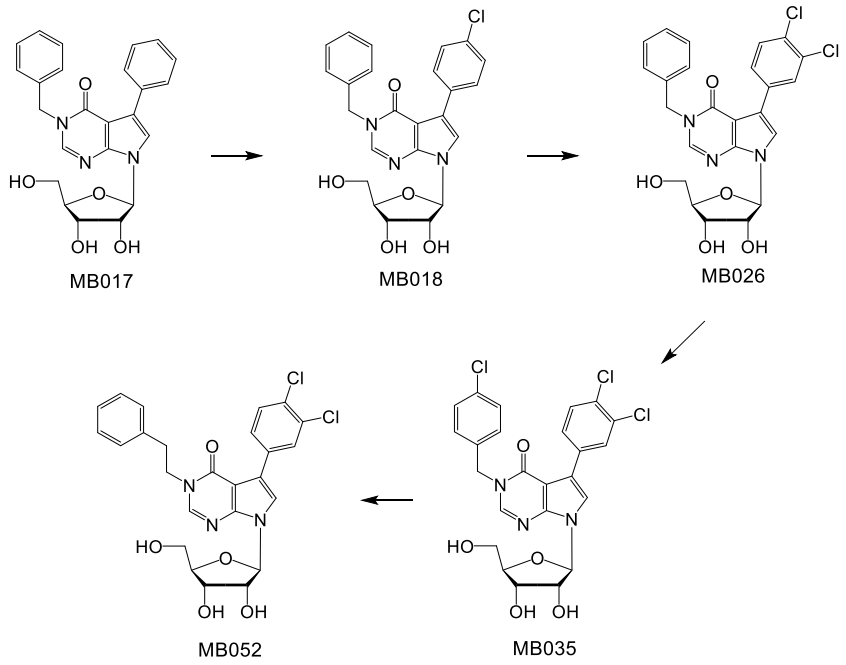

Compound	MB017	MB018	MB026	MB035	MB052
EC_{50} (nM)	1,200	1,100	8,810	14,000	> 64,000
K_D (nM)	21 ± 3	18 ± 4	23.7 ± 5.5	~ 50	-
EC_{50} / K_D	60	60	371	280	-

Fig 3.40 comparison of the structures of the N1 and C7 modified inosine analogs. The table lists the EC_{50} and K_D values of the compounds.

Computational docking suggests a very similar binding pattern of MB017, MB018 and MB026. This is in agreement with their similar K_D values. In particular, MB026 can form

a halogen bond with R413 (Fig 3.41 A). The docking of MB035 (orange sticks) and MB052 (yellow sticks) in the NBD-B are shown in Fig 3.41B. In comparison with MB026 (cyan sticks), MB035 can interact with W423 by π-stacking via the N1 benzyl group. MB052, however, docks very differently. The extended flexibility of the phenethyl group in MB052 compared to benzyl derivatives suggests the option of a favorable edge-to-face interaction with F425. For MB052 this results in a changed orientation of the dichlorophenyl ring. The differently positioned N1 and C7 groups of MB052 might restrict the flexibility of the α-D helix and thereby prevent it to approach the B-site, causing the strikingly high EC_{50} (> 64 μM). However, the high EC_{50} can also be due to low binding affinity.

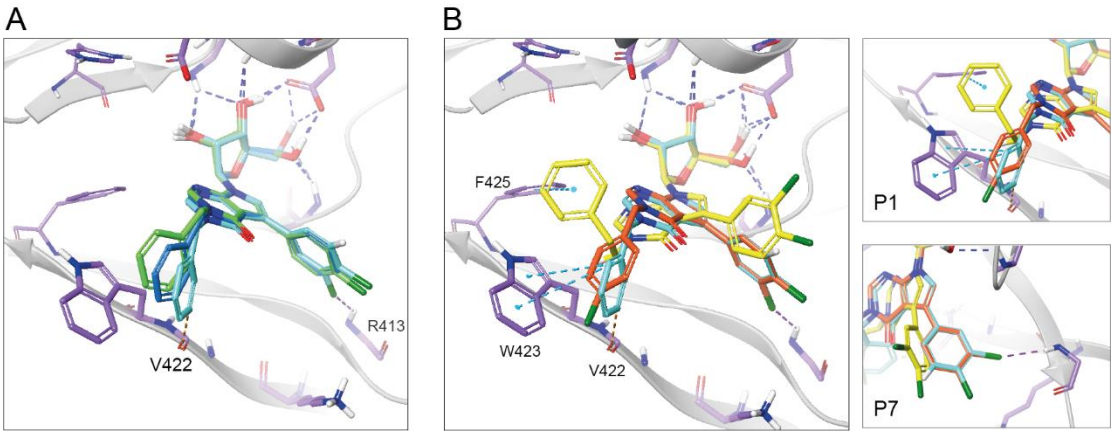

Fig 3.41, A, docking of MB017 (green), MB018 (blue) and MB026 (cyan). B, docking of MB026 (cyan), MB035 (orange) and MB052 (yellow). The 2 smaller panels on the right represent the binding of N1 and C7 side groups in a close view, respectively. The representation of other structural components is similar as Fig 3.36.

The binding affinity (K_D is around 1 μM) of adenosine to the B-site is lower than the compounds discussed above, while the K_D for binding both A- and B-sites of PKAR is in low nanomolar range (George Githure & Yuri Volpato, manuscript, 2021), suggesting a high binding affinity to the A-site. A competition assay was performed using MB052 to compete with adenosine for binding and activating PKAR. A fixed concentration of MB052 (10 μM) was used, since it only slightly activates TbPKA at this concentration. Therefore, we expected to see a right-shifted dose-response curve of adenosine in the presence of MB052. As shown in Fig 3.42, the adenosine EC_{50} strikingly increased 5-times by the competition of MB052. This result suggests MB052 is a potential antagonist and better antagonists can be further developed based on it. Nevertheless, the competition effect is not as strong as we expected, one possible explanation is that

the binding of MB052 to the B-site opens the A-site so that adenosine can active PKA by binding to the A-site.

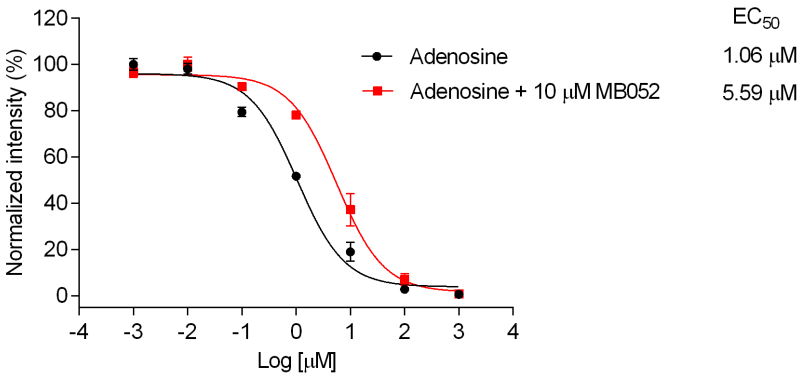

Fig 3.42, competition assay assessing the antagonist potential of MB052. Two independent experiments were performed and both demonstrated a 5-fold increase of EC_{50} of adenosine. The cells used were membrane permeabilized by 2% NanoGlo buffer.

3.4.2 Converting inosine to PKA inhibitor by substituting the ribose group

The interaction between the ribose group and the RBC domain was proven to be essential for purine nucleosides binding in PKAR in *T. brucei*. Modification on the ribose group very likely results in significant reduction of the activation potency. Same for mammalian PKA, the interaction of cAMP with the PBC domain is of extremely importance and it was considered to initiate the conformation change of mammalian PKAR through a charge relay pathway (Wu *et al.*, 2004b). The most potent cAMP antagonist identified so far is Rp-cAMPS. A simple replacement of the equatorial oxygen on the phosphate group with a sulphur atom converts cAMP to an antagonist. Whether *T. brucei* PKAR has a similar charge relay pathway is not clear, while it might be an alternative way of developing a PKA inhibitor by rational modifying or replacing the ribose group. We expected to obtain some compounds capable of binding the NBD domain but not triggering PKAR conformation change.

A series of N9 modified compounds were synthesized. Among them, the following three compounds show inhibitory activity to PKA, though the effect is still weak. As shown in Fig 3.43, the three compounds elevate the luminescence intensity by at least 25% at 100 μM. MB019 is the strongest among them, rising up the luminescence by more than 50%. Strikingly, ITC detected no binding of this compound to the B-site, probably due to extremely low binding affinity. Nevertheless, competition assay that uses 100 μM MB019 as competitor was conducted. The EC_{50} of the tested activators

increased only slightly (data not shown).

Interestingly, small modifications on the above compounds can eliminate the inhibitory activity. For example, substitution of the C6 methoxy group of MB019 by carbonyl group resulted in a compound that slightly induces PKA activation. Probably, introduction of the methoxy group at C6 position completely change the hydrogen bond pattern and even electronic properties of the compounds, converting them to inhibitor. Although more explorations can be done in this category of compound, it would be more helpful to address the detailed TbPKA activation mechanism, in particular the cooperativity of A- and B-site. A potent PKA inhibitor has not been obtained from these compounds, but they have been precious chemical tools to study PKA activation mechanism. For example, co-crystallization of a N1, C7-modified compound and PKAR can be performed to verify compound binding in B-site and study the role of the α-D helix.

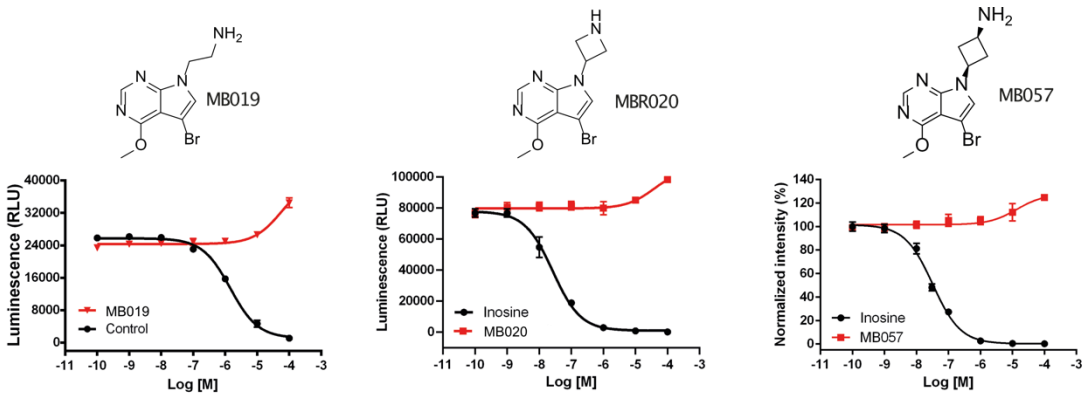

Fig 3.43, compounds tested to inhibit PKA activation via replacement of the ribose moiety. Membrane permeabilized cell were used in the NanoBiT assay experiments.

3.5 BRET assay development for genome-wide RNAi screening for PKA upstream signaling components

PKA activation by cold shock and indirectly by dipyridamole provides evidence for the existence of upstream PKA regulators in *T. brucei*. Genome-wide RNAi screen has proven to be powerful in gene identification in many studies of trypanosomes as introduced in chapter 1.3.4.3. In these studies, the positive cells were selected either by antibiotics or cell viability assay. However, PKA activation cannot be directly selected, especially when the activation is transient and reversible. To tackle the issue, assays that are able to trace the change of cellular PKA activation and indicate it by fluorescence signal were considered for development of a genome-wide RNAi screen using Fluorescence-activated cell sorting (FACS). Förster resonance energy transfer (FRET) assay is a good tool, it detects not only the fluorescence intensity but also the FRET ratio, which can reflect the targeted protein-protein interaction change, regardless of the expression level of proteins in individual cell. However, the featured high background signal resulted from the simultaneous excitation of the energy acceptor by the laser and the low dynamic range which likely makes it hard to distinguish the change in PKA activation by FACS (George Abraham *et al.*, 2015). Nluc based Bioluminescence resonance energy transfer (BRET) assay is an alternative and becoming popular for assay development. It uses Nluc, the brightest luciferase so far, as energy donor and a fluorescent protein as energy acceptor. Fig 3.44 shows the mechanism of BRET. The signal is cleaner and the dynamic range is higher than traditional BRET using Renilla luciferase (Rluc) or FRET (Machleidt *et al.*, 2015).

The idea is to use Tet inducible genome-wide RNAi to induce random gene knockdown in different cells. Then, PKA activation upon cold shock or dipyridamole treatment will be compared between these cells and wildtype control. The cells with altered PKA activation property will be detected and sorted out by FACS, the gene depleted will be identified by next generation sequencing.

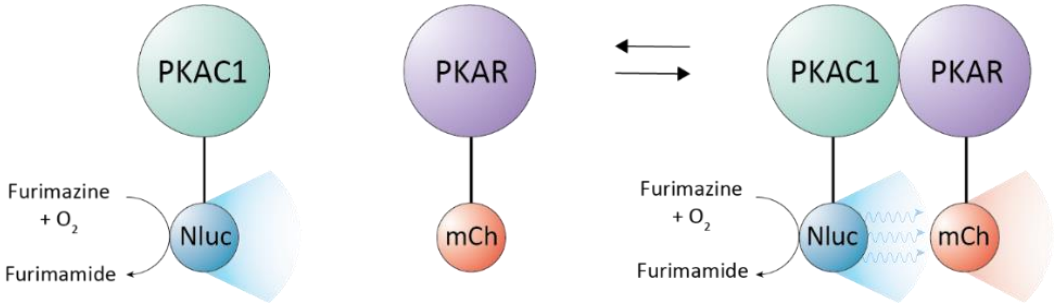

Fig 3.44 Illustration of NanoBRET assay. In the present of Nluc substrate, furimazine, strong luminescence signal will be generated and be absorbed by the fluorescent protein in close proximity, resulting in the emission of fluorescent signal. The energy transfer will only happen when the two target proteins interact.

3.5.1 Development of BRET assay

In our design, the energy donor is NLuc and mCherry is the energy acceptor in the BRET assay. Nluc and mCherry genes were fused *in situ* to *PKAR* and *PKAC1* loci using pPOTv4 vector as described previously (see chapter 3.1.1). To facilitate the detection by western blot, HA and Ty epitope tags were fused to the N-terminus of Nluc and mCherry, respectively. In addition, the same GS linker used for using NanoBiT tags to PKA subunits (see chapter 3.1.1) was used to improve the flexibility of reporter proteins. The cell line (referred to as Nluc-C1/R) constitutively expressing HA-Nluc-PKAC1 was firstly generated. Ty-mCherry was N-terminally tagged to PKAR on top of this cell line. A second cell line using YFP as the energy acceptor was also generated. The YFP excitation spectrum has broader overlap with the emission spectrum of Nluc, so this BRET pair was expected to generate higher BRET ratio, albeit the background signal might be higher.

In the end, two NanoBRET cell lines were made. They were referred to as Nluc-C1/mCherry-R and Nluc-C1/YFP-R. Western blot analysis indicates the correct expression of the fusion proteins in the two cell lines as expected (Fig 3.45A). Live cell imaging was performed according to 2.2.1.8 using GE Delta-Vision Elite microscope. As shown on Fig 3.45B, Ty-mCherry-PKAR and Ty-YFP-PKAR are well localized on the flagellum of the parasite as the endogenous PKAR.

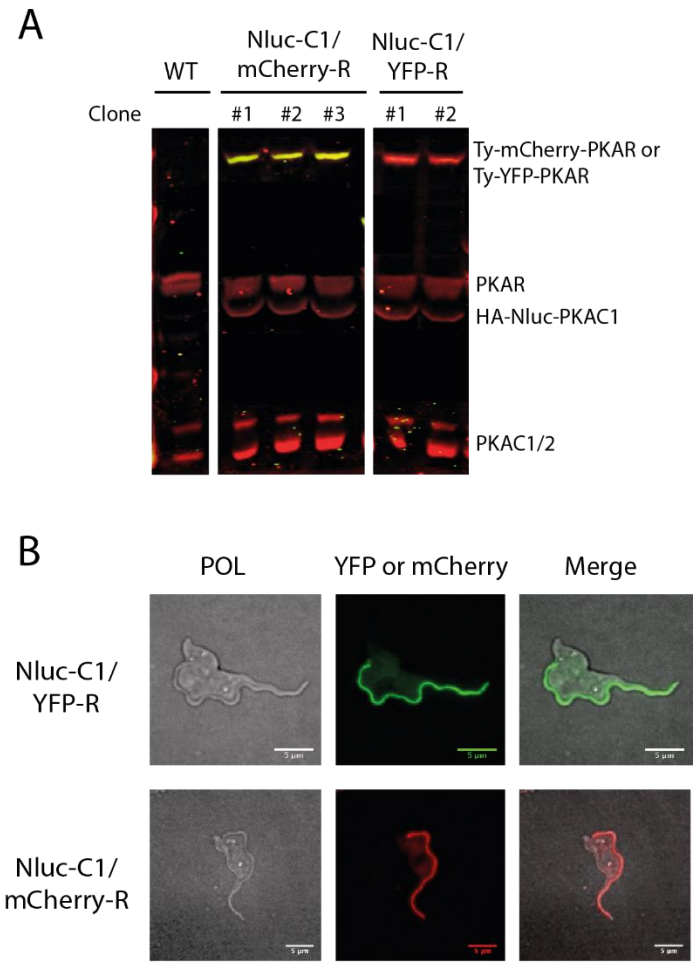

Fig 3.45, development of BRET assay. A, WB verification of BRET cell lines. Anti-Ty epitope, anti-PKAC1/2, anti-PKAR and anti-PFR antibodies were used. B, live cell imaging of BRET cells. The cells were fixed on agar pads and imaged by GE Deltavision microscope (see section 2.2.6).

3.5.2 BRET assay measuring PKA activation

Strong luminescence signal was detected in both cell lines by Tecan plate reader, indicating the expression of Nluc-PKAC1. In the two cell lines, PKA was activated as described in 2.2.7. As shown in Fig 3.46, the EC_{50} of Toyocamycin, 5-I-tubercidin and 5-Br-tubercidin were determined. The EC_{50} of individual compounds are similar in the two cell lines, suggesting the BRET method is reliable and reproducible. Most importantly, the values are close to the ones measured by NanoBiT assay. However, the dynamic range of the readout is lower. The BRET ratio of Nluc-C1:mCherry-R cells is relatively low (<0.01), very likely due to the weak excitation of mCherry. The overlap between the emission spectrum of Nluc and the excitation spectrum of mCherry is small. On the other hand, although the Nluc-C1:YFP-R cells show a better BRET ratio

(~ 0.4), the dynamic range is also narrow.

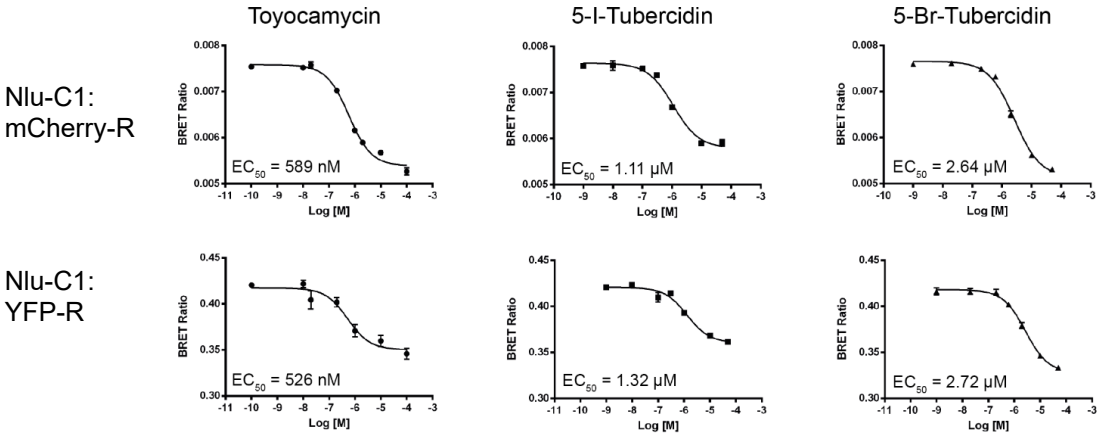

Fig 3.46, PKA activation measured by BRET assay. The intact cells were incubated with different concentrations of compounds for 15 min before measurement by GloMax® plate reader (Promega). The luminescence filter used in the detection is 450 nm (8 nm BP). The fluorescence filters used are 530 nm LP for YFP and 600 nm LP for mCherry.

Compound	*In vitro* kinase assay[1]	*In vivo* VASP assay[2]	NanoBiT assay[3]	NanoBiT assay (permeabilized cells)[4]	BRET (Nluc-C1:mCherry-R)	BRET (Nluc-C1:YFP-R)
Toyocamycin	180 nM	88 ± 10 nM	354 ± 37 nM	285 ± 20 nM	589 nM	526 nM
5-I-Tubercidin	230 nM	390 ± 20 nM	822 ± 52 nM	161 ± 19 nM	1.11 µM	1.32 nM
5-Br-Tubercidin	≥ 700 nM	625 ± 66 nM	2.13 ± 0.12 µM	2.77 ± 0.32 µM	2.64 µM	2.72 µM

Table 7, comparison of the EC_{50} values measured by BRET and other assays

[1] data from (PhD thesis Githure, 2014)

[2] data from (Bachmaier *et al.*, 2019)

[3]data taken from Table1, see chapter 3.1.2.1

[4] data taken from Fig 3.8, see chapter 3.1.2.2

3.5.3 BRET assay is not compatible with FACS

FACS and the GloMax plate reader have different settings and filters for fluorescence. FACS actually measures the fluorescence from individual cells, while GloMax plate reader measures luminescence of a collection of cells. To make sure the YFP or mCherry signal are detectable in a single trypanosome, cells were analyzed by flow cytometry. The parent cell line Nluc-C1/R was used as the negative control and a PKAR-GFP overexpression cell line was used as the positive control. As shown in Fig 3.47, 99.86% of the gated Nluc-C1/YFP-R cells were YFP positive, 97.59% of the gated Nluc-C1/mCherry-R cells were mCherry positive, albeit the florescent intensity

was more than 10-fold lower than that of the PKAR-GFP overexpression cell line.

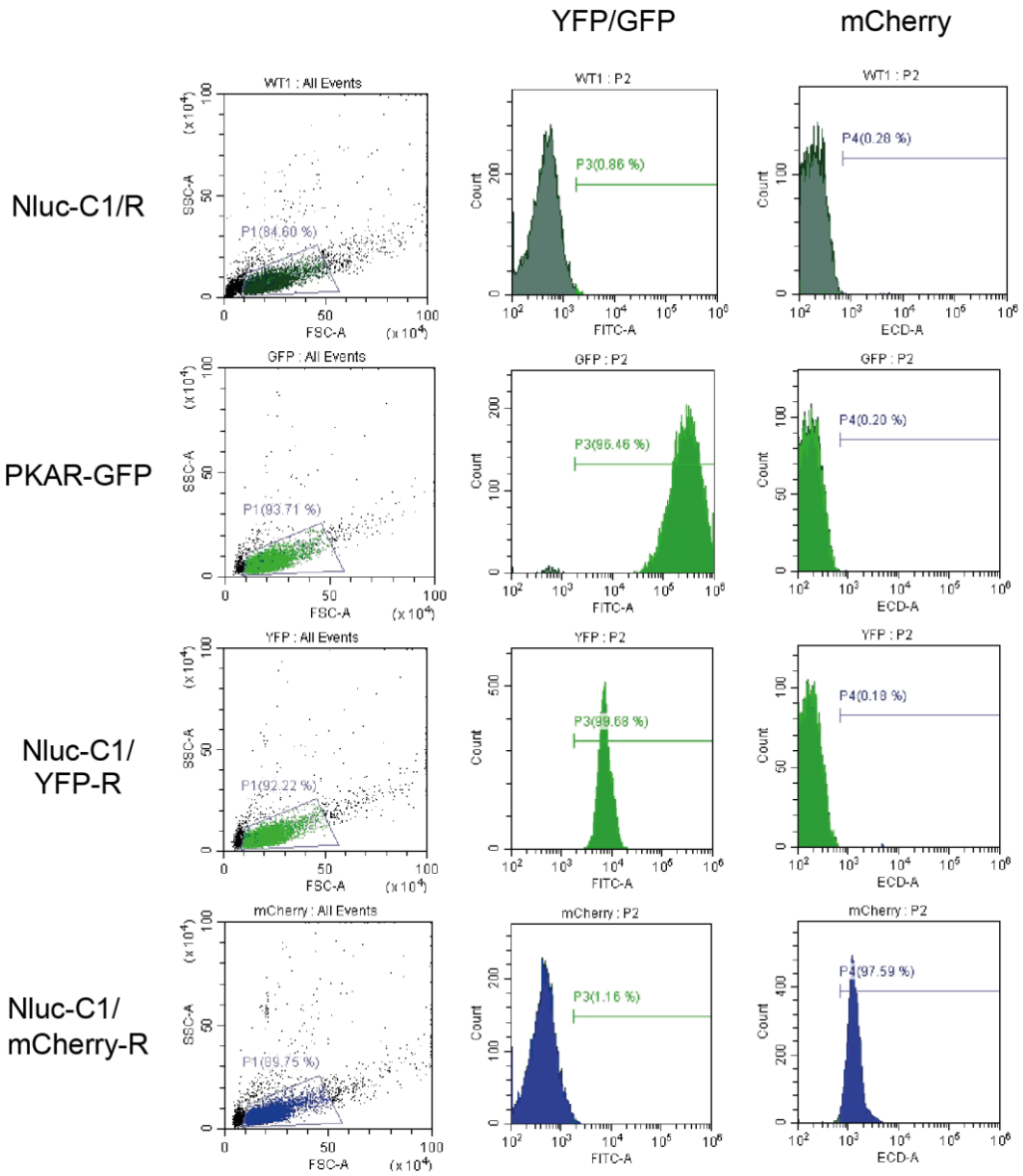

Fig 3.47, Detection of the fluorescence in single cells by flow cytometry. The fluorescent signal from the Nluc-C1/YFP-R and Nluc-C1/mCherry-R cells were measured by a flow cytometry (Beckmann coulter Cytoflex).

The BRET signal of single cell was subsequently measured in FACS as described in section 2.2.8. A laser must be turned on during FACS measurement, so the laser for exciting DAPI (375 nm) was used to avoid excitation of the fluorescent proteins in the cell lines. As shown in Fig 3.48, the addition of substrate increased the mCherry signal of the control cell line (Nluc-C1/R) by 100-fold, suggesting autofluorescence from the added substrate. Unexpectedly, the mCherry signal in the cell line Nluc-C1/mCherry-R is more or less the same as that in the control in the presence of substrate, suggesting the autofluorescence of the substrate is excessive and overlaps the BRET

signal. Same phenomenon was observed in the Nluc-C1/YFP-R cell line (data not shown). The substrate solution is brown colored liquid. Whether the autofluorescence is from the substrate Furimazine or the additives in the solution is yet to be investigated. Therefore, BRET assay is not compatible with FACS. A further development of the screening such as using improved FRET assays as reporter was considered but preference was given to the study of PKA activation mechanisms as described in chapter 3.4.

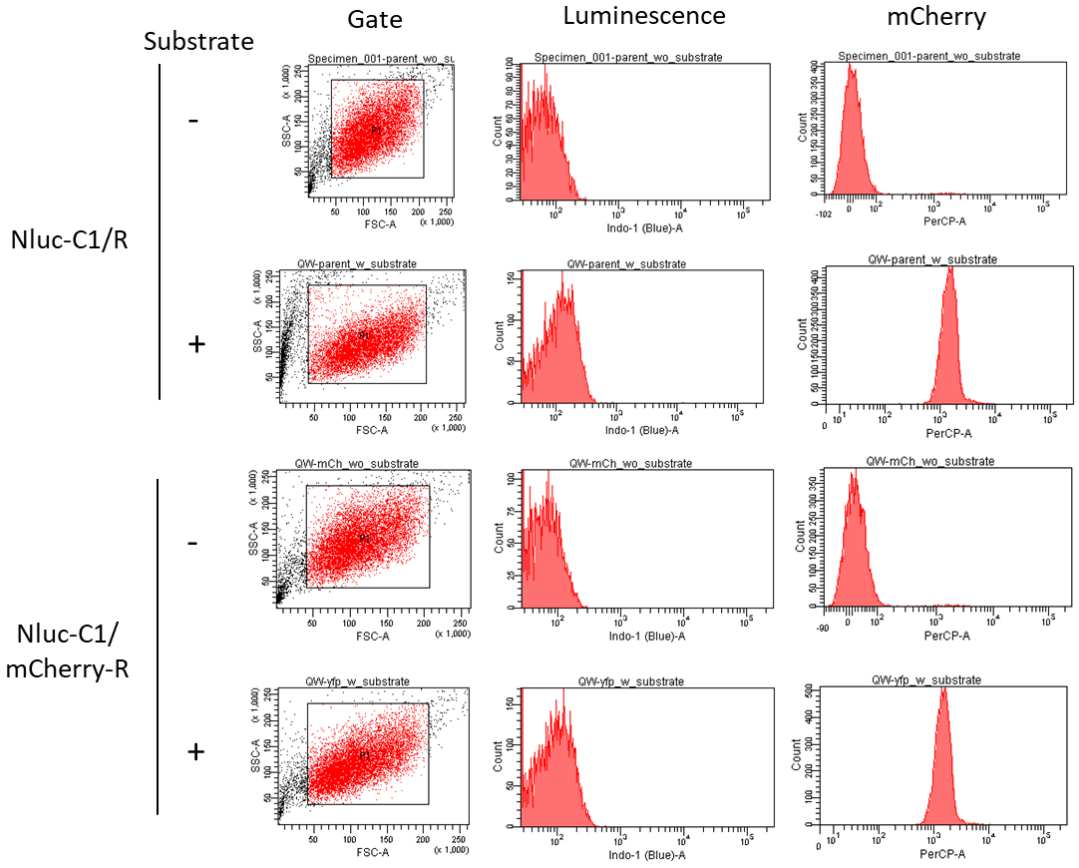

Fig 3.48, Detection of BRET signal by FACS. Cells were resuspended in PBSG and subjected to FACSAria-II for analysis in the presence and absence of Nluc substrate. Filter settings for dye Indo-1, which detects an emission at around 450 nm close to Nluc emission peak, were used for the detection of luminescence, while PerCP-A and FITC settings were used for the detection of mCherry and YFP signals respectively.

4 Discussion

4.1 The unconventional PKA holoenzyme formation and activation mechanisms in *T. brucei*

Besides of the NBD-domain for nucleoside binding, *T. brucei* PKA has two other kinetoplastid-specific features, the large N-terminal domain and the C-terminal extended α-D helix. The findings that the N-terminal domain is implicated in PKA holoenzyme formation and the α-D helix is critical for PKA activation suggest an unconventional but yet unclear PKA allosteric regulation mechanism, which seems to be conserved in kinetoplastids according to sequence homology and data from this thesis. In this chapter, the potential mechanisms of PKA holoenzyme formation and activation in *T. brucei* are discussed.

4.1.1 How is the N-terminal domain involved in R-C holoenzyme formation?

Chapter 3.2.1 shows that the N-terminal domain is critical for *T. brucei* PKA holoenzyme formation *in vivo.* Loss of this domain results in significantly reduced PKA holoenzyme level as shown by NanoBiT assay in spite of comparable expression level (Fig 3.11). This result is perfectly consistent with the previous pull-down experiment showing that the N-terminal domain truncated PKAR is unable to bind the C-subunits (PhD thesis Krumbholz, 2006). The involvement of N-terminal domain in PKA holoenzyme formation is an unconventional feature for *T. brucei*, because in RI or RII subunits of higher eukaryotes, the N-terminal domain has no or negligible effect on R-C association. This is evident by the fact that a number of recombinant PKARs used for *in vitro* kinase assay or co-crystallization with the catalytic subunit are N-terminal domain truncated mutants (Kim *et al.*, 2007; Wu *et al.*, 2007). Our first thought was that the N-terminal domain provides an additional R-C interface other than the 4 sites identified in mammalian PKAR, the inhibitory sequence (site 1), CNB-A (site 2), the α-B/C helix of CNB-A (site 3) and the CNB-B (site 4). The additional interface between the N-terminal domain and C subunit contributes to the R-C complex stabilization. A systematic dissection of the N-terminal domain of *T. brucei* PKAR performed in a previous study (PhD thesis Krumbholz, 2006) showed that deletion of the whole subdomain or a small part within the N-terminal domain leads to mutants with disrupted flagellar localization and incapability of binding C-subunits. These results suggest that

a correctly folded N-terminal domain is needed for R-C association. In this study, we proposed a TbPKA holoenzyme structure model and tested potential interaction sites by mutagenesis by NanoBiT assay. The predicted interaction interface (Fig 3.12) was not confirmed. To understand the mechanism of the N-terminal domain, a PKA holoenzyme structure will be needed to identify the critical interaction sites.

Substitution of the substrate site $RRTT^{205}$ by a pseudosubstrate site $RRTA^{205}$ resulted in undissociated PKA holoenzymes in *T. brucei* (Fig 3.14). This is consistent with previous observations using the VASP kinase reporter assay, which showed the T205A mutant did not respond to toyocamycin treatment (Schmitz, 2011). This likely results from increased R-C affinity. In mammalian PKA, replacement of the serine residue of the P-site to an alanine in a RII subunit has been shown to result in a 40-fold increased R-C affinity (Diskar *et al.*, 2007). Other studies have also shown that the P-site phosphorylation destabilizes and thus sensitizes the R-C complex to activation (Diskar *et al.*, 2007; Isensee *et al.*, 2018). Therefore, we concluded that the phosphorylation on the P-site is crucial for PKA dissociation (activation).

Combining the data, the N-terminal domain and T205 phosphorylation seem to be antagonistic to each other. Interestingly, the effect of the N-terminal domain deletion can be compensated by T205A mutation as shown in Fig 3.16. The resulted R(191-499, T205A):C holoenzyme showed resistance to toyocamycin activation. Therefore, we concluded that the P-site phosphorylation is a strong modulator on R-C dissociation, while the N-terminal domain serves as a complement to stabilize R-C holoenzyme upon T205 phosphorylation. Based on this, we propose a model of TbPKA activation as shown in Fig 4.1. It presents the two states of PKA holoenzyme, a stable state and a metastable or sensitized state. The stable state PKA occurs shortly upon R-C interaction, while it switches to metastable state upon phosphorylation of T205. The sensitized state of PKA holoenzyme has been reported in mammalian RIα (Haushalter *et al.*, 2018), in which phosphorylation at the Ser101 (P+2 site) by PKG has been shown to sensitize PKA, resulting in partially restored kinase activity without R-C dissociation. In *T. brucei*, the P+2 arginine has been shown to have negligible effect on PKA activation (Fig 3.15). The model can be further validated by 1) generation of a PKAC1 dead mutant (PhD thesis Kramer, 2004), which lacks the kinase activity, so T205 should not be phosphorylated. The resulting PKA holoenzymes are supposed to be in the stable state and show resistance to ligand activation; 2) resolving the structure of the holoenzyme by X-ray or cryo-EM to see how the N-terminal domain interacts the C-subunit.

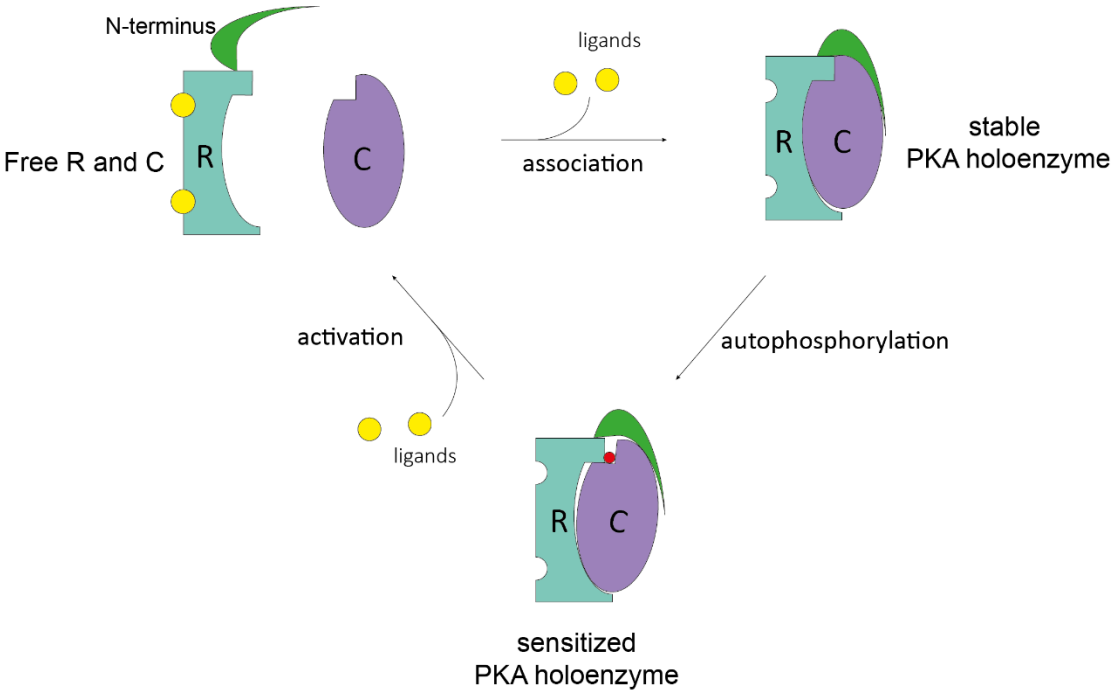

Fig 4.3, a cartoon model describing PKA holoenzyme formation. Autophosphorylation of T205 (the phosphoryl group is represented as a red ball) sensitizes the holoenzyme, making it primed to ligand activation.

4.1.2 is the N-terminal domain related to cold shock induced PKA activation?

There are two possible mechanisms behind the temperature-dependent PKA activation. One is that PKA itself responds to cold shock by conformation change. Indeed, studies have shown that the PKAC orthologues from several hibernating animals and cold-hardy insects undergoes conformation change which causes increased substrate affinity and higher tolerance to ion inhibition (MacDonald & Storey, 1998; Holden & Storey, 2000; Pfister & Storey, 2002); however, this possibility is excluded given the fact that cold shock induced PKA activation was not observed in PKAR homozygous knockout cells. Alternatively, it could be PKAR or the holoenzyme rather than PKAC undergoes conformation change upon cold shock, which leads to the release of the bound PKAC. In low temperatures, water surrounding the protein surface become more ordered and form less hydrogen bonds with the protein, driving the protein towards an unfolded and unstable state (Fernandez & Scheraga, 2003; Chaplin, 2006; Koizumi *et al.*, 2007). For PKA, a such change may result in a conformation change that either dissociates or enhances the heterodimeric R-C complex. It is possible that the N-terminal domain suffers a conformation change upon cold shock, resulting in holoenzyme dissociation. Increased molecular dynamics by

temperature downshift has been seen in a couple of proteins such as SARS-CoV-2 spike protein. Spike protein is a surface protein of SARS-CoV-2 virus which interacts with the Angiotensin Converting Enzyme 2 (ACE2) in human lung cells, whereby it enters the respiratory system (Wang *et al.*, 2008). The N-terminal domain of the spike protein is found to be more active in lower temperatures and the active N-terminal domain is required for the binding of the spike protein to ACEs through a receptor binding domain (Rath & Kumar, 2020). To investigate the possible molecular dynamics of the N-terminal domain of PKAR, molecular dynamics simulations can be used once the holoenzyme structure is available. Alternatively, biophysical methods such as single molecule FRET can be used to detect the dynamic conformation change of the N-terminal domain upon cold shock treatment *in vivo* (Hellenkamp *et al.*, 2018; de Boer *et al.*, 2019a; de Boer *et al.*, 2019b; Mazal & Haran, 2019).

If PKA itself is unchanged by cold shock, then there might be upstream signaling regulating PKA activity. Temperature downshift might change the membrane fluidity of trypanosomes and activate cation channels such as calcium channels. Indeed, crosstalk between calcium and the conventional PKA signaling has been observed in many organisms (Volotovski *et al.*, 1998; Gorbunova & Spitzer, 2002; Zaccolo & Pozzan, 2003; Bencina *et al.*, 2005). Calcium is found to regulate the activity of a number of signaling enzymes, e.g., ACs (DeBernardi & Brooker, 1996) and PDEs (Moore *et al.*, 1998). On the other hand, PKA has been found to activate calcium channels, by which it regulates calcium homeostasis (Sorrentino & Rizzuto, 2001; Wetzel *et al.*, 2001). The enrichment of calcium signaling and PKA subunits in the parasite flagellum suggests a possible signaling crosstalk (Broadhead *et al.*, 2006; Oberholzer *et al.*, 2007; Saada *et al.*, 2014; Subota *et al.*, 2014).

4.1.3 Other functions of the N-terminal domain

The unusual large N-terminal domain is conserved in all identified kinetoplastid PKARs. It consists of nearly 200 aa, which is twice that of human PKARs and four times that of *Dictyostelium discoideum* and *Paramecium tetraurelia* PKARs. Amino acid sequence alignment of the N-terminal domains of TbPKAR, TcPKAR and LdPKAR reveals a 62% consensus between each other (Fig S8). In addition, all kinetoplastid PKARs contain the substrate site (RRxT), which means they are all similar to type II PKARs in that respect. These findings suggest that kinetoplastid PKAs share a conserved mechanism of R-C dissociation/association with the N-terminal domain involved. The D/D domain locates at the N-terminal region of PKARs in higher eukaryotes. As introduced, it is responsible for forming PKAR dimers and binding AKAP proteins. The

lack of D/D domain in kinetoplastid PKARs is compatible with the heterodimeric (R_1C_1), rather than tetrameric (R_2C_2), holoenzyme composition in *T. brucei*. PKA was found enriched in the flagellum of trypanosomes (PhD thesis Krumbholz, 2006; Oberholzer *et al.*, 2011). PKA localization in *T. brucei* is clearly related to the N-terminal domain as evident by the mis-localization of the N-terminal deletion mutants (PhD thesis Krumbholz, 2006). However, attempts to identify the tethering partners of PKAR by proximity labelling failed (data from this lab).

4.1.4 The role of the α-D helix in ligand binding

The α-D helix is a conserved feature of kinetoplastid PKARs. The studies in chapter 3.2.2 demonstrate a close relationship between the α-D helix and PKA activation. The PBC motif in mammalian cAMP-dependent PKA forms a strong ionic interaction with the phosphate group of cAMP as well as hydrogen bonds with the ribose moiety, while the Ribose Binding Cassette (RBC) motif forms only hydrogen bonds with the ribose moiety. This would predict a lower affinity of nucleosides compared to cAMP. However, ITC experiments reveal a low nanomolar equilibrium dissociation constant (K_d) of inosine for TbPKAR (5-15 nM). The K_d value is at least 2-fold lower than that of cAMP for mammalian PKARs. Due to this, we speculated that the α-D helix serves as a complement of the RBC motif to strengthen the ligand binding. The hypothesis was evident by NanoBiT assay with the α-D helix deletion mutant and the Y→A mutants (Table 06). Structural analysis reveals that Y484 and Y485 are responsible for anchoring the α-D helix onto the binding pocket (B-site), by which the α-D helix acts like a lid, locking the ligand in the B-site without exposure to the solvent. This can also be explained by receptor-ligand binding kinetics. Studies have shown that the residence time, which is the reciprocal of the ligand dissociation rate constant (K_{off}), has significant impacts on physiological function of a receptor-ligand binary complex (Tummino & Copeland, 2008; Hoffmann *et al.*, 2015; Rinken *et al.*, 2016). The relationship between K_{off} and K_d can be formalized as $K_d = K_{off}/K_{on}$. Ligand being wrapped in the B-site by the α-D helix resulted in extended residence time, which means smaller K_{off} and thus higher binding affinity. A similar triad motif has been observed in the monomer PKG of *Plasmodium falciparum* (Kim *et al.*, 2015; El Bakkouri *et al.*, 2019). Three resides (R484, Q532 and D533) form a strong interaction network that shield the bound cGMP within *Pf*CNB-D domain while not directly interacts with the cGMP.

Second, the conserved amino acids on the α-D helix play a role on ligand selectivity. Among the three nucleosides tested, inosine is the strongest agonist followed by

guanosine and adenosine. The common feature of inosine and guanosine is the keto group at 6-position of the purine ring, which serves as a hydrogen bond acceptor sharing an electron donated by the hydrogen of Y485 (N-H). In contrast, the amine group at the 6-position of adenosine serves as a hydrogen bond donor donating an electron to the nitrogen of Y485. In addition, the 1-position nitrogen of inosine is an electron acceptor, whilst the counterpart in adenosine donates an electron to N481. These differences likely result in significant changes in ligand binding affinity as well as activation potency. For *T. cruzi* and *L. donovani* PKAR, the same potency order of nucleosides was demonstrated (Fig 3.25). However, guanosine showed 10-times higher K_d for TcR and LdR compared to TbR. Possibly, the 2-position amine group of guanosine is less preferable for TcR and LdR. Truncation of the α-D helix in TcR resulted in strong resistance to ligand activation, as observed in TbR. Although the role of the α-D helix is yet to be examined in *Leishmania*, it is highly likely to be conserved as in *T. brucei* and *T. cruzi*.

4.1.5 The role of the α-D helix in PKAR conformation change

As discussed above, the α-D helix is crucial for ligand binding. However, its role in PKAR conformation change is unclear. In mammalian PKA, the capping residue interaction with the ligand initiates the motion of the α-C helix, which results in the breakage of the critical salt bridge (E261:R366) and then triggers a series of conformational changes on PKAR (Kim *et al.*, 2007). This salt bridge is conserved in *T. brucei* PKA. Removing both the capping residue and the α-D helix totally blocked PKA activation by toyocamycin *in vivo* as seen in Fig 3.20. Interestingly, deletion of the α-D helix only was shown to have a similar result (Fig. 3.26). Combining these observations, it is speculated that the activation mechanisms of mammalian PKAs and *T. brucei* PKA are in general similar except for that the involvement of the α-D helix. We speculated that the capping residue alone is not sufficient to induce the complete conformation change required for PKA activation, the interactions of Y484 and Y485 of the α-D helix with the B-site are needed to reinforce the activation. A single mutation of the capping residue would further clarify this point. Loss of the α-D helix not only decreases ligand binding affinity but also results in disrupted allosteric regulation of PKA. Observations in developing PKA inhibitors (chapter 3.4) give support for the hypothesis. For example, some N1, C7-inosine analogs were found to retain high binding affinity for the B-site while show significantly reduced PKA activation potency. Moreover, computational docking has shown that the spatial positions of Y484 and/or Y482 of the α-D helix in the scenario of inosine binding are occupied by either the N1

or C7 moiety of those compounds. In general, the function of the α-D helix in PKAR conformation change is still poorly understood. A systematic and quantitative study comparing the impacts of Y485A mutation and the α-D helix deletion on compound binding and PKA activation is expected to provide more information.

4.2 PKAC1 and PKAC2

PKAC1 and PKAC2 share 94% identity but show distinct expression regulation in the life cycle of the parasite. Whereas PKAC2 knockout succeeded in both BSF and PCF cells, all attempts to knock out both PKAC1 alleles failed and RNAi of PKAC1/2 was found lethal to a monomorphic BSF strain (PhD thesis Kramer, 2004; K. Malenica, this lab; PhD thesis Bachmaier, 2015; Bachmaier *et al.*, 2019). In addition, a recent study of leishmania kinome by gene deletion using CRISPR-CAS9 also suggested an essential role of PKAC1 for promastigote *Leishmania mexicana* (living in mammalian macrophages) (Baker *et al.*, 2021). These different lines of evidence bring up the questions: 1) is PKAC essential for *T. brucei* BSF cells and can PKAC1 be replaced by PKAC2? 2) Is there a specific function of PKAC1 and PKAC2 in trypanosomes? In this chapter, we will discuss the two questions.

4.2.1 Is PKAC1 essential in BSFs?

Although many attempts have been conducted to deplete PKAC1 or PKAC1/2 of BSF by knockout or RNAi, the essentiality of PKAC1 is not formally documented. This is because 1) no PKAC1 homozygous knockout cell line was obtained before; 2) different RNAi phenotypes in different strains were puzzling. In chapter 3.3, we intended to provide additional evidence and a tool to study PKAC1 function by knocking out both PKAC1 alleles with an inducible KO strategy. The knockout cell lines were successfully generated and the integration of resistance makers into the PKAC1 alleles were verified (Fig. 3.28 and Fig 3.29). With the exception of [Δ*pkac1*/Δ*pkac1 Ty-PKAC2*^{Ti}] cell line, in which Ty-C2 expression was uncontrollable by tetracycline, depletion of PKAC1 protein was achieved 24 h post Tet removal in both [Δ*pkac1*/Δ*pkac1 Ty-C1C2*^{Ti}] and [Δ*pkac1*/Δ*pkac1 Ty-C2C1*^{Ti}] cell lines as no PKAC1 nor rescue protein signal was detected by western blot (Fig 3.30). Surprisingly, these cells were able to survive up to 4 days without showing significant phenotypes in the absence of rescue protein expression. This result plausibly suggests that PKAC1 is not essential under culture conditions, it contrasts with the lethal effect observed in the monomorphic MiTat1.2 strain (PhD thesis Kramer, 2004). Table 9 summarizes all the experiments studying

PKAC1/2 by reverse genetics. Some of the results are contradictory. For example, the RNAi of PKAC1/2 done in (PhD thesis Kramer, 2004) and (PhD thesis Bachmaier, 2015). Two MiTat1.2 derived cell lines were used while the phenotypes were distinct. The hairpin-based RNAi was regulated by a parasite endogenous *PRAP* promoter while another RNAi was regulated by a T7 promoter which, in the presence of T7 polymerase, enables high-efficient production of siRNA. The kinome-wide RNAi screening used a ribosomal RNA promoter to control the RNAi and the knockdown of PKAC1 resulted in a mild growth and cytokinesis phenotype (Jones *et al.*, 2014). These experiments suggest the different phenotypes might depend on the efficiency or kinetics of RNAi. It is possible that the cells can adapt to a low PKAC activity in the slow process of PKAC1 or PKAC1/2 depletion.

Target gene	PKAC1 and PKAC2	PKAC1	PKAC1 and PKAC2	PKAC1	PKAC1	PKAC1
cell line	MiTat1.2 1313-514 monomorphic	MiTat1.2 monomorphic	MiTat1.2 1313 monomorphic	MiTat1.2 1313 monomorphic	2T1 cell line (derived from MiTat1.2) monomorphic	Antat1.1 E 1313 pleomorphic
Method	RNAi controlled by T7 promoter, inducible	knockout	Hairpin-based RNAi, inducible	Hairpin-based RNAi, inducible	RNAi controlled by a ribosomal RNA promoter, inducible	inducible knockout
Result and phenotype	severe growth phenotype, cell died in 2 days	only a hemizygous PKAC1 KO cell line obtained with mild growth phenotype	very slight growth phenotype	very slight growth phenotype	mild growth and cytokinesis phenotype	very slight or no growth phenotype
Reference	(PhD thesis Kramer, 2004)		(PhD thesis Bachmaier, 2015)		(Jones *et al.*, 2014)	This thesis

Table 9, Reverse genetics targeting PKAC1 or PKAC1/2.

Another explanation is that the three PKAC isoforms are functionally redundant. The loss of PKAC1 or PKAC1/2 might be compensated by the increased expression of PKAC2 and/or PKAC3. Actually, the expression of PKAC3 was not carefully checked in these studies. Knockout of PKAC3 in BSF Antat1.1 cells has been attempted but failed, while RNAi of PKAC3 in MiTat1.2 has shown a severe growth and cytokinesis phenotype (PhD thesis Kramer, 2004). This indicates PKAC3 is also important for growth and viability. Therefore, we think BSF trypanosomes might regulate PKAC expression to maintain the least PKAC activity required for cell surviving and proliferation. Here we show that a dominant-negative PKAR mutant is able to block PKAC activity in BSFs (Fig 3.24). To avoid the possible compensatory regulation in response to gene manipulation of PKAC isoforms, an inducible overexpression of a robust dominant-negative PKAR mutant is expected to significantly block the kinase activity of all three PKAC isoforms. Although sufficient overexpression of DN PKAR is

challenging, different overexpression vectors will be attempted in the future. In addition, the DN PKAR can be expressed in the PKAR KO cell line (PhD thesis Bachmaier, 2015). In this case, there would be no wild type PKAR that competes for free PKACs with the DN PKAR and a remarkable or complete depletion of PKAC activity can be achieved. Alternatively, a triple RNAi targeting the three PKAC isoforms can be attempted.

Interestingly, animal infection experiments have shown that the PKAR knockout cell line is unable to proliferate in mice (Collaboration work with Luisa Figueiredo, Lison, unpublished). This suggests that trypanosomes might be more sensitive to PKAC activity levels in animals than in lab culturing. To explore the role of different PKAC isoforms and the possible regulations, a systematic reverse genetics study should be carried out in animals.

4.2.2 a specific role of PKAC1 and PKAC2?

A specific function of PKAC2 had not been identified, since homozygous PKAC2 knockouts have been obtained in both BSF and PCF and they showed no noticeable phenotype (PhD thesis Kramer, 2004; K. Malenica, this lab; PhD thesis Bachmaier, 2015; Bachmaier *et al.*, 2019). Moreover, neither cold shock nor toyocamycin treatment of PCF cells expressing only PKAC2, resulted in a significantly increase in PKA substrate phosphorylation, whereas in BSF cells that express PKAC1, PKA substrate phosphorylation can be significantly elevated in response to cold shock or toyocamycin treatment (see Fig 3.24). It was thus suspected that the R:C2 holoenzyme is resistant to activation or PKAC2 is nonfunctional in terms of kinase activity. The first hypothesis was rejected by comparing the activation of different PKA holoenzymes in BSF and PCF cells by NanoBiT assays (chapter 3.3.2). The activation profiles of these PKA holoenzymes by activators are similar in BSF and PCF when using membrane permeabilized cells, suggesting the R:C2 holoenzyme is not resistant to activation. A difference in catalytic activity between PKAC1 and PKAC2 is unlikely, since the kinase core of the two isoforms are identical. Whether replacement of PKAC1 by PKAC2 at similar expression levels in BSF results in inducibility by cold shock, remains to be tested.

4.3 PKA upstream signaling in *T. brucei*

4.3.1 The possible mechanism of dipyridamole induced PKA activation

Dipyridamole was initially synthesized as a coronary vasodilator and later it was found inhibiting adenosine re-uptake in platelets, erythrocytes and endothelial cells by blocking the nucleoside transporters (Born & Cross, 1963; Elkeles *et al.*, 1968; Gamboa *et al.*, 2005). In *T. brucei*, dipyridamole was found inhibiting adenosine uptake in both BSFs (James & Born, 1980) and PCFs (Al-Salabi *et al.*, 2007). Moreover, it acts as an inhibitor of PDEs in both mammals (Harker & Kadatz, 1983; Balakumar *et al.*, 2014) and trypanosomes (Zoraghi *et al.*, 2001; Rascon *et al.*, 2002), resulting in intracellular cAMP concentration increase, which has no effect to *T. brucei* PKA activation (Bachmaier *et al.*, 2019). However, dipyridamole was surprisingly found to activate PKA *in vivo* while not activating purified PKA holoenzyme *in vitro* with (PhD thesis Githure, 2014). Therefore, it is likely to activate PKA via an upstream mechanism targeting PKA that is unrelated to cAMP (Bachmaier *et al.*, 2019). To explore this putative pathway, a systematic genome-wide RNAi screen was initially planned (see chapter 3.5). Trypanosomes are unable to synthesize the purine ring *de novo* (Berens *et al*., 1995), so they rely on nucleobase/ nucleoside transporters for acquiring purine nucleobases/nucleosides from the host. The inhibition of adenosine uptake by dipyridamole might disrupt the purine salvage pathway and probably alter the concentrations of other nucleosides or of nucleoside-derived second messenger molecules activating TbPKA.

4.3.2 Genome-scale RNAi screen studying the PKA upstream signaling

Genome-scale RNAi library screen is well established in *T. brucei* facilitated by the generation of the *T. brucei* RNAi library (Morris *et al.*, 2002; Alsford *et al.*, 2011). In most cases, the positive hits were selected by antibiotics or drugs (Baker *et al.*, 2011; Gould *et al.*, 2013; Fernandez-Cortes *et al.*, 2017; Rico *et al.*, 2017). Intracellular transient PKA activation is rapid, reversible and phenotypes cannot be traced in this assay. Putative genes regulating PKA activation upon cold shock or dipyridamole treatment are thus hard to be screened by genome-wide RNAi. NanoBRET assay was developed (chapter 3.5) attempting to trace the dynamic PKA association/dissociation in single cells by FACS. Although NanoBRET is able to measure PKA dissociation in real-time, it has a low dynamic range (Fig 3.46). Most importantly, it turned out to be not compatible with FACS, because the luminescence signal is too weak to be detected by the fluorescence detectors in FACS (Fig 3.47). FRET-based cell sorting by FACS was reported in mammalian cells (Banning *et al.*, 2010), while a weak FRET signal due to the relatively low PKA level in trypanosomes, the small cell size and the commonly low signal-to-noise ratio (SNR) in FRET assays are problematic. Recently, an

excitation-ratiometric PKA activity biosensor, which contains a PKA substrate peptide, a circularly permuted fluorescent protein (cpFP) and a phosphoamino acid-binding forkhead-associated 1 (FHA1) domain creating, was reported (Mehta *et al.*, 2018; Zhang *et al.*, 2021). The three components were properly joined together with optimized peptide linkers, constituting a very sensitive PKA activity sensor that the peak excitation wavelength of the coupled cpFP (e.g., cpEGFP) can be modulated in response to phosphorylation of the substrate peptide by PKA in living cells. This biosensor has been proven to be capable of detecting dynamic PKA activity in living cells by multiple fluorescence detection modalities, including plate reading and cell sorting. Therefore, integrating this biosensor and the genome-wide RNAi screening might be a potent method for searching for TbPKA upstream regulators in the future. For this PhD project, the technology came too late to be integrated and the failure of the NanoBRET approach led to change in project focus as detailed in chapter 4.4.

4.4 Development of anti-trypanosomal drug targeting PKA

Trypanosomatid parasites caused diseases, especially the Chagas disease and cutaneous (CL) and visceral (VL) leishmaniasis, are threatening millions of people worldwide. Drug resistance, adverse side effects and low efficacy of current drugs are the main limitations of current therapies, especially for late-stage disease patients. Our attempt to develop PKA inhibitors targeting PKAR NBD-B is based on the structural and functional study of *T. brucei* PKAR. Separating the binding affinity from activation potency has been achieved in some of the N1, C7-modified inosine analogs (Fig 3.40). What's more, the promising compound MB-052 shows an antagonistic effect to adenosine activation, although it also has intrinsic activation potency for TbPKA. Nevertheless, development of a potent PKA inhibitor seems possible but needs better understanding of *T. brucei* PKA activation mechanism. Computational docking has shown that the α-D helix is displaced upon the binding of these compounds to the B-site, while this does not disable the activation of PKA as revealed by NanoBiT assay. Therefore, we have to reconsider our initial hypothesis about the role of the α-D helix in PKA activation. One interpretation is that this kinetoplastids-specific α-D helix is not required for inducing PKAR conformation change, but only important for ligand binding and selectivity. Inosine EC_{50} increased 100-fold in the absence of the α-D helix (Fig 3.26). The data is in agreement with the 100-fold increase of inosine K_d measured with the Y484 and Y485 mutated PKAR mutant (Githure, manuscript, 2021), in which the α-D helix cannot properly interact with the B-site. Moreover, new interactions formed

between the added N1 and C7 moieties of the designed compounds and the β-strands of the B-site likely stabilize the compounds in the B-site. To validate the hypothesis, the α-D helix deletion mutant can be applied. By comparing the activation profile of this mutant by natural nucleosides and the modified compounds and the binding affinity of these compounds to the α-D helix deleted B-site, which is measured with the refolded PKAR(199-482)_PBCA protein by ITC, the role of the α-D helix in PKA activation can be further understood.

If the α-D helix would still be critical for the conformation change required for activation of PKA, it would mean that the currently designed compounds did not, or at least not fully, interrupt the interactions of the α-D helix. In this case, a co-crystal structure of one of the compounds and PKAR is needed for further inhibitor design. If it is proven to be the opposite, it means that we have to search again for key elements inducing PKAR conformation change. In this scenario, the previous studies with the Rp-cAMPS are helpful (Dostmann & Taylor, 1991; Dostmann, 1995; Badireddy *et al.*, 2011). There is an ensemble allosteric model of PKA proposed based on x-ray crystallography and amide hydrogen/deuterium exchange mass spectrometry (Badireddy *et al.*, 2011), which was further rationalized by molecular dynamics (MD) simulation and nuclear magnetic resonance (NMR) recently (Byun *et al.*, 2020). In this model, addition of the PKA inhibitor, Rp-cAMPS, to PKA holoenzymes is supposed to stabilize the A-site in an open topological structure (H-form) while the B-site is in an equilibrium of H-form and the closed state (B-form). The distance between the equatorial sulfur (of Rp-cAMPS) and the residue Ala 202 and Arg 209 (of human RIα) are critical for maintaining the H-form state. In addition, substitution of the capping residue of the A-site, which is important for A- and B-site communication, is thought to stress the A-site of the APO PKAR to H-form. The model can be verified in *T. brucei* PKA and compounds mimicking Rp-cAMPS can be designed. The accessibility of the A-site in a mammalian PKA holoenzyme is thought to highly depend on the state of the B-site, whether this rule works for T. brucei PKA is yet to be studied. A PKAR mutant with a malfunctional B-site that not binds any ligands can be tested by NanoBiT assay to see whether PKA activation can happen. Moreover, the PKAR mutant containing a malfunctional A-site plus (or not) the α-D helix deletion can be tested to see whether B-site conformation change alone is sufficient to activate PKA. In summary, a better understanding of the PKA activation mechanism is the basis for further inhibitor development.

5 References

Al-Salabi, M. I., Wallace, L. J., Luscher, A., Maser, P., Candlish, D., Rodenko, B., et al. (2007). Molecular interactions underlying the unusually high adenosine affinity of a novel Trypanosoma brucei nucleoside transporter. *Mol Pharmacol, 71*(3), 921-929. doi:10.1124/mol.106.031559

Alfituri, O. A., Quintana, J. F., MacLeod, A., Garside, P., Benson, R. A., Brewer, J. M., et al. (2020). To the Skin and Beyond: The Immune Response to African Trypanosomes as They Enter and Exit the Vertebrate Host. *Front Immunol, 11*, 1250. doi:10.3389/fimmu.2020.01250

Alsford, S., Eckert, S., Baker, N., Glover, L., Sanchez-Flores, A., Leung, K. F., et al. (2012). High-throughput decoding of antitrypanosomal drug efficacy and resistance. *Nature, 482*(7384), 232-236. doi:10.1038/nature10771

Alsford, S., & Horn, D. (2008). Single-locus targeting constructs for reliable regulated RNAi and transgene expression in Trypanosoma brucei. *Mol Biochem Parasitol, 161*(1), 76-79. doi:10.1016/j.molbiopara.2008.05.006

Alsford, S., Turner, D. J., Obado, S. O., Sanchez-Flores, A., Glover, L., Berriman, M., et al. (2011). High-throughput phenotyping using parallel sequencing of RNA interference targets in the African trypanosome. *Genome Res, 21*(6), 915-924. doi:10.1101/gr.115089.110

Andriani, G., Amata, E., Beatty, J., Clements, Z., Coffey, B. J., Courtemanche, G., et al. (2013). Antitrypanosomal lead discovery: identification of a ligand-efficient inhibitor of Trypanosoma cruzi CYP51 and parasite growth. *J Med Chem, 56*(6), 2556-2567. doi:10.1021/jm400012e

Ashcroft, M. T. (1960). A comparison between a syringe-passaged and a tsetse-fly-transmitted line of a strain of Trypanosoma rhodesiense. *Ann Trop Med Parasitol, 54*, 44-53. doi:10.1080/00034983.1960.11685955

Azad, T., Singaravelu, R., Brown, E. E. F., Taha, Z., Rezaei, R., Arulanandam, R., et al. (2021). SARS-CoV-2 S1 NanoBiT: A nanoluciferase complementation-based biosensor to rapidly probe SARS-CoV-2 receptor recognition. *Biosens Bioelectron, 180*, 113122. doi:10.1016/j.bios.2021.113122

Bachmaier, S., & Boshart, M. (2013). Kinetoplastid AGC Kinases. In *Protein Phosphorylation in Parasites* (pp. 99-122).

Bachmaier, S., Thanner, T., & Boshart, M. (2020). Culturing and Transfection of Pleomorphic Trypanosoma brucei. *Methods Mol Biol, 2116*, 23-38. doi:10.1007/978-1-0716-0294-2_2

Bachmaier, S., Volpato Santos, Y., Kramer, S., Githure, G. B., Klockner, T., Pepperl, J., et al. (2019). Nucleoside analogue activators of cyclic AMP-independent protein kinase A of Trypanosoma. *Nat Commun, 10*(1), 1421. doi:10.1038/s41467-019-09338-z

Badireddy, S., Yunfeng, G., Ritchie, M., Akamine, P., Wu, J., Kim, C. W., et al. (2011). Cyclic AMP analog blocks kinase activation by stabilizing inactive conformation: conformational selection highlights a new concept in allosteric inhibitor design. *Mol Cell Proteomics, 10*(3), M110 004390. doi:10.1074/mcp.M110.004390

Baker, N., Alsford, S., & Horn, D. (2011). Genome-wide RNAi screens in African trypanosomes identify the nifurtimox activator NTR and the eflornithine transporter AAT6. *Mol Biochem Parasitol, 176*(1), 55-57. doi:10.1016/j.molbiopara.2010.11.010

Baker, N., Catta-Preta, C. M. C., Neish, R., Sadlova, J., Powell, B., Alves-Ferreira, E. V. C., et al. (2021). Systematic functional analysis of Leishmania protein kinases identifies regulators of differentiation or survival. *Nat Commun, 12*(1), 1244. doi:10.1038/s41467-021-21360-8

Balakumar, P., Nyo, Y. H., Renushia, R., Raaginey, D., Oh, A. N., Varatharajan, R., et al. (2014). Classical and pleiotropic actions of dipyridamole: Not enough light to illuminate the dark tunnel? *Pharmacol Res, 87*, 144-150. doi:10.1016/j.phrs.2014.05.008

Bandje, K., Naissant, B., Bigey, P., Lohezic, M., Vayssieres, M., Blaud, M., et al. (2016). Characterization of an A-kinase anchoring protein-like suggests an alternative way of PKA anchoring in Plasmodium falciparum. *Malar J, 15*, 248. doi:10.1186/s12936-016-1275-9

Banning, C., Votteler, J., Hoffmann, D., Koppensteiner, H., Warmer, M., Reimer, R., et al. (2010). A flow cytometry-based FRET assay to identify and analyse protein-protein interactions in living cells. *PLoS One, 5*(2), e9344. doi:10.1371/journal.pone.0009344

Barry, J. D., & McCulloch, R. (2001). Antigenic variation in trypanosomes: enhanced phenotypic variation in a eukaryotic parasite. *Adv Parasitol, 49*, 1-70. doi:10.1016/s0065-308x(01)49037-3

Bastidas, A. C., Deal, M. S., Steichen, J. M., Keshwani, M. M., Guo, Y., & Taylor, S. S. (2012). Role of N-terminal myristylation in the structure and regulation of cAMP-dependent protein kinase. *J Mol Biol, 422*(2), 215-229. doi:10.1016/j.jmb.2012.05.021

Bencina, M., Legisa, M., & Read, N. D. (2005). Cross-talk between cAMP and calcium signalling in Aspergillus niger. *Mol Microbiol, 56*(1), 268-281. doi:10.1111/j.1365-2958.2005.04541.x

Berriman, M., Ghedin, E., Hertz-Fowler, C., Blandin, G., Renauld, H., Bartholomeu, D. C., et al. (2005). The genome of the African trypanosome Trypanosoma brucei. *Science, 309*(5733), 416-422. doi:10.1126/science.1112642

Bertherat, J., Horvath, A., Groussin, L., Grabar, S., Boikos, S., Cazabat, L., et al. (2009). Mutations in regulatory subunit type 1A of cyclic adenosine 5'-monophosphate-dependent protein kinase (PRKAR1A): phenotype analysis in 353 patients and 80 different genotypes. *J Clin Endocrinol Metab, 94*(6), 2085-2091. doi:10.1210/jc.2008-2333

Beuschlein, F., Fassnacht, M., Assie, G., Calebiro, D., Stratakis, C. A., Osswald, A., et al. (2014). Constitutive activation of PKA catalytic subunit in adrenal Cushing's syndrome. *N Engl J Med, 370*(11), 1019-1028. doi:10.1056/NEJMoa1310359

Bhattacharya, A., Biswas, A., & Das, P. K. (2012). Identification of a protein kinase A regulatory subunit from Leishmania having importance in metacyclogenesis through induction of autophagy. *Mol Microbiol, 83*(3), 548-564. doi:10.1111/j.1365-2958.2011.07950.x

Born, G. V., & Cross, M. J. (1963). Effect of adenosine diphosphate on the concentration of platelets in circulating blood. *Nature, 197*, 974-976. doi:10.1038/197974a0

Bringaud, F., & Baltz, T. (1993). Differential regulation of two distinct families of glucose transporter genes in Trypanosoma brucei. *Mol Cell Biol, 13*(2), 1146-1154. doi:10.1128/mcb.13.2.1146

Broadhead, R., Dawe, H. R., Farr, H., Griffiths, S., Hart, S. R., Portman, N., et al. (2006). Flagellar motility is required for the viability of the bloodstream trypanosome. *Nature, 440*(7081), 224-227. doi:10.1038/nature04541

Brun, R., Blum, J., Chappuis, F., & Burri, C. (2010). Human African trypanosomiasis. *Lancet, 375*(9709), 148-159. doi:10.1016/S0140-6736(09)60829-1

Bubis, J., Martinez, J. C., Calabokis, M., Ferreira, J., Sanz-Rodriguez, C. E., Navas, V., et al. (2018). The gene product of a Trypanosoma equiperdum ortholog of the cAMP-dependent protein kinase regulatory subunit is a monomeric protein that is not capable of binding cyclic nucleotides. *Biochimie, 146*, 166-180. doi:10.1016/j.biochi.2017.12.010

Byun, J. A., Akimoto, M., VanSchouwen, B., Lazarou, T. S., Taylor, S. S., & Melacini,

G. (2020). Allosteric pluripotency as revealed by protein kinase A. *Sci Adv, 6*(25), eabb1250. doi:10.1126/sciadv.abb1250

Cadd, G., & McKnight, G. S. (1989). Distinct patterns of cAMP-dependent protein kinase gene expression in mouse brain. *Neuron, 3*(1), 71-79. doi:10.1016/0896-6273(89)90116-5

Carr, D. W., Stofko-Hahn, R. E., Fraser, I. D., Bishop, S. M., Acott, T. S., Brennan, R. G., et al. (1991). Interaction of the regulatory subunit (RII) of cAMP-dependent protein kinase with RII-anchoring proteins occurs through an amphipathic helix binding motif. *J Biol Chem, 266*(22), 14188-14192.

Cauthron, R. D., Carter, K. B., Liauw, S., & Steinberg, R. A. (1998). Physiological phosphorylation of protein kinase A at Thr-197 is by a protein kinase A kinase. *Mol Cell Biol, 18*(3), 1416-1423. doi:10.1128/mcb.18.3.1416

Chaplin, M. (2006). Do we underestimate the importance of water in cell biology? *Nat Rev Mol Cell Biol, 7*(11), 861-866. doi:10.1038/nrm2021

Chaves, I., Rudenko, G., Dirks-Mulder, A., Cross, M., & Borst, P. (1999). Control of variant surface glycoprotein gene-expression sites in Trypanosoma brucei. *EMBO J, 18*(17), 4846-4855. doi:10.1093/emboj/18.17.4846

Cheng, H. C., van Patten, S. M., Smith, A. J., & Walsh, D. A. (1985). An active twenty-amino-acid-residue peptide derived from the inhibitor protein of the cyclic AMP-dependent protein kinase. *Biochem J, 231*(3), 655-661. doi:10.1042/bj2310655

Cheng, X., Ma, Y., Moore, M., Hemmings, B. A., & Taylor, S. S. (1998). Phosphorylation and activation of cAMP-dependent protein kinase by phosphoinositide-dependent protein kinase. *Proc Natl Acad Sci U S A, 95*(17), 9849-9854. doi:10.1073/pnas.95.17.9849

Colledge, M., Dean, R. A., Scott, G. K., Langeberg, L. K., Huganir, R. L., & Scott, J. D. (2000). Targeting of PKA to glutamate receptors through a MAGUK-AKAP complex. *Neuron, 27*(1), 107-119. doi:10.1016/s0896-6273(00)00013-1

Cooper, D. M. (2005). Compartmentalization of adenylate cyclase and cAMP signalling. *Biochem Soc Trans, 33*(Pt 6), 1319-1322. doi:10.1042/BST20051319

Courter, J. R., Madani, N., Sodroski, J., Schon, A., Freire, E., Kwong, P. D., et al. (2014). Structure-based design, synthesis and validation of CD4-mimetic small molecule inhibitors of HIV-1 entry: conversion of a viral entry agonist to an antagonist. *Acc Chem Res, 47*(4), 1228-1237. doi:10.1021/ar4002735

Croft, S. L., & Coombs, G. H. (2003). Leishmaniasis--current chemotherapy and recent advances in the search for novel drugs. *Trends Parasitol, 19*(11), 502-508. doi:10.1016/j.pt.2003.09.008

Cross, G. A. (1975). Identification, purification and properties of clone-specific glycoprotein antigens constituting the surface coat of Trypanosoma brucei. *Parasitology, 71*(3), 393-417. doi:10.1017/s003118200004717x

Cross, G. A., & Manning, J. C. (1973). Cultivation of Trypanosoma brucei sspp. in semi-defined and defined media. *Parasitology, 67*(3), 315-331. doi:10.1017/s0031182000046540

Das, R., Esposito, V., Abu-Abed, M., Anand, G. S., Taylor, S. S., & Melacini, G. (2007). cAMP activation of PKA defines an ancient signaling mechanism. *Proc Natl Acad Sci U S A, 104*(1), 93-98. doi:10.1073/pnas.0609033103

de Boer, M., Gouridis, G., Muthahari, Y. A., & Cordes, T. (2019a). Single-Molecule Observation of Ligand Binding and Conformational Changes in FeuA. *Biophys J, 117*(9), 1642-1654. doi:10.1016/j.bpj.2019.08.005

de Boer, M., Gouridis, G., Vietrov, R., Begg, S. L., Schuurman-Wolters, G. K., Husada, F., et al. (2019b). Conformational and dynamic plasticity in substrate-binding proteins underlies selective transport in ABC importers. *Elife, 8*. doi:10.7554/eLife.44652

Dean, S., Marchetti, R., Kirk, K., & Matthews, K. R. (2009). A surface transporter family conveys the trypanosome differentiation signal. *Nature, 459*(7244), 213-217.

doi:10.1038/nature07997
Dean, S., Sunter, J., Wheeler, R. J., Hodkinson, I., Gluenz, E., & Gull, K. (2015). A toolkit enabling efficient, scalable and reproducible gene tagging in trypanosomatids. *Open Biol, 5*(1), 140197. doi:10.1098/rsob.140197
DeBernardi, M. A., & Brooker, G. (1996). Single cell Ca2+/cAMP cross-talk monitored by simultaneous Ca2+/cAMP fluorescence ratio imaging. *Proc Natl Acad Sci U S A, 93*(10), 4577-4582. doi:10.1073/pnas.93.10.4577
Deeks, E. D. (2019). Fexinidazole: First Global Approval. *Drugs, 79*(2), 215-220. doi:10.1007/s40265-019-1051-6
Delauw, M. F., Pays, E., Steinert, M., Aerts, D., Van Meirvenne, N., & Le Ray, D. (1985). Inactivation and reactivation of a variant-specific antigen gene in cyclically transmitted Trypanosoma brucei. *EMBO J, 4*(4), 989-993.
Dessauer, C. W. (2009). Adenylyl cyclase--A-kinase anchoring protein complexes: the next dimension in cAMP signaling. *Mol Pharmacol, 76*(5), 935-941. doi:10.1124/mol.109.059345
Diskar, M., Zenn, H. M., Kaupisch, A., Prinz, A., & Herberg, F. W. (2007). Molecular basis for isoform-specific autoregulation of protein kinase A. *Cell Signal, 19*(10), 2024-2034. doi:10.1016/j.cellsig.2007.05.012
Dixon, A. S., Schwinn, M. K., Hall, M. P., Zimmerman, K., Otto, P., Lubben, T. H., et al. (2016). NanoLuc Complementation Reporter Optimized for Accurate Measurement of Protein Interactions in Cells. *ACS Chem Biol, 11*(2), 400-408. doi:10.1021/acschembio.5b00753
Dostmann, W. R. (1995). (RP)-cAMPS inhibits the cAMP-dependent protein kinase by blocking the cAMP-induced conformational transition. *FEBS Lett, 375*(3), 231-234. doi:10.1016/0014-5793(95)01201-o
Dostmann, W. R., & Taylor, S. S. (1991). Identifying the molecular switches that determine whether (Rp)-cAMPS functions as an antagonist or an agonist in the activation of cAMP-dependent protein kinase I. *Biochemistry, 30*(35), 8710-8716. doi:10.1021/bi00099a032
Duthie, M. S., Favila, M., Hofmeyer, K. A., Tutterrow, Y. L., Reed, S. J., Laurance, J. D., et al. (2016). Strategic evaluation of vaccine candidate antigens for the prevention of Visceral Leishmaniasis. *Vaccine, 34*(25), 2779-2786. doi:10.1016/j.vaccine.2016.04.067
El-Sayed, N. M., Myler, P. J., Bartholomeu, D. C., Nilsson, D., Aggarwal, G., Tran, A. N., et al. (2005). The genome sequence of Trypanosoma cruzi, etiologic agent of Chagas disease. *Science, 309*(5733), 409-415. doi:10.1126/science.1112631
El Bakkouri, M., Kouidmi, I., Wernimont, A. K., Amani, M., Hutchinson, A., Loppnau, P., et al. (2019). Structures of the cGMP-dependent protein kinase in malaria parasites reveal a unique structural relay mechanism for activation. *Proc Natl Acad Sci U S A, 116*(28), 14164-14173. doi:10.1073/pnas.1905558116
Elkeles, R. S., Hampton, J. R., Honour, A. J., Mitchell, J. R., & Prichard, J. S. (1968). Effect of a pyrimido-pyrimidine compound on platelet behaviour in vitro and in vivo. *Lancet, 2*(7571), 751-754. doi:10.1016/s0140-6736(68)90952-5
Ellison, K. E., & Gandhi, G. (2005). Optimising the use of beta-adrenoceptor antagonists in coronary artery disease. *Drugs, 65*(6), 787-797. doi:10.2165/00003495-200565060-00006
Engstler, M., & Boshart, M. (2004). Cold shock and regulation of surface protein trafficking convey sensitization to inducers of stage differentiation in Trypanosoma brucei. *Genes Dev, 18*(22), 2798-2811. doi:10.1101/gad.323404
Fernandez-Cortes, F., Serafim, T. D., Wilkes, J. M., Jones, N. G., Ritchie, R., McCulloch, R., et al. (2017). RNAi screening identifies Trypanosoma brucei stress response protein kinases required for survival in the mouse. *Sci Rep, 7*(1), 6156. doi:10.1038/s41598-017-06501-8

Fernandez, A., & Scheraga, H. A. (2003). Insufficiently dehydrated hydrogen bonds as determinants of protein interactions. *Proc Natl Acad Sci U S A, 100*(1), 113-118. doi:10.1073/pnas.0136888100

Field, M. C., & Carrington, M. (2009). The trypanosome flagellar pocket. *Nat Rev Microbiol, 7*(11), 775-786. doi:10.1038/nrmicro2221

Flynn, I. W., & Bowman, I. B. (1973). The metabolism of carbohydrate by pleomorphic African trypanosomes. *Comp Biochem Physiol B, 45*(1), 25-42. doi:10.1016/0305-0491(73)90281-2

Francisco, A. F., Jayawardhana, S., Lewis, M. D., White, K. L., Shackleford, D. M., Chen, G., et al. (2016). Nitroheterocyclic drugs cure experimental Trypanosoma cruzi infections more effectively in the chronic stage than in the acute stage. *Sci Rep, 6*, 35351. doi:10.1038/srep35351

Francisco, A. F., Jayawardhana, S., Olmo, F., Lewis, M. D., Wilkinson, S. R., Taylor, M. C., et al. (2020). Challenges in Chagas Disease Drug Development. *Molecules, 25*(12). doi:10.3390/molecules25122799

Franco, J. R., Cecchi, G., Priotto, G., Paone, M., Diarra, A., Grout, L., et al. (2020). Monitoring the elimination of human African trypanosomiasis at continental and country level: Update to 2018. *PLoS Negl Trop Dis, 14*(5), e0008261. doi:10.1371/journal.pntd.0008261

Freitas-Junior, L. H., Chatelain, E., Kim, H. A., & Siqueira-Neto, J. L. (2012). Visceral leishmaniasis treatment: What do we have, what do we need and how to deliver it? *Int J Parasitol Drugs Drug Resist, 2*, 11-19. doi:10.1016/j.ijpddr.2012.01.003

Gadelha, F. R., Moreno, S. N., De Souza, W., Cruz, F. S., & Docampo, R. (1989). The mitochondrion of Trypanosoma cruzi is a target of crystal violet toxicity. *Mol Biochem Parasitol, 34*(2), 117-126. doi:10.1016/0166-6851(89)90003-0

Gamboa, A., Abraham, R., Diedrich, A., Shibao, C., Paranjape, S. Y., Farley, G., et al. (2005). Role of adenosine and nitric oxide on the mechanisms of action of dipyridamole. *Stroke, 36*(10), 2170-2175. doi:10.1161/01.STR.0000179044.37760.9d

Garbers, D. L., Chrisman, T. D., Wiegn, P., Katafuchi, T., Albanesi, J. P., Bielinski, V., et al. (2006). Membrane guanylyl cyclase receptors: an update. *Trends Endocrinol Metab, 17*(6), 251-258. doi:10.1016/j.tem.2006.06.006

Genovesio, A., Giardini, M. A., Kwon, Y. J., de Macedo Dossin, F., Choi, S. Y., Kim, N. Y., et al. (2011). Visual genome-wide RNAi screening to identify human host factors required for Trypanosoma cruzi infection. *PLoS One, 6*(5), e19733. doi:10.1371/journal.pone.0019733

George Abraham, B., Sarkisyan, K. S., Mishin, A. S., Santala, V., Tkachenko, N. V., & Karp, M. (2015). Fluorescent Protein Based FRET Pairs with Improved Dynamic Range for Fluorescence Lifetime Measurements. *PLoS One, 10*(8), e0134436. doi:10.1371/journal.pone.0134436

Gibson, W., & Bailey, M. (2003). The development of Trypanosoma brucei within the tsetse fly midgut observed using green fluorescent trypanosomes. *Kinetoplastid Biol Dis, 2*(1), 1. doi:10.1186/1475-9292-2-1

Glover, L., Alsford, S., Baker, N., Turner, D. J., Sanchez-Flores, A., Hutchinson, S., et al. (2015). Genome-scale RNAi screens for high-throughput phenotyping in bloodstream-form African trypanosomes. *Nat Protoc, 10*(1), 106-133. doi:10.1038/nprot.2015.005

Gorbunova, Y. V., & Spitzer, N. C. (2002). Dynamic interactions of cyclic AMP transients and spontaneous Ca(2+) spikes. *Nature, 418*(6893), 93-96. doi:10.1038/nature00835

Gould, M. K., Bachmaier, S., Ali, J. A., Alsford, S., Tagoe, D. N., Munday, J. C., et al. (2013). Cyclic AMP effectors in African trypanosomes revealed by genome-scale RNA interference library screening for resistance to the phosphodiesterase inhibitor CpdA. *Antimicrob Agents Chemother, 57*(10),

4882-4893. doi:10.1128/AAC.00508-13
Grab, D. J., & Kennedy, P. G. (2008). Traversal of human and animal trypanosomes across the blood-brain barrier. *J Neurovirol, 14*(5), 344-351. doi:10.1080/13550280802282934
Gruszynski, A. E., van Deursen, F. J., Albareda, M. C., Best, A., Chaudhary, K., Cliffe, L. J., et al. (2006). Regulation of surface coat exchange by differentiating African trypanosomes. *Mol Biochem Parasitol, 147*(2), 211-223. doi:10.1016/j.molbiopara.2006.02.013
Guo, C., & Zhou, H. X. (2016). Unidirectional allostery in the regulatory subunit RIalpha facilitates efficient deactivation of protein kinase A. *Proc Natl Acad Sci U S A, 113*(44), E6776-E6785. doi:10.1073/pnas.1610142113
Hammarton, T. C. (2007). Cell cycle regulation in Trypanosoma brucei. *Mol Biochem Parasitol, 153*(1), 1-8. doi:10.1016/j.molbiopara.2007.01.017
Hammerl, J. (2018). *Dominant negative mutants of the regulatory subunit of protein kinase A in Trypanosoma brucei.* (Bachelor Bachelor thesis), Ludwig-Maximilians Universität München, München.
Hanks, S. K., Quinn, A. M., & Hunter, T. (1988). The protein kinase family: conserved features and deduced phylogeny of the catalytic domains. *Science, 241*(4861), 42-52. doi:10.1126/science.3291115
Hao, Y., England, J. P., Bellucci, L., Paci, E., Hodges, H. C., Taylor, S. S., et al. (2019). Activation of PKA via asymmetric allosteric coupling of structurally conserved cyclic nucleotide binding domains. *Nat Commun, 10*(1), 3984. doi:10.1038/s41467-019-11930-2
Harker, L. A., & Kadatz, R. A. (1983). Mechanism of action of dipyridamole. *Thromb Res Suppl, 4*, 39-46. doi:10.1016/0049-3848(83)90356-0
Haste, N. M., Talabani, H., Doo, A., Merckx, A., Langsley, G., & Taylor, S. S. (2012). Exploring the Plasmodium falciparum cyclic-adenosine monophosphate (cAMP)-dependent protein kinase (PfPKA) as a therapeutic target. *Microbes Infect, 14*(10), 838-850. doi:10.1016/j.micinf.2012.05.004
Haston, W. S. (1972). Development of Trypanosoma brucei in the gut of Glossina morsitans. *Trans R Soc Trop Med Hyg, 66*(4), 548.
Haushalter, K. J., Casteel, D. E., Raffeiner, A., Stefan, E., Patel, H. H., & Taylor, S. S. (2018). Phosphorylation of protein kinase A (PKA) regulatory subunit RIalpha by protein kinase G (PKG) primes PKA for catalytic activity in cells. *J Biol Chem, 293*(12), 4411-4421. doi:10.1074/jbc.M117.809988
Hellenkamp, B., Schmid, S., Doroshenko, O., Opanasyuk, O., Kuhnemuth, R., Rezaei Adariani, S., et al. (2018). Precision and accuracy of single-molecule FRET measurements-a multi-laboratory benchmark study. *Nat Methods, 15*(9), 669-676. doi:10.1038/s41592-018-0085-0
Herberg, F. W., Zimmermann, B., McGlone, M., & Taylor, S. S. (1997). Importance of the A-helix of the catalytic subunit of cAMP-dependent protein kinase for stability and for orienting subdomains at the cleft interface. *Protein Sci, 6*(3), 569-579. doi:10.1002/pro.5560060306
Hirimburegama, K., Durnez, P., Keleman, J., Oris, E., Vergauwen, R., Mergelsberg, H., et al. (1992). Nutrient-induced activation of trehalase in nutrient-starved cells of the yeast Saccharomyces cerevisiae: cAMP is not involved as second messenger. *J Gen Microbiol, 138*(10), 2035-2043. doi:10.1099/00221287-138-10-2035
Hoffmann, C., Castro, M., Rinken, A., Leurs, R., Hill, S. J., & Vischer, H. F. (2015). Ligand Residence Time at G-protein-Coupled Receptors-Why We Should Take Our Time To Study It. *Mol Pharmacol, 88*(3), 552-560. doi:10.1124/mol.115.099671
Holden, C. P., & Storey, K. B. (2000). Purification and characterization of protein kinase A from liver of the freeze-tolerant wood frog: role in glycogenolysis during

freezing. *Cryobiology, 40*(4), 323-331. doi:10.1006/cryo.2000.2252
Holdgate, G. A. (2007). Thermodynamics of binding interactions in the rational drug design process. *Expert Opin Drug Discov, 2*(8), 1103-1114. doi:10.1517/17460441.2.8.1103
Huang, H., Weiss, L. M., Nagajyothi, F., Tanowitz, H. B., Wittner, M., Orr, G. A., et al. (2006). Molecular cloning and characterization of the protein kinase A regulatory subunit of Trypanosoma cruzi. *Mol Biochem Parasitol, 149*(2), 242-245. doi:10.1016/j.molbiopara.2006.05.008
Huang, H., Werner, C., Weiss, L. M., Wittner, M., & Orr, G. A. (2002). Molecular cloning and expression of the catalytic subunit of protein kinase A from Trypanosoma cruzi. *Int J Parasitol, 32*(9), 1107-1115. doi:10.1016/s0020-7519(02)00085-1
Ilouz, R., Bubis, J., Wu, J., Yim, Y. Y., Deal, M. S., Kornev, A. P., et al. (2012). Localization and quaternary structure of the PKA RIbeta holoenzyme. *Proc Natl Acad Sci U S A, 109*(31), 12443-12448. doi:10.1073/pnas.1209538109
Ilouz, R., Lev-Ram, V., Bushong, E. A., Stiles, T. L., Friedmann-Morvinski, D., Douglas, C., et al. (2017). Isoform-specific subcellular localization and function of protein kinase A identified by mosaic imaging of mouse brain. *Elife, 6*. doi:10.7554/eLife.17681
Isensee, J., Kaufholz, M., Knape, M. J., Hasenauer, J., Hammerich, H., Gonczarowska-Jorge, H., et al. (2018). PKA-RII subunit phosphorylation precedes activation by cAMP and regulates activity termination. *J Cell Biol, 217*(6), 2167-2184. doi:10.1083/jcb.201708053
Ivens, A. C., Peacock, C. S., Worthey, E. A., Murphy, L., Aggarwal, G., Berriman, M., et al. (2005). The genome of the kinetoplastid parasite, Leishmania major. *Science, 309*(5733), 436-442. doi:10.1126/science.1112680
Jahnsen, T., Hedin, L., Lohmann, S. M., Walter, U., & Richards, J. S. (1986). The neural type II regulatory subunit of cAMP-dependent protein kinase is present and regulated by hormones in the rat ovary. *J Biol Chem, 261*(15), 6637-6639.
James, D. M., & Born, G. V. (1980). Uptake of purine bases and nucleosides in African trypanosomes. *Parasitology, 81*(2), 383-393. doi:10.1017/s0031182000056110
Jaski, B. E., Fifer, M. A., Wright, R. F., Braunwald, E., & Colucci, W. S. (1985). Positive inotropic and vasodilator actions of milrinone in patients with severe congestive heart failure. Dose-response relationships and comparison to nitroprusside. *J Clin Invest, 75*(2), 643-649. doi:10.1172/JCI111742
Jelesarov, I., & Bosshard, H. R. (1999). Isothermal titration calorimetry and differential scanning calorimetry as complementary tools to investigate the energetics of biomolecular recognition. *J Mol Recognit, 12*(1), 3-18. doi:10.1002/(SICI)1099-1352(199901/02)12:1<3::AID-JMR441>3.0.CO;2-6
Jones, N. G., Thomas, E. B., Brown, E., Dickens, N. J., Hammarton, T. C., & Mottram, J. C. (2014). Regulators of Trypanosoma brucei cell cycle progression and differentiation identified using a kinome-wide RNAi screen. *PLoS Pathog, 10*(1), e1003886. doi:10.1371/journal.ppat.1003886
Kannan, N., Haste, N., Taylor, S. S., & Neuwald, A. F. (2007). The hallmark of AGC kinase functional divergence is its C-terminal tail, a cis-acting regulatory module. *Proc Natl Acad Sci U S A, 104*(4), 1272-1277. doi:10.1073/pnas.0610251104
Kim, C., Cheng, C. Y., Saldanha, S. A., & Taylor, S. S. (2007). PKA-I holoenzyme structure reveals a mechanism for cAMP-dependent activation. *Cell, 130*(6), 1032-1043. doi:10.1016/j.cell.2007.07.018
Kim, C., Xuong, N. H., & Taylor, S. S. (2005). Crystal structure of a complex between the catalytic and regulatory (RIalpha) subunits of PKA. *Science, 307*(5710), 690-696. doi:10.1126/science.1104607
Kim, J., & Grailhe, R. (2016). Nanoluciferase signal brightness using furimazine substrates opens bioluminescence resonance energy transfer to widefield

microscopy. *Cytometry A, 89*(8), 742-746. doi:10.1002/cyto.a.22870
Kim, J. J., Flueck, C., Franz, E., Sanabria-Figueroa, E., Thompson, E., Lorenz, R., et al. (2015). Crystal structures of the carboxyl cGMP binding domain of the Plasmodium falciparum cGMP-dependent protein kinase reveal a novel capping triad crucial for merozoite egress. *PLoS Pathog, 11*(2), e1004639. doi:10.1371/journal.ppat.1004639
Kirschner, L. S., Carney, J. A., Pack, S. D., Taymans, S. E., Giatzakis, C., Cho, Y. S., et al. (2000). Mutations of the gene encoding the protein kinase A type I-alpha regulatory subunit in patients with the Carney complex. *Nat Genet, 26*(1), 89-92. doi:10.1038/79238
Kleppe, R., Krakstad, C., Selheim, F., Kopperud, R., & Doskeland, S. O. (2011). The cAMP-dependent protein kinase pathway as therapeutic target: possibilities and pitfalls. *Curr Top Med Chem, 11*(11), 1393-1405. doi:10.2174/156802611795589629
Kobayashi, T., & Dynlacht, B. D. (2011). Regulating the transition from centriole to basal body. *J Cell Biol, 193*(3), 435-444. doi:10.1083/jcb.201101005
Kohl, L., Sherwin, T., & Gull, K. (1999). Assembly of the paraflagellar rod and the flagellum attachment zone complex during the Trypanosoma brucei cell cycle. *J Eukaryot Microbiol, 46*(2), 105-109. doi:10.1111/j.1550-7408.1999.tb04592.x
Koizumi, H., Kimata, Y., Shiraishi, Y., & Hirai, T. (2007). Temperature-controlled changeable oxygenation selectivity by singlet oxygen with a polymeric photosensitizer. *Chem Commun (Camb)*(18), 1846-1848. doi:10.1039/b617718b
Komander, D., Kular, G., Deak, M., Alessi, D. R., & van Aalten, D. M. (2005). Role of T-loop phosphorylation in PDK1 activation, stability, and substrate binding. *J Biol Chem, 280*(19), 18797-18802. doi:10.1074/jbc.M500977200
Koning, H. P. D. (2020). The Drugs of Sleeping Sickness: Their Mechanisms of Action and Resistance, and a Brief History. *Trop Med Infect Dis, 5*(1). doi:10.3390/tropicalmed5010014
Kornev, A. P., Haste, N. M., Taylor, S. S., & Eyck, L. F. (2006). Surface comparison of active and inactive protein kinases identifies a conserved activation mechanism. *Proc Natl Acad Sci U S A, 103*(47), 17783-17788. doi:10.1073/pnas.0607656103
Kornev, A. P., & Taylor, S. S. (2010). Defining the conserved internal architecture of a protein kinase. *Biochim Biophys Acta, 1804*(3), 440-444. doi:10.1016/j.bbapap.2009.10.017
Laemmli, U. K. (1970). Cleavage of structural proteins during the assembly of the head of bacteriophage T4. *Nature, 227*(5259), 680-685. doi:10.1038/227680a0
Lawson, C. L., Swigon, D., Murakami, K. S., Darst, S. A., Berman, H. M., & Ebright, R. H. (2004). Catabolite activator protein: DNA binding and transcription activation. *Curr Opin Struct Biol, 14*(1), 10-20. doi:10.1016/j.sbi.2004.01.012
Leal, S., Acosta-Serrano, A., Morris, J., & Cross, G. A. (2004). Transposon mutagenesis of Trypanosoma brucei identifies glycosylation mutants resistant to concanavalin A. *J Biol Chem, 279*(28), 28979-28988. doi:10.1074/jbc.M403479200
Leighfield, T. A., Barbier, M., & Van Dolah, F. M. (2002). Evidence for cAMP-dependent protein kinase in the dinoflagellate, Amphidinium operculatum. *Comp Biochem Physiol B Biochem Mol Biol, 133*(3), 317-324. doi:10.1016/s1096-4959(02)00148-3
Li, Z. (2012). Regulation of the cell division cycle in Trypanosoma brucei. *Eukaryot Cell, 11*(10), 1180-1190. doi:10.1128/EC.00145-12
Lindner, A. K., Lejon, V., Chappuis, F., Seixas, J., Kazumba, L., Barrett, M. P., et al. (2020). New WHO guidelines for treatment of gambiense human African trypanosomiasis including fexinidazole: substantial changes for clinical practice.

Lancet Infect Dis, 20(2), e38-e46. doi:10.1016/S1473-3099(19)30612-7

Lu, T. W., Wu, J., Aoto, P. C., Weng, J. H., Ahuja, L. G., Sun, N., et al. (2019). Two PKA RIalpha holoenzyme states define ATP as an isoform-specific orthosteric inhibitor that competes with the allosteric activator, cAMP. *Proc Natl Acad Sci U S A, 116*(33), 16347-16356. doi:10.1073/pnas.1906036116

Luis García-Fuentes, R., Téllez-Sanz, Indalecio Quesada-Soriano, Carmen Barón. (2011). Thermodynamics of Molecular Recognition by Calorimetry. In J. C. Moreno-Piraján (Ed.), *Thermodynamics - Physical Chemistry of Aqueous Systems*: IntechOpen.

MacDonald, J. A., & Storey, K. B. (1998). cAMP-dependent protein kinase from brown adipose tissue: temperature effects on kinetic properties and enzyme role in hibernating ground squirrels. *J Comp Physiol B, 168*(7), 513-525. doi:10.1007/s003600050172

Machleidt, T., Woodroofe, C. C., Schwinn, M. K., Mendez, J., Robers, M. B., Zimmerman, K., et al. (2015). NanoBRET--A Novel BRET Platform for the Analysis of Protein-Protein Interactions. *ACS Chem Biol, 10*(8), 1797-1804. doi:10.1021/acschembio.5b00143

Manning, G., Whyte, D. B., Martinez, R., Hunter, T., & Sudarsanam, S. (2002). The protein kinase complement of the human genome. *Science, 298*(5600), 1912-1934. doi:10.1126/science.1075762

Matthews, K. R. (2005). The developmental cell biology of Trypanosoma brucei. *J Cell Sci, 118*(Pt 2), 283-290. doi:10.1242/jcs.01649

Mazal, H., & Haran, G. (2019). Single-molecule FRET methods to study the dynamics of proteins at work. *Curr Opin Biomed Eng, 12*, 8-17. doi:10.1016/j.cobme.2019.08.007

McKeage, K., & Keam, S. J. (2009). Salmeterol/fluticasone propionate: a review of its use in asthma. *Drugs, 69*(13), 1799-1828. doi:10.2165/11202210-000000000-00000

McKean, P. G. (2003). Coordination of cell cycle and cytokinesis in Trypanosoma brucei. *Curr Opin Microbiol, 6*(6), 600-607. doi:10.1016/j.mib.2003.10.010

Mehta, S., Zhang, Y., Roth, R. H., Zhang, J. F., Mo, A., Tenner, B., et al. (2018). Single-fluorophore biosensors for sensitive and multiplexed detection of signalling activities. *Nat Cell Biol, 20*(10), 1215-1225. doi:10.1038/s41556-018-0200-6

Moore, T. M., Chetham, P. M., Kelly, J. J., & Stevens, T. (1998). Signal transduction and regulation of lung endothelial cell permeability. Interaction between calcium and cAMP. *Am J Physiol, 275*(2), L203-222. doi:10.1152/ajplung.1998.275.2.L203

Moreau, M. J., & Schaeffer, P. M. (2013). Dissecting the salt dependence of the Tus-Ter protein-DNA complexes by high-throughput differential scanning fluorimetry of a GFP-tagged Tus. *Mol Biosyst, 9*(12), 3146-3154. doi:10.1039/c3mb70426b

Morris, J. C., Wang, Z., Drew, M. E., & Englund, P. T. (2002). Glycolysis modulates trypanosome glycoprotein expression as revealed by an RNAi library. *EMBO J, 21*(17), 4429-4438. doi:10.1093/emboj/cdf474

Moss, C. X., Brown, E., Hamilton, A., Van der Veken, P., Augustyns, K., & Mottram, J. C. (2015). An essential signal peptide peptidase identified in an RNAi screen of serine peptidases of Trypanosoma brucei. *PLoS One, 10*(3), e0123241. doi:10.1371/journal.pone.0123241

Mutzel, R., Lacombe, M. L., Simon, M. N., de Gunzburg, J., & Veron, M. (1987). Cloning and cDNA sequence of the regulatory subunit of cAMP-dependent protein kinase from Dictyostelium discoideum. *Proc Natl Acad Sci U S A, 84*(1), 6-10. doi:10.1073/pnas.84.1.6

Newlon, M. G., Roy, M., Hausken, Z. E., Scott, J. D., & Jennings, P. A. (1997). The A-kinase anchoring domain of type IIalpha cAMP-dependent protein kinase is highly helical. *J Biol Chem, 272*(38), 23637-23644.

doi:10.1074/jbc.272.38.23637
Newlon, M. G., Roy, M., Morikis, D., Carr, D. W., Westphal, R., Scott, J. D., et al. (2001). A novel mechanism of PKA anchoring revealed by solution structures of anchoring complexes. *EMBO J, 20*(7), 1651-1662. doi:10.1093/emboj/20.7.1651
Ngo, H., Tschudi, C., Gull, K., & Ullu, E. (1998). Double-stranded RNA induces mRNA degradation in Trypanosoma brucei. *Proc Natl Acad Sci U S A, 95*(25), 14687-14692. doi:10.1073/pnas.95.25.14687
Nirula, A., Ho, M., Phee, H., Roose, J., & Weiss, A. (2006). Phosphoinositide-dependent kinase 1 targets protein kinase A in a pathway that regulates interleukin 4. *J Exp Med, 203*(7), 1733-1744. doi:10.1084/jem.20051715
Oberholzer, M., Langousis, G., Nguyen, H. T., Saada, E. A., Shimogawa, M. M., Jonsson, Z. O., et al. (2011). Independent analysis of the flagellum surface and matrix proteomes provides insight into flagellum signaling in mammalian-infectious Trypanosoma brucei. *Mol Cell Proteomics, 10*(10), M111 010538. doi:10.1074/mcp.M111.010538
Oberholzer, M., Marti, G., Baresic, M., Kunz, S., Hemphill, A., & Seebeck, T. (2007). The Trypanosoma brucei cAMP phosphodiesterases TbrPDEB1 and TbrPDEB2: flagellar enzymes that are essential for parasite virulence. *FASEB J, 21*(3), 720-731. doi:10.1096/fj.06-6818com
Ogbadoyi, E. O., Robinson, D. R., & Gull, K. (2003). A high-order trans-membrane structural linkage is responsible for mitochondrial genome positioning and segregation by flagellar basal bodies in trypanosomes. *Mol Biol Cell, 14*(5), 1769-1779. doi:10.1091/mbc.e02-08-0525
Overath, P., Czichos, J., & Haas, C. (1986). The effect of citrate/cis-aconitate on oxidative metabolism during transformation of Trypanosoma brucei. *Eur J Biochem, 160*(1), 175-182. doi:10.1111/j.1432-1033.1986.tb09955.x
Pays, E., Tebabi, P., Pays, A., Coquelet, H., Revelard, P., Salmon, D., et al. (1989). The genes and transcripts of an antigen gene expression site from T. brucei. *Cell, 57*(5), 835-845. doi:10.1016/0092-8674(89)90798-8
Peng, D., Kurup, S. P., Yao, P. Y., Minning, T. A., & Tarleton, R. L. (2014). CRISPR-Cas9-mediated single-gene and gene family disruption in Trypanosoma cruzi. *MBio, 6*(1), e02097-02014. doi:10.1128/mBio.02097-14
Perkins, G. A., Wang, L., Huang, L. J., Humphries, K., Yao, V. J., Martone, M., et al. (2001). PKA, PKC, and AKAP localization in and around the neuromuscular junction. *BMC Neurosci, 2*, 17. doi:10.1186/1471-2202-2-17
Pfister, T. D., & Storey, K. B. (2002). Protein kinase A: purification and characterization of the enzyme from two cold-hardy goldenrod gall insects. *Insect Biochem Mol Biol, 32*(5), 505-515. doi:10.1016/s0965-1748(01)00128-x
PhD thesis Bachmaier, S. (2015). *Evolutionary Repurposing of cAMP and PKA Signaling Pathways in Kinetoplastids.* (Doktor Dissertation), Ludwig-Maximilians-Universität München, München.
PhD thesis Githure, G. B. (2014). *Evolutionary Divergent Ligand Activation of PKA-like Kinase from Trypanosoma brucei.* (PhD Dissertations), Ludwig-Maximilians Universität München, München.
PhD thesis Klöckner, T. (1996). *cAMP Signaltransduktion in Trypanosoma brucei: Klonierung und Charakterisierung von Proteinkinase A- und Phosphodiesterase-Homologen. .* (Doctorarbeit Dissertation), Ludwig-Maximilians-Universität München,
PhD thesis Kramer, S. (2004). *Characterization of a PKA-like kinase from Trypanosoma brucei.* (Doktorarbeit), Ludwig-Maximilians-Universität München, München.
PhD thesis Krumbholz, C. (2006). *A PKA-like kinase important for coordination of flagellar motility in Trypanosoma brucei.* (Doktorarbeit), Ludwig-Maximilians-

Universität München, München.
Pinger, J., Nesic, D., Ali, L., Aresta-Branco, F., Lilic, M., Chowdhury, S., et al. (2018). African trypanosomes evade immune clearance by O-glycosylation of the VSG surface coat. *Nat Microbiol, 3*(8), 932-938. doi:10.1038/s41564-018-0187-6
Priest, J. W., & Hajduk, S. L. (1994). Developmental regulation of Trypanosoma brucei cytochrome c reductase during bloodstream to procyclic differentiation. *Mol Biochem Parasitol, 65*(2), 291-304. doi:10.1016/0166-6851(94)90080-9
Rangel-Aldao, R., & Rosen, O. M. (1976). Dissociation and reassociation of the phosphorylated and nonphosphorylated forms of adenosine 3':5' - monophosphate-dependent protein kinase from bovine cardiac muscle. *J Biol Chem, 251*(11), 3375-3380.
Rascon, A., Soderling, S. H., Schaefer, J. B., & Beavo, J. A. (2002). Cloning and characterization of a cAMP-specific phosphodiesterase (TbPDE2B) from Trypanosoma brucei. *Proc Natl Acad Sci U S A, 99*(7), 4714-4719. doi:10.1073/pnas.002031599
Rath, S. L., & Kumar, K. (2020). Investigation of the Effect of Temperature on the Structure of SARS-CoV-2 Spike Protein by Molecular Dynamics Simulations. *Front Mol Biosci, 7*, 583523. doi:10.3389/fmolb.2020.583523
Ribeiro, V., Dias, N., Paiva, T., Hagstrom-Bex, L., Nitz, N., Pratesi, R., et al. (2020). Current trends in the pharmacological management of Chagas disease. *Int J Parasitol Drugs Drug Resist, 12*, 7-17. doi:10.1016/j.ijpddr.2019.11.004
Rico, E., Ivens, A., Glover, L., Horn, D., & Matthews, K. R. (2017). Genome-wide RNAi selection identifies a regulator of transmission stage-enriched gene families and cell-type differentiation in Trypanosoma brucei. *PLoS Pathog, 13*(3), e1006279. doi:10.1371/journal.ppat.1006279
Rico, E., Jeacock, L., Kovarova, J., & Horn, D. (2018). Inducible high-efficiency CRISPR-Cas9-targeted gene editing and precision base editing in African trypanosomes. *Sci Rep, 8*(1), 7960. doi:10.1038/s41598-018-26303-w
Rico, E., Rojas, F., Mony, B. M., Szoor, B., Macgregor, P., & Matthews, K. R. (2013). Bloodstream form pre-adaptation to the tsetse fly in Trypanosoma brucei. *Front Cell Infect Microbiol, 3*, 78. doi:10.3389/fcimb.2013.00078
Rinken, A., Veiksina, S., & Kopanchuk, S. (2016). Dynamics of ligand binding to GPCR: Residence time of melanocortins and its modulation. *Pharmacol Res, 113*(Pt B), 747-753. doi:10.1016/j.phrs.2016.05.030
Riviere, L., van Weelden, S. W., Glass, P., Vegh, P., Coustou, V., Biran, M., et al. (2004). Acetyl:succinate CoA-transferase in procyclic Trypanosoma brucei. Gene identification and role in carbohydrate metabolism. *J Biol Chem, 279*(44), 45337-45346. doi:10.1074/jbc.M407513200
Robinson, D. R., & Gull, K. (1991). Basal body movements as a mechanism for mitochondrial genome segregation in the trypanosome cell cycle. *Nature, 352*(6337), 731-733. doi:10.1038/352731a0
Romano, R. A., Kannan, N., Kornev, A. P., Allison, C. J., & Taylor, S. S. (2009). A chimeric mechanism for polyvalent trans-phosphorylation of PKA by PDK1. *Protein Sci, 18*(7), 1486-1497. doi:10.1002/pro.146
Rose, C., Casas-Sanchez, A., Dyer, N. A., Solorzano, C., Beckett, A. J., Middlehurst, B., et al. (2020). Trypanosoma brucei colonizes the tsetse gut via an immature peritrophic matrix in the proventriculus. *Nat Microbiol, 5*(7), 909-916. doi:10.1038/s41564-020-0707-z
Rotureau, B., & Van Den Abbeele, J. (2013). Through the dark continent: African trypanosome development in the tsetse fly. *Front Cell Infect Microbiol, 3*, 53. doi:10.3389/fcimb.2013.00053
Saada, E. A., Kabututu, Z. P., Lopez, M., Shimogawa, M. M., Langousis, G., Oberholzer, M., et al. (2014). Insect stage-specific receptor adenylate cyclases are localized to distinct subdomains of the Trypanosoma brucei Flagellar membrane.

Eukaryot Cell, 13(8), 1064-1076. doi:10.1128/EC.00019-14

Sales Junior, P. A., Molina, I., Fonseca Murta, S. M., Sanchez-Montalva, A., Salvador, F., Correa-Oliveira, R., et al. (2017). Experimental and Clinical Treatment of Chagas Disease: A Review. *Am J Trop Med Hyg, 97*(5), 1289-1303. doi:10.4269/ajtmh.16-0761

Sanchez, M. A., Tryon, R., Green, J., Boor, I., & Landfear, S. M. (2002). Six related nucleoside/nucleobase transporters from Trypanosoma brucei exhibit distinct biochemical functions. *J Biol Chem, 277*(24), 21499-21504. doi:10.1074/jbc.M202319200

Sandrini, F., & Stratakis, C. (2003). Clinical and molecular genetics of Carney complex. *Mol Genet Metab, 78*(2), 83-92. doi:10.1016/s1096-7192(03)00006-4

Sastri, M., Barraclough, D. M., Carmichael, P. T., & Taylor, S. S. (2005). A-kinase-interacting protein localizes protein kinase A in the nucleus. *Proc Natl Acad Sci U S A, 102*(2), 349-354. doi:10.1073/pnas.0408608102

Saye, M., Gauna, L., Valera-Vera, E., Reigada, C., Miranda, M. R., & Pereira, C. A. (2020). Crystal violet structural analogues identified by in silico drug repositioning present anti-Trypanosoma cruzi activity through inhibition of proline transporter TcAAAP069. *PLoS Negl Trop Dis, 14*(1), e0007481. doi:10.1371/journal.pntd.0007481

Schmitz, F. (2011). *Bedeutung von Phosphorylierungen für die Aktivierung der PKA-ähnlichen Kinase in Trypanosoma brucei.* (Diplomarbeit), Ludwig-Maximilians-Universität München, München.

Schothorst, J., Zeebroeck, G. V., & Thevelein, J. M. (2017). Identification of Ftr1 and Zrt1 as iron and zinc micronutrient transceptors for activation of the PKA pathway in Saccharomyces cerevisiae. *Microb Cell, 4*(3), 74-89. doi:10.15698/mic2017.03.561

Schultz, S. C., Shields, G. C., & Steitz, T. A. (1991). Crystal structure of a CAP-DNA complex: the DNA is bent by 90 degrees. *Science, 253*(5023), 1001-1007. doi:10.1126/science.1653449

Schuster, S., Kruger, T., Subota, I., Thusek, S., Rotureau, B., Beilhack, A., et al. (2017). Developmental adaptations of trypanosome motility to the tsetse fly host environments unravel a multifaceted in vivo microswimmer system. *Elife, 6*. doi:10.7554/eLife.27656

Scott, J. D., Fischer, E. H., Demaille, J. G., & Krebs, E. G. (1985). Identification of an inhibitory region of the heat-stable protein inhibitor of the cAMP-dependent protein kinase. *Proc Natl Acad Sci U S A, 82*(13), 4379-4383. doi:10.1073/pnas.82.13.4379

Seebeck, T., Whittaker, P. A., Imboden, M. A., Hardman, N., & Braun, R. (1983). Tubulin genes of Trypanosoma brucei: a tightly clustered family of alternating genes. *Proc Natl Acad Sci U S A, 80*(15), 4634-4638. doi:10.1073/pnas.80.15.4634

Seed, J. R., & Wenck, M. A. (2003). Role of the long slender to short stumpy transition in the life cycle of the african trypanosomes. *Kinetoplastid Biol Dis, 2*(1), 3. doi:10.1186/1475-9292-2-3

Semisotnov, G. V., Rodionova, N. A., Razgulyaev, O. I., Uversky, V. N., Gripas, A. F., & Gilmanshin, R. I. (1991). Study of the "molten globule" intermediate state in protein folding by a hydrophobic fluorescent probe. *Biopolymers, 31*(1), 119-128. doi:10.1002/bip.360310111

Shalaby, T., Liniger, M., & Seebeck, T. (2001). The regulatory subunit of a cGMP-regulated protein kinase A of Trypanosoma brucei. *Eur J Biochem, 268*(23), 6197-6206. doi:10.1046/j.0014-2956.2001.02564.x

Shaw, S., Knusel, S., Hoenner, S., & Roditi, I. (2020). A transient CRISPR/Cas9 expression system for genome editing in Trypanosoma brucei. *BMC Res Notes, 13*(1), 268. doi:10.1186/s13104-020-05089-z

Shetty, S. K., Walzem, R. L., & Davies, B. S. J. (2020). A novel NanoBiT-based assay

monitors the interaction between lipoprotein lipase and GPIHBP1 in real time. *J Lipid Res, 61*(4), 546-559. doi:10.1194/jlr.D119000388

Shi, H., Wormsley, S., Tschudi, C., & Ullu, E. (2002). Efficient transposition of preformed synaptic Tn5 complexes in Trypanosoma brucei. *Mol Biochem Parasitol, 121*(1), 141-144. doi:10.1016/s0166-6851(02)00020-8

Shih, M., Lin, F., Scott, J. D., Wang, H. Y., & Malbon, C. C. (1999). Dynamic complexes of beta2-adrenergic receptors with protein kinases and phosphatases and the role of gravin. *J Biol Chem, 274*(3), 1588-1595. doi:10.1074/jbc.274.3.1588

Shoji, S., Titani, K., Demaille, J. G., & Fischer, E. H. (1979). Sequence of two phosphorylated sites in the catalytic subunit of bovine cardiac muscle adenosine 3':5'-monophosphate-dependent protein kinase. *J Biol Chem, 254*(14), 6211-6214.

Siman-Tov, M. M., Aly, R., Shapira, M., & Jaffe, C. L. (1996). Cloning from Leishmania major of a developmentally regulated gene, c-lpk2, for the catalytic subunit of the cAMP-dependent protein kinase. *Mol Biochem Parasitol, 77*(2), 201-215. doi:10.1016/0166-6851(96)02601-1

Siman-Tov, M. M., Ivens, A. C., & Jaffe, C. L. (2002). Molecular cloning and characterization of two new isoforms of the protein kinase A catalytic subunit from the human parasite Leishmania. *Gene, 288*(1-2), 65-75. doi:10.1016/s0378-1119(02)00403-1

Simon, M. N., Pelegrini, O., Veron, M., & Kay, R. R. (1992). Mutation of protein kinase A causes heterochronic development of Dictyostelium. *Nature, 356*(6365), 171-172. doi:10.1038/356171a0

Skalhegg, B. S., & Tasken, K. (2000). Specificity in the cAMP/PKA signaling pathway. Differential expression,regulation, and subcellular localization of subunits of PKA. *Front Biosci, 5*, D678-693. doi:10.2741/skalhegg

Sorrentino, V., & Rizzuto, R. (2001). Molecular genetics of Ca(2+) stores and intracellular Ca(2+) signalling. *Trends Pharmacol Sci, 22*(9), 459-464. doi:10.1016/s0165-6147(00)01760-0

Steinberg, R. A., Cauthron, R. D., Symcox, M. M., & Shuntoh, H. (1993). Autoactivation of catalytic (C alpha) subunit of cyclic AMP-dependent protein kinase by phosphorylation of threonine 197. *Mol Cell Biol, 13*(4), 2332-2341. doi:10.1128/mcb.13.4.2332

Steyfkens, F., Zhang, Z., Van Zeebroeck, G., & Thevelein, J. M. (2018). Multiple Transceptors for Macro- and Micro-Nutrients Control Diverse Cellular Properties Through the PKA Pathway in Yeast: A Paradigm for the Rapidly Expanding World of Eukaryotic Nutrient Transceptors Up to Those in Human Cells. *Front Pharmacol, 9*, 191. doi:10.3389/fphar.2018.00191

Stortz, J. A., Serafim, T. D., Alsford, S., Wilkes, J., Fernandez-Cortes, F., Hamilton, G., et al. (2017). Genome-wide and protein kinase-focused RNAi screens reveal conserved and novel damage response pathways in Trypanosoma brucei. *PLoS Pathog, 13*(7), e1006477. doi:10.1371/journal.ppat.1006477

Stratakis, C. A., Kirschner, L. S., & Carney, J. A. (2001). Clinical and molecular features of the Carney complex: diagnostic criteria and recommendations for patient evaluation. *J Clin Endocrinol Metab, 86*(9), 4041-4046. doi:10.1210/jcem.86.9.7903

Su, Y., Dostmann, W. R., Herberg, F. W., Durick, K., Xuong, N. H., Ten Eyck, L., et al. (1995). Regulatory subunit of protein kinase A: structure of deletion mutant with cAMP binding domains. *Science, 269*(5225), 807-813. doi:10.1126/science.7638597

Subota, I., Julkowska, D., Vincensini, L., Reeg, N., Buisson, J., Blisnick, T., et al. (2014). Proteomic analysis of intact flagella of procyclic Trypanosoma brucei cells identifies novel flagellar proteins with unique sub-localization and dynamics. *Mol Cell Proteomics, 13*(7), 1769-1786. doi:10.1074/mcp.M113.033357

Sundar, S. (2001). Drug resistance in Indian visceral leishmaniasis. *Trop Med Int Health, 6*(11), 849-854. doi:10.1046/j.1365-3156.2001.00778.x

Tagoe, D. N., Kalejaiye, T. D., & de Koning, H. P. (2015). The ever unfolding story of cAMP signaling in trypanosomatids: vive la difference! *Front Pharmacol, 6*, 185. doi:10.3389/fphar.2015.00185

Tao, J., Wang, H. Y., & Malbon, C. C. (2003). Protein kinase A regulates AKAP250 (gravin) scaffold binding to the beta2-adrenergic receptor. *EMBO J, 22*(24), 6419-6429. doi:10.1093/emboj/cdg628

Taylor, S. S., Ilouz, R., Zhang, P., & Kornev, A. P. (2012). Assembly of allosteric macromolecular switches: lessons from PKA. *Nat Rev Mol Cell Biol, 13*(10), 646-658. doi:10.1038/nrm3432

Taylor, S. S., Kim, C., Cheng, C. Y., Brown, S. H., Wu, J., & Kannan, N. (2008). Signaling through cAMP and cAMP-dependent protein kinase: diverse strategies for drug design. *Biochim Biophys Acta, 1784*(1), 16-26. doi:10.1016/j.bbapap.2007.10.002

Taylor, S. S., Radzio-Andzelm, E., Knighton, D. R., Ten Eyck, L. F., Sowadski, J. M., Herberg, F. W., et al. (1993a). Crystal structures of the catalytic subunit of cAMP-dependent protein kinase reveal general features of the protein kinase family. *Receptor, 3*(3), 165-172.

Taylor, S. S., Zhang, P., Steichen, J. M., Keshwani, M. M., & Kornev, A. P. (2013). PKA: lessons learned after twenty years. *Biochim Biophys Acta, 1834*(7), 1271-1278. doi:10.1016/j.bbapap.2013.03.007

Taylor, S. S., Zheng, J., Radzio-Andzelm, E., Knighton, D. R., Ten Eyck, L. F., Sowadski, J. M., et al. (1993b). cAMP-dependent protein kinase defines a family of enzymes. *Philos Trans R Soc Lond B Biol Sci, 340*(1293), 315-324. doi:10.1098/rstb.1993.0073

Ten Eyck, L. F., Taylor, S. S., & Kornev, A. P. (2008). Conserved spatial patterns across the protein kinase family. *Biochim Biophys Acta, 1784*(1), 238-243. doi:10.1016/j.bbapap.2007.11.002

Terrin, A., Monterisi, S., Stangherlin, A., Zoccarato, A., Koschinski, A., Surdo, N. C., et al. (2012). PKA and PDE4D3 anchoring to AKAP9 provides distinct regulation of cAMP signals at the centrosome. *J Cell Biol, 198*(4), 607-621. doi:10.1083/jcb.201201059

Tolbert, W. D., Daugherty, J., Gao, C., Xie, Q., Miranti, C., Gherardi, E., et al. (2007). A mechanistic basis for converting a receptor tyrosine kinase agonist to an antagonist. *Proc Natl Acad Sci U S A, 104*(37), 14592-14597. doi:10.1073/pnas.0704290104

Trotter, K. W., Fraser, I. D., Scott, G. K., Stutts, M. J., Scott, J. D., & Milgram, S. L. (1999). Alternative splicing regulates the subcellular localization of A-kinase anchoring protein 18 isoforms. *J Cell Biol, 147*(7), 1481-1492. doi:10.1083/jcb.147.7.1481

Tu, X., Kumar, P., Li, Z., & Wang, C. C. (2006). An aurora kinase homologue is involved in regulating both mitosis and cytokinesis in Trypanosoma brucei. *J Biol Chem, 281*(14), 9677-9687. doi:10.1074/jbc.M511504200

Tummino, P. J., & Copeland, R. A. (2008). Residence time of receptor-ligand complexes and its effect on biological function. *Biochemistry, 47*(20), 5481-5492. doi:10.1021/bi8002023

Ullu, E., Djikeng, A., Shi, H., & Tschudi, C. (2002). RNA interference: advances and questions. *Philos Trans R Soc Lond B Biol Sci, 357*(1417), 65-70. doi:10.1098/rstb.2001.0952

van Weelden, S. W., Fast, B., Vogt, A., van der Meer, P., Saas, J., van Hellemond, J. J., et al. (2003). Procyclic Trypanosoma brucei do not use Krebs cycle activity for energy generation. *J Biol Chem, 278*(15), 12854-12863. doi:10.1074/jbc.M213190200

Vanhollebeke, B., De Muylder, G., Nielsen, M. J., Pays, A., Tebabi, P., Dieu, M., et al. (2008). A haptoglobin-hemoglobin receptor conveys innate immunity to Trypanosoma brucei in humans. *Science, 320*(5876), 677-681. doi:10.1126/science.1156296

Vassella, E., & Boshart, M. (1996). High molecular mass agarose matrix supports growth of bloodstream forms of pleomorphic Trypanosoma brucei strains in axenic culture. *Mol Biochem Parasitol, 82*(1), 91-105. doi:10.1016/0166-6851(96)02727-2

Vassella, E., Reuner, B., Yutzy, B., & Boshart, M. (1997). Differentiation of African trypanosomes is controlled by a density sensing mechanism which signals cell cycle arrest via the cAMP pathway. *J Cell Sci, 110 (Pt 21)*, 2661-2671.

Vaughan, S., & Gull, K. (2015). Basal body structure and cell cycle-dependent biogenesis in Trypanosoma brucei. *Cilia, 5*, 5. doi:10.1186/s13630-016-0023-7

Verner, Z., Paris, Z., & Lukes, J. (2010). Mitochondrial membrane potential-based genome-wide RNAi screen of Trypanosoma brucei. *Parasitol Res, 106*(5), 1241-1244. doi:10.1007/s00436-010-1754-9

Vickerman, K. (1985). Developmental cycles and biology of pathogenic trypanosomes. *Br Med Bull, 41*(2), 105-114. doi:10.1093/oxfordjournals.bmb.a072036

Vickerman K, P. J. M., Stuart KD. (1993). African trypanosomiasis. In K. S. Warren (Ed.), *Immunology and Molecular Biology of Parasitic Infections* Boston, MA: Blackwell Scientific Publications.

Villalta, F., & Rachakonda, G. (2019). Advances in preclinical approaches to Chagas disease drug discovery. *Expert Opin Drug Discov, 14*(11), 1161-1174. doi:10.1080/17460441.2019.1652593

Volotovski, I. D., Sokolovsky, S. G., Molchan, O. V., & Knight, M. R. (1998). Second messengers mediate increases in cytosolic calcium in tobacco protoplasts. *Plant Physiol, 117*(3), 1023-1030. doi:10.1104/pp.117.3.1023

Walsh, D. A., Ashby, C. D., Gonzalez, C., Calkins, D., & Fischer, E. H. (1971). Krebs EG: Purification and characterization of a protein inhibitor of adenosine 3',5'-monophosphate-dependent protein kinases. *J Biol Chem, 246*(7), 1977-1985.

Walsh, D. A., Perkins, J. P., & Krebs, E. G. (1968). An adenosine 3',5'-monophosphate-dependant protein kinase from rabbit skeletal muscle. *J Biol Chem, 243*(13), 3763-3765.

Wang, D., Harper, J. F., & Gribskov, M. (2003). Systematic trans-genomic comparison of protein kinases between Arabidopsis and Saccharomyces cerevisiae. *Plant Physiol, 132*(4), 2152-2165. doi:10.1104/pp.103.021485

Wang, H., Yang, P., Liu, K., Guo, F., Zhang, Y., Zhang, G., et al. (2008). SARS coronavirus entry into host cells through a novel clathrin- and caveolae-independent endocytic pathway. *Cell Res, 18*(2), 290-301. doi:10.1038/cr.2008.15

Wells, C. I., Vasta, J. D., Corona, C. R., Wilkinson, J., Zimprich, C. A., Ingold, M. R., et al. (2020). Quantifying CDK inhibitor selectivity in live cells. *Nat Commun, 11*(1), 2743. doi:10.1038/s41467-020-16559-0

Wetzel, C. H., Spehr, M., & Hatt, H. (2001). Phosphorylation of voltage-gated ion channels in rat olfactory receptor neurons. *Eur J Neurosci, 14*(7), 1056-1064. doi:10.1046/j.0953-816x.2001.01722.x

Wong, W., & Scott, J. D. (2004). AKAP signalling complexes: focal points in space and time. *Nat Rev Mol Cell Biol, 5*(12), 959-970. doi:10.1038/nrm1527

Wu, J., Brown, S., Xuong, N. H., & Taylor, S. S. (2004a). RIalpha subunit of PKA: a cAMP-free structure reveals a hydrophobic capping mechanism for docking cAMP into site B. *Structure, 12*(6), 1057-1065. doi:10.1016/j.str.2004.03.022

Wu, J., Brown, S. H., von Daake, S., & Taylor, S. S. (2007). PKA type IIalpha holoenzyme reveals a combinatorial strategy for isoform diversity. *Science, 318*(5848), 274-279. doi:10.1126/science.1146447

Wu, J., Jones, J. M., Nguyen-Huu, X., Ten Eyck, L. F., & Taylor, S. S. (2004b). Crystal structures of RIalpha subunit of cyclic adenosine 5'-monophosphate (cAMP)-dependent protein kinase complexed with (Rp)-adenosine 3',5'-cyclic monophosphothioate and (Sp)-adenosine 3',5'-cyclic monophosphothioate, the phosphothioate analogues of cAMP. *Biochemistry, 43*(21), 6620-6629. doi:10.1021/bi0302503

Wurst, M., Robles, A., Po, J., Luu, V. D., Brems, S., Marentije, M., et al. (2009). An RNAi screen of the RRM-domain proteins of Trypanosoma brucei. *Mol Biochem Parasitol, 163*(1), 61-65. doi:10.1016/j.molbiopara.2008.09.001

Yang, J., Cron, P., Thompson, V., Good, V. M., Hess, D., Hemmings, B. A., et al. (2002). Molecular mechanism for the regulation of protein kinase B/Akt by hydrophobic motif phosphorylation. *Mol Cell, 9*(6), 1227-1240. doi:10.1016/s1097-2765(02)00550-6

Yonemoto, W., Garrod, S. M., Bell, S. M., & Taylor, S. S. (1993a). Identification of phosphorylation sites in the recombinant catalytic subunit of cAMP-dependent protein kinase. *J Biol Chem, 268*(25), 18626-18632.

Yonemoto, W., McGlone, M. L., & Taylor, S. S. (1993b). N-myristylation of the catalytic subunit of cAMP-dependent protein kinase conveys structural stability. *J Biol Chem, 268*(4), 2348-2352.

Yun, O., Priotto, G., Tong, J., Flevaud, L., & Chappuis, F. (2010). NECT is next: implementing the new drug combination therapy for Trypanosoma brucei gambiense sleeping sickness. *PLoS Negl Trop Dis, 4*(5), e720. doi:10.1371/journal.pntd.0000720

Zaccolo, M., & Pozzan, T. (2003). CAMP and Ca2+ interplay: a matter of oscillation patterns. *Trends Neurosci, 26*(2), 53-55. doi:10.1016/s0166-2236(02)00017-6

Zhang, H., Kong, Q., Wang, J., Jiang, Y., & Hua, H. (2020). Complex roles of cAMP-PKA-CREB signaling in cancer. *Exp Hematol Oncol, 9*(1), 32. doi:10.1186/s40164-020-00191-1

Zhang, J. F., Liu, B., Hong, I., Mo, A., Roth, R. H., Tenner, B., et al. (2021). An ultrasensitive biosensor for high-resolution kinase activity imaging in awake mice. *Nat Chem Biol, 17*(1), 39-46. doi:10.1038/s41589-020-00660-y

Zhang, P., Kornev, A. P., Wu, J., & Taylor, S. S. (2015). Discovery of Allostery in PKA Signaling. *Biophys Rev, 7*(2), 227-238. doi:10.1007/s12551-015-0170-x

Zhang, P., Smith-Nguyen, E. V., Keshwani, M. M., Deal, M. S., Kornev, A. P., & Taylor, S. S. (2012). Structure and allostery of the PKA RIIbeta tetrameric holoenzyme. *Science, 335*(6069), 712-716. doi:10.1126/science.1213979

Zhang, W. W., & Matlashewski, G. (2015). CRISPR-Cas9-Mediated Genome Editing in Leishmania donovani. *MBio, 6*(4), e00861. doi:10.1128/mBio.00861-15

Zhou, Q., Hu, H., & Li, Z. (2014). New insights into the molecular mechanisms of mitosis and cytokinesis in trypanosomes. *Int Rev Cell Mol Biol, 308*, 127-166. doi:10.1016/B978-0-12-800097-7.00004-X

Zoraghi, R., Kunz, S., Gong, K., & Seebeck, T. (2001). Characterization of TbPDE2A, a novel cyclic nucleotide-specific phosphodiesterase from the protozoan parasite Trypanosoma brucei. *J Biol Chem, 276*(15), 11559-11566. doi:10.1074/jbc.M005419200

Curriculum Vitae

Acknowledgements

I want to express my deepest appreciation to my supervisor Prof. Michael Boshart for offering this captivating project, for all interesting and productive discussions, for the innumerable support and encouragement for my study and live in Germany.

I would like to thank Prof. Daniel Krappmann for being the second examiner of the thesis. I am also grateful to Prof. Kirsten Jung, Dr. Sebastian Bultmann, Prof. Torben Cordes and Prof. Christof Osman for being the members of my thesis examination board.

Dr. Sebastian Bultmann has also been in my Thesis Advisory Committee together with Prof. Caroline Gutjahr, thank you for the helpful suggestions.

Special thanks to our collaborators (Prof. Oliver Plettenburg, Dr. Matjaz, Brvar, Dr. Frank Schwede, Dr. Andreas Rentsch) for your essential contributions and the practical suggestions in the inhibitor development project and my thesis.

I would like to extend my sincere thanks to all the members of AG Boshart, for the invaluable help and support. To Sabine, many thanks for guiding me to the field and your patient instructions and all the fruitful discussions. To Kristina, Astrid and Theresa, thank you for your support, company and the fun in and outside the lab. I very much appreciate Yuri for your support and help in structural biology, working with you and Veronica is a great pleasure. To George, thank you for your help in the early stage of my PhD.

The last but the most important persons I want to thank are my parents and my grandma, thank you for your continuous support and love, I cannot wait to see you again.

Supplementary data

Fig S1

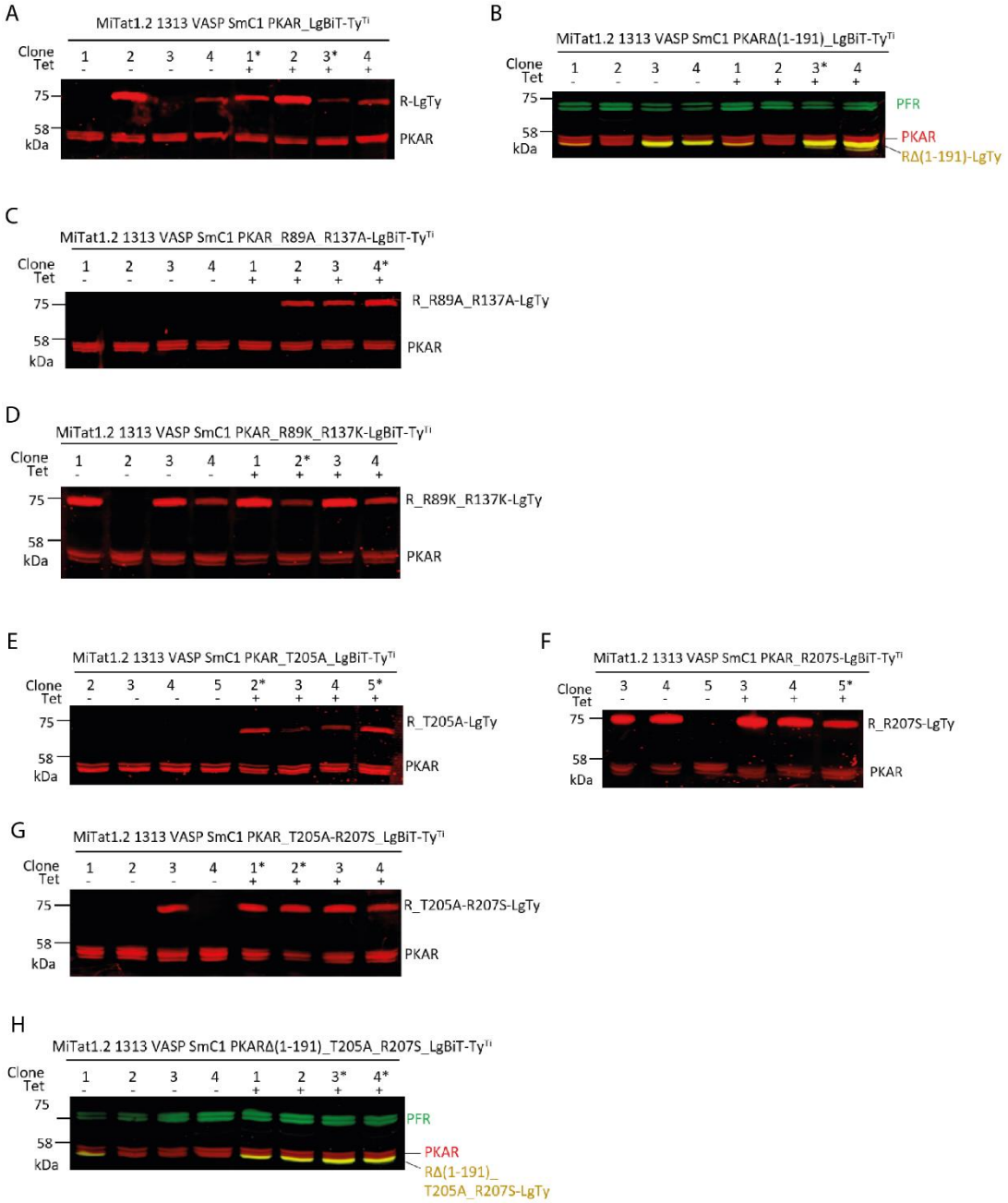

Fig S1, Western blot probing the expression of PKAR-LgBiT-Ty and the mutants. A, PKAR-LgTy; B, PKARΔ(1-191)-LgTy; C, PKAR_R89A_R137A-LgTy; D, PKAR_R89K_R137K-LgTy; E, , PKAR_T205A-LgTy; F, PKAR_R207S-LgTy; G, PKAR_T205A_R207S-LgTy; H, PKAR Δ(1-191)_T205A_R207S-LgTy. Anti-PKAR, anti-PFR and anti-Ty were used. PFR signal was used as loading control. In graph B and H, the band of the N-terminal domain deleted PKAR mutant (yellow band) overlaps with the endogenous one (red band), they were labelled with corresponding colors.

Fig S2

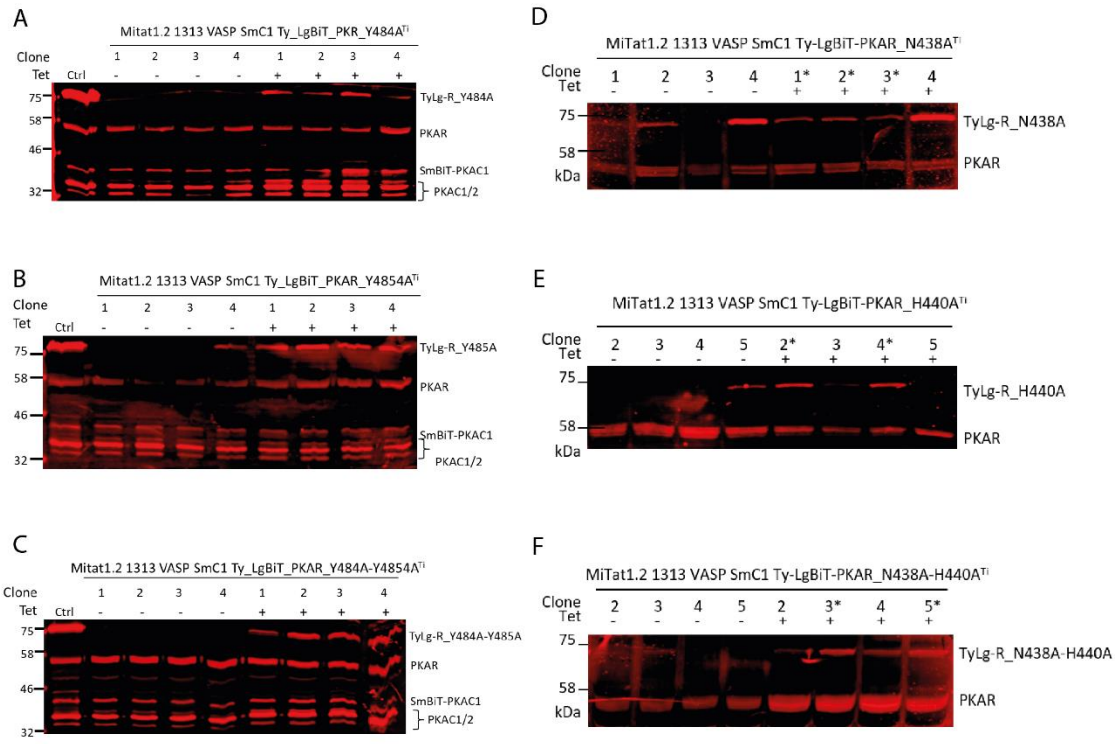

Fig S2, Western blot probing the expression of α-D helix and its contacts mutants. A, TyLg-PKAR_Y484A; B, TyLg-PKAR_Y485A; C, TyLg-PKAR_Y484A_Y485A; D, TyLg-PKAR_N438A; E, TyLg-PKAR_H440A; F, TyLg-PKAR_N438A_H440A. Anti-PKAR, anti-PKAC1/2, anti-PFR and anti-Ty were used. PFR signal was used as loading control. The molecular weight of the TyLgBiT fused PKAR mutants are very close to that of PFR, so PFR signal was hidden for visualization. SmBiT-PKAC1 and PKAC1/2 signals were omitted in graph D, E and F for better visualization.

Fig S3

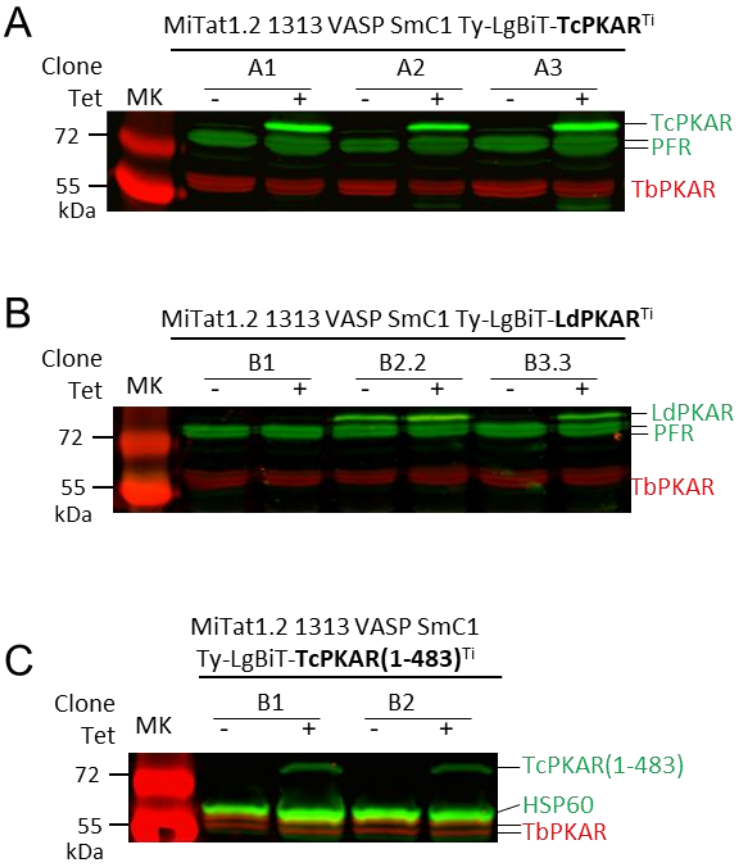

Fig S3, Western blot probing the expression of TcPKAR and LdPKAR. A, TyLg-TcPKAR; B, TyLg-LdPKAR; C, TyLg-TcPKAR(1-483). Anti-PKAR, anti-PFR and anti-Ty were used in graph A and B. anti- HSP60 was used for loading control rather than anti-PFR as the molecular weight of the TyLgBiT-TcPKAR(1-483) and PFR are very close.

Fig S4

A

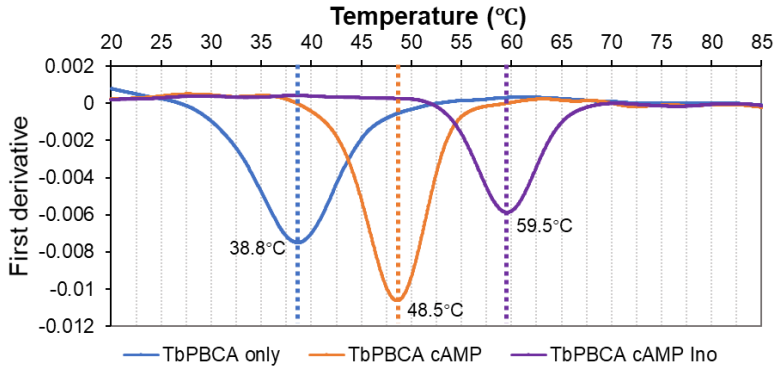

B

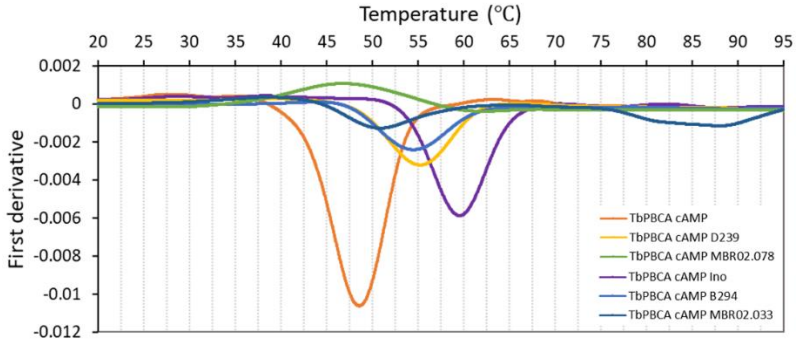

C

Sample	Tm	Compound K_D
R-PBCA + cAMP	48,5°C	-
R-PBCA + cAMP + Ino	59,5°C	3.1 ± 1.5 nM
R-PBCA + cAMP + D239	55,4°C	10.5 ± 2.0 nM
R-PBCA + cAMP + B294	54,5°C	26.5 ± 4.0 nM
R-PBCA + cAMP + MBR02.033	51,6°C	ND
R-PBCA + cAMP + MBR02.078	46,9°C	435.5 ± 37 nM

Fig S4, NanoDSF testing protein thermostability. A, the thermostability of PKAR(199-499, PBCA) proteins refolded in addition of nothing, cAMP or cAMP plus inosine. B, cAMP refolded PKAR(199-499, PBCA) stability in the treatment of different compounds. C, table listing the Tm values.

Fig S5

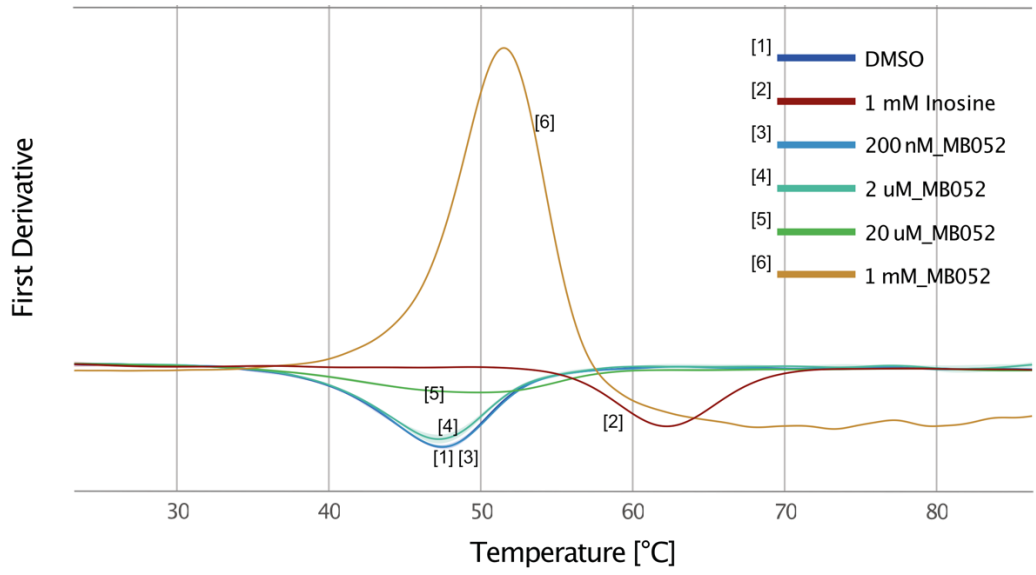

Treatment	Tm(°C)
Solvent (DMSO)	47,37
Ino 1 mM	62,25
MB052 200 nM	47,42
MB052 2 µM	47,18
MB052 20 µM	49,74
MB052 1 mM	51,38

Fig S5, NanoDSF testing PKAR stabilization by MB052. PKAR(199-499, PBCA) was refolded in the presence of cAMP. Protein was treated with different concentrations of MB052 and then measured by NanoDSF. Higher concentration of MB052 resulted in a higher Tm of the protein. The first derivative curve of 1 mM MB052 treated protein is inverted compared to the others, suggesting a different protein state upon binding of MB052.

Fig S6

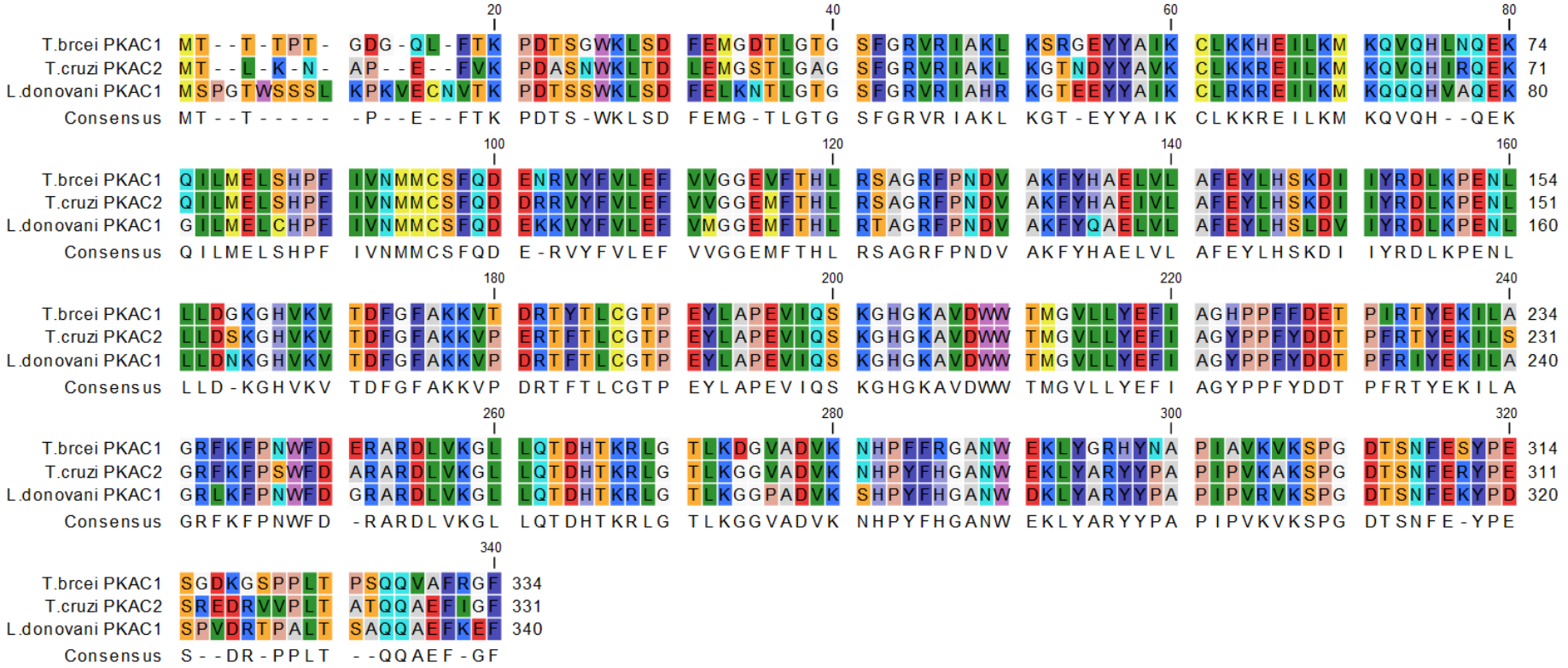

Fig S6, Amino acid sequence alignment of TbPKAC1, TcPKAC2 and LdPKAC1. The three genes are on the similar gene locus in the genome, although the naming is different. TcPKAC2 and LdPKAC1 are 82.5% and 78.4% identical with TbPKAC1 in amino acid sequence, respectively.

Fig S7

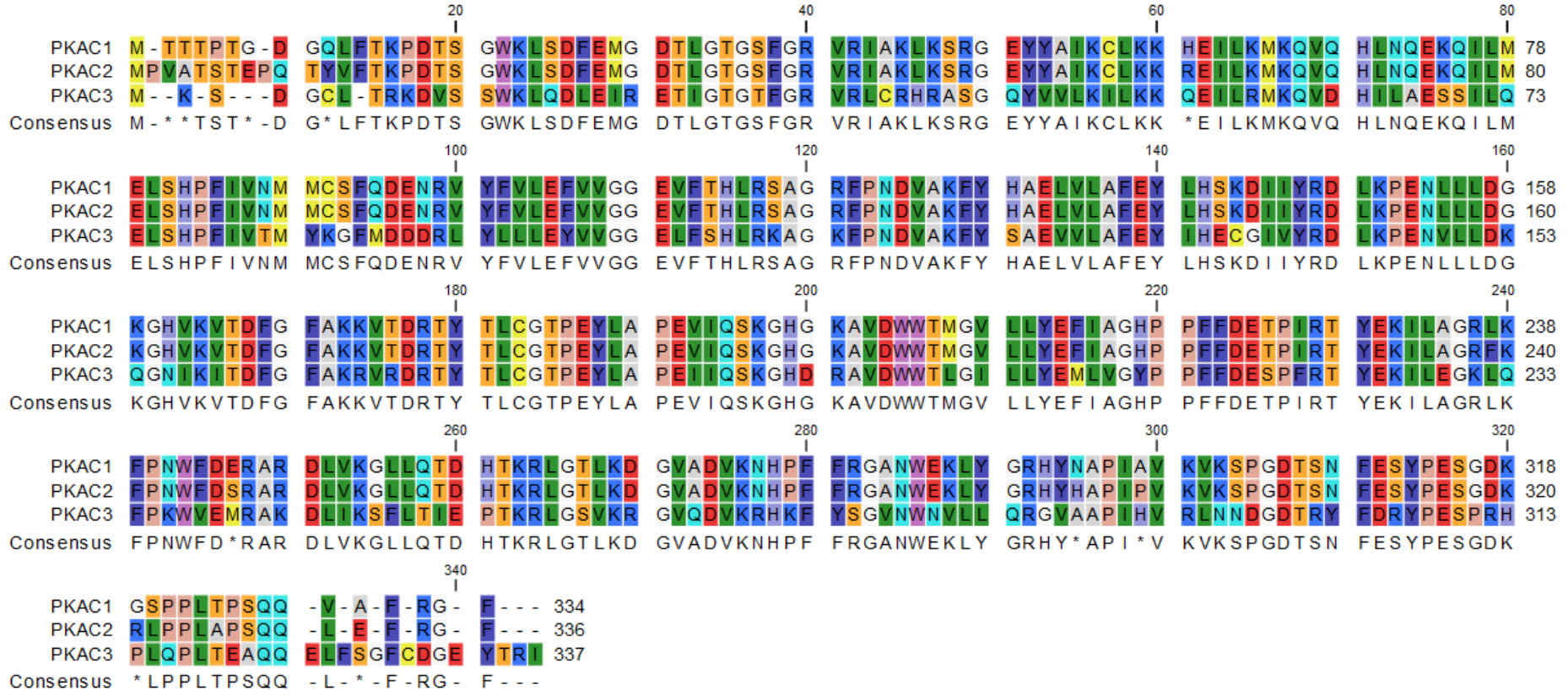

Fig S7, Amino acid sequence alignment of PKAC1, PKAC2 and PKAC3 of *T. brucei*. PKAC1 and PKAC2 are 94.01% identical. PKAC3 share 59.88% and 59.57% homology with PKAC1 and PKAC2, respectively.

Fig S8

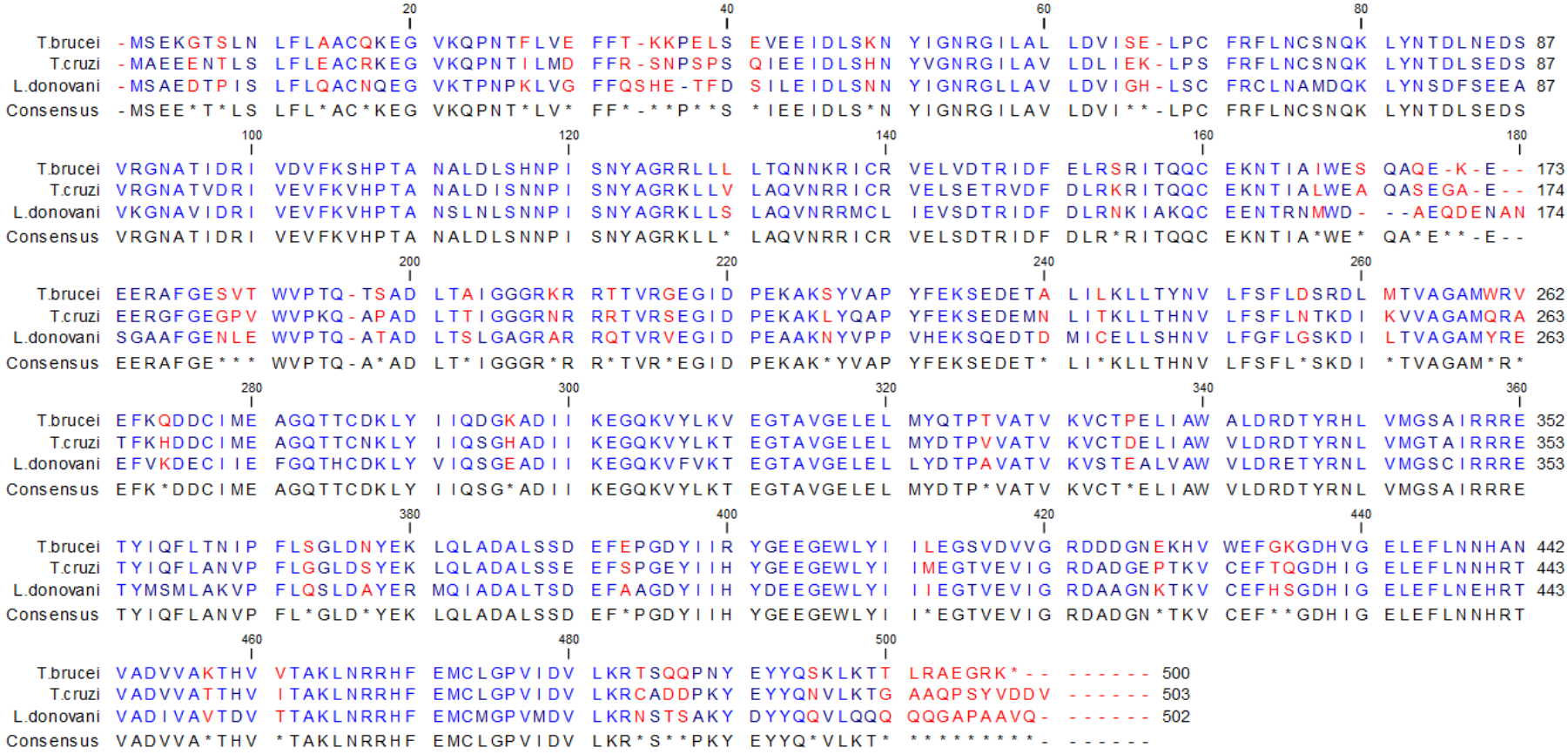

Fig S8, Amino acid sequence alignment of PKARs from *T. brucei*, *T. cruzi* and *L. donovani*. 100% consensus is indicated by blue color, while consensus lower than 40% and between 40-70% were indicated with red and black colors, respectively.

Fig S9

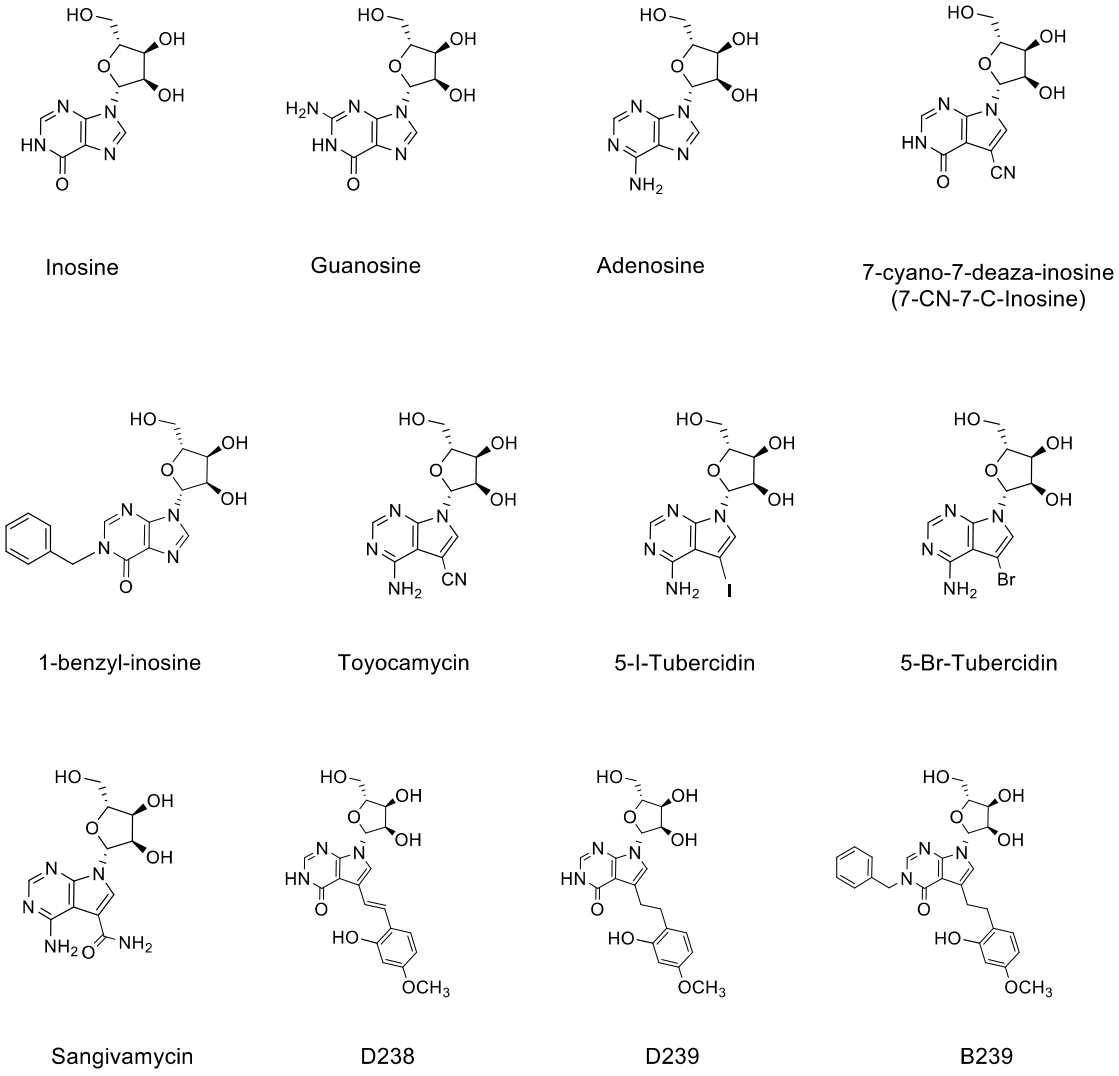

Fig S9, Chemical structure of compounds.

Table S1 PKA inhibitor candidate evaluation

Compound ID	Modification position	Activation/Inhibition	Mean of EC_{50} (μM)	Mean of K_D by ITC (nM)	EC_{50}/K_D
Inosine	-	activation	0.035	5	7
D238	C7	activation	0.31	9.9	31.3
D239	C7	activation	0.14	10	14.0
B294	N1, C7	activation	2.39	26.5	90.2
MB002	N1, C8	activation	13.2	N.D.	-
MB003	N1, C9	activation	9.8	436	22.5
MB004	N1	activation	1.16	N.D.	-
MB005	N1, N9	activation	undetectable	N.D.	-
MB006	C6	activation	0.3	N.D.	-
MB007	N9	activation	undetectable	N.D.	-
MB-008	C7	activation	0.02	N.D.	-
MB-009	N1, C7	activation	1.87	undetectable	-
MB-010	N1, C7	activation	1.8	undetectable	-
MB-011	N1, C7	activation	10.1	123	82.1
MB-012	N1, N9	activation	undetectable	N.D.	-
MB-013	N1, C7	activation	3.63	57	63.7
MB-014	N1, C7	activation	5.53	N.D.	-
MB-015	N1, C7	activation	1.45	N.D.	-
MB-016	N9	activation	no effect	N.D.	-
MB-017	N1, C7	activation	1.17	21.6	54.2
MB-018	N1, C7	activation	1.09	17.7	61.6
MB-019	C6, N9	weak inhibition	> 30	N.D.	-
MB-020	C6, N9	weak inhibition	> 30	N.D.	-
MB-022	C6, N9	weak activation	> 100	N.D.	-
MB-023	N1, C7	activation	1.86	40.3	46.2
MB-024	N1, C7	activation	2.42	43.2	56.0
MB-025	N1, C7	activation	1.65	15	110.0
MB-026	N1, C7	activation	8.81	23.7	371.7
MB-027	N1, C7	activation	10.04	35.7	281.2
MB-028	N1, C7	activation	4.61	43.1	107.0
MB-029	N9	weak activation	> 20	54.2	-
MB-030	N9	weak activation	> 20	N.D.	-
MB-031	N1, C7	activation	3.84	54	71.1
MB-032	N9	weak activation	-	N.D.	-
MB-033	N9	weak activation	-	N.D.	-
MB-034	N1, C7	activation	0.198	N.D.	-

MB-035	N1, C7	activation	14	50	280.0
MB-036	C6	activation	0.164	N.D.	-
MB-037	C6	activation	0.534	N.D.	-
MB-038	C6	activation	0.119	N.D.	-
MB-039	C6	activation	0.904	N.D.	-
MB-040	C6	activation	1.228	N.D.	-
MB-041	C6	activation	0.262	N.D.	-
MB-042	C6	activation	0.108	N.D.	-
MB-043	C6	activation	0.191	N.D.	-
MB-044	C6	activation	0.532	N.D.	-
MB-045	C6	activation	0.437	N.D.	-
MB-046	C6	activation	0.862	N.D.	-
MB-047	C6	activation	1.161	N.D.	-
MB-048	C6	activation	0.52	N.D.	-
MB-049	C6	activation	0.125	N.D.	-
MB-050	C6	activation	0.089	N.D.	-
MB-051	N1, C7	activation	0.446	N.D.	-
MB-052	N1, C7	weak activation	>60	N.D.	-
MB-053	C6	activation	0.127	N.D.	-
MB-054	N1, C7	activation		N.D.	-
MB-055	C6	activation	7.82	N.D.	-
MB-056	C6	activation	0.14	N.D.	-
MB-057	C6, N9	weak inhibition	>30	N.D.	-
MB-058	C6	activation	0.14	N.D.	-
MB-059	C6	activation	0.222	N.D.	-